NUMERICAL SOLUTION OF THE COMPLETE TWO-PHASE MODEL FOR LAMINAR FILM CONDENSATION WITH A NONCONDENSABLE GAS

by

Yu-Shan (Sammy) Chin

A Thesis Presented to

The University of Manitoba

in Partial Fulfillment of the

Requirements for the degree of

Master of Science in Mechanical Engineering

Winnipeg, Manitoba, Canada

August 1995

National Library
of Canada

Acquisitions and
Bibliographic Services Branch

395 Wellington Street
Ottawa, Ontario
K1A 0N4

Bibliothèque nationale
du Canada

Direction des acquisitions et
des services bibliographiques

395, rue Wellington
Ottawa (Ontario)
K1A 0N4

Your file *Votre référence*

Our file *Notre référence*

ISBN 0-612-13028-2

Canada

Name Yu-Shan Chin

Dissertation Abstracts International is arranged by broad, general subject categories. Please select the one subject which most nearly describes the content of your dissertation. Enter the corresponding four-digit code in the spaces provided.

Heat and Thermodynamics
SUBJECT TERM

0348
SUBJECT CODE

U·M·I

Subject Categories

THE HUMANITIES AND SOCIAL SCIENCES

COMMUNICATIONS AND THE ARTS
Architecture 0729
Art History 0377
Cinema 0900
Dance 0378
Fine Arts 0357
Information Science 0723
Journalism 0391
Library Science 0399
Mass Communications 0708
Music 0413
Speech Communication 0459
Theater 0465

EDUCATION
General 0515
Administration 0514
Adult and Continuing 0516
Agricultural 0517
Art 0273
Bilingual and Multicultural 0282
Business 0688
Community College 0275
Curriculum and Instruction 0727
Early Childhood 0518
Elementary 0524
Finance 0277
Guidance and Counseling 0519
Health 0680
Higher 0745
History of 0520
Home Economics 0278
Industrial 0521
Language and Literature 0279
Mathematics 0280
Music 0522
Philosophy of 0998
Physical 0523
Psychology 0525
Reading 0535
Religious 0527
Sciences 0714
Secondary 0533
Social Sciences 0534
Sociology of 0340
Special 0529
Teacher Training 0530
Technology 0710
Tests and Measurements 0288
Vocational 0747

LANGUAGE, LITERATURE AND LINGUISTICS
Language
- General 0679
- Ancient 0289
- Linguistics 0290
- Modern 0291

Literature
- General 0401
- Classical 0294
- Comparative 0295
- Medieval 0297
- Modern 0298
- African 0316
- American 0591
- Asian 0305
- Canadian (English) 0352
- Canadian (French) 0355
- English 0593
- Germanic 0311
- Latin American 0312
- Middle Eastern 0315
- Romance 0313
- Slavic and East European 0314

PHILOSOPHY, RELIGION AND THEOLOGY
Philosophy 0422
Religion
- General 0318
- Biblical Studies 0321
- Clergy 0319
- History of 0320
- Philosophy of 0322

Theology 0469

SOCIAL SCIENCES
American Studies 0323
Anthropology
- Archaeology 0324
- Cultural 0326
- Physical 0327

Business Administration
- General 0310
- Accounting 0272
- Banking 0770
- Management 0454
- Marketing 0338

Canadian Studies 0385
Economics
- General 0501
- Agricultural 0503
- Commerce-Business 0505
- Finance 0508
- History 0509
- Labor 0510
- Theory 0511

Folklore 0358
Geography 0366
Gerontology 0351
History
- General 0578
- Ancient 0579
- Medieval 0581
- Modern 0582
- Black 0328
- African 0331
- Asia, Australia and Oceania 0332
- Canadian 0334
- European 0335
- Latin American 0336
- Middle Eastern 0333
- United States 0337

History of Science 0585
Law 0398
Political Science
- General 0615
- International Law and Relations 0616
- Public Administration 0617

Recreation 0814
Social Work 0452
Sociology
- General 0626
- Criminology and Penology 0627
- Demography 0938
- Ethnic and Racial Studies 0631
- Individual and Family Studies 0628
- Industrial and Labor Relations 0629
- Public and Social Welfare 0630
- Social Structure and Development 0700
- Theory and Methods 0344

Transportation 0709
Urban and Regional Planning 0999
Women's Studies 0453

THE SCIENCES AND ENGINEERING

BIOLOGICAL SCIENCES
Agriculture
- General 0473
- Agronomy 0285
- Animal Culture and Nutrition 0475
- Animal Pathology 0476
- Food Science and Technology 0359
- Forestry and Wildlife 0478
- Plant Culture 0479
- Plant Pathology 0480
- Plant Physiology 0817
- Range Management 0777
- Wood Technology 0746

Biology
- General 0306
- Anatomy 0287
- Biostatistics 0308
- Botany 0309
- Cell 0379
- Ecology 0329
- Entomology 0353
- Genetics 0369
- Limnology 0793
- Microbiology 0410
- Molecular 0307
- Neuroscience 0317
- Oceanography 0416
- Physiology 0433
- Radiation 0821
- Veterinary Science 0778
- Zoology 0472

Biophysics
- General 0786
- Medical 0760

EARTH SCIENCES
Biogeochemistry 0425
Geochemistry 0996
Geodesy 0370
Geology 0372
Geophysics 0373
Hydrology 0388
Mineralogy 0411
Paleobotany 0345
Paleoecology 0426
Paleontology 0418
Paleozoology 0985
Palynology 0427
Physical Geography 0368
Physical Oceanography 0415

HEALTH AND ENVIRONMENTAL SCIENCES
Environmental Sciences 0768
Health Sciences
- General 0566
- Audiology 0300
- Chemotherapy 0992
- Dentistry 0567
- Education 0350
- Hospital Management 0769
- Human Development 0758
- Immunology 0982
- Medicine and Surgery 0564
- Mental Health 0347
- Nursing 0569
- Nutrition 0570
- Obstetrics and Gynecology 0380
- Occupational Health and Therapy 0354
- Ophthalmology 0381
- Pathology 0571
- Pharmacology 0419
- Pharmacy 0572
- Physical Therapy 0382
- Public Health 0573
- Radiology 0574
- Recreation 0575
- Speech Pathology 0460
- Toxicology 0383

Home Economics 0386

PHYSICAL SCIENCES
Pure Sciences
Chemistry
- General 0485
- Agricultural 0749
- Analytical 0486
- Biochemistry 0487
- Inorganic 0488
- Nuclear 0738
- Organic 0490
- Pharmaceutical 0491
- Physical 0494
- Polymer 0495
- Radiation 0754

Mathematics 0405
Physics
- General 0605
- Acoustics 0986
- Astronomy and Astrophysics 0606
- Atmospheric Science 0608
- Atomic 0748
- Electronics and Electricity 0607
- Elementary Particles and High Energy 0798
- Fluid and Plasma 0759
- Molecular 0609
- Nuclear 0610
- Optics 0752
- Radiation 0756
- Solid State 0611

Statistics 0463

Applied Sciences
Applied Mechanics 0346
Computer Science 0984
Engineering
- General 0537
- Aerospace 0538
- Agricultural 0539
- Automotive 0540
- Biomedical 0541
- Chemical 0542
- Civil 0543
- Electronics and Electrical 0544
- Heat and Thermodynamics 0348
- Hydraulic 0545
- Industrial 0546
- Marine 0547
- Materials Science 0794
- Mechanical 0548
- Metallurgy 0743
- Mining 0551
- Nuclear 0552
- Packaging 0549
- Petroleum 0765
- Sanitary and Municipal 0554
- System Science 0790

Geotechnology 0428
Operations Research 0796
Plastics Technology 0795
Textile Technology 0994

PSYCHOLOGY
General 0621
Behavioral 0384
Clinical 0622
Developmental 0620
Experimental 0623
Industrial 0624
Personality 0625
Physiological 0989
Psychobiology 0349
Psychometrics 0632
Social 0451

NUMERICAL SOLUTION OF THE COMPLETE TWO-PHASE MODEL FOR LAMINAR FILM CONDENSATION WITH A NONCONDENSABLE GAS

BY

YU-SHAN(SAMMY) CHIN

A Thesis submitted to the Faculty of Graduate Studies of the University of Manitoba in partial fulfillment of the requirements of the degree of

MASTER OF SCIENCE

ABSTRACT

Laminar film condensation, of a vapor-noncondensable gas mixture on a flat isothermal surface, with quiescent or moving mixtures, is analyzed. Surface temperature and free stream conditions are kept uniform, surface orientation varied from vertical to horizontal and variable properties are used. Using a finite control volume approach, the full boundary layer equations for conservation of mass, momentum, energy and species (mixture only) for both the liquid and vapor-gas mixture phases are solved in primitive variable form. The focus of this thesis is on developing the velocity and temperature fields in both phases and gas concentration profile in the vapor-gas mixture phase, as well as the film thickness, the heat transfer coefficients and the condensation rate. These results are then used to assess the effects of neglecting the inertia terms in the liquid momentum equation and the energy convection terms from the liquid energy equation. Dimensionless parameters are also developed allowing the results to be presented in a generalized format.

Results are obtained for three different vapor-gas mixtures to examine a wide range of Prandtl number, Pr_L. The vapor-gas combinations are: steam-air ($Pr_L \approx 2$), sodium-argon ($Pr_L \approx 0.006$) and glycerine-bromine ($Pr_L \approx 1000$). Along with the complete numerical solution, simplified solutions are also obtained by modifying the numerical model to neglect either the inertia terms in the liquid momentum equation or the energy convection terms in the liquid energy equation. Results are presented for any plate inclinations (between veritical and horizontal), any gravity force, any free stream velocity and for specific wall temperature, and free stream temperature and gas concentration.

The inertia terms in the liquid momentum equation were found to have negligible effect on the hydrodynamic and thermal characteristics of the flow for both the steam-air and glycerine-bromine mixtures. The inertia terms had the greatest effect on pure sodium, with the deviation decreasing with increasing argon gas concentrations, such that when the free

stream gas concentration is increased to 10^{-3}, the effect of the inertia terms became negligible.

Furthermore, the energy convection terms in the liquid energy equation were found to have negligible effect on the hydrodynamic and thermal characteristics of the flow for both the steam-air and sodium-argon mixtures. The effect of neglecting the energy convection terms for the glycerine-bromine is to underpredict the heat transfer coefficient, with the error reaching a maximum between the horizontal forced convection limit and the free convection limit.

ACKNOWLEDGEMENTS

The author would like to thank Dr. S. Ormiston and Dr. H.M. Soliman for all of their help in completing this thesis. The author is also grateful for the financial assistance in the form of teaching and research assistantships provided by the Department of Mechanical and Industrial Engineering.

TABLE OF CONTENTS

LIST OF FIGURES

LIST OF TABLES

NOMENCLATURE

c_P	specific heat, J/kg·K
D	diffusion coefficient, m^2/s
Fr_x	Froude number = $\dfrac{u_\infty^{\,2}}{g\ x\cos\alpha}$
g	gravitational acceleration, m/s^2
Ga_x	Galileo number = $\dfrac{g\,x^3}{\nu_L^{\,2}}$
g_{mx}	local mass-transfer coefficient = $-\dfrac{\rho D}{W_i - W_\infty}\dfrac{\partial W}{\partial y}$
h_{fg}	latent heat of vaporization, J/kg
h_x	local heat transfer coefficient = $q/\Delta T$, $W/m^2\cdot K$
i	nodal index
j	nodal index
Ja	Jakob number = $c_P\,\Delta T/h_{fg}$
k	thermal conductivity, W/m·K
m	number of nodes in the χ direction

$\dot{m}''$ mass flux at the interface, kg/s·m^2

$\dot{m}$ mass flow per unit depth, kg/s

$\tilde{M}$ molecular weight

n number of nodes in the η direction within the liquid film

nv number of nodes in the η direction within the mixture layer

Nu_x local Nusselt number = $h_x\, x/k_L$

P Pressure, kPa

Pe Peclet number = $\dfrac{\dot{m}\delta\,\Delta\eta_+\, c_P}{k\,\Delta\chi}$, $\dfrac{\dot{m}\delta\,\Delta\eta_+}{\mu\,\Delta\chi}$, $\dfrac{\dot{m}\delta\,\Delta\eta_+}{\rho\, D\,\Delta\chi}$

Pr Prandtl number = $\mu\, c_P/k$

q local wall heat flux, W/m^2

R $\left[\rho_L\,\mu_L/\rho\,\mu\right]^{1/2}$

$\overline{\mathrm{R}}$ universal gas constant = 8.3144 kJ/kmol·K

Re_δ film Reynolds number = $4\Gamma/\mu_L$

Re_x local Reynolds number = $\rho_L\, x\, \mathrm{u}_\infty/\mu_L$

Sc Schmidt number = $\mu/(\rho\, D)$, evaluated with mixture properties

Sh_x local Sherwood number = $\frac{g_{mx}\, x}{\rho\, D}$

T temperature, K

T^* $\frac{T - T_{wall}}{T_\infty - T_{wall}}$

ΔT overall temperature difference = $\left(T_\infty - T_{wall}\right)$, K

u velocity component in the x direction, m/s

u^* $\frac{\mathrm{u}}{\mathrm{u}_\infty}$

v velocity component in the y direction, m/s

v^* $\frac{\mathrm{v}}{\sqrt{g\, x \cos\alpha}}$

W noncondensable gas mass fraction

x co-ordinate direction along the plate, m

x^* $\frac{g\, x \cos\alpha}{\mathrm{u}_\infty{}^2}$

x_δ axial location at which transition from laminar to turbulent flow occurs in the liquid film, m

y co-ordinate direction normal to the plate, m

y^* $\quad y\sqrt{\frac{g\cos\alpha}{u_\infty \nu_L}}$

Z_x $\quad Sh_x\, Re_x^{-1/2}$

Greek Symbols

α angle of plate inclination, measured from the vertical, radians

β coefficient used in evaluating the reference temperature as defined by $\left[T_r = T_{wall} + \beta\,(T_\infty - T_{wall})\right]$.

Γ condensate flow rate per unit width of film, kg/m·s

χ co-ordinate used in the transformation $\chi = x$

δ liquid film thickness, m

δ_m $\quad \frac{\delta_e + \delta_w}{2}$, m

δ^* $\quad \delta\sqrt{\frac{g\cos\alpha}{u_\infty \nu_L}}$

ϕ general variable used to represent u_L, T_L, u, T or W

η co-ordinate transformation, $\eta = y/\delta$

$\Delta\eta$, $\Delta\eta_+$, $\Delta\eta_-$	see Figure 4.3
μ	viscosity, $N \cdot s/m^2$
ν	μ/ρ , m^2/s
ρ	density, kg/m^3
σ	condensation coefficient
τ	shear stress, N/m^2

Subscripts

b	control volume face (see Figure 4.3)
CP	complete numerical solution
E	control volume at $(i+1, j)$
e	east face of the control volume at (i, j)
g	noncondensable gas
i	at the interface
L	liquid
m	mean value over length of plate

NC	numerical solution neglecting the energy convection terms in the liquid energy equation
NI	numerical solution neglecting the inertia terms in the liquid momentum equation
NU	Nusselt's solution
N	control volume at (i, j+1)
n	north face of the control volume at (i, j)
r	used to denote reference temperature
relx	coefficient that has been modified by applying relxation through the inertia terms
sat	saturated vapor
S	control volume at (i, j-1)
s	south face of the control volume at (i, j)
v	vapor
wall	at the wall
W	control volume at (i-*1*, j)
w	west face of the control volume at (i, j)
x	local value at axial location x
∞	at the free stream

Chapter 1

INTRODUCTION

Since the pioneering work of Nusselt (1916), considerable attention has been directed towards the problem of condensation on plates and tubes. The interest in this problem has been motivated by its fundamental nature and relevance to many industrial applications where a phase change occurs. One example is in the containment buildings of nuclear reactors where core pressure is reduced by condensing the steam against the walls of the containment buildings. Another is on the condensation of a vapor on the shell side of shell and tube heat exchangers. In these cases, it is usually impossible to seal the operating fluid from unwanted outside gas, such as air, and small concentrations of gas would eventually end up within the system. Therefore, rather than having just pure vapor, the system would be operating with a vapor-gas mixture. Thus, the condensation of a vapor with a noncondensable gas on surfaces is important for industrial applications. A recent review of the theoretical studies of laminar film condensation (natural and forced convection) on plates and tubes has been reported by Rose (1988).

For laminar film condensation on vertical plates, some of the frequently used assumptions in previous studies were to ignore the inertia forces, energy convection, and interfacial shear in the condensate layer (e.g., Jacobs 1966; Fujii and Uehara 1972; Sparrow and Lin 1964; Minkowycz and Sparrow 1966; Denny *et al.* 1971). These assumptions may be valid only for thin films, as shown by Koh *et al.* (1961) for quiescent pure vapors

condensing on a vertical plate and by Koh (1962) for flowing pure vapors condensing on a horizontal plate. Gaddis (1979) examined the validity of these assumptions for the condensation of flowing pure vapors on a horizontal tube. He concluded that these simplifying assumptions can cause significant errors in estimating the heat transfer rate for liquid metals and viscous liquids, while the influence is insignificant for water over a wide range of pressures.

For the case of forced-convection condensation in the presence of a noncondensable gas, there have been no studies, to the author's best knowledge, where variable properties were used and the inertia forces, energy convection and interfacial shear have all been included in the governing equations of the liquid film. Even though the elimination of these terms may be justified in many situations, it is necessary to develop a method for solving the complete two-phase boundary layer equations in the liquid and mixture (vapor and gas) regions.

The aim of this work is to develop a numerical code to solve the complete two-phase boundary-layer equations including inertia forces, energy convection, interfacial shear and variable properties. The same numerical code can then be used to obtain solutions without either the inertia forces or energy convection. This allows a direct comparison between the complete and simplified solutions and shows the single effect of neglecting either inertia forces or energy convection. The effect of interfacial shear is not studied in this work since it has already been shown by Koh *et al.* (1961) to be important.

Results will then be obtained for three different vapor-gas mixtures to examine a wide range of Pr_L. The vapor-gas combinations are: steam-air ($Pr_L \approx 2$), sodium-argon ($Pr_L \approx 0.006$) and glycerine-bromine ($Pr_L \approx 1000$). For each mixture, results will be obtained neglecting either the inertia forces or energy convection and compared to the complete solution. This will determine the conditions under which the inertia and convection terms in the model are important and to quantify the predicted deviation in heat transfer that would result from their exclusion. Knowing that, it would be possible to determine the conditions for which the results from the complete model are necessary for good accuracy and the conditions under which simplified versions of the model can be used to provide satisfactory results.

Chapter 2

LITERATURE REVIEW

The pioneering work by Nusselt (1916) on the condensation of a saturated quiescent pure vapor, upon a vertical isothermal flat plate, was based on the assumptions that the inertia forces, energy convection, interfacial shear and subcooling in the condensate layer were negligible. As well, constant properties were assumed in the vapor and liquid regions. Subsequent studies by other authors dealing with quiescent or flowing vapors have applied one or more of Nusselt's assumptions, and the review of their work in this chapter will point out their limitations. There are four subsections in this chapter that discuss previous work for the cases of pure quiescent condensation, pure forced convection condensation, and the addition of a noncondensable gas to either quiescent or forced convection condensation.

2.1 Pure Vapors

2.1.1 Quiescent

An analytical solution for the condensation of a saturated pure vapor on a vertical isothermal plate was first obtained by Nusselt (1916). His mathematical model assumed constant properties, a very thin film, linear temperature profile across the film, zero shear forces at the interface and negligible effects of liquid inertia, energy convection and liquid

subcooling. The results of this analysis include simple algebraic equations for the condensate thickness, the velocity profile and most importantly, the local heat flux along the plate as given by:

$$q_{NU} = \left[\frac{g\, \rho_L^{\,2}\, h_{fg}\, k_L^{\,3} \left(T_\infty - T_{wall}\right)^3}{4\, \mu_L\, x} \right]^{\frac{1}{4}} \tag{2.1}$$

Rohsenow (1956) extended the work of Nusselt (1916) by including the effect of a non-linear temperature profile. This was accomplished by solving the partial differential and integral equations obtained from separate energy and momentum balances performed on a control volume in the liquid film. The algebraic form of the results predicted a higher heat flux and a thicker film than the earlier results by Nusselt. They also showed that the significance of the non-linear temperature profile depended on Ja_L. Rohsenow concluded that the effect of the non-linear temperature profile is only important at high values of liquid subcooling or high values of Ja_L. Thus, for $Ja_L < 0.2$, the linear temperature assumption is valid.

Sparrow and Gregg (1959) solved the complete set of boundary-layer equations for the liquid film, which included conservation of mass, momentum and energy, with the standard (Nusselt) boundary conditions at the wall and free stream, along with an overall energy balance to solve for film thickness. Essentially, their work improved on Nusselt's work by including the effects of energy convection and liquid inertia, but still maintaining the assumption of zero shear stress at the interface and constant properties. Their method

of solution was to apply a similarity transformation to the set of partial differential equations and iterate to solve the resulting set of ordinary differential equations. They studied the effect of neglecting the liquid inertia terms over a range of liquid Prandtl numbers between 1 and 100 with Ja_L numbers between 0.003 and 0.3. They also included an appendix that extended their study to liquid metals with Pr_L between 0.003 and 0.03, and Ja_L between 0.0001 and 0.1. The effect of including the inertia terms is to lower the Nusselt number with the effects becoming more pronounced at higher Ja_L and lower Pr_L. For $Pr_L = 100$, the effects are negligible, and at $Pr_L = 1.0$, the highest deviation, for the range of Ja_L studied, occurred at $Ja_L = 2.0$ and is about 5%. Similar trends were shown for low Pr_L. However, the deviation is much more significant at higher Ja_L numbers. For example, with $Pr_L = 0.003$ and $Ja_L = 0.1$, their predicted values of q were almost 45% lower than that predicted by Nusselt's theory. They also showed the effect of Ja_L on the temperature profile, and supported the earlier claim by Rohsenow (1956) that the temperature profile is essentially linear for $Ja_L < 0.2$.

The complete model for the condensation of a quiescent pure vapor on a vertical flat plate with constant properties was solved by Koh *et al.* (1961). Using the solution method of Sparrow and Gregg (1959), they added the interfacial shear by solving the equations of motion in the vapor and examined its effect for a range of liquid Prandtl numbers, $0.003 < Pr_L < 810$. The use of constant properties allowed them to nondimensionalize the boundary-layer equations so that all results were expressed with the dimensionless

parameters Pr_L, Ja_L and $[\rho_L\mu_L/\rho_v\mu_v]^{1/2}$. They also made a minor assumption that $\rho_L >> \rho_v$. Earlier work had always assumed a zero shear at the interface for simplicity. However, the quiescent vapor causes a negative shear in the liquid film at the interface, which acts to retard the downward flow of the condensed liquid, thereby increasing the film thickness and lowering the heat transfer. This effect was shown to be less than 1% for fluids with $Pr_L \geq 10$, because of the viscous nature of these fluids. The effect becomes much more pronounced with lower Pr_L and higher Ja_L numbers and was shown to be over 25% at $Pr_L = 0.003$ and $Ja_L > 0.028$.

Chen (1961) solved the same problem as Koh *et al.* (1961), except that he used a perturbation method to solve a set of modified integral boundary-layer equations. Rather than equating the vapor and liquid shear stresses at the interface, he used an order-of-magnitude estimation to approximate the shear stress at the interface. As well, he assumed that $[\rho_v \mu_v/\rho_L \mu_L]= 0$. His results showed the same trends as reported by Koh *et al.*.

Poots and Miles (1967) used the same equation set as Koh *et al.* (1961) but added the effect of variable liquid properties and included the effect of $\partial C_{P_L}/\partial T_L$ in the energy balance used to calculate the film thickness. Similarity transformations were used to reduce the differential equations to a set of ordinary differential equations, which were then solved numerically using a modified form of the Runge-Kutta method. Results were

obtained for saturated steam at 100 °C and wall temperatures ranging from 0 to 90 °C. Their variable property analysis was first compared to the constant property analysis of Nusselt(1916), with the constant properties evaluated at T_∞. This showed that the error was increasing with increasing $(T_\infty - T_{wall})$, reaching about 25% for the local heat transfer coefficient and about 8% for the Nusselt number at $(T_\infty - T_{wall}) = 100\,^\circ\mathrm{C}$. They then proposed a reference temperature $T_r = T_{wall} + \beta(T_\infty - T_{wall})$ at which to evaluate the constant properties for the Nusselt solution, with the value of β dependent on $(T_\infty - T_{wall})$. Using this reference temperature, the error in Nusselt's constant-properties solution was reduced to less than 0.5% for $(T_\infty - T_{wall}) \leq 30\,^\circ\mathrm{C}$.

2.1.2 Forced Convection

Using a similar approach to Nusselt (1916), Rohsenow *et al.* (1956) studied laminar and turbulent forced convection condensation of a pure saturated vapor on a vertical plate. They used constant properties, linear temperature profile across the liquid film, and neglected the effect of inertia in the liquid and vapor layers. A criterion was also developed to determine the transition from laminar to turbulent flow based on the film Reynolds number:

$$(\mathrm{Re}_\delta)_{\text{transition}} = 1800 - 246\left(\frac{1-\rho}{\rho_L}\right)^{1/3}\tau_i^* + 0.667\left(\frac{1-\rho}{\rho_L}\right)(\tau_i^*)^3 \qquad (2.2)$$

where: $\tau_i^* = \dfrac{\tau_i}{g(\rho_L - \rho)\left(\dfrac{\nu_L^2}{g}\right)^{1/3}}$

τ_i = shear stress at the interface

Equation (2.2) indicates that $(\mathrm{Re}_\delta)_{\text{transition}}$ varies along the plate because of it's dependence on the shear stress at the interface. Plots of heat transfer results, $\dfrac{h_m}{k_L}\left(\dfrac{\mu_L^2}{\rho_L^2 g}\right)^{1/3}$ *vs.* Re_δ, were given showing the transition from laminar to turbulent flows. Transition occurs when the local Re_δ exceeds $(\mathrm{Re}_\delta)_{\text{transition}}$.

Cess (1960) obtained a constant-property solution to the forced convection condensation of a pure saturated vapor on a horizontal flat plate. Similarity was used to transform the boundary-layer equations to a set of ordinary differential equations. It was further simplified by using the solution for the suction at a wall as the solution for the ordinary differential equation for vapor momentum. Rather than numerically solving the three differential equations, for the liquid layer, Cess used an infinite series solution for each of the differential equations, and truncated the higher order terms. The loss of the higher order terms is the same as neglecting the inertia terms in the liquid momentum equation and the energy convection terms in the liquid energy equation. Heat transfer results were shown to be represented by a single curve when plotted on a graph of $\mathrm{Nu}_x \mathrm{Re}_x^{-1/2}$ *vs.* $R\mathrm{Ja}_L/\mathrm{Pr}_L$. Asymptotic relations were also given for the limiting

cases as $R\,\mathrm{Ja}_L/\mathrm{Pr}_L$ goes to zero (no suction or no condensation) and infinity (infinite suction or infinite condensation).

Koh (1962) extended the study by Cess (1960) to include inertia and energy convection and numerically solved the set of ordinary differential equations. Koh showed that the heat transfer parameter $\mathrm{Nu}_x\,\mathrm{Re}_x^{-1/2}$ was dependent on more than just $R\,\mathrm{Ja}_L/\mathrm{Pr}_L$, because his plots of $\mathrm{Nu}_x\,\mathrm{Re}_x^{-1/2}$ *vs.* $R\,\mathrm{Ja}_L/\mathrm{Pr}_L$ showed that varying Pr_L and R separately led to different curves. Thus, on Koh's plots of $\mathrm{Nu}_x\,\mathrm{Re}_x^{-1/2}$ *vs.* $R\,\mathrm{Ja}_L/\mathrm{Pr}_L$, Cess's results were represented by a single curve, and the deviation from Koh's results at different Pr_L and R showed the effects of neglecting liquid inertia and convection. For low Pr_L ($\mathrm{Pr}_L < 0.03$), the combined effects were found to be more significant at lower R and higher values of $R\,\mathrm{Ja}_L/\mathrm{Pr}_L$. For $\mathrm{Pr}_L \geq 1$, the effects became more significant at higher Pr_L, lower R and higher values of $R\,\mathrm{Ja}_L/\mathrm{Pr}_L$.

Jacobs (1966) solved the set of boundary-layer equations for forced convection condensation of a pure freon–113 vapor on a vertical plate. Constant properties were used with the following assumptions: $\rho_L >> \rho_v$, inertia terms in the liquid have a negligible effect, and a linear temperature profile (which would neglect the energy convection terms). Results were obtained for a pressure of 1 atm with $T_\infty - T_{wall} = 10$, 40 and 70 °F. For each of the three cases, the dependence of $\mathrm{Nu}_x\,\mathrm{Fr}_x^{1/2}\,\mathrm{Re}_x^{-1/2}$ on $1/\mathrm{Fr}_x$ was obtained for $1/\mathrm{Fr}_x$ ranging from 10^{-4} to 10^3. This range showed the solution for

combined forced convection and body force condensation between the two limits, forced convection only ($1/\mathrm{Fr}_x \to 0$) and body force only ($1/\mathrm{Fr}_x \to \infty$). The numerical results were compared with experimental data and were found to show agreement within ± 20%.

Shekriladze and Gomelauri (1966) obtained an analytical expression for the heat transfer coefficient during forced convection condensation on vertical and horizontal plates. They employed a similar model to Jacobs (1966) for the liquid and simplified the effect of the vapor by comparing the condensation process to that of a vapor undergoing suction at the plate's surface. With sufficiently high suction rates, the shear stress on the plate's surface is essentially equal to the momentum transferred to the condensing mass. Thus, the interfacial shear stress in the liquid film was approximated by $\tau_i = \dot{m}''(u_\infty - u_i)$, where u_i accounts for the motion of the liquid film. Algebraic expressions were obtained for the heat transfer coefficient as a function of $\mathrm{Ja}_L/\mathrm{Pr}_L$, free stream velocity, ΔT and axial location (or plate length for average heat transfer coefficients). Correction factors were also obtained to account for the effect on the heat transfer coefficient of either liquid inertia or energy convection. These correlations showed that inertia effect is negligible for non-metallic liquids with $\mathrm{Ja}_L/\mathrm{Pr}_L < 0.1$. They also showed that liquid energy convection is negligible for ordinary liquids with $\mathrm{Ja}_L/\mathrm{Pr}_L << 0.1$.

Denny and Mills (1969) included the inertia and convection terms in the liquid momentum and energy equations. The effect of the vapor was approximated using the asymptotic solution of the vapor momentum equation, as given by Shekriladze and Gomelauri (1966).

Algebraic expressions solved by a least-mean-squares procedure were used to obtain correlations between the properties and the temperature. The equations were solved numerically using the method developed by Patankar and Spalding (1967). They validated their work by comparing with the free convection results by Koh *et al.* (1961) and their numerical results were shown to be in good agreement over the range of Pr_L and Ja_L studied by Koh *et al.* Plots of the local heat transfer coefficient were given for ethylene glycol (at $T_\infty = 140\ ^\circ\mathrm{F}$), n-propyl alcohol (at $T_\infty = 140\ ^\circ\mathrm{F}$), and water (at $T_\infty = 150\ ^\circ\mathrm{F}$) with $\Delta T = 40\ ^\circ\mathrm{F}$ and $u_\infty = 20$ and 50 ft/s. Results were also presented for a non-isothermal wall with a co-current and counter-current coolant flows.

Denny *et al.* (1970) extended the earlier work of Denny and Mills (1969) by numerically solving the case of constant property, quiescent and forced convection condensation of liquid metals on a vertical surface. By neglecting the inertia and convection terms in the liquid conservation equations, they were also able to obtain a closed form solution. Their numerical results were then compared to their closed form solution to determine the effect of inertia alone, since for liquid metals ($\mathrm{Pr}_L << 1$) the convection terms are negligible and the temperature profile is essentially linear. Results were obtained for sodium, potassium, cesium, lithium, rubidium, and mercury for $0 \le u_\infty \le 100$ ft/s, $1100 \le T_\infty \le 2400$ R, and $3 \le \Delta T \le 20$ R. For these substances, the error in neglecting the inertia terms was less than 3% for the range of variables studied.

Fujii and Uehara (1972) performed a constant property analysis using the same boundary layer equations and boundary conditions as Jacobs (1966) with one different boundary condition. They replaced the condition of zero liquid thickness at the leading edge with a mass balance over a discrete step along the plate, Δx. Along with the numerical results for forced convection condensation on a vertical plate, they also obtained approximate analytical expressions for the Nusselt number at the two limiting cases of body force only (quiescent, $1/\mathrm{Fr}_x \to \infty$) and forced convection only (horizontal plate, $1/\mathrm{Fr}_x \to 0$). Results were obtained for four combinations of properties and were shown to have the correct limits. For the complete case, they proposed an approximate expression which correlated the local Nusselt number with Re_x, Fr_x, Ja_L, Pr_L and R. The maximum discrepancy between the numerical results and the expression was about 2.5%. Fujii and Uehara's results for the limiting case of a horizontal plate agreed well with those of Cess (1960) who also neglected the liquid inertia and convection terms. However, these results disagreed with the results of Koh (1962) for a horizontal plate, since Koh included the liquid inertia and convection terms.

Rose (1989) examined the effect of liquid inertia and convection for condensation on horizontal plates by plotting the results of Shekriladze and Gomelauri (1966) and Fujii and Uehara (1972) against those of Koh (1962). Plots of $\mathrm{Nu}_x \mathrm{Re}_x^{-1/2}$ *vs.* $\mathrm{Ja}_L/\mathrm{Pr}_L$ showed that the solution by Fujii and Uehara have the incorrect limit for high $\mathrm{Ja}_L/\mathrm{Pr}_L$. Likewise, plots of $\mathrm{Nu}_x \mathrm{Re}_x^{-1/2}$ *vs.* $R\,\mathrm{Ja}_L/\mathrm{Pr}_L$ showed that Shekriladze and Gomelauri's solution have the incorrect limit as $R\,\mathrm{Ja}_L/\mathrm{Pr}_L$ approaches zero. Rose proposed a new algebraic

expression that more closely approximates the solution by Koh, within the range of $0.01 < \mathrm{Ja}_L/\mathrm{Pr}_L < 10$ and $0.1 < R\,\mathrm{Ja}_L/\mathrm{Pr}_L < 100$.

2.2 Mixtures of a Vapor and a Noncondensable Gas

2.2.1 Quiescent

Condensation of a quiescent mixture of a vapor and a noncondensable gas on a vertical wall was studied by Sparrow and Lin (1964). The authors assumed constant properties, and dropped the inertia and convection terms from the liquid momentum and energy conservation equations. As well, they applied a zero shear stress condition at the interface. They also rationalized that since Sparrow and Eckert (1961) showed that the effect of superheat is low even with a highly superheated vapor (on the order of hundreds of degrees), and that the mixture would be at or near free stream conditions, the mixture energy equation could also be neglected. Similarity transformations were used and the resulting ordinary differential equations were solved numerically. The mechanism by which the noncondensable gas lowers the heat transfer is that convection in the mixture carries gas to the interface. Since the interface is impermeable, the gas concentration increases enough to create a gradient allowing for the diffusion of the gas away from the interface. The high gas concentration at the interface lowers the partial pressure of the vapor. The corresponding interfacial vapor temperature decreases, leading to a reduction in the thermal driving force (T_i - T_{wall}). Plots of the interfacial gas concentration, W_i,

showed that W_i increases (heat transfer decreases) with $\frac{C_{P_L}(T_i - T_{wall})}{h_{fg}\,\mathrm{Pr}_L}$ and the effect is even greater at higher free stream gas concentrations, W_∞. They also noted two other trends for W_i. The first trend is that greater buildup of gas occurs at higher Sc, which corresponds to lower diffusion coefficients limiting the diffusion of gas away from the interface. The second trend is that W_i also increases with R . An iterative process is required that uses plots of W_i along with the pressure-gas concentration equation and a set of saturation pressure-temperature data in order to obtain the heat transfer, q.

Minkowycz and Sparrow (1966) extended the work of Sparrow and Lin (1964) by including the mixture energy equation and the effects of thermal diffusion and diffusion thermo. Properties for steam as the vapor and air as the noncondensing gas were fitted to algebraic expressions and mixture rules derived by Mason and Monchik (1963) were used to calculate the mixture properties (except for ρ and C_P which were calculated by standard additive procedures). Similarity transformations were used and the resulting equations were solved numerically. In order to normalize their heat transfer results, they defined a reference temperature, $T_r = T_{wall} + 0.31(T_i - T_{wall})$, for evaluating the properties used to calculate q_{NU} using Equation (2.1). This allowed them to normalize q, evaluated with variable properties, by dividing by q_{NU} . Their model was used to determine the effect of noncondensable gas, interfacial resistance, superheating, and diffusion. The effect of superheat on the condensation of pure steam was found to be minimal, since even a superheat of 400 °F was shown to increase heat transfer by less than 5%. Superheating

became more significant with the addition of a noncondensing gas, especially at higher T_∞, and lower ΔT . The interface itself acts as a resistance to the conduction of energy from the mixture to the liquid and causes a temperature jump between the liquid and mixture side of the interface. The effect of interfacial resistance depended on the selected value for σ, the condensation coefficient. Paul (1962) and Nabavian (1962) suggested values of σ ranging from 0.004 to 1.0, and Mills (1965) performed experiments on the condensation of pure steam and showed that σ was essentially equal to one. The numerical results of Minkowycz and Sparrow for quiescent pure steam showed that the heat transfer results with $\sigma = 1$ compare very well with Nusselt's theory. As σ was lowered, so too was the heat transfer rate. When adding a noncondensing gas with or without superheat, the results with interfacial resistance were shown to closely match the solutions without interfacial resistance, even with the low value of $\sigma = 0.04$. Thermal diffusion and diffusion thermo were found to have negligible effects in this situation. The most important effect was that of the noncondensable gas, as just 0.5% gas concentration in the bulk resulted in more than 50% reduction in the heat transfer rate. Increasing W_∞, decreased the heat transfer results monotonically. For the same W_∞, increasing the temperature difference resulted in an increase in the heat transfer rate. As well, the effect of the noncondensable gas became more pronounced at lower T_∞.

Rose (1969) solved the problem by considering only the vapor-gas region. He applied arbitrary velocity and gas concentration profiles to solve the integral continuity, momentum and diffusion conservation equations. Comparison with the steam-air mixture

results by Sparrow and Lin (1964) showed that although these profiles followed the same trends, Rose's results over predicted W_i. No indication was given on how the value of W_i was used to evaluate the heat flux, but q/q_{NU} was compared with the steam-air mixture results of Minkowycz and Sparrow (1966). Rose's solution underestimated the heat transfer at low W_∞, but improved with higher W_∞ and showed good agreement for $W_\infty > 0.02$.

Fujii *et al.* (1992) performed a constant property analysis on a steam-air mixture using the complete boundary layer equations and boundary conditions, but neglecting interfacial resistance, thermal diffusion and diffusion thermo (all of which were shown to be negligible by Minkowycz and Sparrow (1966)). Similarity transformations were applied, and the resulting equations were solved numerically. They then performed an approximate analytical analysis based on their numerical data to obtain algebraic expressions for the mass flux and the heat flux. The heat flux was a function of properties, the temperature drop across the liquid, temperate gradient, axial location and the Galileo number, Ga_x. The mass flux was a function of properties, the interfacial gas concentration, gradient of the gas concentration, axial location and the Galileo number. Algebraic expression for the mass flux of the condensing vapor was within 10% of the experimental data. Calculated heat fluxes did not compare as favorably and were generally within 30% of the experimental results.

2.2.2 Forced Convection

Sparrow *et al.* (1967) followed-up on the earlier work of Sparrow and Lin (1964) by extending it to cover forced convection condensation of a vapor-noncondensable gas mixture on a horizontal flat plate. Like Sparrow and Lin, they also neglected the mixture energy equation, and assumed negligible effects of inertia and energy convection in the liquid. The boundary conditions were similar, except that they imposed continuity of shear stress at the interface and assumed that $u_{L,i} = u_i = 0$, since $u_\infty >> u_i$. As well, a variable property analysis was performed on a steam-air mixture. Similarity transformations were used and the resulting equations were solved both numerically and by an approximate integral method as described in their appendix. The heat transfer results were normalized by dividing the heat flux of steam in the presence of air with the heat flux for pure steam, thereby eliminating the dependence on x and u_∞. Results for steam-air were plotted for W_∞ ranging from 0.005 to 0.1, ΔT ranging from 2 to 40 °F and T_∞ ranging from 80 to 212 °F. The quiescent results by Minkowycz and Sparrow (1966) were also plotted on some of the graphs to highlight the marked improvement in heat transfer due to forced convection. They also examined the effect of interfacial resistance for steam undergoing forced convection condensation on a horizontal plate and concluded that since the interfacial resistance is negligible for pure steam, it would also be negligible for a steam-air mixture.

Minkowycz and Sparrow (1969) added the effect of superheating to the work of Sparrow *et al.* (1967) by solving the mixture energy equation. Their results showed that the effect of superheat was to increase the heat transfer. This increase was less than 10%, but it became more significant at lower values of ΔT and higher W_∞.

A variable property analysis on steam-air mixtures was performed by Denny *et al.* (1971). The liquid film was modeled using the Nusselt assumptions, whereby inertia and energy convection were neglected. Although variable properties were used for steam and air, liquid properties were only allowed to vary axially, and was evaluated at their reference temperature defined by; $T_r = T_{wall} + 0.33(T_i + T_{wall})$. No assumptions were made to simplify the mixture conservation equations. Solutions were obtained by the finite difference method of Patankar and Spalding (1967), using a forward marching technique. Local values of q/q_{NU} were presented for a plate length of 0.5 ft with T_∞ ranging from 100 to 212 °F, ΔT ranging from 5 to 40 °F, bulk air concentrations ranging from 0.001 to 0.1, and free stream vapor velocities ranging from 0.1 to 10 ft/s. They observed that "..effects of interfacial velocity and induced natural convection may be ignored as u_∞ becomes large, the magnitude of the vapor drag being essentially equal to the asymptotic value $\dot{m}'' u_\infty$ which is characteristic of boundary-layer flows undergoing strong suction". Two other papers followed which used the same numerical model but studied other fluids. The first was by Denny and Jusionis (1972) which reported results for six vapors (water, ammonia, freon-12, ethanol, butanol, and carbon tetrachloride) with air as the noncondensable gas. Condensation of liquid metals with a noncondensable gas was then

presented by Turner *et al.* (1973) for the mercury-air and sodium-argon systems. The mercury-air system presented a special problem in that a negative buoyancy force was set up because the molecular mass of air is lower than that of mercury. Thus, as the air builds up at the interface, the density of the mixture decreases and the resulting buoyancy force is directed opposite to the mixture flow, causing the mixture boundary layer to separate at some distance down the plate.

Rose (1980) obtained an approximate expression for forced convection condensation of a vapor-gas mixture on a horizontal flat plate. In an earlier work, he obtained an approximate expression to the solution of the liquid momentum and energy equation for forced convection condensation of a pure vapor on a horizontal plate. This resulted in the following expression for $\mathrm{Nu}_x \mathrm{Re}_x^{-1/2}$ as a function of Pr_L:

$$\mathrm{Nu}_x \mathrm{Re}_x^{-1/2} = \frac{\mathrm{Pr}_L^{1/2}}{\left[27.8 + 75.9\,\mathrm{Pr}_L^{0.306} + 657\,\mathrm{Pr}\right]^{1/6}} \tag{2.3}$$

In his present work, he neglected the temperature profile in the mixture, assumed that the interface velocity to be zero (assumed the problem to be just like a mixture undergoing suction as it flowed across a plate) and took W_i to be constant. Thus he only needed to solve the mixture momentum and diffusion equations. With the similarity of the present equation set to that for his earlier pure vapor case, the solution of the mixture momentum and diffusion equation would have the same form as Equation (2.3), but with Sh_x replacing Nu_x and Pr_L being replaced by Sc. He then used the impermeability condition

at the interface to relate the Sh_x number to the interfacial gas concentration. His final result gives an implicit relation for Sh_x:

$$Z_x + 0.941 Sc^{-0.21} (1-\omega)^{1.14} Z_x^{2.14} - \zeta/\omega = 0 \tag{2.4}$$

where: $$Z_x = Sh_x Re_x^{-1/2} \tag{2.5}$$

$$\omega = W_\infty / W_i \tag{2.6}$$

$$\zeta = \frac{Sc^{1/2}}{\left[27.8 + 75.9\, Sc^{0.306} + 657\, Sc\right]^{1/6}} \tag{2.7}$$

which can be solved iteratively. The main drawback to the use of Equation (2.4) is that to obtain Sh_x, W_i must be known. Comparisons with the results of Sparrow *et al.* (1967) shows very good agreement for a steam-air mixture.

Legay-Desequelles and Prunet-Foch (1985, 1986) performed an experimental study on steam-air mixtures undergoing forced convection condensation over a horizontal isothermal plate under laminar and turbulent conditions. Comparisons were made to their numerical model, which used partial condensation of the steam within the mixture to maintain a saturated steam-air mixture everywhere. The liquid film was assumed to be thin and not have any effect on the mixture layer (they assumed that the liquid-mixture interface coincided with the wall). Buoyancy effects were ignored. The mixture conservation equations (continuity, momentum, energy and diffusion) were solved numerically. This condensation process was compared to results obtained by imposing a uniform suction velocity (without a temperature difference) at the wall and the equivalent suction rate was predicted from the results of the mass flux at the wall. Plots of the

temperature profiles show a good agreement, within 10%, between their experimental and numerical data. Nusselt number and mass flow results for laminar condensation were given for $Pr_L = 0.7$ and $Sc = 0.6$ and compared to the work by Hijikata and Mori (1973). Nusselt number was shown to be in good agreement for $10^4 < Re_x < 3.5x10^4$. Plots of their mass flow rate showed that for $T_\infty = 30$, 40 and 50 °C, there was good agreement with Hijikata and Mori's results for $\Delta T < 20$ °C.

2.3 Closing Remarks

This literature review of laminar condensation of saturated vapor-gas mixtures or pure vapors on isothermal flat plate, under quiescent or forced convection conditions show that the following general observations can be made:

1. Nusselt (1916) neglected the interfacial shear as one of his simplifying assumptions. For pure vapors, Koh *et al.* (1961) showed that this is only valid for high Pr_L fluids and the error increases with lower Pr_L. Furthermore, the effect of interfacial shear also increases with higher Ja_L.

2. Energy convection and subcooling have been shown to be negligible for low Pr_L fluids such as liquid metals and even steam ($0.1 \leq Pr_L \leq 10$). However, energy convection and subcooling play very important roles in the condensation of viscous fluids (high Pr_L), especially at higher Ja_L.

3. The liquid inertia forces play an important role only in the condensation of low Pr_L fluids, with the effects becoming greater at higher Ja_L.

4. None of the earlier authors have solved the complete model which included the boundary layer equations for both the mixture and liquid (including the inertia, energy convection and subcooling), interfacial shear and variable properties. The one exception is the study by Poots and Miles (1970) who limited their work to quiescent pure steam and only showed the combined effects of interfacial shear and variable properties.

The purpose of this thesis is to solve the complete boundary layer equations, which includes inertia forces, energy convection, subcooling in the condensate layer, interfacial shear, and variable properties. Solution of the complete model can be used as the basis for evaluating the effects of neglecting the inertia terms from the liquid momentum equation and the energy convection terms from the liquid energy equation. Using the complete model, solutions will be obtained for quiescent and forced convection condensation at various plate inclinations from horizontal to vertical. Three fluids are to be studied to cover a wide range of Pr_L: sodium ($\mathrm{Pr}_L \approx 0.006$, with and without argon), steam ($\mathrm{Pr}_L \approx 2.0$, with and without air), and glycerine ($\mathrm{Pr}_L \approx 1000$, with and without bromine). Gas concentrations are to be varied for each mixture, with pure vapor being one of the cases, along with varying ΔT. Results for sodium without the liquid inertia terms will be compared with the complete solutions to determine the effect of liquid inertia (checks were also made for steam and glycerine to ensure that inertia had negligible effect). Results will then be obtained for glycerine without the liquid convection terms. Comparison with the complete solutions will show the combined effect of neglecting

energy convection and subcooling (checks were also done to ensure that these effects were negligible for steam and sodium).

Chapter 3

STATEMENT OF THE PROBLEM

3.1 Physical Model

The focus of this study is on laminar film condensation on the isothermal flat plate as shown in Figure 3.1. Orientation of the plate in the figure is vertical, but can be oriented at any angle from the vertical, to the horizontal. The inclination of the plate is given by α, the angle between the plate and the x axis. The layer next to the wall is the liquid condensate film that is separated from the mixture layer by the liquid-mixture interface. Beyond the mixture layer is the external flow, where velocity, temperature and gas mass fraction remain uniform at the free stream values and saturated conditions are assumed. The origin of the axis is located at the leading edge of the plate, with x directed along the plate, and y directed normal to the plate. The plate is assumed to be of infinite width, so that the edges have no effect and velocity, temperature and concentration gradients only occur in the x and y directions.

For a pure quiescent vapor, the temperature in the vapor layer is uniform at T_∞. Convection in both x and y directions carries the vapor to the interface where condensation releases the latent heat to the liquid. The temperature gradient within the liquid layer results in conduction of heat from the interface to the plate. Liquid subcooling also occurs which adds to the heat transferred to the wall. The main limiting factor in the

heat transfer for a pure vapor is the thickness of the condensate since the potential remains the same, ΔT constant along the plate. Thus, as the condensate builds up along the plate, the heat transfer decreases. Forced convection condensation will increase heat transfer over the quiescent case because the free stream velocity will speed up the condensate layer, thereby thinning the condensate layer and increasing the in heat transfer.

As discussed in the literature review, the addition of a denser noncondensing gas to the vapor leads to a decrease in the heat transfer. Convection will carry the vapor-gas mixture to the interface where the vapor condenses. Since the interface is impermeable to the gas, it builds on the mixture side of the interface. This build up of gas at the interface can only be moved away from the interface by diffusion. Diffusion away from the interface requires a negative gradient, so a high concentration is required at the interface so that enough of a gradient exists for diffusion to occur. Thus, the gas concentration is a maximum at the interface and decreases until its minimum value is reached at the free stream. The total pressure, P_∞ is assumed to be invariant in the y direction, and because of the change in gas concentrations, the partial pressure of the gas and vapor vary. The partial pressure of the gas, P_g, increases with W (gas concentration) and the difference between the total pressure and P_g is the partial pressure of the vapor, P_v . The decreasing value of P_v towards the interface leads to a corresponding drop in the saturation temperature of the vapor. Since the free stream temperature is assumed to be the saturation temperature of the vapor at the P_v corresponding to W_∞ , a value of W_i greater than W_∞ produces a value of T_i that is lower than T_∞ . Thus there is a lower ΔT acting as the driving potential in the

conduction heat transfer across the condensate layer. This effect of noncondensing gas is much more significant when the mixture is at rest, and becomes less so with increasing free stream velocity. The forced convection will tend to sweep the gas along, and helps to lower the gas concentration at the interface.

3.2 Mathematical Model

The following mathematical model is valid for a steady-state incompressible, laminar, Newtonian boundary-layer flow on an isothermal flat plate. Thermodynamic and transport properties are taken to be dependent on the temperature and gas concentration and are calculated at the local conditions. The model consists of seven partial differential equations: three for the liquid layer, and four for the mixture. They are:

- **Liquid Continuity Equation**

$$\frac{\partial}{\partial x}(\rho_L u_L) + \frac{\partial}{\partial y}(\rho_L v_L) = 0 \tag{3.1}$$

- **Liquid Momentum Equation**

$$\frac{\partial}{\partial x}(\rho_L u_L u_L) + \frac{\partial}{\partial y}(\rho_L v_L u_L) = \frac{\partial}{\partial y}\left(\mu_L \frac{\partial u_L}{\partial y}\right) + g(\rho_L - \rho_\infty)\cos\alpha \tag{3.2}$$

The $\cos\alpha$ accounts for the component of gravity directed along the plate.

- **Liquid Energy Equation**

$$\frac{\partial}{\partial x}\left(\rho_L u_L C_{P_L} T_L\right) + \frac{\partial}{\partial y}\left(\rho_L v_L C_{P_L} T_L\right) = \frac{\partial}{\partial y}\left(k_L \frac{\partial T_L}{\partial y}\right) \tag{3.3}$$

- **Mixture Continuity Equation**

$$\frac{\partial}{\partial x}(\rho u) + \frac{\partial}{\partial y}(\rho v) = 0 \tag{3.4}$$

- **Mixture Momentum Equation**

$$\frac{\partial}{\partial x}(\rho u u) + \frac{\partial}{\partial y}(\rho v u) = \frac{\partial}{\partial y}\left(\mu \frac{\partial u}{\partial y}\right) + g(\rho - \rho_\infty)\cos\alpha \tag{3.5}$$

- **Mixture Energy Equation**

$$\frac{\partial}{\partial x}(\rho u C_p T) + \frac{\partial}{\partial y}(\rho v C_p T) = \frac{\partial}{\partial y}\left(k \frac{\partial T}{\partial y}\right) + \frac{\partial}{\partial y}\left(\rho D\left(C_{Pg} - C_{Pv}\right)\frac{\partial W}{\partial y} T\right) \tag{3.6}$$

The second term on the right hand side of Equation (3.6) arises from the transport of energy by mass transfer due to diffusion.

- **Mixture Mass Diffusion Equation**

$$\frac{\partial}{\partial x}(\rho u W) + \frac{\partial}{\partial y}(\rho v W) = \frac{\partial}{\partial y}\left(\rho D \frac{\partial W}{\partial y}\right) \tag{3.7}$$

The twelve applicable boundary conditions are:

- At the plate surface $(y = 0)$

$$u_L = 0 \tag{3.8}$$

$$v_L = 0 \tag{3.9}$$

$$T_L = T_{wall} \tag{3.10}$$

- At the free stream $(y \rightarrow \infty)$

$$u = u_{\infty} \tag{3.11}$$

$$T = T_{\infty} \tag{3.12}$$

$$W = W_{\infty} \tag{3.13}$$

- At the liquid-mixture interface $(y = \delta)$

$$u_L = u \tag{3.14}$$

$$\mu_L \frac{\partial u_L}{\partial y} = \mu \frac{\partial u}{\partial y} \tag{3.15}$$

$$T_L = T = T_i \tag{3.16}$$

$$T_i = T_{v,sat,i}\left(W_i, W_{\infty}, T_{\infty}, \tilde{M}_v, \tilde{M}_g\right) \tag{3.17}$$

$$\dot{m}'' = \rho_L u_L \frac{d\delta}{dx} - \rho_L v_L = \rho u \frac{d\delta}{dx} - \rho v \tag{3.18}$$

$$\dot{m}'' W + \rho D \frac{\partial W}{\partial y} = 0 \tag{3.19}$$

Equation (3.17) indicates that the mixture temperature at the interface is equal to the saturated temperature of the vapor at its partial pressure. The partial pressure of the vapor is a function of the system pressure, P_{∞}, gas concentration and molecular weights and is given by:

$$\frac{P_v}{P_{\infty}} = \frac{1-W}{1+W\left(\tilde{M}_v / \tilde{M}_g - 1\right)} \tag{3.20}$$

This relation assumes that the mixture and its components behave like perfect gases. The value of P_∞ was calculated from Equation (3.20) assuming that at the free stream conditions (T_∞ and W_∞) the mixture is saturated with the partial pressure of the vapor equal to the saturation pressure corresponding to T_∞. The total pressures at the free stream and at the interface are equal.

Equation (3.18) states that the mass flux entering the interface from the mixture side is equal to the mass flux leaving the interface from the liquid side, and assumes that $\dot{m}''$ is positive in the negative y direction. The boundary condition given by Equation (3.19) is the gas impermeability condition which shows that the mass flux of gas being convected to the interface, $\dot{m}''W$, is equal to the mass diffused away from the interface.

One additional equation is required for the evaluation of the liquid film thickness, δ. Two different methods may be used: one method is to perform an energy balance at the interface, and the other method is to perform an overall energy balance within the condensate layer. The first method, when applied to a control volume at the interface as shown in Figure 3.2, yields:

$$k_L \frac{\partial T_L}{\partial y} = k\frac{\partial T}{\partial y} + h_{fg}\left(\rho u \frac{d\delta}{dx} - \rho v\right) = k\frac{\partial T}{\partial y} + \dot{m}'' h_{fg} \qquad (3.21)$$

replace $\dot{m}''$ with the change in liquid condensate flow rates to obtain:

$$k_L \frac{\partial T_L}{\partial y} = k\frac{\partial T}{\partial y} + h_{fg}\frac{d}{dx}\left(\int_0^\delta \rho_L u_L \, dy\right) \qquad (3.22)$$

Alternatively, an application of overall energy balance across the liquid condensate, as shown in Figure 3.3, results in the following equation:

$$\left(h_{fg} + C_{P_L} T_i\right) \frac{d}{dx} \left\{ \int_0^{\delta} \rho_L \, u_L \, dy \right\} dx \quad + \quad k \, dx \left(\frac{\partial T}{\partial y} \right)_i$$

$$+ \int_0^{\delta_{x-dx/2}} \rho_L \, C_{P_L} \left(u_L \, T_L \right)_{x-dx/2} dy \qquad (3.23)$$

$$= \int_0^{\delta_{x+dx/2}} \rho_L \, C_{P_L} \left(u_L \, T_L \right)_{x+dx/2} dy \quad + \quad k_L \, dx \left(\frac{\partial T_L}{\partial y} \right)_{wall}$$

Either Equation (3.22) or Equation (3.23) can be used to solve for δ, since there is a negligible difference between the results produced by the two methods. Generally, Equation (3.22) was used in this investigation because it is easier to compute. Equation (3.23) would be more convenient for two particular cases. The first case would be the examination of omitting only subcooling and the second case would consider the effect of subcooling while neglecting energy convection. More details concerning these cases will be given later in this chapter.

One of the objectives of this thesis work was to study the effect of liquid inertia. The liquid inertia effect is given by the two terms on the left hand side of Equation (3.2). A direct comparison of the results obtained by dropping the two liquid inertia terms with the results from the complete solution will show the effects of liquid inertia. Another objective was to examine the combined effects of neglecting the liquid convection and subcooling. The liquid convection terms are those on the left hand side of Equation (3.3).

Neglecting these terms and using Equation (3.22) will give the combined effect of neglecting liquid convection and subcooling. The separate effects of liquid convection and subcooling can be studied by using Equation (3.23). Solutions can be obtained without the effect of subcooling by dropping the terms in Equation (3.23) that contain the specific heat. Likewise, results without energy convection can be obtained by neglecting the convection terms in the liquid energy equation, and using Equation (3.23) to solve for δ. These last two cases were not studied because they were outside the scope of this thesis.

Equations (3.1) to (3.19) and (3.22) above were transformed from the *x-y* coordinate plane to the χ-η plane using the following transformation parameters:

$$\eta = \frac{y}{\delta}, \qquad \text{and} \qquad \chi = x \tag{3.24}$$

The partial derivatives $\frac{\partial \phi}{\partial x}$ and $\frac{\partial \phi}{\partial y}$ of an arbitrary variable ϕ will now have to be rewritten in terms of χ and η by using the chain rule:

$$\frac{\partial \phi}{\partial x} = \frac{\partial \phi}{\partial \chi}\frac{\partial \chi}{\partial x} + \frac{\partial \phi}{\partial \eta}\frac{\partial \eta}{\partial x} \tag{3.25}$$

and

$$\frac{\partial \phi}{\partial y} = \frac{\partial \phi}{\partial \eta}\frac{\partial \eta}{\partial y} + \frac{\partial \phi}{\partial \chi}\frac{\partial \chi}{\partial y} \tag{3.26}$$

In Equation (3.25) $\frac{\partial \chi}{\partial x} = 1$, and $\frac{\partial \eta}{\partial x}$ can be rewritten as:

$$\frac{\partial \eta}{\partial x} = y\frac{\partial}{\partial x}\left(\frac{1}{\delta}\right) = \delta\,\eta\frac{\partial}{\partial x}\left(\frac{1}{\delta}\right) \tag{3.27}$$

which can be easily formulated as:

$$\frac{\partial \eta}{\partial x} = \delta \eta \frac{d}{d\chi}\left(\frac{1}{\delta}\right) = -\frac{\eta}{\delta}\frac{d\delta}{d\chi} \tag{3.28}$$

Finally, since χ is not a function of y, $\frac{\partial \chi}{\partial y} = 0$, and

$$\frac{\partial \eta}{\partial y} = \frac{1}{\delta} \tag{3.29}$$

the partial derivatives for a general variable, as described in Equations (3.25) and (3.26), can be defined by:

$$\left.\begin{aligned} \frac{\partial \phi}{\partial x} &= \frac{\partial \phi}{\partial \chi} - \frac{\eta}{\delta}\frac{d\delta}{d\chi}\frac{\partial \phi}{\partial \eta} \\ \frac{\partial \phi}{\partial y} &= \frac{1}{\delta}\frac{\partial \phi}{\partial \eta} \\ \frac{\partial^2 \phi}{\partial y^2} &= \frac{1}{\delta^2}\frac{\partial^2 \phi}{\partial \eta^2} \end{aligned}\right\} \tag{3.30}$$

Applying the above equations for the partial derivatives, with the following two relations:

$$\left.\begin{aligned} \frac{\partial}{\partial \chi}(\delta \rho u \phi) &= \delta \frac{\partial}{\partial \chi}(\rho u \phi) + \rho u \phi \frac{d\delta}{d\chi} \\ \frac{d\delta}{d\chi}\frac{\partial}{\partial \eta}(\eta \rho u \phi) &= \eta \frac{d\delta}{d\chi}\frac{\partial}{\partial \eta}(\rho u \phi) + \rho u \phi \frac{d\delta}{d\chi} \end{aligned}\right\} \tag{3.31}$$

results in the following transformed boundary layer equations:

- **Liquid Continuity Equation**

$$\frac{\partial}{\partial \chi}(\delta \rho_L u_L) - \frac{d\delta}{d\chi}\frac{\partial}{\partial \eta}(\eta \rho_L u_L) + \frac{\partial}{\partial \eta}(\rho_L v_L) = 0 \tag{3.32}$$

- **Liquid Momentum Equation**

$$\frac{\partial}{\partial \chi}\left(\delta \rho_L u_L u_L\right) - \frac{d\delta}{d\chi}\frac{\partial}{\partial \eta}\left(\eta \rho_L u_L u_L\right) + \frac{\partial}{\partial \eta}\left(\rho_L v_L u_L\right) = \frac{\partial}{\partial \eta}\left(\frac{\mu_L}{\delta}\frac{\partial u_L}{\partial \eta}\right) + \delta g \left(\rho_L - \rho_\infty\right)\cos\alpha \tag{3.33}$$

- **Liquid Energy Equation**

$$\frac{\partial}{\partial \chi}\left(\delta \rho_L c_{P_L} u_L T_L\right) - \frac{d\delta}{d\chi}\frac{\partial}{\partial \eta}\left(\eta \rho_L c_{P_L} u_L T_L\right) + \frac{\partial}{\partial \eta}\left(\rho_L c_{P_L} v_L T_L\right) = \frac{\partial}{\partial \eta}\left(\frac{k_L}{\delta}\frac{\partial T_L}{\partial \eta}\right) \tag{3.34}$$

- **Mixture Continuity Equation**

$$\frac{\partial}{\partial \chi}\left(\delta \rho u\right) - \frac{d\delta}{d\chi}\frac{\partial}{\partial \eta}\left(\eta \rho u\right) + \frac{\partial}{\partial \eta}\left(\rho v\right) = 0 \tag{3.35}$$

- **Mixture Momentum Equation**

$$\frac{\partial}{\partial \chi}\left(\delta \rho u u\right) - \frac{d\delta}{d\chi}\frac{\partial}{\partial \eta}\left(\eta \rho u u\right) + \frac{\partial}{\partial \eta}\left(\rho v u\right) = \frac{\partial}{\partial \eta}\left(\frac{\mu}{\delta}\frac{\partial u}{\partial \eta}\right) + \delta g \left(\rho - \rho_\infty\right)\cos\alpha \tag{3.36}$$

- **Mixture Energy Equation**

$$\frac{\partial}{\partial \chi}\left(\delta \rho c_P u T\right) - \frac{d\delta}{d\chi}\frac{\partial}{\partial \eta}\left(\eta \rho c_P u T\right) + \frac{\partial}{\partial \eta}\left(\rho c_P v T\right) = \frac{\partial}{\partial \eta}\left(\frac{k}{\delta}\frac{\partial T}{\partial \eta}\right) + \frac{\partial}{\partial \eta}\left(\frac{\rho D\left(c_{P_g} - c_{P_v}\right)}{\delta} T \frac{\partial W}{\partial \eta}\right) \tag{3.37}$$

- **Mixture Mass Diffusion Equation**

$$\frac{\partial}{\partial \chi}(\delta \rho u W) - \frac{d\delta}{d\chi}\frac{\partial}{\partial \eta}(\eta \rho u W) + \frac{\partial}{\partial \eta}(\rho v W) = \frac{\partial}{\partial \eta}\left(\frac{\rho D}{\delta}\frac{\partial W}{\partial \eta}\right) \tag{3.38}$$

With the transformation, the variables u_L, v_L, T_L, u, v, T, W, and δ will be evaluated at (χ-η), but the direction of the velocities are still Cartesian (x-y).

The transformed boundary conditions are:

- At the plate surface $(\eta = 0)$

$$u_L = 0 \tag{3.39}$$

$$v_L = 0 \tag{3.40}$$

$$T_L = T_{wall} \tag{3.41}$$

- At the free stream $(\eta \rightarrow \infty)$

$$u = u_\infty \tag{3.42}$$

$$T = T_\infty \tag{3.43}$$

$$W = W_\infty \tag{3.44}$$

- At the liquid-mixture interface $(\eta = 1)$

$$u_L = u \tag{3.45}$$

$$\mu_L \frac{\partial u_L}{\partial \eta} = \mu \frac{\partial u}{\partial \eta} \tag{3.46}$$

$$T_L = T = T_i \tag{3.47}$$

$$T_i = T_{v,sat,i}\left(W_i, W_\infty, T_\infty, \tilde{M}_v, \tilde{M}_g\right) \tag{3.48}$$

$$\dot{m}'' = \rho_L u_L \frac{d\delta}{d\chi} - \rho_L v_L = \rho u \frac{d\delta}{d\chi} - \rho v \tag{3.49}$$

$$\dot{m}'' W + \frac{\rho D}{\delta} \frac{\partial W}{\partial \eta} = 0 \tag{3.50}$$

The transformed form of the energy balance used to evaluate δ is:

$$\frac{k_L}{\delta}\left(\frac{\partial T_L}{\partial \eta}\right)_{\eta=1} = \frac{k}{\delta}\left(\frac{\partial T}{\partial \eta}\right)_{\eta=1} + h_{fg} \frac{d}{d\chi} \int_0^1 \rho_L u_L \delta \, d\eta \tag{3.51}$$

3.3 Fluid Properties

Three vapor-gas combinations were used in this study: steam-air, sodium-argon, and glycerine-bromine. Properties were evaluated at the local temperature. Correlations were found for the temperature dependence of some properties, but for others, tabulated data were used. The tabulated data were used in two ways. One method used a linear interpolation to evaluate the property at the desired temperature between two tabulated points. The other method used functions fitted to the tabulated data by a polynomial approximations as shown below for liquid sodium density:

For example, Table 3.1 shows the dependence of liquid sodium density on temperature. The first two columns contain the tabulated data relating density to temperature. Four of the tabulated data points, shown in bold face in the table, were selected to obtain a polynomial correlation of the form:

$$\rho_L = a_0 + a_1 T_L + a_2 T_L^2 + a_3 T_L^3 \qquad (3.52)$$

The four data points were used to form four linear equations which were solved simultaneously to obtain the coefficients a_0, a_1, a_2, and a_3. The above polynomial expression can then be used with the coefficients to solve for ρ_L at the desired temperature.

Table 3.1: Liquid sodium density.

T_L (K) tabulated data	ρ_L (kg/m^3) tabulated data	ρ_L (kg/m^3) calculated	% error of calculated ρ_L
3.66483300e+02	**9.27588000e+02**	9.27588000e+02	0.00000000e+00
4.77594400e+02	9.03528000e+02	9.01334641e+02	-2.42754904e-01
5.88705600e+02	**8.74692000e+02**	8.74692000e+02	0.00000000e+00
6.99816700e+02	8.49060000e+02	8.47656376e+02	-1.65314999e-01
8.10927800e+02	**8.20224000e+02**	8.20224000e+02	0.00000000e+00
9.22038900e+02	7.86582000e+02	7.92391124e+02	7.38527392e-01
1.03315000e+03	**7.64154000e+02**	7.64154000e+02	-1.48774773e-14

Steam and air was the first combination to be studied. Linear interpolations were used to evaluate the specific heat, thermal conductivity, and viscosity for the liquid and vapor states of steam from the tabulated data given in Incropera and DeWitt (1985). Steam saturation temperature and pressure, liquid density and latent heat were calculated from functions provided by Irvine and Liley (1984). They also provided functions to evaluate the specific heat, thermal conductivity and viscosity of air. The densities of air and steam (vapor) were obtained using the ideal gas equation of state.

The values ρ_L, μ_L, and k_L for sodium were found using functions fitted to tabulated data provided in Bolz and Tuve (1973). Functions fitted to the data given in Hultgren *et al.* (1973) and Rohsenow *et al.* (1985) were used to calculate c_{P_L} and h_{fg}, respectively, for sodium. Sodium vapor properties μ_v, and k_v were obtained using correlations given in Reid *et al.* (1977), as were μ_g, and k_g for argon. Specific heat for the sodium vapor and argon gas was obtained from Hultgren *et al.* and Irvine and Liley (1984), respectively. The densities for both sodium vapor and argon were obtained from the ideal gas equation of state. The condensation of a mixture of sodium and argon resulted in very small $(T_i - T_{wall})$ and a very accurate method was required in the evaluation of the saturation temperature and pressure such that when a pressure is calculated for a given temperature, the reverse process must result in the same temperature. This was obtained by determining a single function, from the tabulated data given by Rohsenow *et al.*, that calculates the temperature for a given pressure. The reverse calculation was performed using a root search by employing a Newton-Raphson method and is shown in Appendix A.

For the transport and thermal properties of glycerine, polynomial functions were fitted to the tabulated data in Gallant (1968). The values of μ_g, C_{Pg} and k_g for bromine was obtained from functions fit to the data given in Touloukian *et al.* (1970). Tabulated data were found for the saturation temperature-pressure relationship for glycerine in Smith and Srivastava (1986) and the data were used in the same method as described above for

sodium. The densities of both glycerine vapor and bromine gas were obtained from the ideal gas equation of state.

For the three vapor-gas combinations, the mixture transport and thermal properties were μ, k and D were evaluated as suggested by Reid *et al.* (1977) and standard additive procedures were used to calculate ρ and C_p. These equations are also given in Appendix A, along with the correlations used to calculate the liquid, vapor and gas properties. Appendix A also includes tables of properties which were the basis for linear interpolation or polynomial curve fits.

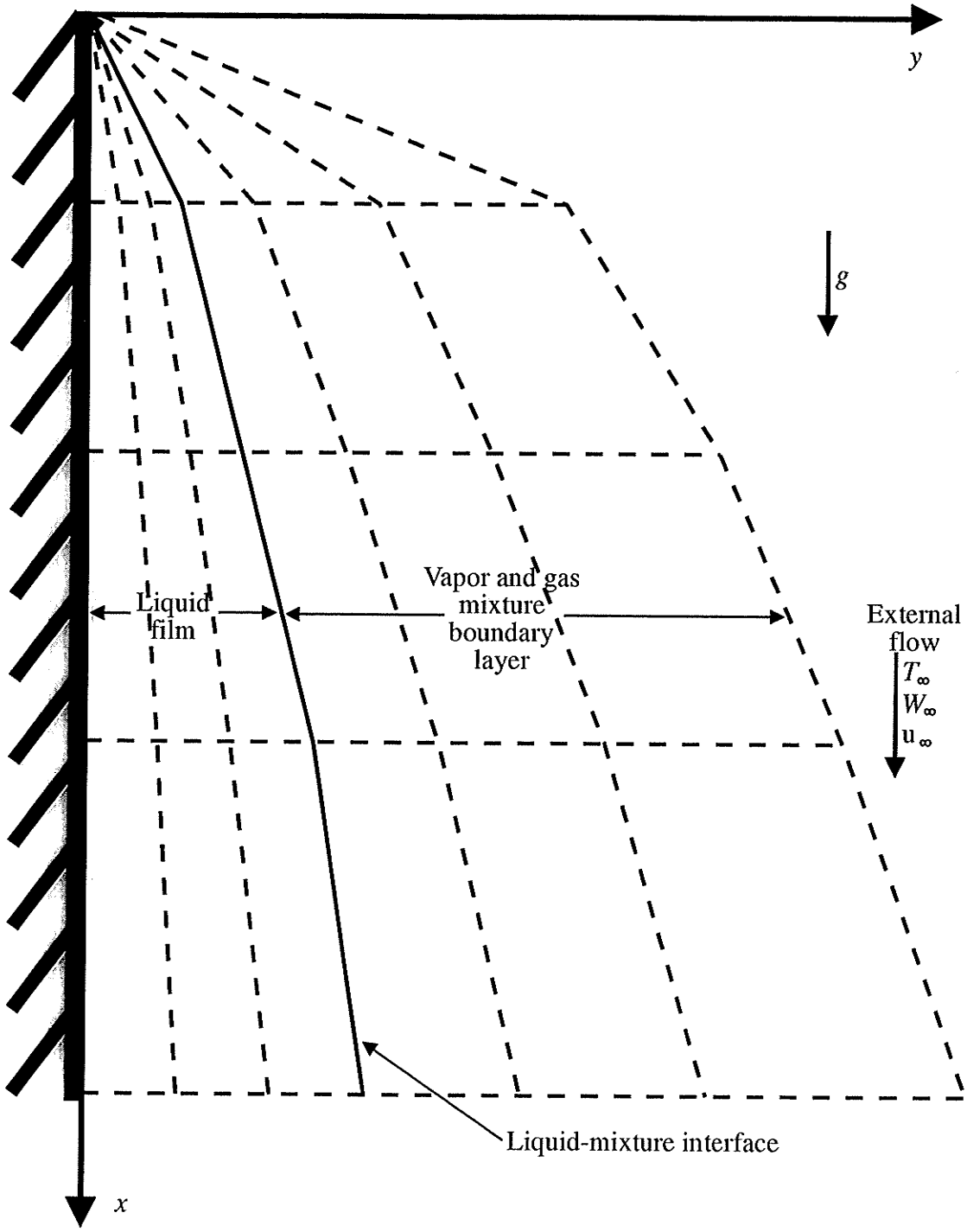

Figure 3.1: Domain and computational grid.

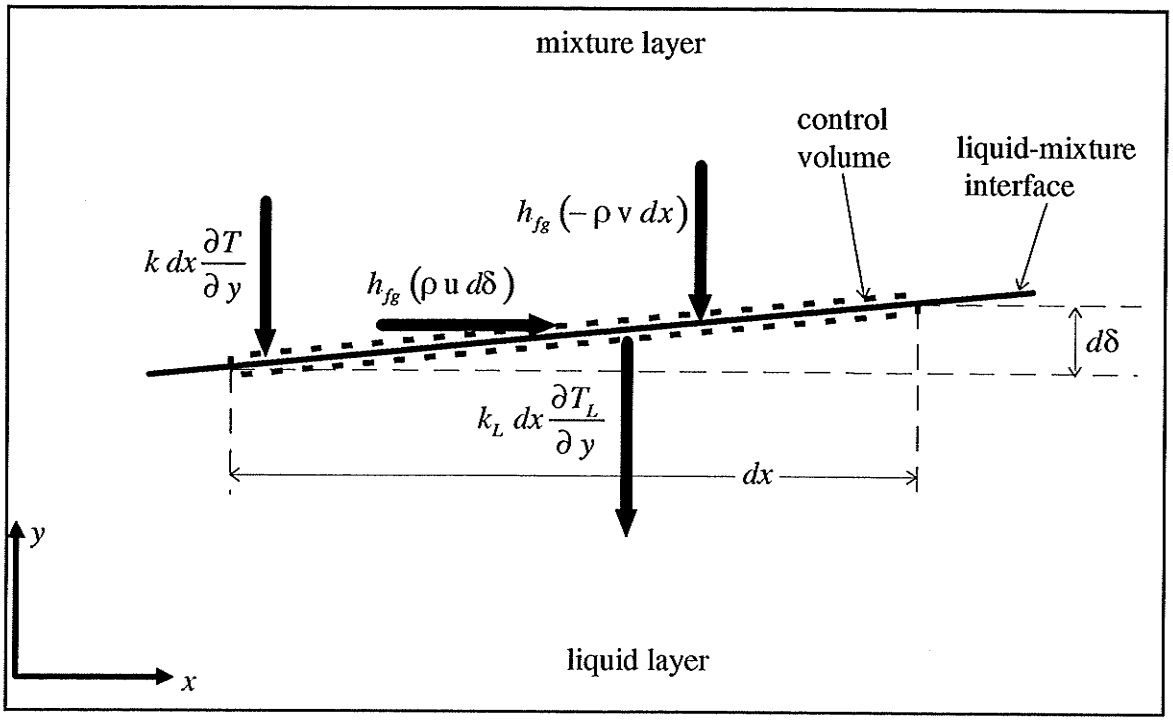

Figure 3.2: Energy balance at the liquid-mixture interface.

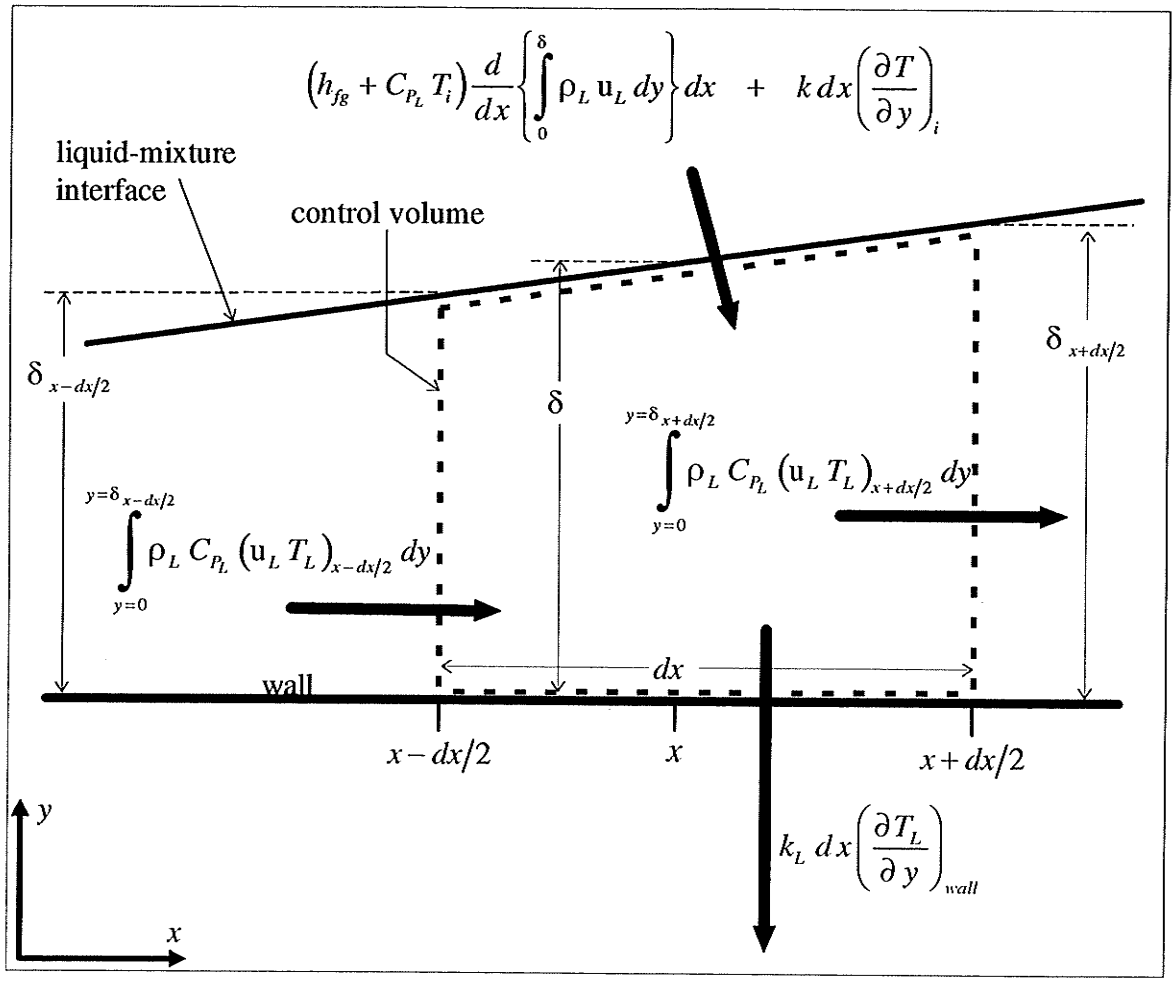

Figure 3.3: Overall energy balance across liquid condensate.

Chapter 4

NUMERICAL SOLUTION METHOD

4.1 Discretization

The coordinate transformation from the x-y plane to the χ-η plane will allow a discretization over orthogonal control volumes in the χ-η plane, as shown in Figure 4.1. The same grid in the x-y plane is shown in Figure 4.2. There are two types of zero width control volumes shown in both figures. The first type has $\Delta\chi = 0$ and occurs at $i = 1$. The second type has $\Delta\eta = 0$ and occurs at $j_L = 1$ and $j_L = n$ on the liquid side and at $j = 1$ and $j = nv$ on the mixture side.

The main grid points for the primary variables u, T, and W are located at the centre of each control volume and the numbering of the control volumes and grid points is as shown in Figure 4.1. The grid points for the other variables are staggered, as shown in Figure 4.1. Mass flows are at the center of the control volume's faces and the grid points for the condensate thickness are situated at the east (downstream) faces.

Expanding grids are used to concentrate the grid points in areas where steep changes take place. The variations of the mixture variables in the η direction are highest near the interface and decrease to zero in the free stream. More nodes are placed near the interface to capture the rapid changes in the variables, and fewer grid points are used farther away

from the interface, where the variables change more slowly. Thus, in the η direction within the mixture layer, the grid spacing near the interface is very small, and increases away from the interface. A uniform grid spacing was used in the η direction within the liquid layer because significant variable changes may occur throughout the liquid film. An expanding grid was also employed for the χ direction because of the rapidly increasing condensate thickness near the leading edge which tapers off further down the plate. Also, there are greater changes in the velocity, temperature and gas concentrations near the leading edge and it is important that the grid spacing in the χ direction be small enough to capture these effects. The details of the algorithm used to generate the expanding grid are given in Appendix B.

The boundary layer equations were discretized over a control volume P at indices (i, j), as shown in Figure 4.3. This figure also shows the four adjacent control volumes and how they are labeled with respect to the present control volume P. The definitions of the spatial quantities are also shown. The primary nodal points, represented by the larger black dot labeled with N, S, E, and W (and i, j indices), are located at the centre of each control volume. Likewise, the nodal points at the four faces, represented by smaller black dots labeled n, s, e, and w, are located at the centre of each face. The details of the discretization of Equations (3.32) to (3.38), along with the boundary conditions described by Equations (3.39) to (3.50) and the energy balance for δ as given by Equation (3.51) are shown in Appendix B. The final results are summarized below.

For the Continuity equations, the discretized form is as follows:

- **Liquid Continuity**

  For $j_L = 1$:

$$\dot{m}_{L,n}(i,1) = 0.0 \tag{4.1}$$

  For $2 \le j_L \le n\text{-}1$:

$$\dot{m}_{L,n}(i,j_L) = \dot{m}_{L,w}(i,j_L) - \dot{m}_{L,e}(i,j_L) + \dot{m}_{L,s}(i,j_L) \tag{4.2}$$

- **Mixture Continuity**

  For $j = 1$:

$$\dot{m}_{n}(i,j=1) = \dot{m}_{L,n}(i,j_L=n-1) \tag{4.3}$$

  For $2 \le j \le nv\text{-}1$:

$$\dot{m}_{n}(i,j) = \dot{m}_{w}(i,j) - \dot{m}_{e}(i,j) + \dot{m}_{s}(i,j) \tag{4.4}$$

Equations (4.1) to (4.4) can be solved by applying the upwind scheme (Patankar (1980)) to the liquid and mixture u-velocity profiles to obtain mass flows at the east and west faces. Then Equation (4.1) is used to obtain a starting value for $\dot{m}_{L,s}(i, j_L=2)$ of Equation (4.2), since:

$$\dot{m}_{L,s}(i, j_L) = \dot{m}_{L,n}(i, j_L-1) \tag{4.5}$$

Likewise, the same approach is used for the mixture continuity equation by using Equations (4.3) and (4.4).

The discretized form of the conservation equations for momentum, energy and diffusion all have the general form of:

$$a_P(i,j)\phi(i,j) = a_N(i,j)\phi(i,j+1) + a_S(i,j)\phi(i,j-1) + b_P(i,j) \tag{4.6}$$

where the general variable ϕ represents either u_L, u, T_L, T or W. The Exponential Differencing Scheme (Patankar (1980)) was used in the calculation of convection and diffusion fluxes. The values of the coefficients are as follows:

- **Liquid and Mixture Momentum Equations**

At $j_L = 1$:

$$\left.\begin{aligned} a_P(i, j_L = 1) &= 1.0 \\ a_S(i, j_L = 1) &= 0.0 \\ a_N(i, j_L = 1) &= 0.0 \\ b_P(i, j_L = 1) &= 0.0 \end{aligned}\right\} \tag{4.7}$$

at $j_L = 2$:

$$a_N(i, j_L) = \dot{m}_{L,n}(i, j_L)\left[\frac{1}{\exp(Pe_{L,n}) - 1}\right] \tag{4.8}$$

$$Pe_{L,n} = \frac{\dot{m}_{L,n}(i, j_L)\delta_m(i)\Delta\eta_{L,+}(j_L)}{\mu_{L,n}(i, j_L)\Delta\chi(i)} \tag{4.9}$$

$$a_S(i, j_L) = \frac{\mu_{L,n}(i, j_L - 1)\Delta\chi(i)}{\delta_m(i)\Delta\eta_{L,+}(j_L - 1)} + \dot{m}_{L,s}(i, j_L) \tag{4.10}$$

$$\begin{aligned} b_P(i, j_L) = {} & \dot{m}_{L,w}(i, j_L)u_L(i-1, j_L) \\ & + g\left[\rho_L(i, j_L) - \rho(i, nv)\right]\cos\theta\,\delta_m(i)\Delta\chi(i)\Delta\eta_L(j_L) \end{aligned} \tag{4.11}$$

$$a_P(i, j_L) = \dot{m}_{L,w}(i, j_L) + a_N(i, j_L) + a_S(i, j_L) \tag{4.12}$$

For $3 \leq j_L \leq n\text{-}2$:

$$a_N(i, j_L) = \dot{m}_{L,n}(i, j_L)\left[\frac{1}{\exp(Pe_{L,n}) - 1}\right] \tag{4.13}$$

$$Pe_{L,n} = \frac{\dot{m}_{L,n}(i, j_L)\delta_m(i)\Delta\eta_{L,+}(j_L)}{\mu_{L,n}(i, j_L)\Delta\chi(i)} \tag{4.14}$$

$$a_S(i, j_L) = \dot{m}_{L,n}(i, j_L - 1)\left[\frac{\exp(Pe_{L,s})}{\exp(Pe_{L,s}) - 1}\right] \tag{4.15}$$

$$Pe_{L,s} = \frac{\dot{m}_{L,n}(i, j_L - 1)\delta_m(i)\Delta\eta_{L,+}(j_L - 1)}{\mu_{L,n}(i, j_L - 1)\Delta\chi(i)} \tag{4.16}$$

$$\begin{aligned} b_P(i, j_L) = {} & \dot{m}_{L,w}(i, j_L)\mathrm{u}_L(i - 1, j_L) \\ & + g\left[\rho_L(i, j_L) - \rho(i, nv)\right]\cos\theta\,\delta_m(i)\Delta\chi(i)\Delta\eta_L(j_L) \end{aligned} \tag{4.17}$$

$$a_P(i, j_L) = \dot{m}_{L,w}(i, j_L) + a_N(i, j_L) + a_S(i, j_L) \tag{4.18}$$

At $j_L = n\text{-}1$:

$$a_N(i, j_L) = \frac{\mu_{L,n}(i, j_L)\Delta\chi(i)}{\delta_m(i)\Delta\eta_{L,+}(j_L)} - \dot{m}_{L,n}(i, j_L) \tag{4.19}$$

$$a_S(i, j_L) = \dot{m}_{L,n}(i, j_L - 1)\left[\frac{\exp(Pe_{L,s})}{\exp(Pe_{L,s}) - 1}\right] \tag{4.20}$$

$$Pe_{L,s} = \frac{\dot{m}_{L,n}(i, j_L - 1)\delta_m(i)\Delta\eta_{L,+}(j_L - 1)}{\mu_{L,n}(i, j_L - 1)\Delta\chi(i)} \tag{4.21}$$

$$\begin{aligned} b_P(i, j_L) = {} & \dot{m}_{L,w}(i, j_L)\mathrm{u}_L(i - 1, j_L) \\ & + g\left[\rho_L(i, j_L) - \rho(i, nv)\right]\cos\theta\,\delta_m(i)\Delta\chi(i)\Delta\eta_L(j_L) \end{aligned} \tag{4.22}$$

$$a_P(i, j_L) = \dot{m}_{L,w}(i, j_L) + a_N(i, j_L) + a_S(i, j_L) \tag{4.23}$$

At $j_L = n$ and $j = 1$:

$$a_N(i,n) = \frac{\mu_n(i,1)\Delta\chi(i)}{\Delta\eta_+(1)\delta_m(i)} \tag{4.24}$$

$$a_S(i,n) = \frac{\mu_{L,n}(i,n-1)\Delta\chi(i)}{\Delta\eta_{L,+}(n-1)\delta_m(i)} \tag{4.25}$$

$$a_P(i,n) = a_N(i,n) + a_S(i,n) \tag{4.26}$$

$$b_P(i,n) = 0 \tag{4.27}$$

At $j = 2$:

$$a_N(i,j) = \dot{m}_n(i,j)\left[\frac{1}{\exp(\mathrm{Pe}_n)-1}\right] \tag{4.28}$$

$$\mathrm{Pe}_n = \frac{\dot{m}_n(i,j)\delta_m(i)\Delta\eta_+(j)}{\mu_n(i,j)\Delta\chi(i)} \tag{4.29}$$

$$a_S(i,j) = \frac{\mu_n(i,j-1)\Delta\chi(i)}{\delta_m(i)\Delta\eta_+(j-1)} + \dot{m}_s(i,j) \tag{4.30}$$

$$\begin{aligned} b_P(i,j) &= \dot{m}_w(i,j)\mathrm{u}(i-1,j) \\ &\quad + g\left[\rho(i,j) - \rho(i,nv)\right]\cos\theta\,\delta_m(i)\Delta\chi(i)\Delta\eta(j) \end{aligned} \tag{4.31}$$

$$a_P(i,j) = \dot{m}_w(i,j) + a_N(i,j) + a_S(i,j) \tag{4.32}$$

For $3 \le j \le nv$-2:

$$a_N(i,j) = \dot{m}_n(i,j)\left[\frac{1}{\exp(\mathrm{Pe}_n)-1}\right] \tag{4.33}$$

$$\mathrm{Pe}_n = \frac{\dot{m}_n(i,j)\delta_m(i)\Delta\eta_+(j)}{\mu_n(i,j)\Delta\chi(i)} \tag{4.34}$$

$$a_S(i,j) = \dot{m}_n(i,j-1)\left[\frac{\exp(\mathrm{Pe}_s)}{\exp(\mathrm{Pe}_s)-1}\right] \tag{4.35}$$

$$\mathrm{Pe}_s = \frac{\dot{m}_n(i,j-1)\delta_m(i)\Delta\eta_+(j-1)}{\mu_n(i,j-1)\Delta\chi(i)} \tag{4.36}$$

$$\begin{aligned} b_P(i,j) &= \dot{m}_w(i,j)\mathrm{u}(i-1,j) \\ &\quad + g\left[\rho(i,j)-\rho(i,nv)\right]\cos\theta\,\delta_m(i)\Delta\chi(i)\Delta\eta(j) \end{aligned} \tag{4.37}$$

$$a_P(i,j) = \dot{m}_w(i,j) + a_N(i,j) + a_S(i,j) \tag{4.38}$$

At $j = nv$-1:

$$a_N(i,j) = \frac{\mu_n(i,j)\Delta\chi(i)}{\delta_m(i)\Delta\eta_+(j)} - \dot{m}_n(i,j) \tag{4.39}$$

$$a_S(i,j) = \dot{m}_n(i,j-1)\left[\frac{\exp(\mathrm{Pe}_s)}{\exp(\mathrm{Pe}_s)-1}\right] \tag{4.40}$$

$$\mathrm{Pe}_s = \frac{\dot{m}_n(i,j-1)\delta_m(i)\Delta\eta_+(j-1)}{\mu_n(i,j-1)\Delta\chi(i)} \tag{4.41}$$

$$\begin{aligned} b_P(i,j) &= \dot{m}_w(i,j)\mathrm{u}(i-1,j) \\ &\quad + g\left[\rho(i,j)-\rho(i,nv)\right]\cos\theta\,\delta_m(i)\Delta\chi(i)\Delta\eta(j) \end{aligned} \tag{4.42}$$

$$a_P(i,j) = \dot{m}_w(i,j) + a_N(i,j) + a_S(i,j) \tag{4.43}$$

At $j = nv$:

$$\left.\begin{aligned} a_P(i,nv) &= 1.0 \\ a_N(i,nv) &= 0.0 \\ a_S(i,nv) &= 0.0 \\ b_P(i,nv) &= \mathrm{u}_\infty \end{aligned}\right\} \tag{4.44}$$

- **Liquid Energy Equation**

At $j_L = 1$:

$$\left.\begin{aligned} a_P(i,1) &= 1.0 \\ a_N(i,1) &= 0.0 \\ a_S(i,1) &= 0.0 \\ b_P(i,1) &= T_{wall} \end{aligned}\right\} \tag{4.45}$$

At $j_L = 2$:

$$a_N(i,j_L) = \dot{m}_{L,n}(i,j_L)\, c_{P_{L,n}}(i,j_L)\left[\frac{1}{\exp\left(Pe_{L,n}\right)-1}\right] \tag{4.46}$$

$$Pe_{L,n} = \frac{\dot{m}_{L,n}(i,j_L)\,\delta_m(i)\,\Delta\eta_{L,+}(j_L)\,c_{P_{L,n}}(i,j_L)}{k_{L,n}(i,j_L)\,\Delta\chi(i)} \tag{4.47}$$

$$a_S(i,j_L) = c_{P_{L,n}}(i,j_L-1)\left[\frac{k_{L,n}(i,j_L-1)\Delta\chi(i)}{c_{P_{L,n}}(i,j_L-1)\delta_m(i)\Delta\eta_{L,+}(j_L-1)} + \dot{m}_{L,s}(i,j_L)\right] \tag{4.48}$$

$$b_P(i,j_L) = \dot{m}_{L,w}(i,j_L)\, c_{P_{L,w}}(i,j_L)\, T_L(i-1,j_L) \tag{4.49}$$

$$\begin{aligned} a_P(i,j_L) = {} & \dot{m}_{L,e}(i,j_L)\, c_{P_{L,e}}(i,j_L) + \dot{m}_{L,n}(i,j_L)\, c_{P_{L,n}}(i,j_L) \\ & - \dot{m}_{L,n}(i,j_L-1)\, c_{P_{L,n}}(i,j_L-1) + a_N(i,j_L) + a_S(i,j_L) \end{aligned} \tag{4.50}$$

For $3 \le j_L \le n\text{-}2$:

$$a_N(i,j_L) = \dot{m}_{L,n}(i,j_L)\, c_{P_{L,n}}(i,j_L)\left[\frac{1}{\exp\left(Pe_{L,n}\right)-1}\right] \tag{4.51}$$

$$Pe_{L,n} = \frac{\dot{m}_{L,n}(i,j_L)\,\delta_m(i)\,\Delta\eta_{L,+}(j_L)\, c_{P_{L,n}}(i,j_L)}{k_{L,n}(i,j_L)\,\Delta\chi(i)} \tag{4.52}$$

$$a_S(i,j_L) = \dot{m}_{L,n}(i,j_L-1)\, c_{P_{L,n}}(i,j_L-1)\left[\frac{\exp\left(Pe_{L,s}\right)}{\exp\left(Pe_{L,s}\right)-1}\right] \tag{4.53}$$

$$Pe_{L,s} = \frac{\dot{m}_{L,n}(i,j_L-1)\,\delta_m(i)\,\Delta\eta_{L,+}(j_L-1)\, c_{P_{L,n}}(i,j_L-1)}{k_{L,n}(i,j_L-1)\,\Delta\chi(i)} \tag{4.54}$$

$$b_P(i,j_L) = \dot{m}_{L,w}(i,j_L)\, c_{P_{L,w}}(i,j_L)\, T_L(i-1,j_L) \tag{4.55}$$

$$\begin{aligned} a_P(i,j_L) = {} & \dot{m}_{L,e}(i,j_L)\, c_{P_{L,e}}(i,j_L) + \dot{m}_{L,n}(i,j_L)\, c_{P_{L,n}}(i,j_L) \\ & - \dot{m}_{L,n}(i,j_L-1)\, c_{P_{L,n}}(i,j_L-1) + a_N(i,j_L) + a_S(i,j_L) \end{aligned} \tag{4.56}$$

At $j_L = n\text{-}1$:

$$a_N(i,j_L) = c_{P_{L,n}}(i,j_L)\left[\frac{k_{L,n}(i,j_L)\,\Delta\chi(i)}{c_{P_{L,n}}(i,j_L)\,\delta_m(i)\,\Delta\eta_{L,+}(j_L)} - \dot{m}_{L,n}(i,j_L)\right] \tag{4.57}$$

$$a_S(i,j_L) = \dot{m}_{L,n}(i,j_L-1)\, c_{P_{L,n}}(i,j_L-1)\left[\frac{\exp\left(Pe_{L,s}\right)}{\exp\left(Pe_{L,s}\right)-1}\right] \tag{4.58}$$

$$Pe_{L,s} = \frac{\dot{m}_{L,n}(i,j_L-1)\,\delta_m(i)\,\Delta\eta_{L,+}(j_L-1)\, c_{P_{L,n}}(i,j_L-1)}{k_{L,n}(i,j_L-1)\,\Delta\chi(i)} \tag{4.59}$$

$$b_P(i,j_L) = \dot{m}_{L,w}(i,j_L)\, c_{P_{L,w}}(i,j_L)\, T_L(i-1,j_L) \tag{4.60}$$

$$a_P(i,j_L) = \dot{m}_{L,e}(i,j_L)\,c_{P_{L,e}}(i,j_L) + \dot{m}_{L,n}(i,j_L)\,c_{P_{L,n}}(i,j_L) - \dot{m}_{L,n}(i,j_L-1)\,c_{P_{L,n}}(i,j_L-1) + a_N(i,j_L) + a_S(i,j_L) \tag{4.61}$$

At $j_L = n$:

$$\left.\begin{aligned} a_P(i,n) &= 1.0 \\ a_N(i,n) &= 0.0 \\ a_S(i,n) &= 0.0 \\ b_P(i,n) &= T_i \end{aligned}\right\} \tag{4.62}$$

- **Mixture Energy Equation**

At $j = 1$

$$\left.\begin{aligned} a_P(i,1) &= 1.0 \\ a_N(i,1) &= 0.0 \\ a_S(i,1) &= 0.0 \\ b_P(i,1) &= T_i \end{aligned}\right\} \tag{4.63}$$

At $j = 2$:

$$a_N(i,j) = \dot{m}_n(i,j)\,c_{P_n}(i,j)\left[\frac{1}{\exp(Pe_n)-1}\right] \tag{4.64}$$

$$Pe_n = \frac{\dot{m}_n(i,j)\,\delta_m(i)\,\Delta\eta_+(j)\,c_{P_n}(i,j)}{k_n(i,j)\,\Delta\chi(i)} \tag{4.65}$$

$$a_S(i,j) = c_{P_n}(i,j-1)\left[\frac{k_n(i,j-1)\Delta\chi(i)}{c_{P_n}(i,j-1)\delta_m(i)\Delta\eta_+(j-1)} + \dot{m}_s(i,j)\right] \tag{4.66}$$

$$b_P(i,j) = \dot{m}_w(i,j)\,c_{P_w}(i,j)\,T(i-1,j) + \frac{1}{\delta_m}\Delta\chi(i)\left\{\rho_n(i,j)D_n(i,j)\left[c_{P_{g,n}}(i,j) - c_{P_{v,n}}(i,j)\right]T_n\left(\frac{\partial W}{\partial \eta}\right)_n - \rho_n(i,j-1)D_n(i,j-1)\left[c_{P_{g,n}}(i,j-1) - c_{P_{v,n}}(i,j-1)\right]T_s\left(\frac{\partial W}{\partial \eta}\right)_s\right\} \quad (4.67)$$

$$T_n = T(i,j) + \alpha_n\left[T(i,j+1) - T(i,j)\right] \quad (4.68)$$

$$T_s = T(i,j-1) + \alpha_s\left[T(i,j) - T(i,j-1)\right] \quad (4.69)$$

$$\left(\frac{\partial W}{\partial \eta}\right)_n = \frac{W(i,j+1) - W(i,j)}{\Delta\eta_+(j)} \quad (4.70)$$

$$\left(\frac{\partial W}{\partial \eta}\right)_s = \frac{W(i,j) - W(i,j-1)}{\Delta\eta_+(j-1)} \quad (4.71)$$

$$a_P(i,j) = \dot{m}_e(i,j)\,c_{P_e}(i,j) + \dot{m}_n(i,j)\,c_{P_n}(i,j) - \dot{m}_n(i,j-1)\,c_{P_n}(i,j-1) + a_N(i,j) + a_S(i,j) \quad (4.72)$$

For $3 \le j \le nv\text{-}2$:

$$a_N(i,j) = \dot{m}_n(i,j)\,c_{P_n}(i,j)\left[\frac{1}{\exp(Pe_n) - 1}\right] \quad (4.73)$$

$$Pe_n = \frac{\dot{m}_n(i,j)\,\delta_m(i)\,\Delta\eta_+(j)\,c_{P_n}(i,j)}{k_n(i,j)\,\Delta\chi(i)} \quad (4.74)$$

$$a_S(i,j) = \dot{m}_n(i,j-1)\,c_{P_n}(i,j-1)\left[\frac{\exp(Pe_s)}{\exp(Pe_s) - 1}\right] \quad (4.75)$$

$$Pe_s = \frac{\dot{m}_n(i,j-1)\delta_m(i)\Delta\eta_+(j-1)c_{P_n}(i,j-1)}{k_n(i,j-1)\Delta\chi(i)} \tag{4.76}$$

$$\begin{aligned} b_P(i,j) = {} & \dot{m}_w(i,j)c_{P_w}(i,j)T(i-1,j) \\ & + \frac{1}{\delta_m}\Delta\chi(i)\Big\{\rho_n(i,j)D_n(i,j)\left[c_{P_{g,n}}(i,j) - c_{P_{v,n}}(i,j)\right]T_n\left(\frac{\partial W}{\partial\eta}\right)_n \\ & - \rho_n(i,j-1)D_n(i,j-1)\left[c_{P_{g,n}}(i,j-1) - c_{P_{v,n}}(i,j-1)\right]T_s\left(\frac{\partial W}{\partial\eta}\right)_s\Big\} \end{aligned} \tag{4.77}$$

$$T_n = T(i,j) \quad + \quad \alpha_n\left[T(i,j+1) - T(i,j)\right] \tag{4.78}$$

$$T_s = T(i,j-1) \quad + \quad \alpha_s\left[T(i,j) - T(i,j-1)\right] \tag{4.79}$$

$$\left(\frac{\partial W}{\partial\eta}\right)_n = \frac{W(i,j+1) - W(i,j)}{\Delta\eta_+(j)} \tag{4.80}$$

$$\left(\frac{\partial W}{\partial\eta}\right)_s = \frac{W(i,j) - W(i,j-1)}{\Delta\eta_+(j-1)} \tag{4.81}$$

$$\begin{aligned} a_P(i,j) = {} & \dot{m}_e(i,j)c_{P_e}(i,j) + \dot{m}_n(i,j)c_{P_n}(i,j) \\ & - \dot{m}_n(i,j-1)c_{P_n}(i,j-1) + a_N(i,j) + a_S(i,j) \end{aligned} \tag{4.82}$$

At $j = nv\text{-}1$:

$$a_N(i,j) = c_{P_n}(i,j)\left[\frac{k_n(i,j)\Delta\chi(i)}{c_{P_n}(i,j)\delta_m(i)\Delta\eta_+(j)} \quad - \quad \dot{m}_n(i,j)\right] \tag{4.83}$$

$$a_S(i,j) = \dot{m}_n(i,j-1)c_{P_n}(i,j-1)\left[\frac{\exp(Pe_s)}{\exp(Pe_s) - 1}\right] \tag{4.84}$$

$$Pe_s = \frac{\dot{m}_n(i,j-1)\delta_m(i)\Delta\eta_+(j-1)c_{P_n}(i,j-1)}{k_n(i,j-1)\Delta\chi(i)} \tag{4.85}$$

$$b_P(i,j) = \dot{m}_w(i,j)\,c_{P_w}(i,j)\,T(i-1,j)$$
$$+ \frac{1}{\delta_m}\Delta\chi(i)\Big\{\rho_n(i,j)D_n(i,j)\left[c_{P_{g,n}}(i,j) - c_{P_{v,n}}(i,j)\right]T_n\left(\frac{\partial W}{\partial \eta}\right)_n \tag{4.86}$$
$$- \rho_n(i,j-1)D_n(i,j-1)\left[c_{P_{g,n}}(i,j-1) - c_{P_{v,n}}(i,j-1)\right]T_s\left(\frac{\partial W}{\partial \eta}\right)_s\Big\}$$

$$T_n = T(i,j) + \alpha_n\left[T(i,j+1) - T(i,j)\right] \tag{4.87}$$

$$T_s = T(i,j-1) + \alpha_s\left[T(i,j) - T(i,j-1)\right] \tag{4.88}$$

$$\left(\frac{\partial W}{\partial \eta}\right)_n = \frac{W(i,j+1) - W(i,j)}{\Delta\eta_+(j)} \tag{4.89}$$

$$\left(\frac{\partial W}{\partial \eta}\right)_s = \frac{W(i,j) - W(i,j-1)}{\Delta\eta_+(j-1)} \tag{4.90}$$

$$a_P(i,j) = \dot{m}_e(i,j)\,c_{P_e}(i,j) + \dot{m}_n(i,j)\,c_{P_n}(i,j)$$
$$- \dot{m}_n(i,j-1)\,c_{P_n}(i,j-1) + a_N(i,j) + a_S(i,j) \tag{4.91}$$

At $j = nv$:

$$\left.\begin{aligned} a_P(i,nv) &= 1.0 \\ a_N(i,nv) &= 0.0 \\ a_S(i,nv) &= 0.0 \\ b_P(i,nv) &= T_\infty \end{aligned}\right\} \tag{4.92}$$

- **Mixture Diffusion Equation**

At $j = 1$:

$$a_N(i,1) = \frac{\rho_n(i,1)D_n(i,1)\Delta\chi(i)}{\delta_m(i)\Delta\eta_+(1)} \tag{4.93}$$

$$a_S(i,1) = 0.0 \cdot \tag{4.94}$$

$$b_P(i,1) = 0.0 \tag{4.95}$$

$$a_P(i,1) = \dot{m}_n(i,1) + a_N(i,1) \tag{4.96}$$

At $j = 2$:

$$a_N(i,2) = \dot{m}_n(i,2)\left[\frac{1}{\exp\left[\mathrm{Pe}_n(i,2)\right]-1}\right] \tag{4.97}$$

$$\mathrm{Pe}_n(i,2) = \frac{\dot{m}_n(i,2)\delta_m(i)\Delta\eta_+(2)}{\rho_n(i,2)\,D_n(i,2)\,\Delta\chi(i)} \tag{4.98}$$

$$a_S(i,2) = 0.0 \tag{4.99}$$

$$b_P(i,2) = \dot{m}_w(i,2)W(i-1,2) \tag{4.100}$$

$$a_P(i,2) = \dot{m}_c(i,2) + \dot{m}_n(i,2) + a_N(i,2) \tag{4.101}$$

For $3 \le j \le nv\text{-}2$:

$$a_N(i,j) = \dot{m}_n(i,j)\left[\frac{1}{\exp(\mathrm{Pe}_n)-1}\right] \tag{4.102}$$

$$\mathrm{Pe}_n = \frac{\dot{m}_n(i,j)\delta_m(i)\Delta\eta_+(j)}{\rho_n(i,j)\,D_n(i,j)\,\Delta\chi(i)} \tag{4.103}$$

$$a_S(i,j) = \dot{m}_n(i,j-1)\left[\frac{\exp(\mathrm{Pe}_s)}{\exp(\mathrm{Pe}_s)-1}\right] \tag{4.104}$$

$$\mathrm{Pe}_s = \frac{\dot{m}_n(i,j-1)\delta_m(i)\Delta\eta_+(j-1)}{\rho_n(i,j-1)\,D_n(i,j-1)\,\Delta\chi(i)} \tag{4.105}$$

$$b_P(i,j) = \dot{m}_w(i,j)W(i-1,j) \tag{4.106}$$

$$a_P(i,j) = \dot{m}_w(i,j) + a_N(i,j) + a_S(i,j) \tag{4.107}$$

At $j = nv\text{-}1$:

$$a_N(i,j) = \frac{\rho_n(i,j) D_n(i,j) \Delta\chi(i)}{\delta_m(i) \Delta\eta_+(j)} \quad - \quad \dot{m}_n(i,j) \tag{4.108}$$

$$a_S(i,j) = \dot{m}_n(i,j-1) \left[\frac{\exp(\mathrm{Pe}_s)}{\exp(\mathrm{Pe}_s) - 1} \right] \tag{4.109}$$

$$\mathrm{Pe}_s = \frac{\dot{m}_n(i,j-1) \delta_m(i) \Delta\eta_+(j-1)}{\rho_n(i,j-1) D_n(i,j-1) \Delta\chi(i)} \tag{4.110}$$

$$b_P(i,j) = \dot{m}_w(i,j) W(i-1,j) \tag{4.111}$$

$$a_P(i,j) = \dot{m}_w(i,j) + a_N(i,j) + a_S(i,j) \tag{4.112}$$

At $j = nv$:

$$\left.\begin{aligned} a_P(i,nv) &= 1.0 \\ a_N(i,nv) &= 0.0 \\ a_S(i,nv) &= 0.0 \\ b_P(i,nv) &= W_\infty \end{aligned}\right\} \tag{4.113}$$

The above equations for the coefficients of Equation (4.6) show that Equation (4.6) is independent of the downstream solution profiles and only depends on the known upstream fields. Thus for each i index, Equation (4.6) can be written for the range of applicable j indices. This will result in n (or nv) equations which are then directly solved using a tri-diagonal matrix solver.

The discretized form of the energy balance, Equation (3.51), needed to evaluate δ is:

$$\delta(i) = \frac{-b+\sqrt{b^2 - 4ac}}{2a} \tag{4.114}$$

where:
$$a = h_{fg}(i)\sum_{j_L=1}^{n} \rho_L(i,j_L)\mathrm{u}_L(i,j_L)\Delta\eta(j_L) \tag{4.115}$$

$$b = \delta(i-1)h_{fg}(i)\left\{\sum_{j_L=1}^{n} \rho_L(i,j_L)\mathrm{u}_L(i,j_L)\Delta\eta(j_L) - \sum_{j_L=1}^{n}\frac{\dot{m}_{L,w}(i,j_L)}{\delta(i-1)}\right\} \tag{4.116}$$

$$\begin{aligned} c = {} & -\delta(i-1)^2 h_{fg}(i)\sum_{j_L=1}^{n}\frac{\dot{m}_{L,w}(i,j_L)}{\delta(i-1)} \\ & - 2\Delta\chi(i)k_L(i,n-1)\left\{\frac{T_L(i,n)-T_L(i,n-1)}{\Delta\eta_{L,+}(n-1)}\right\} \\ & + 2\Delta\chi(i)k(i,1)\left\{\frac{T(i,2)-T(i,1)}{\Delta\eta_{+}(1)}\right\} \end{aligned} \tag{4.117}$$

Thus $\delta(i)$ can be obtained from a known solution field for T, T_L, u and $\delta(i-1)$.

4.2 Solution Procedure

The form of the discretized equations in Section 4.1 shows that the solution for a particular χ location is only dependent on the upstream fields, and is independent of what is happening downstream. Thus the entire solution field can be obtained by marching

down the plate, and independently solving the equation set at each $\chi(i)$station. However, in order to solve for any $\chi(i)$ station, the solution for $\chi(i-1)$ must be known, and a starting condition at $x = 0$ is therefore required. The initial solution field at $i = 1$ is:

$$\chi(1) = 0.0 \tag{4.118}$$

$$\delta(1) = 0.0 \tag{4.119}$$

$$u_L(1, j_L) = 0.0 \quad , \quad \text{for } 1 \le j_L \le n \tag{4.120}$$

$$T_L(1, j_L) = T_{wall} \quad , \quad \text{for } 1 \le j_L \le n \tag{4.121}$$

$$u(1, j) = 0.0 \quad , \quad \text{for } 1 \le j \le nv \tag{4.122}$$

$$T(1, j) = T_\infty \quad , \quad \text{for } 1 \le j \le nv \tag{4.123}$$

$$W(1, j) = 0.0 \quad , \quad \text{for } 1 \le j \le nv \tag{4.124}$$

The properties at $i = 1$ are then evaluated at T_{wall} and T_∞ for the liquid and mixture, respectively.

With an initial solution field at $i = 1$, the solutions at $\chi(i)$, $2 \le i \le m$, can then be obtained. However, at each $\chi(i)$ station, an iterative method is required because the equations are non-linear and coupled. To start this iterative process, an initial (guess) solution field is required for each $\chi(i)$, $i \ge 2$. For $i \ge 3$, the solution field for i-1 is used as the initial guess for the three vapor-gas mixtures. The only difference is for the steam-air mixture where the following equation is used to guess an initial value for $\delta(i)$:

$$\delta(i) = \delta(i-1)\left[\frac{\chi_b(i)}{\chi_b(i-1)}\right]^{1/4} \tag{4.125}$$

However, at $i = 2$, a different approach is required since the solution field at i-1 cannot be used for an initial guess. Appendix C contains the details of the initial guess solution field used to start the iterative process at $i = 2$.

Relaxation is required in order to solve the set of equations described above. Two different relaxation methods are used. The first is to solve the equations, and then apply relaxation using the following formula:

$$\phi = \phi_{old} + relx(\phi_{new} - \phi_{old}) \tag{4.126}$$

Where *relx* is the relaxation factor.

The second method is to apply the relaxation through the inertia terms (Patankar (1980)) prior to solving the equations. Thus Equation (4.6) is changed to:

$$\begin{aligned} a_{P,relx}(i,j)\phi(i,j) = {} & a_{N,relx}(i,j)\phi(i,j+1) + a_{S,relx}(i,j)\phi(i,j-1) \\ & + b_{P,relx}(i,j) \end{aligned} \tag{4.127}$$

and the coefficients are defined as:

$$\left.\begin{aligned} a_{P,relx}(i,j) &= a_P(i,j)\left[1 + \frac{1}{relx}\right] \\ a_{N,relx}(i,j) &= a_N(i,j) \\ a_{S,relx}(i,j) &= a_S(i,j) \\ b_{P,relx}(i,j) &= b_P(i,j) + a_P(i,j)\frac{\phi_{old}(i,j)}{relx} \end{aligned}\right\} \tag{4.128}$$

The maximum gas concentration, W_{max}, needs to be defined so that when the diffusion equation is solved, it's validity can be determined. The variable W_{max} is defined as the gas concentration that would result in a mixture temperature that is equal to T_{wall}. The equation used to calculate W_{max} is:

$$W_{\max} = \frac{\frac{P_{g,i}}{P_\infty}\tilde{M}_g}{\frac{P_{g,i}}{P_\infty}\tilde{M}_g + \frac{P_{v,i}}{P_\infty}\tilde{M}_v} \tag{4.129}$$

where: $P_{v,i}$ is the partial pressure of the vapor at $T_i = T_{wall}$

$P_{g,i} = P_\infty - P_{v,i}$

An effective solution procedure is to first use Equations (4.118) to (4.124) to evaluate the solution field at $\chi(1) = 0$, the start of the plate. Then the following steps are used to solve for the rest of the $\chi(i)$ stations along the plate.

1. For i = 2, use the appropriate initial guess solution field as given in Appendix C.
2. Solve for $\delta(i)$ using Equation (4.114) to (4.117). Then apply relaxation using Equation (4.126).
3. Solve the liquid and mixture continuity equations using Equations (4.1) to (4.4).
4. Solve the coupled liquid and mixture momentum equation by using Equations (4.7) to (4.44) to evaluate the coefficients of Equation (4.6). The equation set was then solved using a TDMA (Tri-Diagonal Matrix) solver. The details of the TDMA algorithm can be found in Patankar (1980). Relaxation was then applied using Equation (4.126).
5. Solve the liquid and mixture continuity equations using Equations (4.1) to (4.4).

6. Set up the coefficients of Equation (4.6) for the diffusion equation by using Equations (4.93) to (4.113). Then apply relaxation through the inertia terms by using Equations (4.127) and (4.128). The TDMA solver was then used to solve Equation (4.127) and obtain a new gas concentration field.

7. Check the results from step 6 to see if $W(j) \leq W_{max}$. If all of the gas concentrations are less than W_{max} then proceed to step 8. Halt the solution procedure if any $W(j)$ exceeds W_{max} and check if a backup solution exists. If so, use the backup solution along with a lower relaxation factor. The different situations for the backup solutions are described later in Section 4.3. If no backup solution exists, the program ends.

8. Evaluate the liquid, vapour, gas, and mixture properties.

9. Solve the mixture energy equation by using Equations (4.63) to (4.92) to evaluate the coefficients of Equation (4.6) and then solve the resulting *nv* equations with the TDMA solver. Obtain a new mixture temperature field by applying Equation (4.126).

10. Solve the liquid energy equation by using Equations (4.45) to (4.62) to evaluate the coefficients of Equation (4.6) and then solve the resulting *n* equations with the TDMA solver. Obtain a new liquid temperature field by applying Equation (4.126).

11. Compare this new solution field with the results of the previous iteration. The converged solution for $\chi(i)$ is obtained when the convergence criteria, defined by Equation (4.130) and (4.131), is satisfied by all of the solution fields for u_L, u, T_L, T, W, $\dot{m}_{L,n}$, $\dot{m}_n$ and δ. If the convergence criteria is not satisfied, repeat the above steps.

12. Advance to next $\chi(i)$ station. Use the results from $\chi(i-1)$ as an initial guess solution field and begin iterative process at step 2.

The convergence check mentioned in step 10 was performed by calculating the error between the newest iterated solution and the results from the previous iteration. Two different methods were used to evaluate the difference:

$$err_1 = \left| \frac{\phi_{iter} - \phi_{iter-1}}{\phi_{iter}} \right| \qquad (4.130)$$

$$err_2 = \left| \frac{\phi_{iter} - \phi_{iter-1}}{\text{range of } \phi_{iter}} \right| \tag{4.131}$$

Both methods will report a large error if the denominator $\rightarrow 0$. Thus both errors were evaluated and the lower was compared to the convergence criteria. Convergence was satisfied when the error was lower than the desired convergence criteria.

4.3 The Input File

A separate program was used for each of the three vapor-gas mixtures (steam-air, sodium-argon and glycerine-bromine). Slight differences among the programs resulted in three slightly different input files. This section gives the details of the input file (named input.in) used by the computer code. The differences between the programs and input.in files will also be discussed. Figures 4.4 to 4.6 show listings of the input files used by the steam-air, sodium-argon and glycerine-bromine programs, respectively. The rest of this section will describe each of the lines of Figures 4.4 to 4.6 in detail.

Lines 1-16: The first 16 lines of each input file were used for the same purposes in each of the three programs. The first line of the input file specifies the magnitude of the gravitational force in the vertical direction. The second line gives the angle by which the plate is inclined from the vertical (vertical is defined as being in the direction of gravity). Generally all results were obtained using standard gravitational force of 9.81 m/s^2 and theta was varied between 0^0(vertical plate) and 90^0(horizontal plate) to examine the effects of plate inclination. Lines 3 to 11 and 16 are used to determine the properties. If they are set to 0.0, then the program will perform a variable property analysis using the property correlations given in Appendix A. A constant property analysis is also possible by just defining a non-zero value for each of the properties with lines 7 to 11 devoted to the constant mixture properties (if $W_\infty \neq 0$). Lines 12 to 15 were used to define the wall temperature and the free stream conditions.

Lines 17-18: Lines 17 and 18 were used to define the axial coordinate at the start and end of the plate to be solved. For steam-air, "xstart" is always equal to zero and "xend" would define the length of the plate. A similar specification was used in the sodium-argon and glycerine-bromine programs. However, for the sodium-argon and glycerine-bromine programs, the last converged solution was saved to a file called "solultion.stop". This file can then be used to restart/continue by renaming the "solution.stop" file to "solution.start". It is recommended in such cases that only lines 17 to 24 and 29 to 32 be changed in the "input.in" file. To have the computer program continue from the last solved $\chi(i)$ station, as defined in the "solution.start" file, just set "xstart" to any non-zero value and "xend" to a new value. It is also useful to be able to restart the program in the event of a crash, using the same grid spacing. To do this, set xstart to a non-zero value and on line 29, set m to 1.

Lines 19-22: Four different relaxation factors are defined in lines 19 to 22 of the "input.in" file. "Relxu" is the relaxation factor for both the liquid and mixture momentum equations and "relxt" was used for both the liquid and mixture energy equations. Lines 19 to 22 for the steam-air's "input.in" file contain only a single number representing the relaxation factors used. Steam-air used Equation (4.126) to apply relaxation to the velocity, temperature and condensate thickness (it was found that no relaxation should be applied to the evaluation of the condensate thickness), and Equations (4.127) and (4.128) to apply relaxation to the diffusion equation. For the other two mixtures, line 19 also represents the relaxation factor used by Equation (4.126) in evaluating the condensate thickness (generally no relaxation was required). Lines 20 and 21 contain two numbers in each line. The first number determines the type of relaxation to be applied, 1 means to use Equation (4.126) and 2 means that Equations (4.127) and (4.128) should be used. The second number is the actual relaxation factor. It was found that for the momentum and energy equations, relaxation should be applied by Equation (4.126). Relaxation is applied through the inertia terms of the diffusion equation in the sodium-argon and glycerine-bromine programs. The "relxw" value is defined by the three numbers on line 22. The first defines the relaxation factor to use at the start of each $\chi(i)$ station (the minimum "relxw" value). The maximum "relxw" is given by the second number and the third defines the factor by which the "relxw" increases from the minimum to the maximum value. For example;
if the three numbers are:

1.0e+1, 1.0e+5, 10.0

then the following "relxw" values would be used.

1.0e+1, 1.0e+2, 1.0e+3, 1.0e+4, 1.0e+5

It should be noted that when the relxw values are increased, relxd, relxu and relxt values are also increased above those specified on lines 19 to 21.

Line 23: The reason for increasing the relaxation factors was to speed up the convergence because it was found that at the start of the iterations for each $\chi(i)$ station, low relaxation factors were needed, but as the solution progresses higher relaxation factors can be used to reduce the solution time. The best indication of when to change the relaxation factors is to define a looser convergence criteria, "relxconcri", which is higher than the final convergence criteria as defined on line 31. Thus, when "relxconcri" is satisfied, the relaxation factors can be increased. Backup solution fields are kept in the event that the increased relaxation factors cause instabilities. In which case, the old relaxation values are used along with the solution fields that were saved. Two numbers are given on line 23: the first is the actual "relxconcri" value and the second value determines the type of double check needed to ensure that relxconcri is met. This double check is described in a later paragraph on the convergence criteria given on line 31.

Line 24: At each $\chi(i)$ station, an iterative method was required to obtain a set of converged solutions. To prevent the program from iterating to infinity, the maximum number of iterations was specified on line 24. Thus if the number of iterations exceeded "itermax" for a particular station, the program was instructed to stop. The choice for the value of "itermax" was dependent on the relaxation factors used, since a greater number of iterations was required when strong under-relaxation was applied.

Lines 25-30: The grid spacing is defined by lines 25 to 30. In the η direction, n and nv represent the number of nodes in the liquid and mixture, respectively. The number of nodes in the χ direction is given by m. The variable yvapor defines the thickness of the mixture boundary layer through the following relation:

$$\text{thickness of mixture layer} = \delta\,(\text{yvapor} - 1) \tag{4.132}$$

Non-uniform grid spacing was used to place more nodes in areas where most of the changes in the solution field occur and less nodes as the changes become smaller. Thus, non-uniform gird spacing were used in the χ direction to place more nodes near the leading edge of the plate. Likewise, in the η direction of the mixture layer, most of the changes occur near the interface, with the changes dropping to zero at the free stream (as given by yvapor). The algorithm used to obtain the non-uniform grid spacing in the χ direction and in the η direction of the mixture layer is given in Appendix B. Lines 28 and 30 define how tightly packed the nodes are at the start of the plate (factorm) and near the interface (factornv).

Line 31: On line 31 of the input file for steam-air, the convergence criterion is specified as the input variable "concri". For the sodium-argon and glycerine-bromine, line 31 contains two values. The first is the convergence criterion. The second value represents the type of double checking to be performed. There are three different types of double checking performed once the convergence criterion was satisfied. Type 1 is to increase the relaxation factors and perform one more iteration and then check to see if the convergence criterion was still satisfied with the higher relaxation factors. If it fails, then false convergence had occurred, and the program continues iterating using the new higher relaxation factors. Type 2 is to perform 100 more iterations using the current relaxation factors and then check to see if the convergence criterion was met between the solutions obtained at "iter" iterations and "iter +100" iterations. If it fails, then false convergence had occurred and the program continues the iteration process. Type 3 is the same as type 1, except that if it fails the double check, the program reuses the old solution field and relaxation factors to continue the iteration process.

Line 32: The values on line 32 defines which nodal temperature, velocity and gas concentrations to output during the iterative process. This information allows the user to get a feel for what the program is doing and to check if the program is heading toward convergence or divergence. There are two different formats for line 32. The first format was used for the steam-air program and contains five numbers. If the first number is 1, then the program uses the other four numbers to define which nodal values to output. The second and third numbers define the first and last j_L nodes of the liquid layer values to be printed. Likewise the fourth and fifth numbers define the first and last j nodes of the mixture solution filed to be printed. If the first number is 0, then no output is desired and the remaining numbers are ignored. For the other two mixtures (sodium-argon and glycerine-bromine), line 32 contains 10 numbers. Setting the first number to 1 lets the program know that outputs of the solution filed during the iteration is desired. Instead of printing out all the results between two defined nodal points, as done for the steam-air, these two programs only print out the nodal values for nodes incremented between the defined first and last nodes. The remaining 9 numbers are split into 3 sets of 3 numbers. For each set, the first number defines the first j node, the second number defines the last j node and the third number gives the increments. The first set is for the liquid velocity and temperature fields, the second set is for the mixture velocity and temperature fields, and the third set is for the gas concentrations in the mixture. To prevent large output files, only the last 100 iterations were written to file (except for the steam-air program where all iterations were printed out). Also, if no output is desired, set the first number to zero.

Line 33: The variable "icond" on line 33 should be set to 1 in order to use Equation (4.114) for evaluating δ. Setting "icond" to 0 will result in simplifying the energy

balance at the interface by neglecting the conduction to the interface from the mixture. This input variable is also used in conjunction with line 39 to neglect only the subcooling as explained later in this section.

Line 34: Checks were performed to ensure that the energy, momentum, continuity and gas species were balanced by setting "balout" on line 34 to 1. This caused the program to perform the balances after each iteration and write them to files.

Line 35: Line 35 gives the option to either use a linear slope for W at the interface in the discretization of the diffusion equation or to apply the interpolation formulae to obtain $dW/d\eta$ at the interface. The input variable "diffgrad" must be set to 0 to use the Equations given by (4.93) to (4.113) for the coefficients of the discretized diffusion equation since a linear slope was assumed for W at the interface. Setting "diffgrad" to 1 will cause the program to use the interpolation formula to obtain $dW/d\eta$ at the interface. Both methods gave very similar results, and in general, "diffgrad" was set to 0.

Line 36: For the cases of pure vapor, it wasn't necessary to solve the mixture energy equation since the vapor temperature remains uniform at T_∞. Thus, setting the input variable on line 36, "enerm", to 0 will cause the program to just assume a uniform T_∞ in the mixture and not solve the mixture energy equation.

Lines 37-39: Part of the focus of this thesis was to examine the effects of neglecting the inertia terms in the liquid momentum equation and also the effects of neglecting liquid convection and subcooling in the liquid energy equation. To remove the inertia terms from the liquid momentum equation, set the input variable "liqinertia" to 1. Likewise, setting "liqconv" to 1 will remove the energy convection terms from the liquid energy equation, thereby neglecting energy convection and subcooling in the liquid. If only subcooling is to be neglected, then set "liqsubcool" to 1 and also set "icond" to 2. To obtain the complete solution, set all three input variables; "liqinertia", "liqconv" and "liqsubcool" to 0.

Line 40: Line 40 is only used for the sodium-argon and glycerine-bromine programs. It contains the input variable "deltaguess" which is the guessed value for $\delta(i=2)$. It's use is described in Appendix C. If too high a value is used, the program will crash with $W_i > W_{max}$, because the large condensate thickness means a high condensation rate which results in a high gas concentration at the interface. Starting with too low a value is also not desirable because it means that more iterations may be required. A good value to use for "deltaguess" was found to be the value obtained from a converged solution. Thus for each substance, a trial and error method was employed

to obtain a solution. Then the converged value of $\delta(i=2)$ was used as "deltaguess" for each of the other cases. It should be noted that as $\chi(i=2)$ becomes closer to the leading edge, smaller values of "deltaguess" may be needed.

Lines 41-43: The last three lines in the input file for sodium-argon and glycerine-bromine are not important and should be left as 0.

4.4 Obtaining a Converged Solution

To obtain a converged solution, the following input variables described in Section 4.3 need to be varied: "concri", "yvapor", *n*, *nv*, and *m*. In theory, each one of these variables needs to be varied to ensure that the final solution, as given by the total heat transferred to the wall, is independent of these five variables.

To determine if the solution is independent of "concri", the program was run at two different convergence criteria, as shown in Table 4.1. These results obtained using a "concri" of 10^{-6} and 10^{-7} show that q_{wall} differs by only 0.001%. Thus, a convergence criteria of either 10^{-6} or 10^{-7} is sufficient for all cases.

The mixture layer thickness, as given by "yvapor", also must be specified by the user and must be high enough to ensure that free stream conditions are satisfied at the free stream edge of the specified mixture boundary. Comparison of results showed that the solution was independent of "yvapor" if du/dy and dW/dy at the mixture boundary were small

(less than 10^{-5}). Thus, for all cases, values of "yvapor" were selected such that du/dy and dW/dy were less than 10^{-9}.

To obtain a grid independent solution, the number of grid nodal points (n, nv and m) were doubled until further doubling resulted in a solution change of less than 0.5%. An example of this is shown in Table 4.1 where n is first doubled until the difference in q_{wall} is 0.0028%. Then nv is doubled until the difference in q_{wall} is 0.082%. Finally, tests on m were performed until the difference in q_{wall} reached 0.181%. Then two final runs were done to determine the combined effects of doubling all nodes. The first run was obtained using $n = 20$, $nv = 200$, and $m = 200$ and was compared to a second run using $n = 40$, $nv = 400$, and $m = 400$. These two runs show that doubling the number of nodes resulted in about 0.26% difference in q_{wall}.

Table 4.1: Sample convergence table for glycerine-bromine at T_∞ = 450 K, T_{wall} = 350 K, u_∞ = 5.0 m/s, W_∞ = 0.1, and length = 30.0 m.

Complete								
"relxd" 1.0		"relxu" 0.01		"relxt" 1.0	"relxw" 10^1, 10^3, 10 ("relxconcri" = 10^{-5})		"factornv" = 5000 "factorm" = 50000	
"concri"	n	nv	"yvapor"	m	q_{wall}	% difference	max. du/dy	max. dW/dy
10e-7	20	50	1e+03	50	5.086006e+04		5e-14	5e-15
10e-7	40	50	1e+03	50	5.085866e+04	0.0028	3e-14	4e-15
10e-7	20	50	1e+03	50	5.086006e+04		5e-14	5e-15
10e-7	20	100	1e+03	50	5.110250e+04	0.474	0.0	2e-14
10e-7	20	200	1e+03	50	5.120112e+04	0.193		
10e-7	20	200	1e+03	50	5.120112e+04			
10e-6	20	200	1e+03	50	5.119718e+04	0.001		
The above two runs with different concri show that the difference between using "concri" = 10e-07 or "concri" = 10e-6 is 0.001% difference in q_{wall} .								
10e-6	20	200	1e+03	50	5.119718e+04			
10e-6	20	400	1e+03	50	5.123910e+04	0.082		
10e-6	20	200	1e+03	50	5.119718e+04			
10e-6	20	200	1e+03	100	5.156412e+04	0.712		
10e-6	20	200	1e+03	200	5.175125e+04	0.362		
10e-6	20	200	1e+03	400	5.184527e+04	0.181	8e-14	4e-14
10e-6	20	200	1e+03	200	5.175125e+04			
10e-6	40	400	1e+03	400	5.188629e+04	0.26	3e-13	2e-13

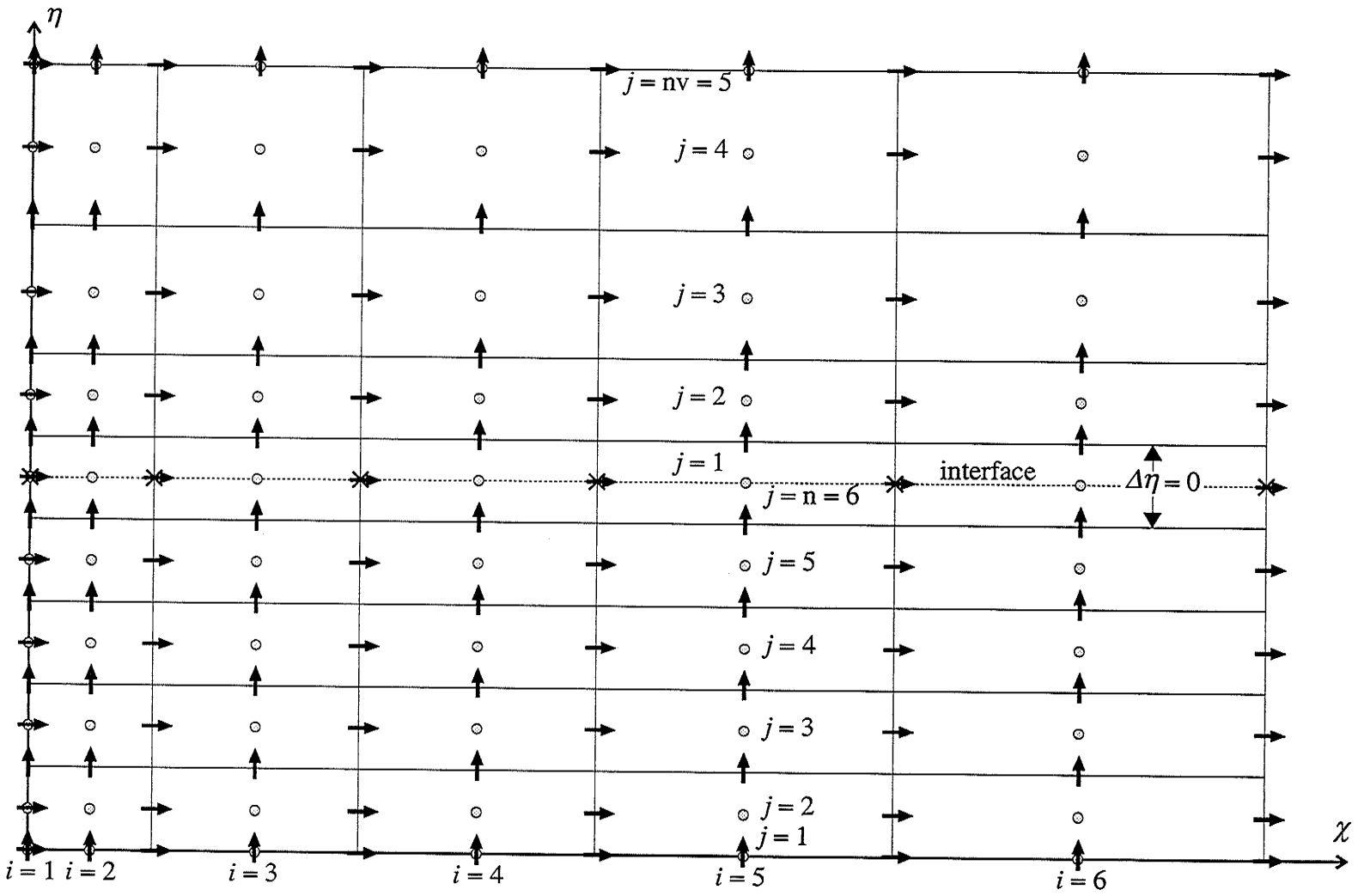

Figure 4.1: Orthogonal control volumes in the χ-η plane with staggered locations for u, T, W = ⊙; $\dot{m}_n$ = ↑; $\dot{m}_e$ = →; and δ = ×.

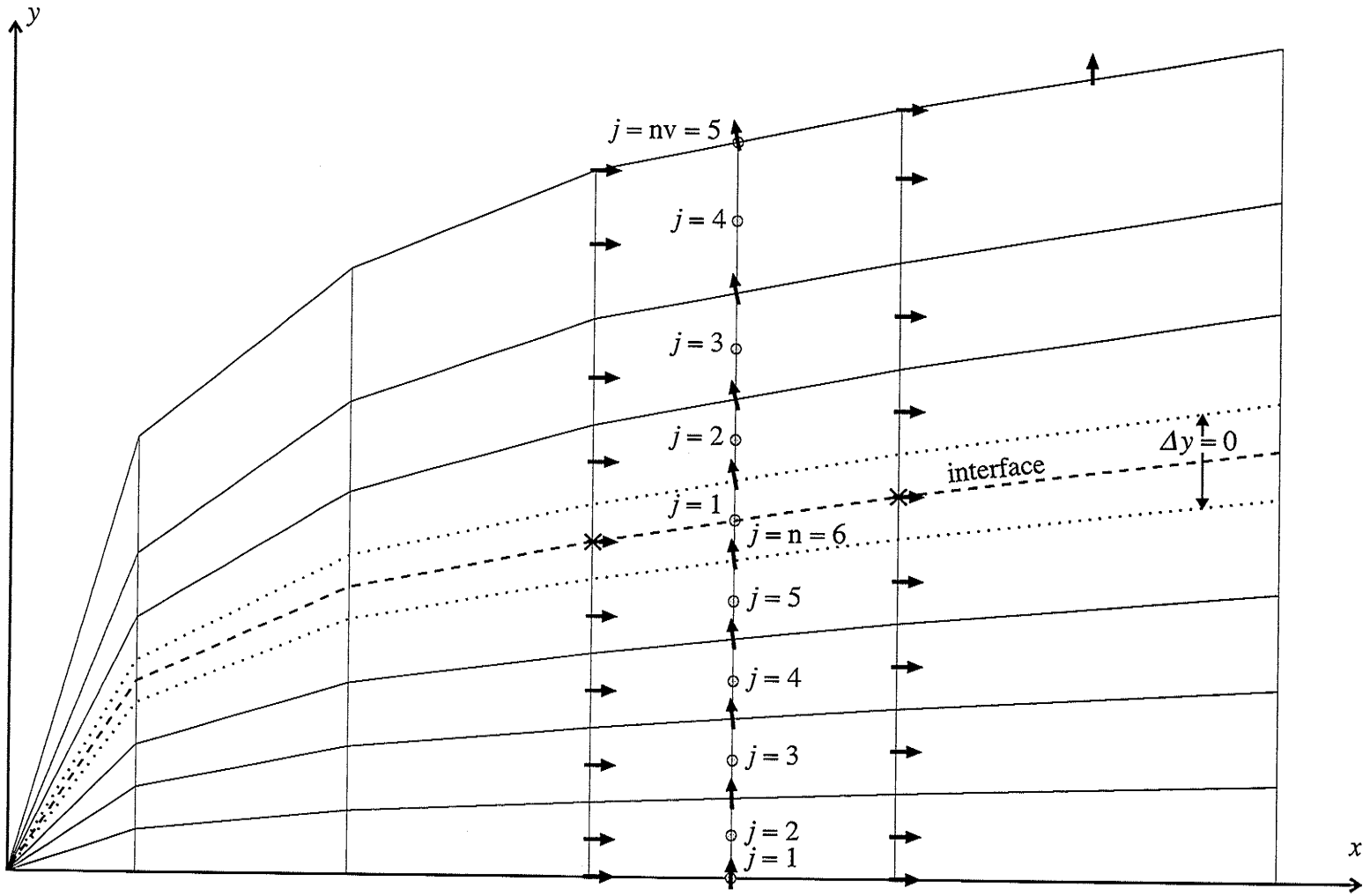

Figure 4.2: Non-orthogonal control volumes in the x-y plane with staggered locations for u, T, W = ○; $\dot{m}_n$ = ↑; $\dot{m}_e$ = →; and δ = ×.

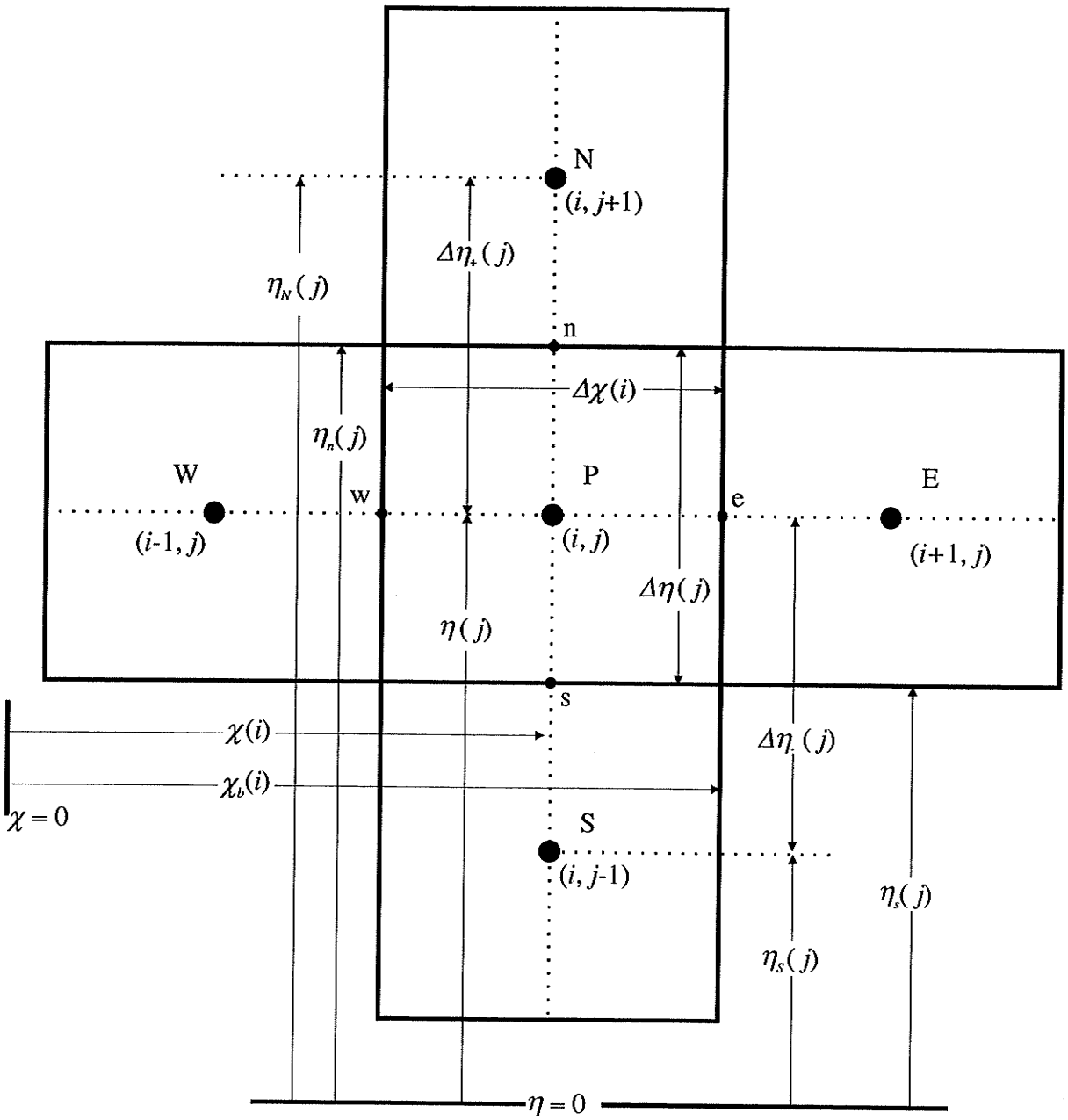

Figure 4.3: Nomenclature used to describe a control volume.

Line 1: 9.81	g (gravity, m/s^2)
Line 2: 0.0	theta (angle of inclination from vertical, degrees)
Line 3: 0.0	roliq (liquid density, kg/m^3)
Line 4: 0.0	visliq (liquid viscosity, $N \cdot s/m^2$)
Line 5: 0.0	cpliq (liquid specific heat, $J/kg \cdot K$)
Line 6: 0.0	kliq (liquid conductivity, $W/m \cdot K$)
Line 7: 0.0	rovap (vapor density, kg/m^3)
Line 8: 0.0	visvap (vapor viscosity, $N \cdot s/m^2$)
Line 9: 0.0	cpvap (vapor specific heat, $J/kg \cdot K$)
Line 10: 0.0	kvap (vapor conductivity, $W/m \cdot K$)
Line 11: 0.0	diffvap (diffusion coefficient, m^2/s)
Line 12: 380.0	tw (wall temperature, K)
Line 13: 400.0	tinf (temp at free stream, K)
Line 14: 5.0	uinf (free stream velocity, m/s)
Line 15: 1.0e-01	winf (free stream mass fraction)
Line 16: 0.0	hfgvap (latent heat, J/kg)
Line 17: 0.0	xstart (start of plate, m)
Line 18: 30.0	xend (end of plate, m)
Line 19: 0.9	relxd (relaxation factor for delta)
Line 20: 0.4	relxu (relaxation factor for U)
Line 21: 0.7	relxt (relaxation factor for T)
Line 22: 0.1	relxw (relaxation factor for W)
Line 24: 10000	itermax (maximum number of iterations)
Line 25: 80	n (nodes in y-dirn of liquid layer)
Line 26: 160	nv (nodes in y-dirn of vapor layer)
Line 27: 400.0	yvapor
Line 28: 2000	factornv
Line 29: 800	m (nodes in x-dirn)
Line 30: 50000	factorm
Line 31: 1.0e-7	concri
Line 32: 0,37,40,1,5	iterprint(1 for output of u,v,t between j1 and j2)
Line 33: 1	icond(set to 1 to use quadratic to solve for delta
Line 34: 0	balout(set to 1 to output balances..energy etc.)
Line 35: 1	diffgrad(0 for linear slope, 1 for EDS scheme)
Line 36: 1	enerm (1 to solve vapor mixture energy equation)
Line 37: 0	liqinertia (set to 1 to neglect liquid inertia terms)
Line 38: 0	liqconv (set to 1 to neglect liquid convection and subcooling)
Line 39: 0	liqsubcool (1 to neglect subcooling, also set icond = 2)

Figure 4.4: The input file for steam-air.

Line 1: 9.81	g (gravity, m/s^2)
Line 2: 0.0	theta(degree - angle of inclination from vertical, degrees)
Line 3: 0.0	roliq (liquid density, kg/m^3)
Line 4: 0.0	visliq (liquid viscosity, $N \cdot s/m^2$)
Line 5: 0.0	cpliq (liquid specific heat, $J/kg \cdot K$)
Line 6: 0.0	kliq (liquid conductivity, $W/m \cdot K$)
Line 7: 0.0	rovap (vapor density, kg/m^3)
Line 8: 0.0	visvap (vapor viscosity, $N \cdot s/m^2$)
Line 9: 0.0	cpvap (vapor specific heat, $J/kg \cdot K$)
Line 10: 0.0	kvap (vapor conductivity, $W/m \cdot K$)
Line 11: 0.0	diffvap (diffusion coefficient, m^2/s)
Line 12: 1000.0	tw (wall temperature, K)
Line 13: 1100.0	tinf (temp at free stream, K)
Line 14: 0.5	uinf (free stream velocity, m/s^2)
Line 15: 1.0e-03	winf (free stream mass fraction)
Line 16: 0.0	hfgvap (latent heat, J/kg)
Line 17: 0.0	xstart (start of plate, m)
Line 18: 0.3	xend (end of plate, m)
Line 19: 1.0	relxd (relaxation factor for delta)
Line 20: 1,0.5	relxu (relaxation factor for U)
Line 21: 1,0.025	relxt (relaxation factor for T)
Line 22: ..... 1.0e+02,1.0e+05,10	relxw (relaxation factor for W)
Line 23: 1.0e-05,1.0	relxconcri
Line 24: 2000000	itermax (maximum number of iterations)
Line 25: 40	n (nodes in y-dirn of liquid layer)
Line 26: 160	nv (nodes in y-dirn of vapor layer)
Line 27: 75.0	yvapor
Line 28: 2000	factornv
Line 29: 200	m (nodes in x-dirn)
Line 30: 200	factorm
Line 31: 1.0e-7,1	concri, dblchk
Line 32: 0,1,20,10,1,200,50,1,100,25	iterprint(1 for output of u,v,t
Line 33: 1	icond(set to 1 to use quadratic to solve for delta
Line 34: 0	balout(set to 1 to output balances..energy etc.)
Line 35: 0	diffgrad(0 for linear slope, 1 for EDS scheme)
Line 36: 1	enerm (1 to solve vapor mixture energy equation)
Line 37: 0	liqinertia (set to 1 to neglect liquid inertia terms)
Line 38: 0	liqconv (set to 1 to neglect liquid convection terms)
Line 40: 1.0e-07	deltaguess
Line 41: 0	dataprint12
Line 42: 0	inittype(0 for using deltaguess, 1 to using initsorm)
Line 43: 0	iabs(absolute value of the change is output at i)

Figure 4.5: The input file for sodium-argon.

Line 1: 9.81	g (gravity, m/s^2)
Line 2: 0.0	theta(degree - angle of inclination from vertical, degrees)
Line 3: 0.0	roliq (liquid density, kg/m^3)
Line 4: 0.0	visliq (liquid viscosity, $N \cdot s/m^2$)
Line 5: 0.0	cpliq (liquid specific heat, $J/kg \cdot K$)
Line 6: 0.0	kliq (liquid conductivity, $W/m \cdot K$)
Line 7: 0.0	rovap (vapor density, kg/m^3)
Line 8: 0.0	visvap (vapor viscosity, $N \cdot s/m^2$)
Line 9: 0.0	cpvap (vapor specific heat, $J/kg \cdot K$)
Line 10: 0.0	kvap (vapor conductivity, $W/m \cdot K$)
Line 11: 0.0	diffvap (diffusion coefficient, m^2/s)
Line 12: 350.0	tw (wall temperature, K)
Line 13: 450.0	tinf (temp at free stream, K)
Line 14: 5.0	uinf (free stream velocity, m/s)
Line 15: 1.0e-01	winf (free stream mass fraction)
Line 16: 0.0	hfgvap (latent heat, J/kg)
Line 17: 0.0	xstart (start of plate, m)
Line 18: 30.0	xend (end of plate, m)
Line 19: 0.1	relxd (relaxation factor for delta)
Line 20: 1,0.01	relxu (relaxation factor for U)
Line 21: 1,1.0	relxt (relaxation factor for T)
Line 22: ..... 1.0e+01,1.0e+03,10.0	relxw (relaxation factor for W)
Line 23: 1.0e-05,1.0	relxconcri
Line 24: 200000	itermax (maximum number of iterations)
Line 25: 40	n (nodes in y-dirn of liquid layer)
Line 26: 400	nv (nodes in y-dirn of vapor layer)
Line 27: ..... 1.0e+03	yvapor
Line 28: 5000	factornv
Line 29: 400	m (nodes in x-dirn)
Line 30: 50000	factorm
Line 31: 1.0e-6,3	concri, dblchk
Line 32: 0,1,40,5,1,200,50,1,100,20	iterprint(1 for output of u,v,t
Line 33: 1	icond(set to 1 to use quadratic to solve for delta
Line 34: 0	balout(set to 1 to output balances..energy etc.)
Line 35: 0	diffgrad(0 for linear slope, 1 for EDS scheme)
Line 36: 1	enerm (1 to solve vapor mixture energy equation)
Line 37: 0	liqinertia (set to 1 to neglect liquid inertia terms)
Line 38: 0	liqconv (set to 1 to neglect liquid convection terms)
Line 39: 0	liqsubcool
Line 40: 1.0e-05	deltaguess
Line 41: 0	dataprint12
Line 42: 0	inittype(0 for using deltaguess, 1 to using initsorm)
Line 43: 0	iabs(absolute value of the change is output at i)

Figure 4.6: The input file for glycerine-bromine.

Chapter 5

VALIDATION OF NUMERICAL RESULTS

To check the validity of the present numerical analysis, results were compared to previous work. Where possible, the present numerical analysis was carried out using the assumptions and simplifications used by previous authors. Some such simplifications were the use of constant properties, neglecting the liquid inertia terms in the momentum equation, and neglecting the energy convection terms in the liquid energy equation. The ability to compare with different authors show the versatility of the present numerical analysis in generating results for forced or quiescent condensation of a vapor, with or without a noncondensing gas.

For quiescent pure vapors, a solution for the complete two-phase boundary layer equations was developed by Koh *et al.* (1961) using a similarity transformation. Their model is identical to the present model for the special case of: $W_\infty = 0$, $u_\infty = 0$, $T = T_\infty$ and constant properties. A comparison between the present numerical solution (using constant properties) and those of Koh *et al.* is given in Table 5.1. These results are presented in terms of the independent dimensionless parameters Pr_L, Ja_L, and R and the dependent parameter q/q_{NU} as given in Koh *et al.*. It is important to note that their solution, using similarity transformation, resulted in constant q/q_{NU}. Also, the present numerical solution produced q/q_{NU} which was essentially invariant along x. For the range of independent parameters presented in Table 5.1, there is excellent agreement between the

present numerical solution and those of Koh *et al.*. With a typical deviation of less than 0.1% and the maximum deviation is less than 2%. These small deviations show that the computer code is properly solving the set of liquid conservation equations along with the vapor momentum equation and energy balance used to obtain the film thickness.

The dimensionless parameter q/q_{NU} in Table 5.1 shows the deviation of the present results from Nusselt's solution. This deviation is shown to be small for $\mathrm{Pr}_L = 1$. For viscous fluids, $\mathrm{Pr}_L = 810$, the deviation is up to 17% and for liquid metals, $\mathrm{Pr}_L = 0.003$, deviations of up to 53% are shown. These deviations can be attributed to Nusselt's assumptions that the liquid inertia, liquid energy convection and interfacial shear have negligible effect. These assumptions are not true for high and low Pr_L fluids.

Table 5.1: Comparison with Koh *et al.* (1961) for pure quiescent vapors.

Pr_L	$R = \sqrt{(\rho_L \mu_L)/(\rho \mu)}$	Ja_L	q/q_{NU}	
			Present Work	Koh *et al.* (1961)
0.003	600	8.746×10^{-2}	0.4634	0.4722
0.003	600	7.497×10^{-5}	0.9931	0.9940
1.0	10	7.442×10^{-1}	0.9945	0.9953
1.0	600	7.704×10^{-2}	0.9943	0.9951
810	10	1.290	1.173	1.174
810	600	8.282×10^{-2}	1.013	1.014

Cess (1960), Koh (1962) and Fujii and Uehara (1972) performed a constant property analysis of the forced convection condensation of a pure vapor on a horizontal flat plate.

Similar equations were used by all authors, except that both Cess and Fujii and Uehara neglected the inertia terms in the liquid momentum equation and the energy convection terms in the liquid energy equation. Their results are compared in Table 5.2 with the present numerical solution obtained with the complete equation set and constant properties. There is a good agreement between the present numerical solution and that of Koh for all Pr_L and Ja_L values presented. Likewise there is a good agreement between the results by Cess and those by Fujii and Uehara since they both neglected the same terms. A comparison between the present solution and that by Fujii and Uehara shows the importance of the missing terms. For low and high Pr_L fluids, the importance of the missing terms becomes more important at higher Ja_L.

Table 5.2: Comparison of horizontal flat plate results.

Pr_L	Ja_L	$H = \frac{Ja_L}{Pr_L}$	$R = \left[\frac{\rho_L \mu_L}{\rho \mu}\right]^{\frac{1}{2}}$	R H	$\frac{Nu}{\sqrt{Re_x}}$			
					Present Numerical Solution	Fujii and Uehara (1972)	Koh (1962)	Cess (1960)
0.003	3.0×10^{-2}	10	100	1000	0.186	0.478	0.19	0.50
0.003	3.0×10^{-3}	1.0	100	100	0.385	0.480	0.38	0.50
0.003	3.0×10^{-4}	0.1	100	10	0.486	0.491	0.49	0.50
1.0	0.1	0.1	100	10	0.491	0.491	0.49	0.50
1.0	0.01	0.01	100	1.0	0.584	0.585	0.58	0.59
100	10.0	0.1	100	10	0.657	0.491	0.76	0.50
100	1.0	0.01	100	1.0	0.645	0.585	0.68	0.59
100	0.3	0.003	100	0.3	0.779	0.745	0.79	0.75

Fujii and Uehara (1972) also performed a constant property analysis on the condensation of pure vapors on flat plates, including the cases of pure forced convection, pure free convection and mixed convection. Figures 5.1 to 5.3 compare their results with the constant property numerical solution for $\mathrm{Pr}_L = 1.0$, 100 and 0.003. Figure 5.1 shows that for $\mathrm{Pr}_L = 1.0$, there is a good agreement with their analysis at both limits of pure forced convection on a horizontal plate ($1/\mathrm{Fr}_x \to 0$) and pure free convection ($1/\mathrm{Fr}_x \to \infty$). Some deviation can be seen at intermediate values of $1/\mathrm{Fr}_x$ corresponding to mixed convection where similarity does not apply. For viscous liquids, Figure 5.2 shows that the liquid convection terms become important since Fujii and Uehara's results differ from the complete numerical model, but is in close agreement with the numerical solutions obtained without the liquid energy convection terms. For liquid metals, Figure 5.3 shows that the difference between the complete numerical solution and that of Fujii and Uehara is small at $\mathrm{Ja}_L = 3\times10^{-4}$, but increases with increasing Ja_L. Analysis by Fujii and Uehara predicts very small effect of Ja_L over the tested range, while our analysis predicts a much greater effect. It must be noted that in Table 5.2, our analysis for pure forced convection agreed very well with Koh *et al.* for the same range of R, Ja_L and Pr_L as presented in Figure 5.3. However, it must also be noted that the equation by Fujii and Uehara gives good accuracy only within the range of $0.01 \le R\,\mathrm{Ja}_L/\mathrm{Pr}_L \le 5$.

Denny *et al.* (1970) obtained numerical solutions for quiescent and forced convection condensation of liquid metals on vertical surfaces. They solved the complete liquid conservation equations, with constant properties, and approximated the effect of the

interfacial shear as the asymptotic value for a vapor boundary layer undergoing strong suction. The present numerical solution imposes the continuity of shear across the interface. Comparison of the results for pure sodium vapors is given in Table 5.3. For the range of parameters in Table 5.3, the deviation ranges from 4 to 10%.

Table 5.3: Comparison with Denny *et al.* (1970) for pure sodium ($x = 0.15$ m).

u_∞ [m/s]	T_∞ [K]	$(T_\infty - T_{wall})$ [K]	$h_x \times 10^{-5}$ [W/m^2 · K]		q/q_{NU}	
			Present Work	Denny *et al.*	Present Work	Denny *et al.*
0	833.3	1.667	3.899	3.548	0.9782	0.8902
0	833.3	5.556	2.763	2.511	0.9368	0.8511
0	1111.1	1.667	3.156	3.087	0.9820	0.9605
0	1111.1	5.556	2.253	2.173	0.9471	0.9134
15.24	833.3	1.667	5.892	5.417	1.478	1.359
15.24	1111.1	1.667	4.612	4.820	1.435	1.500

All of the above comparisons have been made to the condensation of pure vapors. For those cases, only the liquid conservation equations, vapor momentum and continuity equations and the energy balance for film thickness were solved. To validate the solution of the vapor energy and diffusion equations, comparisons to vapor-gas mixtures are required. The first comparison is to the work by Minkowycz and Sparrow (1966) on the condensation of a quiescent steam-air mixture on a vertical flat plate. They assumed a linear temperature profile, a parabolic velocity distribution, and zero interfacial shear in the liquid film. The present numerical solution was obtained using the complete equation set, along with the continuity of interfacial shear. Figure 5.4 shows excellent agreement

between the present numerical solution and those by Minkowycz and Sparrow. This indicates that the inertia and convection terms and interfacial shear have insignificant effects within the tested range of parameters.

Excellent agreement with the results by Denny *et al.* (1971) are shown in Figures 5.5 and 5.6 for the forced convection condensation of a steam-air mixture on a vertical flat surface. Denny *et al.* assumed a linear temperature and parabolic velocity distributions in the liquid film, while solving numerically in the mixture boundary layer, using governing equations similar to the present set of conservation equations. The good agreement for the steam-air mixtures at $T_\infty = 100\ ^\circ C$ is to be expected due to the small effects of inertia and convection terms in the liquid governing equations for these parameters.

A comparison was also made with the forced convection condensation of a sodium-argon mixture from Turner *et al.* (1973). Their analysis ignored the inertia forces, and energy convection in the liquid film. Other simplifications included setting $T_i = T_{wall}$ for high W_∞, setting $u_i = 0$ for high u_∞, neglecting subcooling in the liquid film, and neglecting the energy transfer due to mass diffusion in the mixture energy equation. They included the interfacial resistance, which was neglected in the present work. Four cases from Turner *et al.* are plotted in Figure 5.7, along with the present numerical solutions obtained with and without the liquid inertia terms (both solutions lie on the same curve). The present numerical solutions show that the effects of liquid inertia are insignificant for these four cases, either because of high W_∞ or low ΔT. Therefore, any deviations of Turner *et al.*'s

results from the present numerical solution cannot be attributed to the liquid inertia effects. For these four cases a fairly good agreement can be seen between the present results and those of Turner *et al.*. The case of $W_\infty = 1\times10^{-5}$ shows significant deviations at low x, probably due to the interfacial resistance, but the two solutions converge for larger x. The deviations in the other cases are not easy to explain, but may be attributed to the many simplifying assumptions adopted by Turner *et al.*.

Finally, a comparison was made with the constant property analytical solution of Rose (1980) for the forced convection condensation of a vapor-gas mixture on a horizontal flat surface. This was done by solving the present numerical model with variable properties. These results were then nondimensionalized by evaluating $Z_x = \mathrm{Sh}_x \, \mathrm{Re}_x^{-1/2}$, with mixture properties $(\rho, \mu \text{ and } D)$ evaluated at T_i and W_i , and the Sh_x number evaluated by:

$$\mathrm{Sh}_x = \frac{g_{mx}\, x}{\rho D} \tag{5.1}$$

$$\text{where:} \quad g_{mx} = -\frac{\rho D}{W_i - W_\infty}\frac{\partial W}{\partial y} \tag{5.2}$$

The gradient $\partial W/\partial y$ was evaluated at the interface. The Z_x values obtained from the numerical solution were then compared to the following implicit relation for Z_x as given by Rose:

$$Z_x + 0.941\,\mathrm{Sc}^{-0.21}(1-\omega)^{1.14}\, Z_x^{2.14} - \frac{\zeta}{\omega} = 0 \tag{5.3}$$

where: $$\omega = \frac{W_\infty}{W_i} \tag{5.4}$$

$$\zeta = \mathrm{Sc}^{1/2}\left(27.8 + 75.9\,\mathrm{Sc}^{0.306} + 657\,\mathrm{Sc}\right)^{-1/6} \tag{5.5}$$

To solve Equation (5.3), the W_i value from the numerical solution was used and Sc was calculated using properties evaluated at T_i and W_i (from the numerical solution). Rose also gives a simpler, less accurate relation for Z_x:

$$Z_x = \frac{\left\{1 + 4.57\,\mathrm{Sc}^{-0.04}\,\zeta\left(\frac{1-\omega}{\omega}\right)\right\}^{1/2} - 1}{2.28\,\mathrm{Sc}^{-0.04}(1-\omega)} \tag{5.6}$$

which was used as the starting value in the iterative solution of Equation (5.3). Rose's relations for Z_x values, as given by (5.3) was compared to the Z_x value obtained from the numerical solution in Tables 5.4 to 5.6 for steam-air, glycerine-bromine and sodium-argon mixtures, respectively. For each mixture, Z_x was evaluated at two axial locations and found to be essentially invariant along x, so the results for only one axial location was presented. In the column containing the results by Rose, the percentage deviation of Rose from the numerical solution is given in parenthesis. Table 5.4 shows the comparison with a steam-air mixture at $T_\infty = 400$ K, $T_{wall} = 380$ K, $u_\infty = 5.0$ m/s and $W_\infty = 10^{-3}$, 10^{-2} and 10^{-1}. There are no clear trends in the deviation of Equation (5.3) from the present numerical solution, with errors ranging from 0.0155% to 5.86%. A comparison is shown for a glycerine-bromine mixture at $T_\infty = 450$ K, $T_{wall} = 350$ K, $u_\infty = 20.0$ m/s and $W_\infty = 10^{-3}$, 10^{-2}, 10^{-1} and 0.5 in Table 5.5. Results for the numerical solution with and without the liquid energy convection terms are shown. The deviation of Equation (5.3)

from the complete numerical solution ranges from about 1% to 18% with less error at lower W_∞. Similar deviations are shown for the numerical solution obtained without the liquid energy convection terms. Table 5.6 shows the results for a sodium-argon mixture at $T_\infty = 1100$ K, $T_{wall} = 1000$ K, $u_\infty = 5.0$ m/s and $W_\infty = 10^{-5}$, 10^{-4} and 10^{-3}. Equation (5.3) deviated between 2% to 18% from the complete numerical solution and similar errors were also found when comparing Rose's results to the numerical solution obtained without the liquid inertia terms.

Table 5.4: Comparison with Rose (1980) for a steam-air mixture at $T_\infty = 400$ K, $T_{wall} = 380$ K and $u_\infty = 5.0$ m/s.

W_∞	Complete			
	W_i	Sc	Z_x ($x = 4.50\times10^{-2}$ m)	
			Numerical	Rose
10^{-3}	6.855×10^{-3}	0.5656	0.9997	0.9887 (1.10%)
10^{-2}	6.390×10^{-2}	0.5679	0.9494	0.9493 (0.0155%)
10^{-1}	3.753×10^{-1}	0.5809	0.6516	0.6898 (5.86%)

Table 5.5: Comparison with Rose (1980) for a glycerine-bromine mixture at $T_\infty = 450$ K, $T_{wall} = 350$ K and $u_\infty = 20.0$ m/s.

W_∞	Complete				No Energy Convection Terms			
	W_i	Sc	Z_x ($x = 4.30\times10^{-2}$ m)		W_i	Sc	Z_x ($x = 4.30\times10^{-2}$ m)	
			Numerical	Rose			Numerical	Rose
10^{-3}	4.323×10^{-3}	0.6680	0.7765	0.7866 (1.30%)	4.738×10^{-3}	0.6680	0.8219	0.8321 (1.25%)
10^{-2}	4.250×10^{-2}	0.6716	0.7641	0.7797 (2.03%)	4.644×10^{-2}	0.6720	0.8068	0.8235 (2.07%)
10^{-1}	3.595×10^{-1}	0.7037	0.6562	0.7126 (8.60%)	3.827×10^{-1}	0.7063	0.6787	0.7418 (9.30%)
5×10^{-1}	9.253×10^{-1}	0.7779	0.4044	0.4768 (17.9%)	9.313×10^{-1}	0.7790	0.4054	0.4791 (18.2%)

Table 5.6: Comparison with Rose (1980) for a sodium-argon mixture at T_∞ = 1100 K, T_{wall} = 1000 K and u_∞ = 5.0 m/s.

W_∞	Complete				No Liquid Inertia Terms			
	W_i	Sc	Z_x ($x = 6.22\times10^{-3}$ m)		W_i	Sc	Z_x ($x = 6.22\times10^{-3}$ m)	
			Numerical	Rose			Numerical	Rose
10-5	0.5290	0.5698	103.08	85.17 (17.5%)	0.4880	0.5454	96.14	80.91 (15.8%)
10-4	0.7337	0.7329	36.80	35.93 (2.37%)	0.7299	0.7290	36.39	35.79 (1.66%)
10-3	0.7695	0.7722	10.93	12.48 (14.2%)	0.7692	0.7718	10.92	12.48 (14.3%)

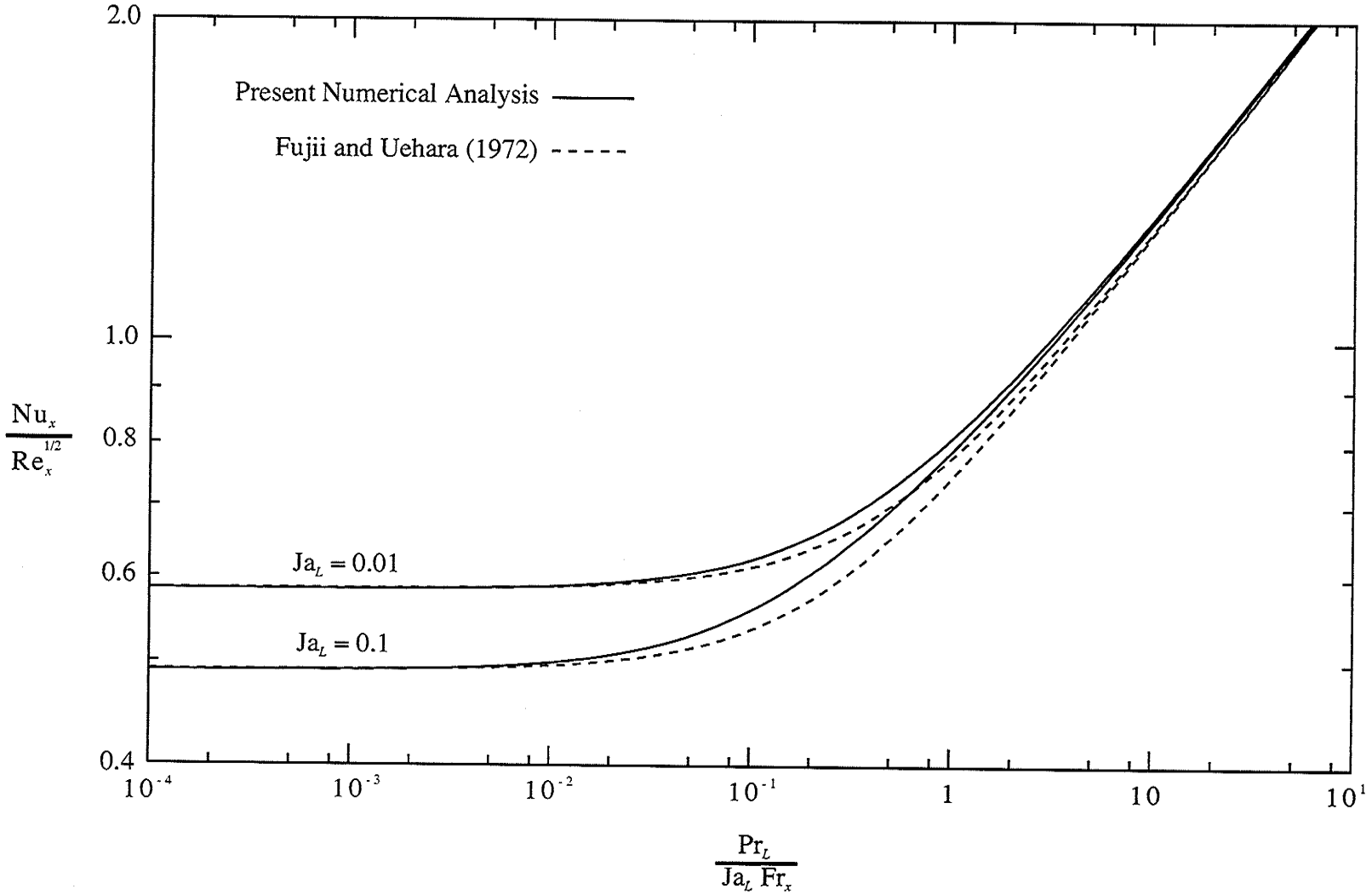

Figure 5.1: Comparison with Fujii and Uehara (1972) at $Pr_L = 1.0$ and $R = 100$.

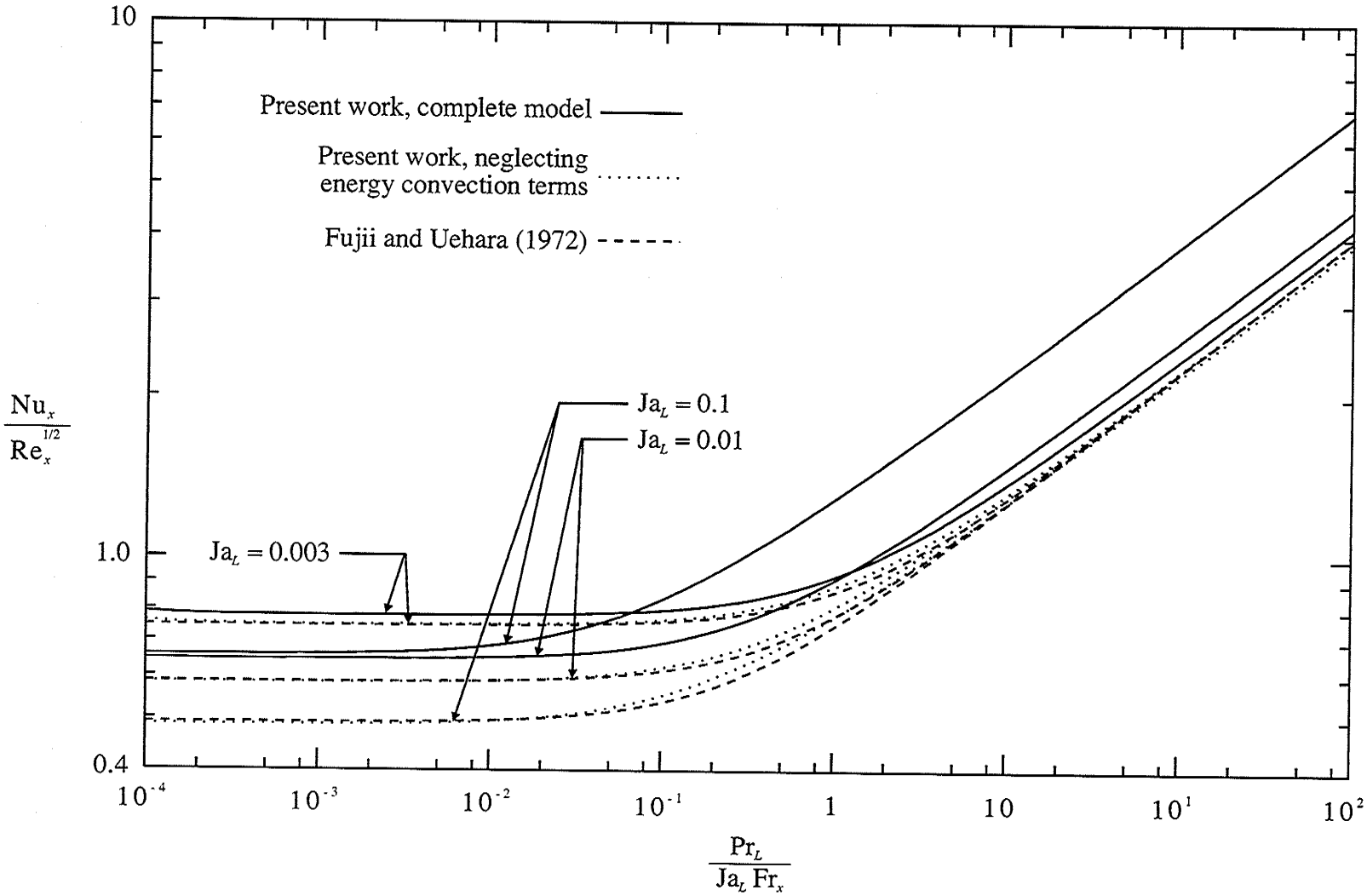

Figure 5.2: Comparison with Fujii and Uehara (1972) at $Pr_L = 100.0$ and $R = 100$.

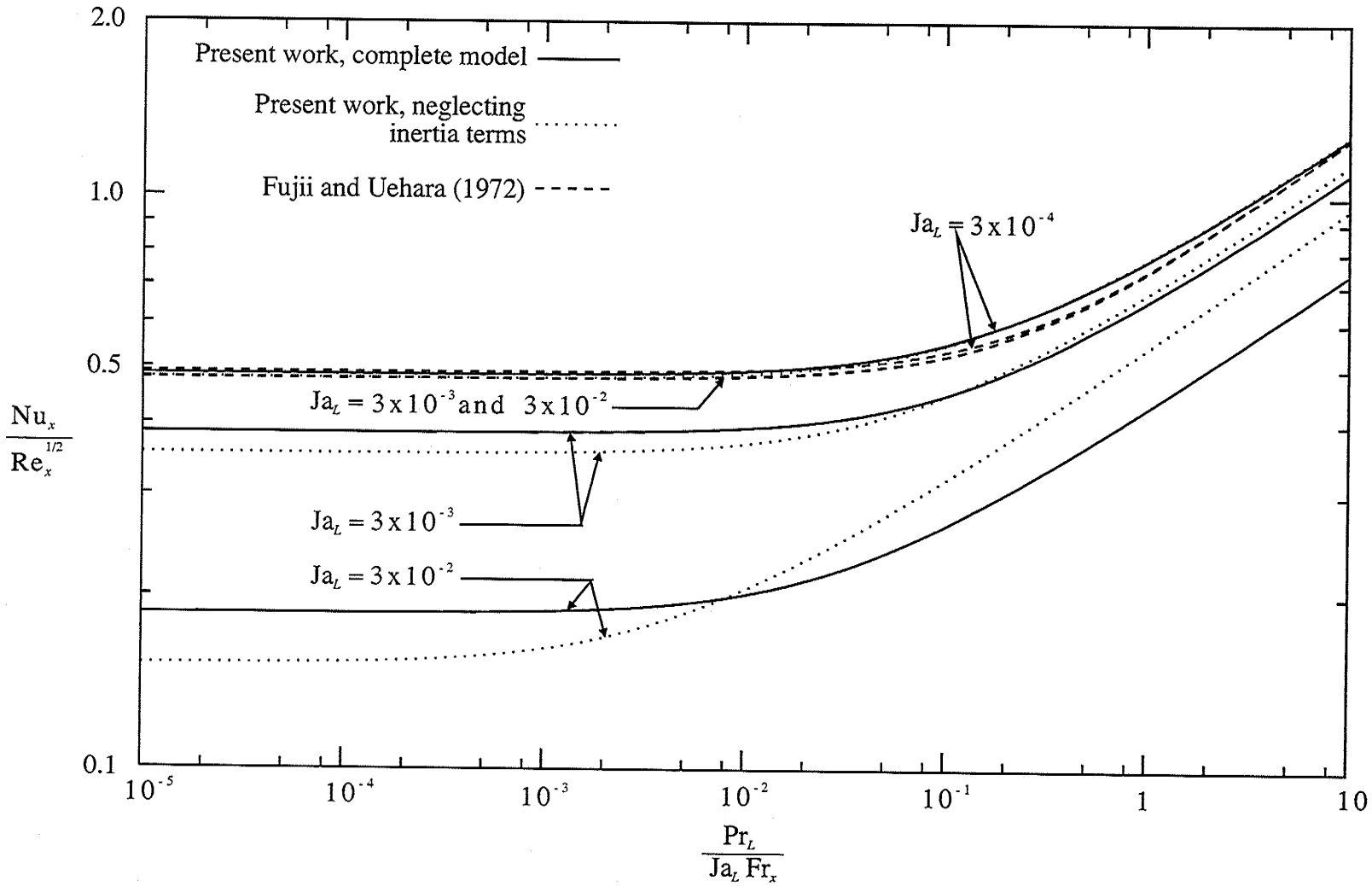

Figure 5.3: Comparison with Fujii and Uehara (1972) at $Pr_L = 0.003$ and $R = 100$.

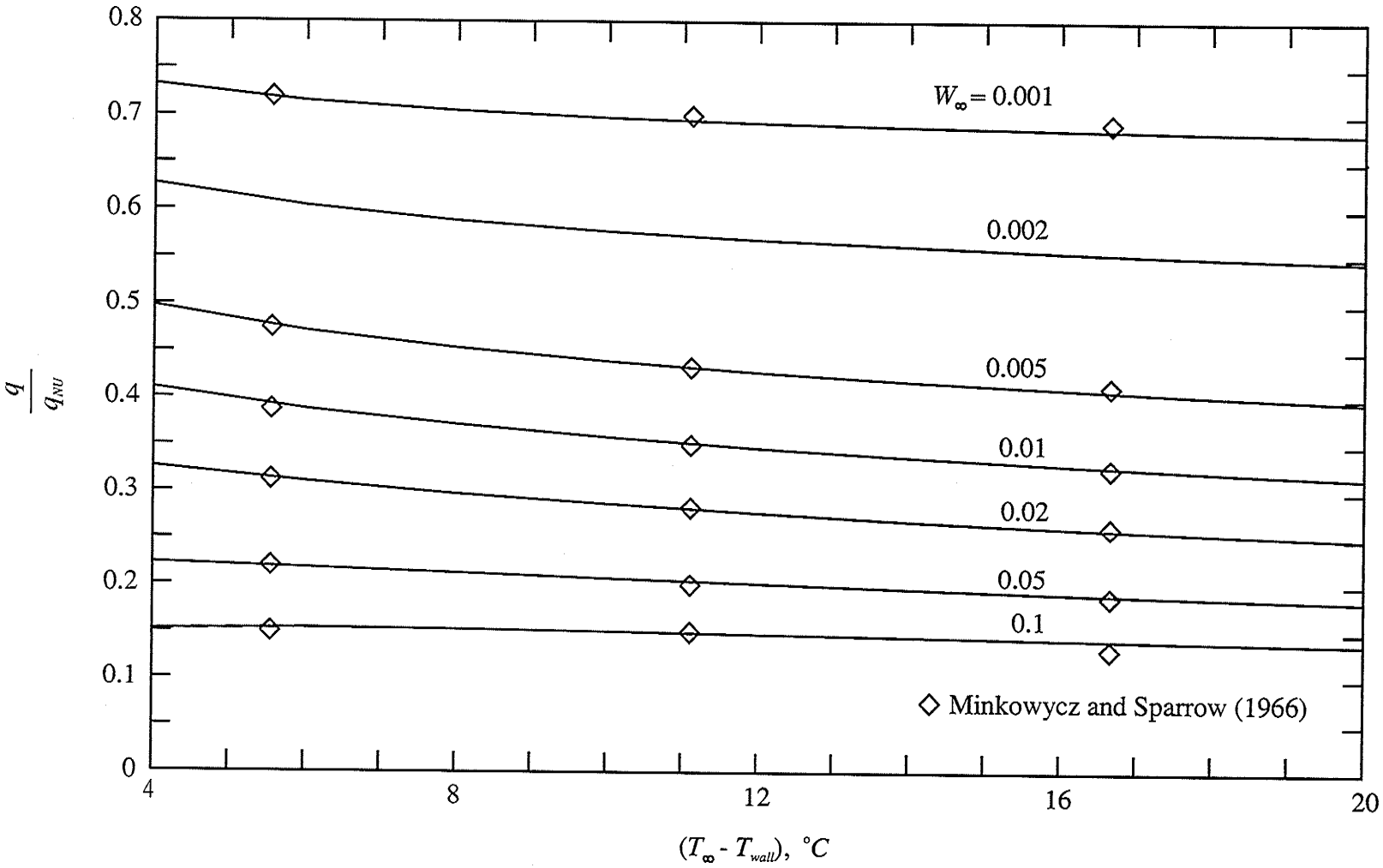

Figure 5.4: Comparison with Minkowycz and Sparrow (1966) for a steam-air mixture at $T_\infty = 100°C$ and $u_\infty = 0$.

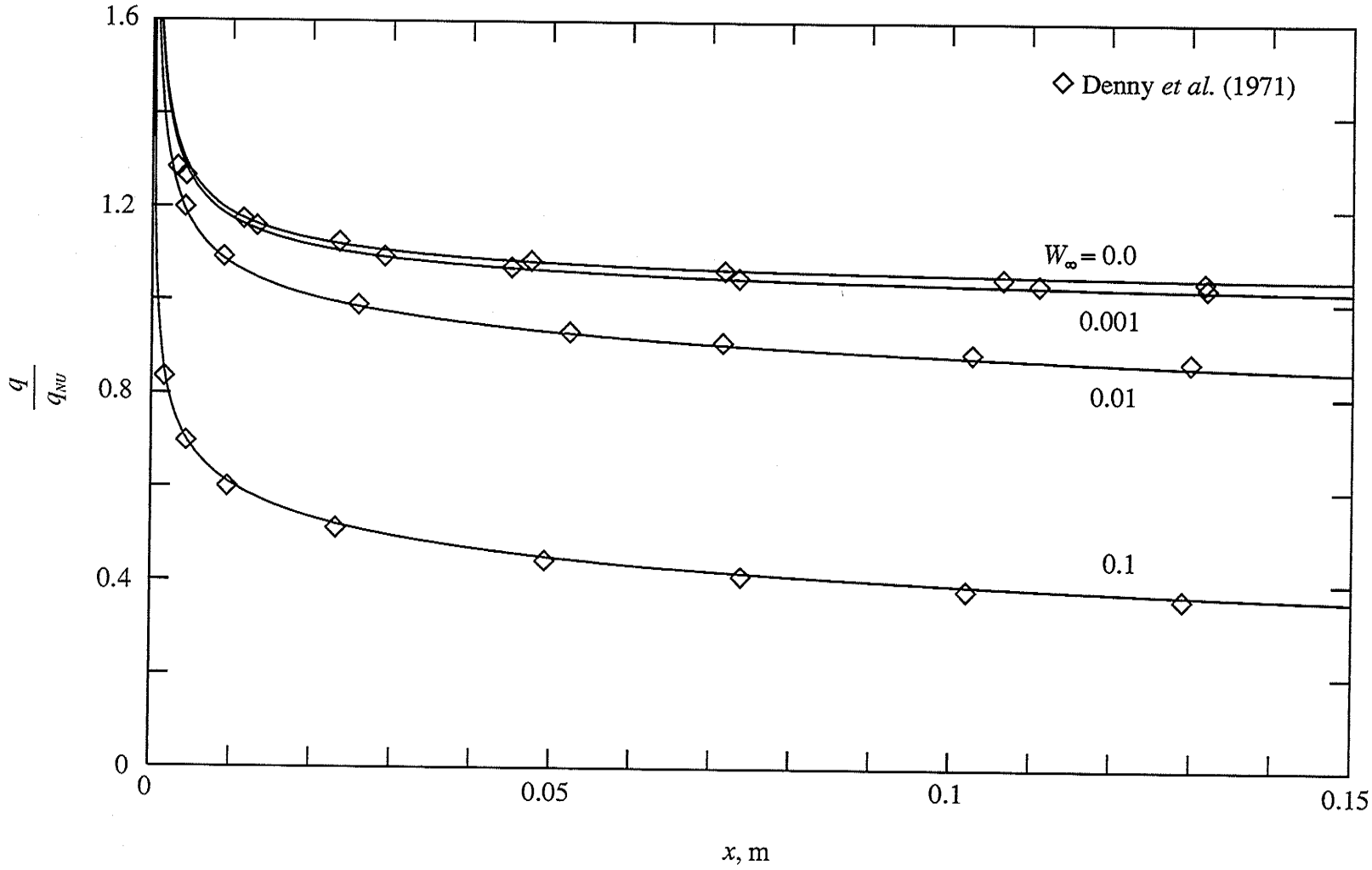

Figure 5.5: Axial distribution of $\frac{q}{q_{NU}}$ for a steam-air mixture at $T_\infty = 100\,°C$, $T_{wall} = 77.8\,°C$, and $u_\infty = 3.05$ m/s.

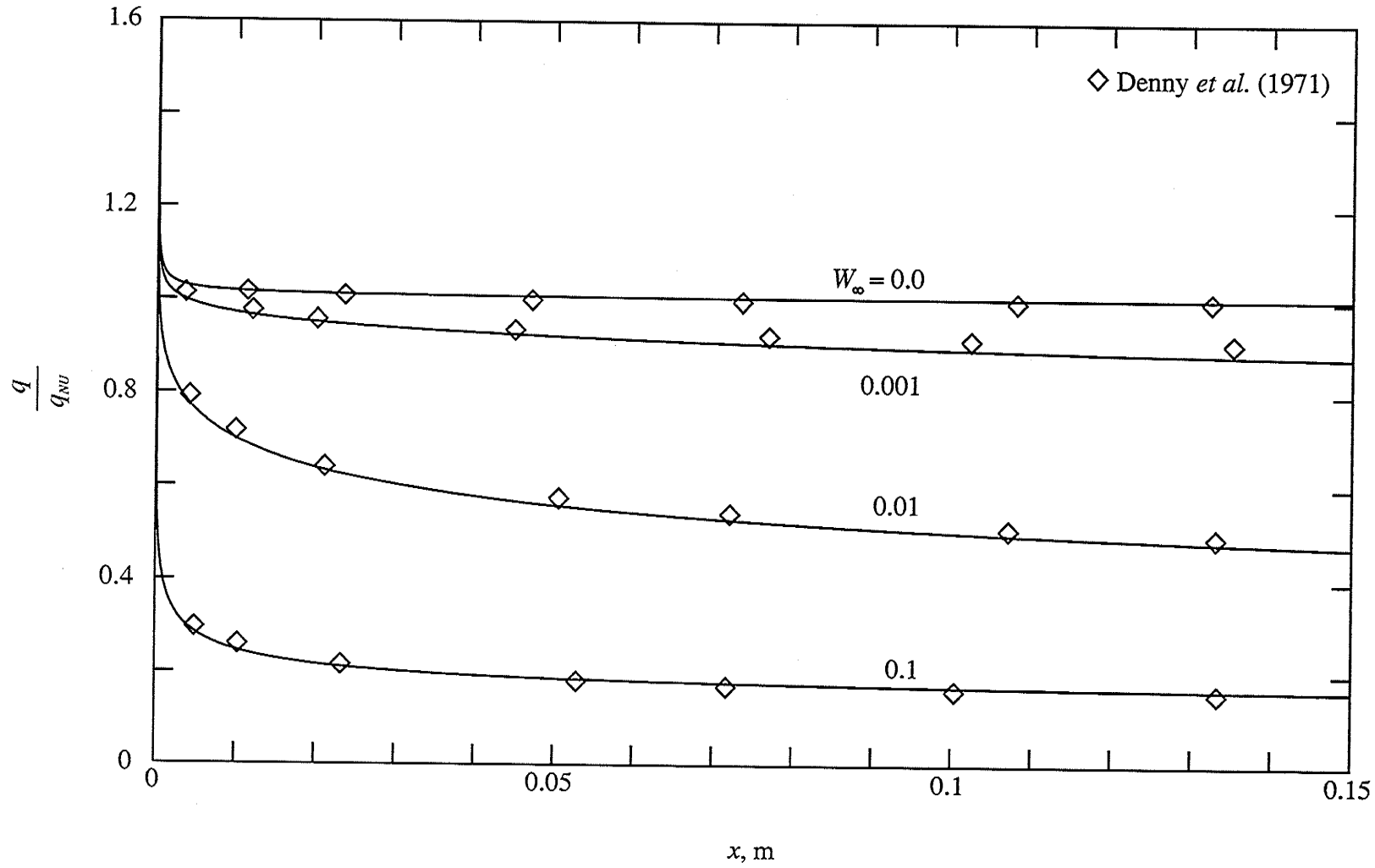

Figure 5.6: Axial distribution of $\frac{q}{q_{NU}}$ for a steam-air mixture at $T_\infty = 100\,^\circ C$, $T_{wall} = 77.8\,^\circ C$, and $u_\infty = 0.305$ m/s.

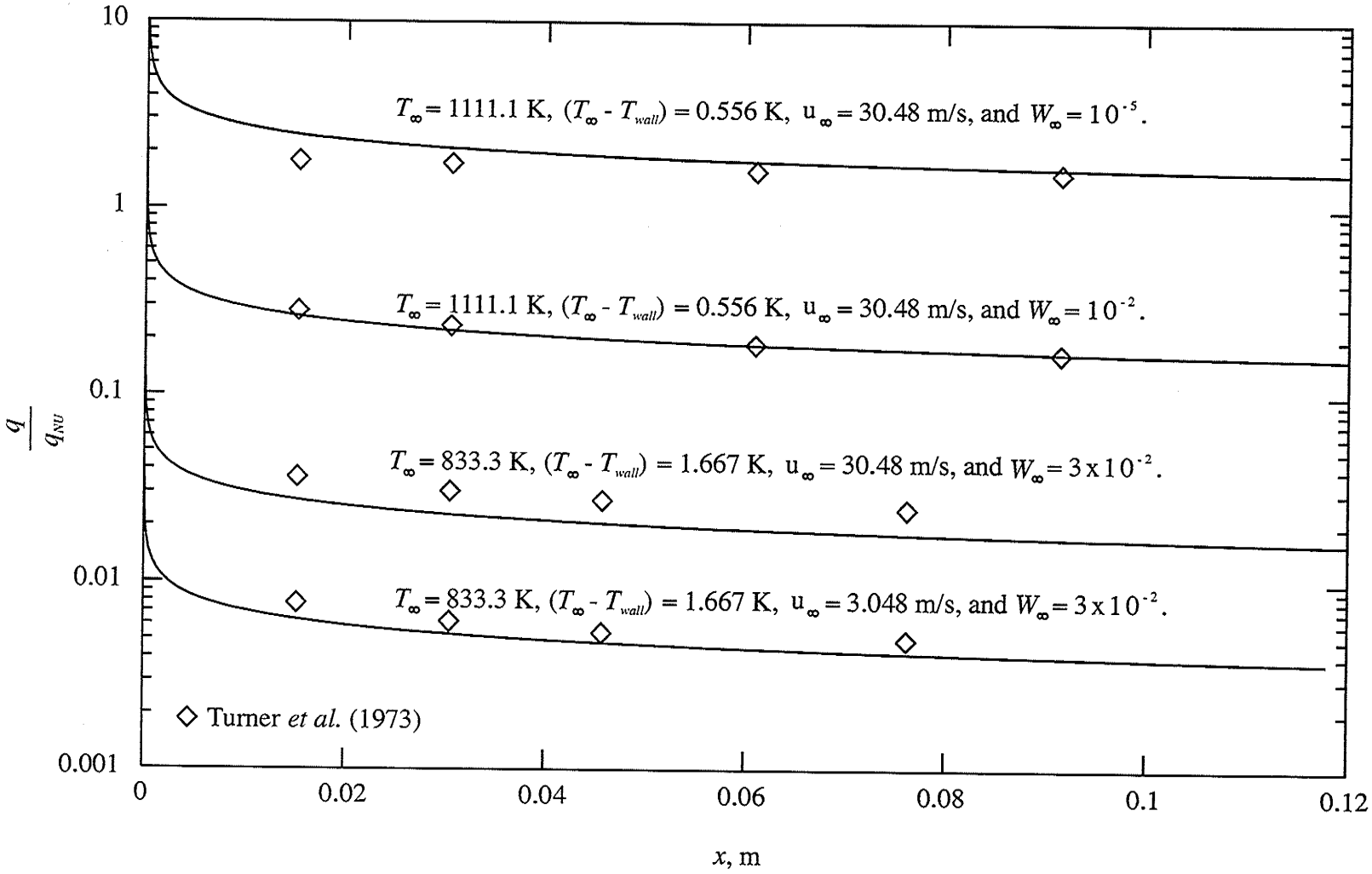

Figure 5.7: Comparison with Turner *et al.* (1973) for sodium-argon.

Chapter 6

RESULTS AND DISCUSSION

Rearranging the governing equations in a nondimensional form resulted in a set of dimensionless groups that eliminates the independent effects of x, u_∞, g, and the angle of inclination. Details of this analysis are shown in Appendix D. Although this nondimensionalization was performed for constant properties, the dimensionless groups were found to be still valid for the present variable property analysis. This was demonstrated by obtaining variable property results for different cases at various u_∞ and g. The numerical results were then nondimensionalized using properties evaluated at $T_r = T_{wall} + 0.31(T_\infty - T_{wall})$. Plotting them showed that the results at different u_∞ and g collapsed onto the same curve.

The heat transfer results can be presented by plotting $Nu_x\, Re_x^{-1/2}$ *vs.* Fr_x^{-1}, where:

$$\frac{1}{Fr_x} = \frac{g\, x \cos\alpha}{u_\infty^{\,2}} \tag{6.1}$$

Thus, a single plot can be used to show the axial variation of Nu_x for all values of x, g, α and u_∞. This dimensionless axis also shows the limiting case of horizontal forced convection at $1/Fr_x = 0$ and the limiting case of quiescent condensation on a vertical plate at $1/Fr_x = \infty$. Likewise, plots of W_i and δ^* *vs.* $1/Fr_x$ show the variations for all values of

x, g, α and u_∞. The dimensionless groups for velocity, temperature and concentration across the liquid and mixture layers can also be plotted against y^* at different values of $1/\mathrm{Fr}_x$.

Three vapor-gas mixtures are selected to demonstrate the effects over a wide Pr_L range. The vapor-gas mixture combinations are: steam-air ($\mathrm{Pr}_L \approx 2$), sodium-argon ($\mathrm{Pr}_L \approx 0.006$) and glycerine-bromine ($\mathrm{Pr}_L \approx 1000$). The numerical code is used to obtain solutions to the complete boundary layer equations. Results are then obtained neglecting either the liquid inertia or the liquid energy convection terms. The effect of neglecting the inertia or energy convection terms is then demonstrated by comparing the simplified model results to the complete solution results.

6.1 Steam-Air Mixture

Results obtained without the liquid inertia terms show negligible deviations from the complete solutions, and likewise the effects of the liquid energy convection terms are also negligible. Thus, no results are shown for solutions without the liquid inertia or energy convection terms.

The heat transfer results for steam-air mixtures at $T_\infty = 400$ K and $T_{wall} = 380$ K are plotted in terms of $\mathrm{Nu}_x \mathrm{Re}_x^{-1/2}$ *vs.* Fr_x^{-1} in Figure 6.1 for four different values of W_∞.

The asymptotic limit, $1/\mathrm{Fr}_x \to 0$, has been found by solving the appropriate forced convection, on a horizontal plate, case and are plotted. In the figure, each curve starts out from the limiting case of horizontal forced convection and increases with $1/\mathrm{Fr}_x$. The increase in $\mathrm{Nu}_x \mathrm{Re}_x^{-1/2}$ is greater for lower gas concentrations, showing that the presence of a noncondensable gas suppresses the condensation process along the plate. Finally the value of $\mathrm{Nu}_x \mathrm{Re}_x^{-1/2}$ is unbounded, approaches infinity, as $1/\mathrm{Fr}_x \to \infty$, which is the expected behaviour for quiescent condensation on a vertical plate

A similar plot for a steam-air mixture with varying ΔT is shown in Figure 6.2 at $T_\infty = 400$ K, for $W_\infty = 0.0$ and 0.1. The effect of ΔT is to decrease the heat transfer coefficient as ΔT is increased. The trend is the same for both $W_\infty = 0.0$ and 0.1.

6.2 Sodium-Argon Mixture

Solutions obtained for the sodium-argon mixture without the liquid energy convection terms show negligible deviation from the complete solution. Thus, this chapter will only examine the effects of the liquid inertia terms on the condensation of a sodium-argon mixture.

The heat transfer for forced convection condensation on a vertical or inclined plate of a sodium-argon mixture at $T_\infty = 1100$ K and $T_{wall} = 1000$ K, are plotted in terms of

$\mathrm{Nu}_x \mathrm{Re}_x^{-1/2}$ *vs.* Fr_x^{-1} in Figure 6.3 for four different W_∞ values. The limiting cases of horizontal forced convection condensation are also displayed. Each curve starts out from the limiting case of horizontal forced convection and increases with $1/\mathrm{Fr}_x$. This increase in $\mathrm{Nu}_x \mathrm{Re}_x^{-1/2}$ over the horizontal limit is due to the presence of gravity acting on the increasing liquid thickness, causing the liquid film to flow faster and become thinner. The thinner liquid film allows for a higher energy conduction, resulting in an increase in heat transfer. The improvement in heat transfer over the horizontal limit is much more significant with lower gas concentrations, showing that the presence of a noncondensable gas (argon) suppresses the condensation process along the plate. Comparing results obtained with argon to the case of pure sodium shows the detrimental effects of the argon gas. Even a tiny amount of argon gas in the free stream ($W_\infty = 1\times10^{-5}$) is sufficient to cause a 33% decrease in heat transfer at low $1/\mathrm{Fr}_x$ with the deviation becoming greater at higher $1/\mathrm{Fr}_x$. This figure also shows that at a relatively high (for sodium-argon mixture) gas concentration, $W_\infty = 1\times10^{-3}$, the condensation is suppressed such that even for an inclined plate, there isn't much increase in heat transfer over the horizontal limiting value.

The effect of ΔT on $\mathrm{Nu}_x \mathrm{Re}_x^{-1/2}$ is shown in Figure 6.4 for pure sodium. These results show that lowering ΔT increases Nu_x. The heat flux is given by $q = h_x \Delta T$, and an examination of the Nu_x values show that while h_x is lower for higher ΔT, the difference in h_x is insufficient to offset the higher value of ΔT. Thus the heat transfer is still higher at higher ΔT.

The effect of the liquid inertia terms on heat transfer for the cases plotted in Figure 6.3 is shown by comparing the results from the complete solution, $Nu_{x,CP}$, with results obtained without the inertia terms, $Nu_{x,NI}$ in terms of their ratio $Nu_{x,NI}/Nu_{x,CP}$. This comparison is plotted in Figure 6.5 and it shows the effect of the liquid inertia terms for all values of x, u_∞, g and plate angles including the horizontal limit ($1/Fr_x = 0$) and the free convection limit ($1/Fr_x \to \infty$). Each curve starts from low values of $1/Fr_x$ where $Nu_{x,NI}/Nu_{x,CP}$ is less than unity in all cases. The curves then rise above one to reach the free convection limit (shown at $1/Fr_x = 100$). From the figure, it appears that each curve crosses $Nu_{x,NI}/Nu_{x,CP} = 1$ at $1/Fr_x \approx 0.1$. However, this is due to the scale chosen for the independent variable and the data table inset in the figure shows that the point where each curve crosses $Nu_{x,NI}/Nu_{x,CP} = 1$ ranges between $0.11179 \le 1/Fr_x \le 0.042481$. An attempt was made to explain the inversion by examining the solution profiles along the plate. The temperature profiles were similar for the range of $1/Fr_x$ studied, essentially linear in the liquid, and a curved profile from T_i to T_∞ in the mixture. Examination of the velocity profiles showed the flow characteristics change from vapor dragging the liquid film (at the horizontal limit, low $1/Fr_x$) to liquid dragging the mixture (at the free convection limit, high $1/Fr_x$). This change is reflected in the direction of the interfacial shear force where the interfacial shear is positive when the vapor is dragging the liquid film, and negative when the liquid is dragging the mixture. Although the direction of the shear force for the two solutions (with and without the liquid inertia terms) changes at

slightly different values of $1/\mathrm{Fr}_x$, it is still close to where $\mathrm{Nu}_{x,\mathrm{NI}}/\mathrm{Nu}_{x,\mathrm{CP}} = 1$. One of the most revealing facts from this figure is that the effects of the liquid inertia terms decrease with increasing free-stream gas concentrations. Thus, with $W_\infty = 1\times10^{-3}$, the effects of the liquid inertia are essentially negligible.

The interfacial gas concentrations for the results plotted in Figure 6.5 are displayed in Figure 6.6. The W_i is independent of Fr_x for both horizontal forced convection and free convection and is plotted as the limits in Figure 6.6. The results for three different values of W_∞ are shown with and without the liquid inertia terms. For all cases, W_i increases along the plate from the horizontal limit to the quiescent vertical plate limit. These curves also show that the liquid inertia effects are most prominent for lower W_∞, and that the inertia terms are more important at lower $1/\mathrm{Fr}_x$, before the two curves cross each other. The point where the two solutions cross over occurs is at a different $1/\mathrm{Fr}_x$ value than in Figure 6.5.

Figure 6.7 shows plots of δ^* *vs.* $1/\mathrm{Fr}_x$ for several values of W_∞. The results show the dimensionless film thickness increasing along the plate for all u_∞, g and plate inclinations (within the range of $1/\mathrm{Fr}_x$ studied) for solutions obtained with and without the liquid inertia terms. The effect of the liquid inertia terms is greatest at $W_\infty = 0$, and decreases with increasing W_∞, becoming insignificant for $W_\infty = 1\times10^{-3}$. The δ^* for the complete solution is thinner than the no-inertia results near the start of the plate (low $1/\mathrm{Fr}_x$).

However, as the solution progresses down the plate, the two film thickness cross over, and then the liquid film for the complete solution becomes thicker than the δ^* obtained without the inertia terms.

The film Reynolds number is given in Figure 6.8 as a plot of $\mathrm{Re}_\delta/\sqrt{\mathrm{Re}_x}$ *vs.* $1/\mathrm{Fr}_x$ for four different W_∞ values. This figure can be used to check if the flow is laminar by satisfying the following condition:

$$\mathrm{Re}_\delta < 30 \tag{6.2}$$

This figure shows that the curves become flatter with higher W_∞. Since the numerical solution is only valid for the laminar region, cases with higher W_∞ will be able to progress further down the plate before hitting the transition region. For example, on a vertical flat plate with $u_\infty = 0.5$ m/s, $g = 9.81$ m/s^2, $T_\infty = 1100$ K and $T_{wall} = 1000$K, the point at which transition occurs, x_δ, for $W_\infty = 0.0$ is 6.64×10^{-5} metres. Increasing W_∞ to 10^{-3} will increase x_δ to 1.38×10^{-3} metres.

Selected velocity, temperature and concentration profiles are plotted for a sodium-argon mixture at $T_\infty = 1100$ K and $T_{wall} = 1000$ K, as shown in Figures 6.9 to 6.11. These profiles are plotted at two different axial locations ($1/\mathrm{Fr}_x = 0.7538$ and 11.6164). Examination of the velocity profiles in Figure 6.9 shows a thicker film for $W_\infty = 0.0$ and a much higher velocity than for $W_\infty = 1\times10^{-3}$. It may appear from Figure 6.9 that for $W_\infty = 0.0$, the liquid always flows faster than the mixture. However, for all forced

convection cases (except for a horizontal plate), the flow starts off with the mixture flowing faster than the liquid film. The liquid film accelerates because of the gravity force. As the liquid film becomes thicker, it will continue to accelerate and eventually the liquid will flow faster than the mixture. It is not possible to see those details in just two velocity profiles. Examination of the profiles obtained with the complete solution and the solution without the liquid inertia terms shows that the liquid inertia terms are only important for $W_\infty = 0.0$, and at $W_\infty = 1\times10^{-3}$, there is not much difference in the velocity profiles.

The temperature profiles shown in Figure 6.10 show the profiles at $1/\mathrm{Fr}_x = 0.7538$ and 11.6164 for $W_\infty = 0.0$ and 1×10^{-3}. For the liquid layer, the temperature profile is essentially linear. The slight deviations are due to the use of variable properties. The range of the independent variable, y^*, is not wide enough to show the complete liquid temperature profile for $W_\infty = 0.0$. It is unnecessary since they continue in a relatively straight line to reach $T^* = 1.0$. The different slopes for $W_\infty = 0.0$ for the solutions with and without the liquid inertia terms are due to the different film thickness. For $W_\infty = 1\times10^{-3}$, the liquid temperature rises almost linearly from $T^* = 0$ to T_i^*, then the mixture temperature curves to $T^* = 1$. Comparison of the temperature profiles obtained with and without the inertia terms show that it is important at $W_\infty = 0.0$ and is negligible at $W_\infty = 1\times10^{-3}$.

The concentration profiles for $W_\infty = 1\times10^{-5}$ and 1×10^{-3} are shown in Figure 6.11. These profiles are plotted at $1/\mathrm{Fr}_x = 0.7538$ and 11.6164. They show the increase in W_i down the plate, with the increase being greater for the lower W_∞. At the same axial location (or $1/\mathrm{Fr}_x$), the slope of the W profile is much greater for the lower W_∞. Subsequently, the mixture boundary layer is much thinner for the lower W_∞. This figure also reinforces the idea that the inertia terms are only important at low W_∞ and become negligible at higher W_∞.

6.3 Glycerine-Bromine Mixture

Solutions obtained for a glycerine-bromine mixture without the liquid inertia terms show negligible deviation from the complete solution. Thus, this chapter will only examine the effects of the liquid energy convection terms on the condensation of a glycerine-bromine mixture.

The effect of bromine on the heat transfer results for forced convection condensation of glycerine on a vertical or inclined plate at $T_\infty = 450$ K and $T_{wall} = 350$ K, is plotted in terms of $\mathrm{Nu}_x \mathrm{Re}_x^{-1/2}$ *vs.* Fr_x^{-1} in Figure 6.12 for five different W_∞ values. The limiting case of forced convection condensation on a horizontal plate is also displayed. For each curve, $\mathrm{Nu}_x \mathrm{Re}_x^{-1/2}$ starts out from the limiting case of horizontal forced convection and increases with $1/\mathrm{Fr}_x$. This increase in heat transfer along $1/\mathrm{Fr}_x$ is much more significant at lower

W_∞ and there isn't much of an increase for $W_\infty = 5\times10^{-1}$ for much of the range of $1/\mathrm{Fr}_x$ studied. This shows the significance that the presence of bromine gas has on the condensation of glycerine, especially at higher $1/\mathrm{Fr}_x$. The limiting case of quiescent condensation occurs as $1/\mathrm{Fr}_x \to \infty$, for which $\mathrm{Nu}_x\,\mathrm{Re}_x^{-1/2}$ is unbounded, which is clearly shown by the direction of the curves for $W_\infty = 0.0$ and 1×10^{-3}.

A similar plot showing the effect of ΔT on the condensation of pure glycerine is shown in Figure 6.13. This figure shows no consistent trend in $\mathrm{Nu}_x\,\mathrm{Re}_x^{-1/2}$ for increasing ΔT. However, this is just due to the evaluation of properties at $T_r = T_{wall} + 0.31(T_\infty - T_{wall})$. Thus T_r is not the same for each case, resulting in a different set of properties used in the nondimensionalization for each ΔT. It is the difference in properties that result in the inconsistent behaviour for $\mathrm{Nu}_x\,\mathrm{Re}_x^{-1/2}$ at different ΔT. Examination of the heat flux at the wall still show that a higher heat transfer occurs at higher ΔT.

The effect of energy convection terms in the liquid energy equation on the heat transfer for the cases plotted on Figure 6.12 are shown in Figure 6.14. This figure shows a plot of $\mathrm{Nu}_{x,\mathrm{NC}}/\mathrm{Nu}_{x,\mathrm{CP}}$ over a range of $1/\mathrm{Fr}_x$ values. $\mathrm{Nu}_{x,\mathrm{NC}}$ is the local Nusselt number obtained without the energy convection terms in the liquid energy equation and $\mathrm{Nu}_{x,\mathrm{CP}}$ is the results from the complete solution. The figure shows the effect of the energy convection terms for all values of x, u_∞, g and plate angles, including the horizontal limits ($1/\mathrm{Fr}_x = 0$) and the free convection limit ($1/\mathrm{Fr}_x \to \infty$) for the complete results. The

general trend for the horizontal limit is that increasing W_∞ results in a lower $\mathrm{Nu}_{x,\mathrm{NC}}/\mathrm{Nu}_{x,\mathrm{CP}}$, indicating a greater effect of the energy convection terms. The reverse is true of the general trend for the free convection limit where, in general, increasing W_∞, increases $\mathrm{Nu}_{x,\mathrm{NC}}/\mathrm{Nu}_{x,\mathrm{CP}}$. The exception for the free convection limit is for $W_\infty = 1\times10^{-3}$, where the limiting value of $\mathrm{Nu}_{x,\mathrm{NC}}/\mathrm{Nu}_{x,\mathrm{CP}}$ is lower than that for $W_\infty = 0.0$. Each curve starts from the horizontal limit and decreases with increasing $1/\mathrm{Fr}_x$. For the pure case, the curve flattens out at the quiescent limit. However, for the other four cases with bromine, it appears that the curves all decrease until a minimum value is reached, then they rise to their quiescent asymptotes. An attempt was made to determine the cause of the minimum by examining the local profiles and also the saturated pressure-temperature relationship. No clear trend, however, was found that led to an explanation of the phenomena. This figure shows that, depending on the W_∞ and $1/\mathrm{Fr}_x$ the errors resulting from neglecting the energy convection terms can be as high at 12%, for $W_\infty = 0.1$, even though the end limits are roughly 5% and 2%.

The interfacial gas concentrations for the cases studied in Figure 6.14 are plotted in Figure 6.15. For the horizontal and free convection limiting cases, W_i is constant and is shown as asymptotic values in the figure. The W_i curves for each of the four different W_∞ values are presented with and without the liquid energy convection terms. All the curves increase from their horizontal limit and rise in an "S"– shaped curve to the free convection limit. In all cases, neglecting the energy convection terms resulted in larger value of W_i.

Figure 6.16 shows a plot of δ^* *vs.* $1/\mathrm{Fr}_x$. For the range of $1/\mathrm{Fr}_x$ shown, it is difficult to examine the effect of the energy convection terms on the film thickness since all curves are very close together. For $W_\infty = 0.5$, the film thickness for the complete solution, is thinner than the solution without the energy convection terms at low $1/\mathrm{Fr}_x$, but the curves cross as $1/\mathrm{Fr}_x$ increases. For the pure case, the complete solution always predicts a thinner liquid film. However, in all cases, the difference between the two solutions is very small.

The film Reynolds number is shown in Figure 6.17 as a plot of $\mathrm{Re}_\delta/\sqrt{\mathrm{Re}_x}$ *vs.* $1/\mathrm{Fr}_x$. This figure is used along with Equation (6.2) to determine the laminar region. It shows that the presence of the bromine gas inhibits the condensation process and allows for a much longer laminar region. For example, using the results of the figure for $u_\infty = 5$ m/s, $g = 9.81$ m/s^2 and $\alpha = 0$, the start of the transition occurs at $x_\delta = 11.9$ metres for $W_\infty = 0.0$. Increasing W_∞ to 10^{-2} will increase x_δ to 17.4 metres and for $W_\infty = 0.1$ and 0.5, x_δ is greater than 30 metres.

Selected velocity, temperature and concentration profiles are plotted for a glycerine-bromine mixture at $T_\infty = 450$ K and $T_{wall} = 350$ K, as shown in Figures 6.18 to 6.20. These profiles are plotted at two different axial locations ($1/\mathrm{Fr}_x = 0.051007$ and 11.6145). Examination of the velocity profiles for $W_\infty = 0.0$ shows a thicker film and a higher velocity than for $W_\infty = 0.1$. For the range of $1/\mathrm{Fr}_x$ studied, the liquid is always flowing

slower than the mixture. Examination of the profiles from the complete solution to the solution without the liquid energy convection terms show that the liquid energy convection terms are only important for $W_\infty = 0.0$, and at $W_\infty = 0.1$, there no significant difference in the velocity profiles.

The temperature profiles in Figure 6.19 show the profiles at $1/\mathrm{Fr}_x = 0.051007$ and 11.6145 for $W_\infty = 0.0$ and 0.1. The temperature profiles for $W_\infty = 0.0$ only vary in the liquid, until it reaches $T^* = 1.0$ at the liquid-mixture interface and then remains at $T^* = 1.0$ throughout the mixture. Although all the liquid temperatures profiles look linear, they are not. The complete solution temperature profile is not linear because of the inclusion of the energy convection and variable properties. The other solution, neglecting the liquid energy convection terms, is not linear because of the variable properties. For $W_\infty = 0.1$, the interfacial temperature decreases with increasing $1/\mathrm{Fr}_x$. This is consistent with the increasing W_i with increasing $1/\mathrm{Fr}_x$. The limited range of y^* doesn't show the mixture temperature rising with a curved profile to reach $T^* = 1.0$. Comparison of the temperature profiles obtained with and without the liquid energy convection terms show that the terms have an important effect at $W_\infty = 0.0$ and have negligible effect at $W_\infty = 0.1$.

Gas mass fraction profiles for $W_\infty = 0.001$ and 0.1 are shown in Figure 6.20. The profiles are plotted at $1/\mathrm{Fr}_x = 0.051007$ and 11.6145. These results show an increase in W_i down the plate (increasing $1/\mathrm{Fr}_x$), with a greater relative increase for lower W_∞. The

concentration boundary layer is also much thinner for lower W_∞ or $1/\mathrm{Fr}_x$. Also, this figure shows that the effect of the energy convection terms on the W profiles mirror the differences shown in Figure 6.14.

6.4 Prandtl Number Effect

The effect of Prandtl Number can be seen by comparing the results obtained for the steam-air mixture ($\mathrm{Pr}_L \approx 2$), sodium-argon mixture ($\mathrm{Pr}_L \approx 0.006$) and glycerine-bromine ($\mathrm{Pr}_L \approx 1000$). Although the effect of the inertia terms were shown only for the sodium-argon mixture, results obtained showed that these terms had insignificant effect on steam, and also didn't effect the higher Pr_L fluids such as glycerine. Likewise, the energy convection terms didn't have significant affects on the steam-air results or the lower Pr_L fluid such as sodium.

Examination of Figures 6.1, 6.3 and 6.12 show that the effect of W_∞ is most significant for the low Pr_L fluid, and decreases with increasing Pr_L. For example, for sodium-argon with $W_\infty = 1\times10^{-3}$, the heat transfer was severely reduced when compared with higher Pr_L fluids.

The W_i plots given by Figure 6.6 for sodium-argon and Figure 6.15 for glycerine-bromine show the reason why a tiny concentration of W_∞ has a much more significant effect on the condensation of sodium than on glycerine. These figures show that with a concentration

of $W_\infty = 1\times10^{-3}$, the argon builds up to a very high concentration (over 75%) at the interface for the entire range of $1/\mathrm{Fr}_x$, whereas the bromine concentration at the interface remains under 10% for about half of the $1/\mathrm{Fr}_x$ range, and then it builds to $W_i = 60\%$ around $1/\mathrm{Fr}_x = 100$. Thus, the higher W_i over much of the range of $1/\mathrm{Fr}_x$ for the sodium severely inhibits the condensation process, which significantly lowers $\mathrm{Nu}_x\,\mathrm{Re}_x^{-1/2}$ (when compared to their respective pure results).

The dimensionless film thickness plotted in Figure 6.7 for sodium-argon and in Figure 6.16 for glycerine-bromine makes it difficult to do a direct comparison between the two because of the different properties. However, a direct comparison between the actual film thickness along the plate length reveal that for $W_\infty = 0.0$, the film thickness for sodium is greater than that of the glycerine.

The plots of the film Reynolds number on Figures 6.8 and 6.17, for sodium-argon and glycerine-bromine respectively, indicate that the glycerine-bromine mixture will remain laminar further down the plate. This has been validated by comparing the axial location along the plate where transition from laminar to turbulent occurs in several specific test cases.

Comparison of the velocity profiles for sodium-argon in Figure 6.9 with glycerine-bromine in Figure 6.18 show that the velocity of the sodium is much greater than that of glycerine. It is difficult to compare the temperature and gas concentration profiles

because different values of W_∞ were used. However, it should be noted that the mixture boundary layers are much thicker for the glycerine-bromine mixtures.

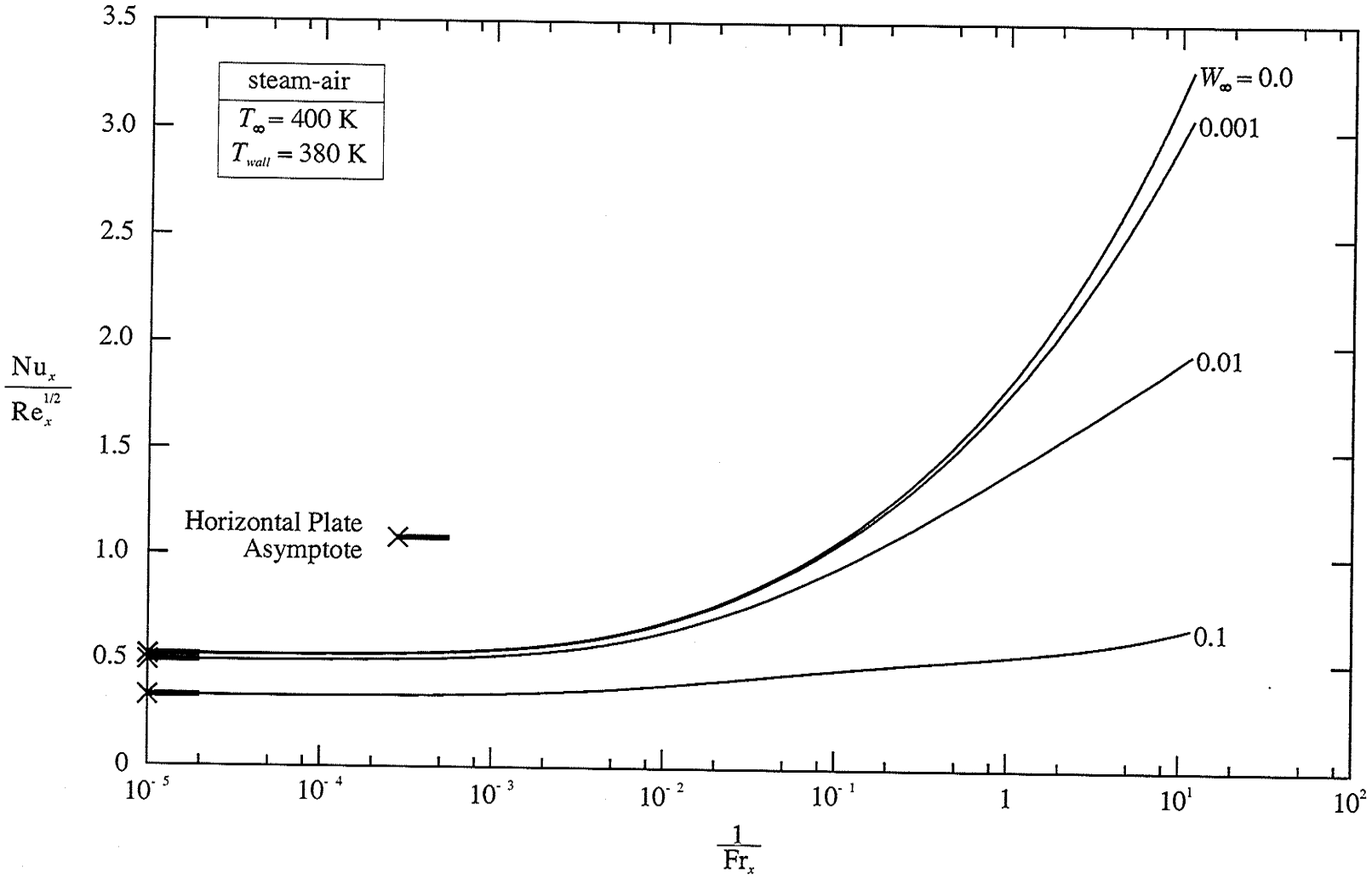

Figure 6.1: Effect of W_∞ on the heat transfer for a steam-air mixture at $T_\infty = 400$ K, and $T_{wall} = 380$ K.

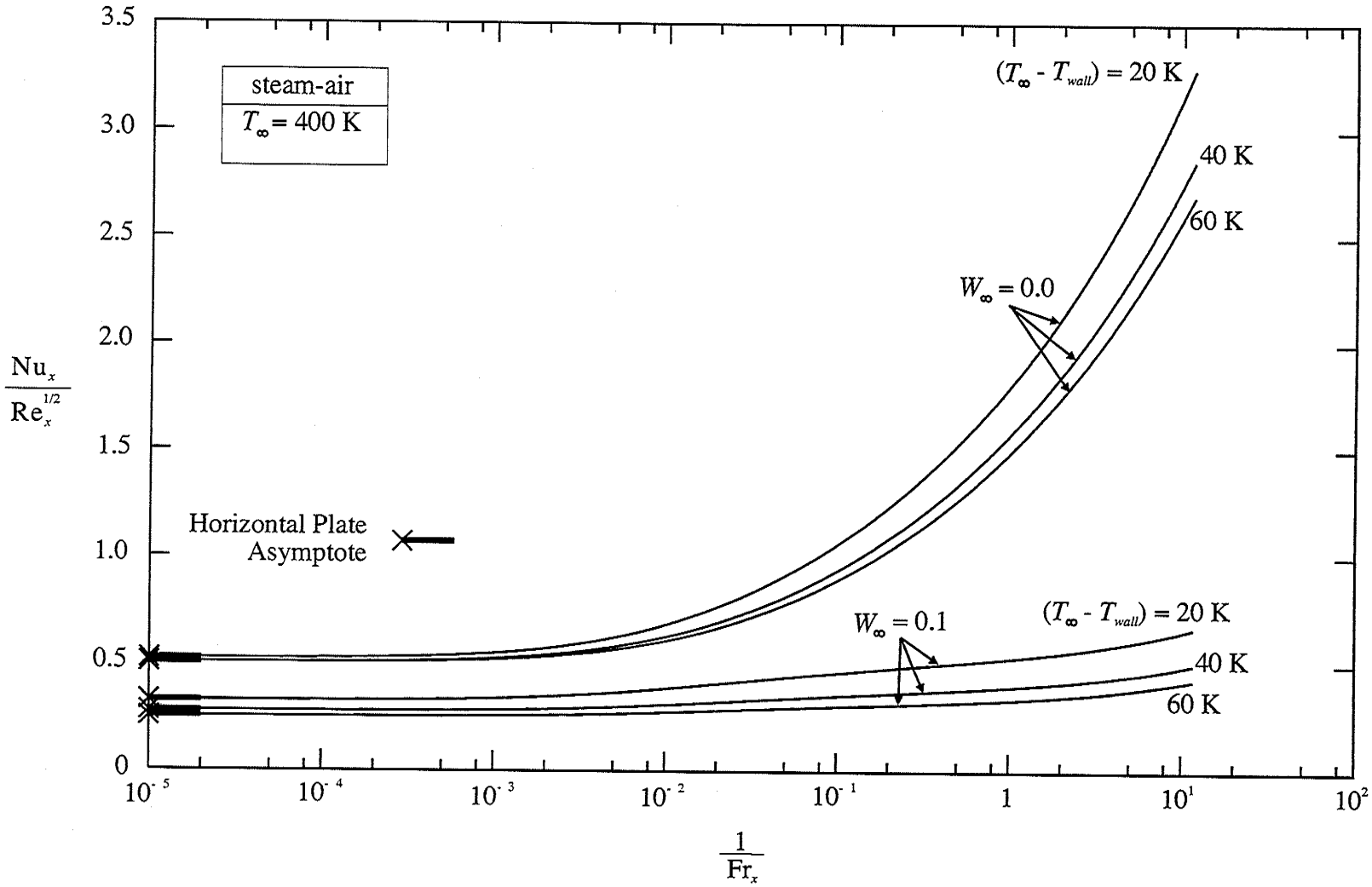

Figure 6.2: Effect of $(T_\infty - T_{wall})$ on the heat transfer for a steam-air mixture at T_∞ = 400 K, and W_∞ = 0.0 and 0.1.

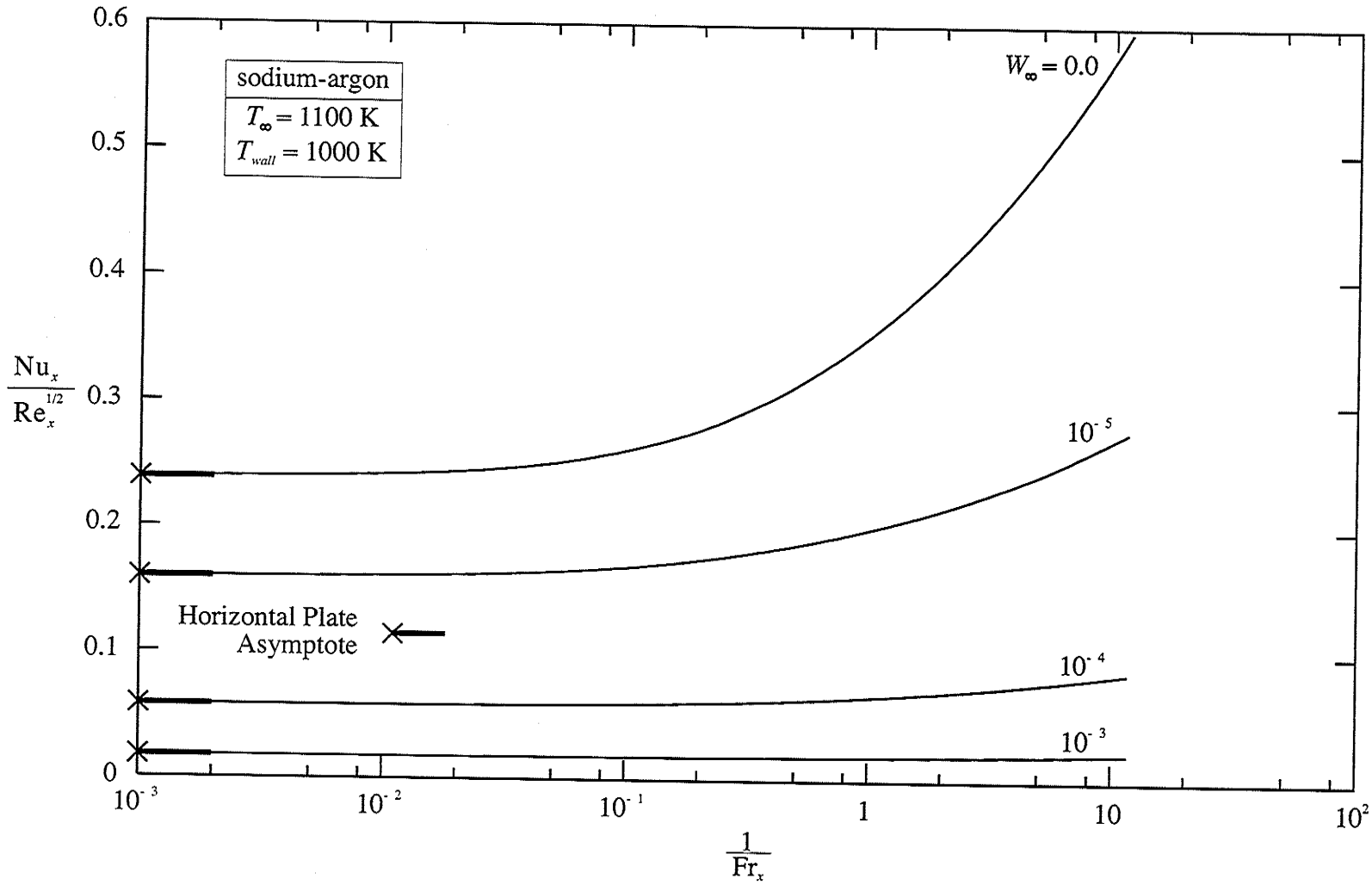

Figure 6.3: Effect of W_∞ on the heat transfer for a sodium-argon mixture at T_∞ = 1100 K, and T_{wall} = 1000 K.

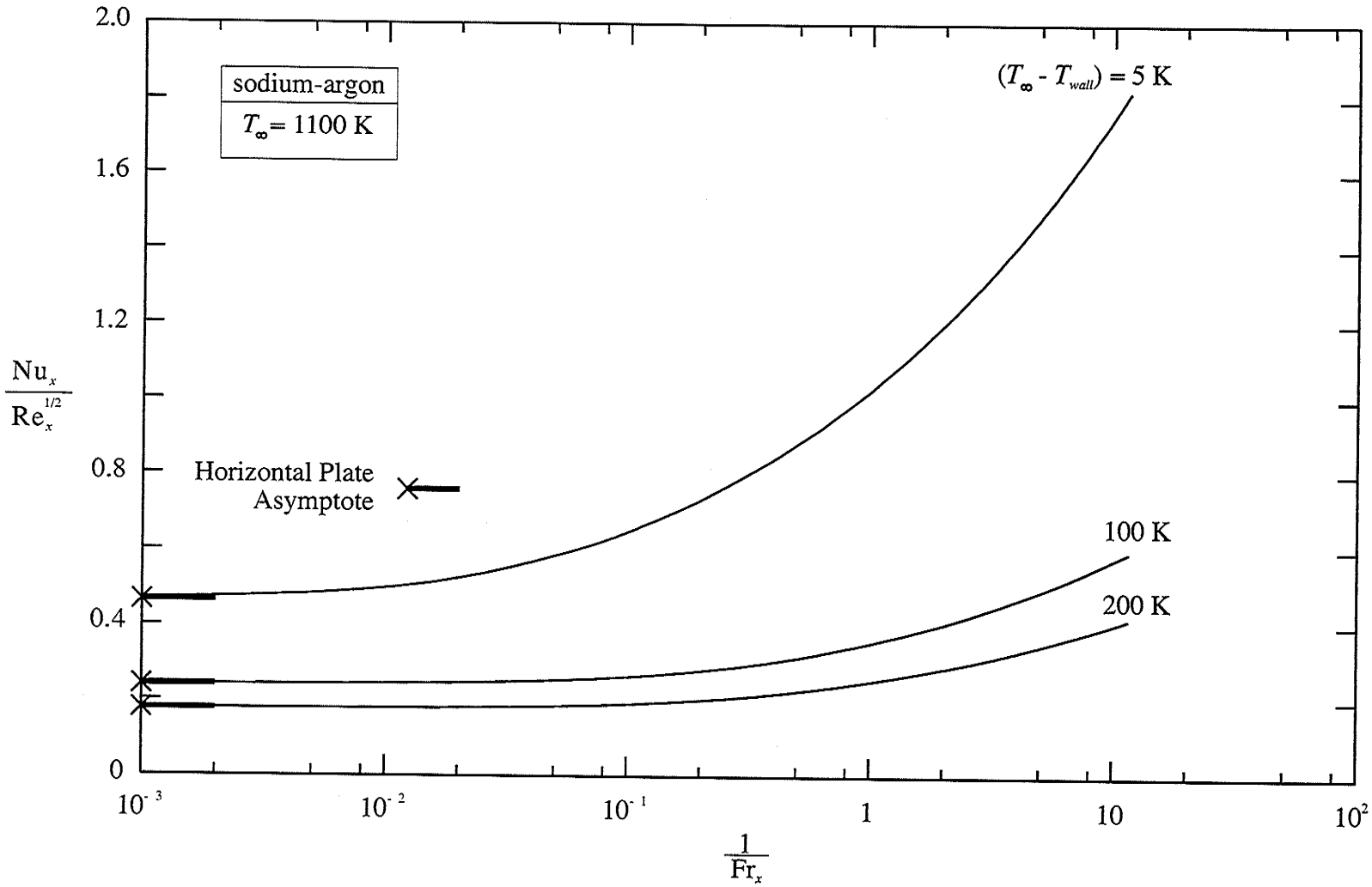

Figure 6.4: Effect of $(T_\infty - T_{wall})$ on the heat transfer for pure sodium at T_∞= 1100 K.

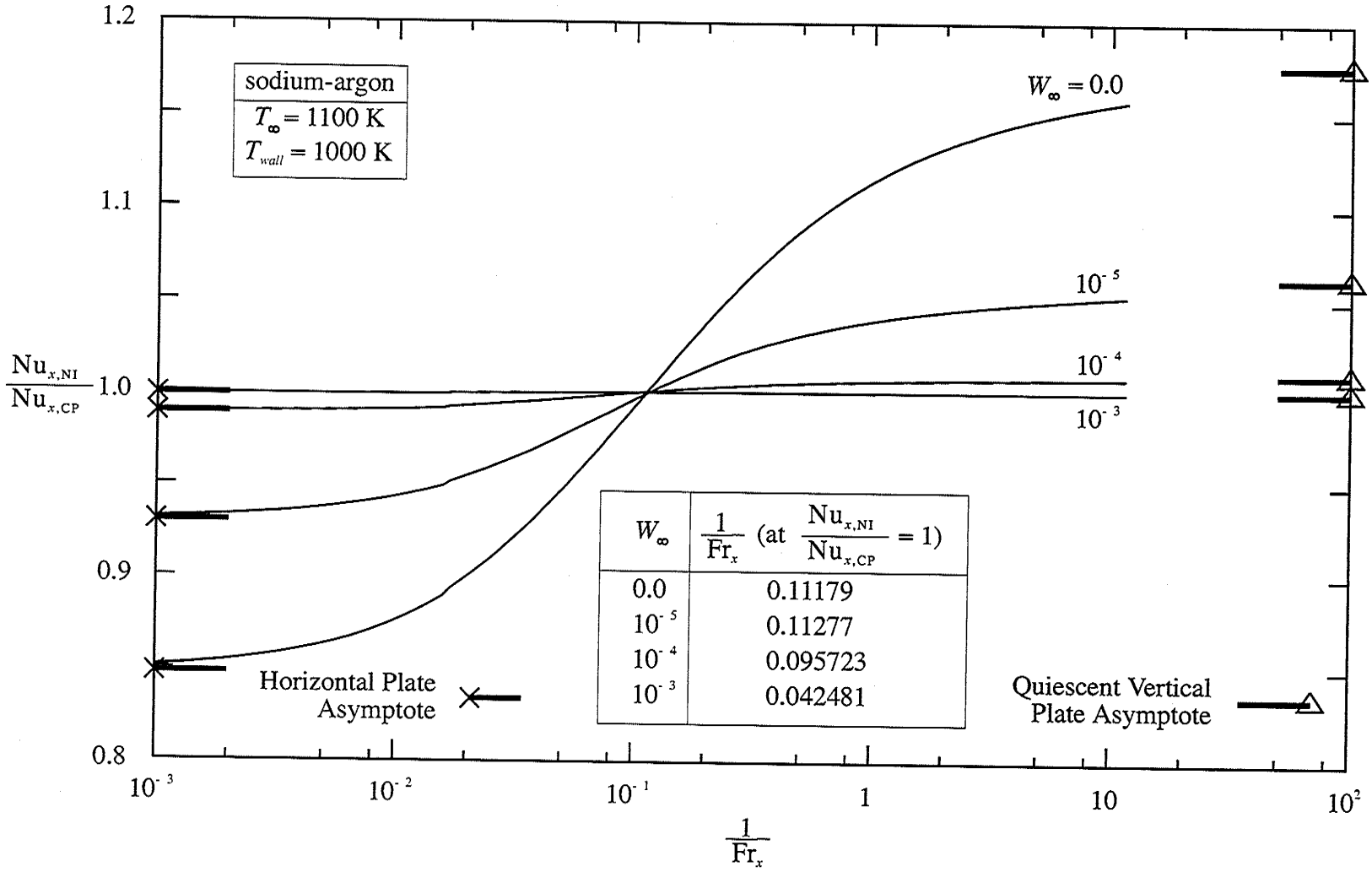

Figure 6.5: Effect of inertia terms in the liquid momentum equation for a sodium-argon mixture at T_∞= 1100 K, and T_{wall} = 1000 K.

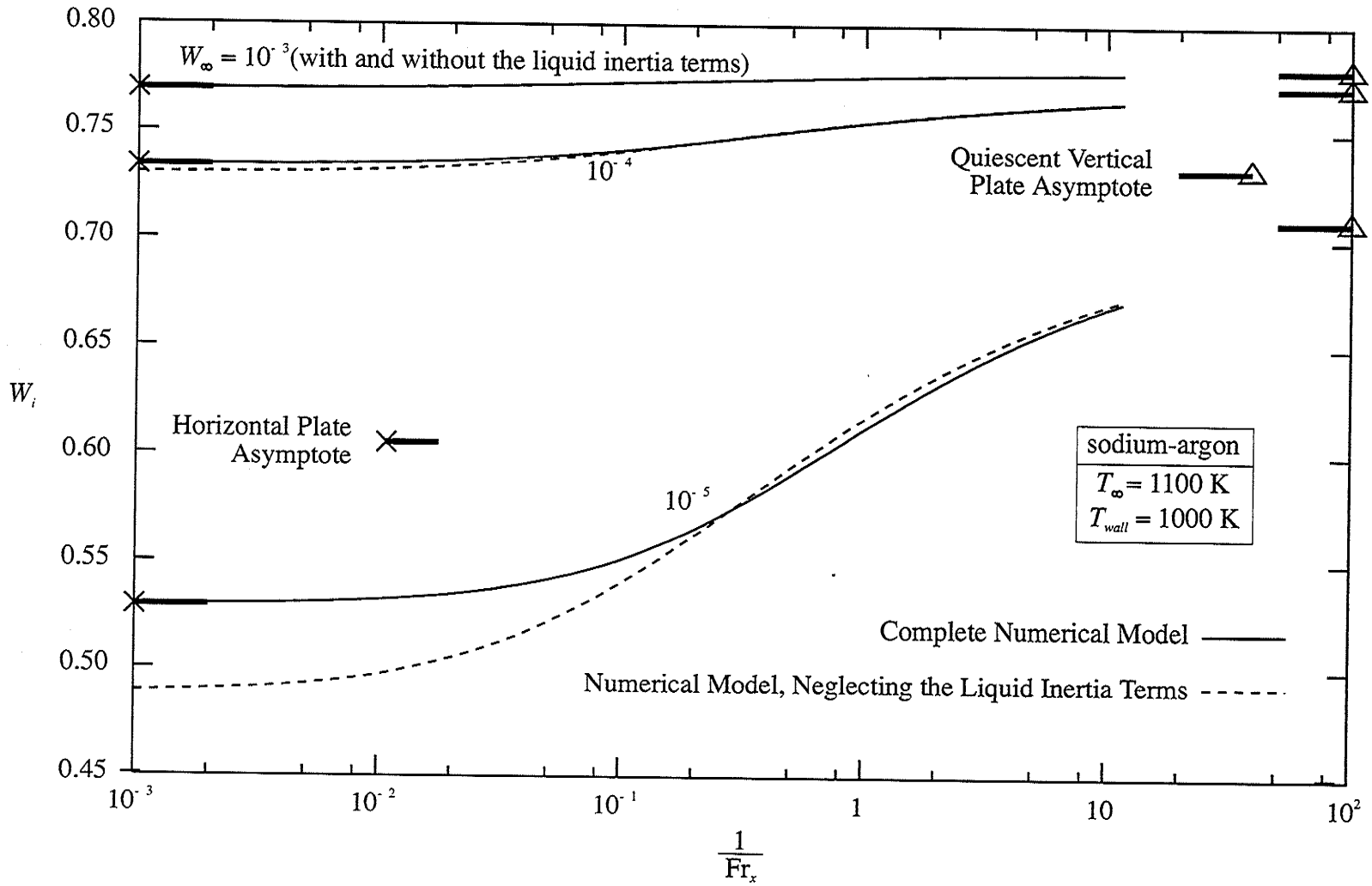

Figure 6.6: Interfacial gas concentrations for a sodium-argon mixture at $T_\infty = 1100$ K, and $T_{wall} = 1000$ K.

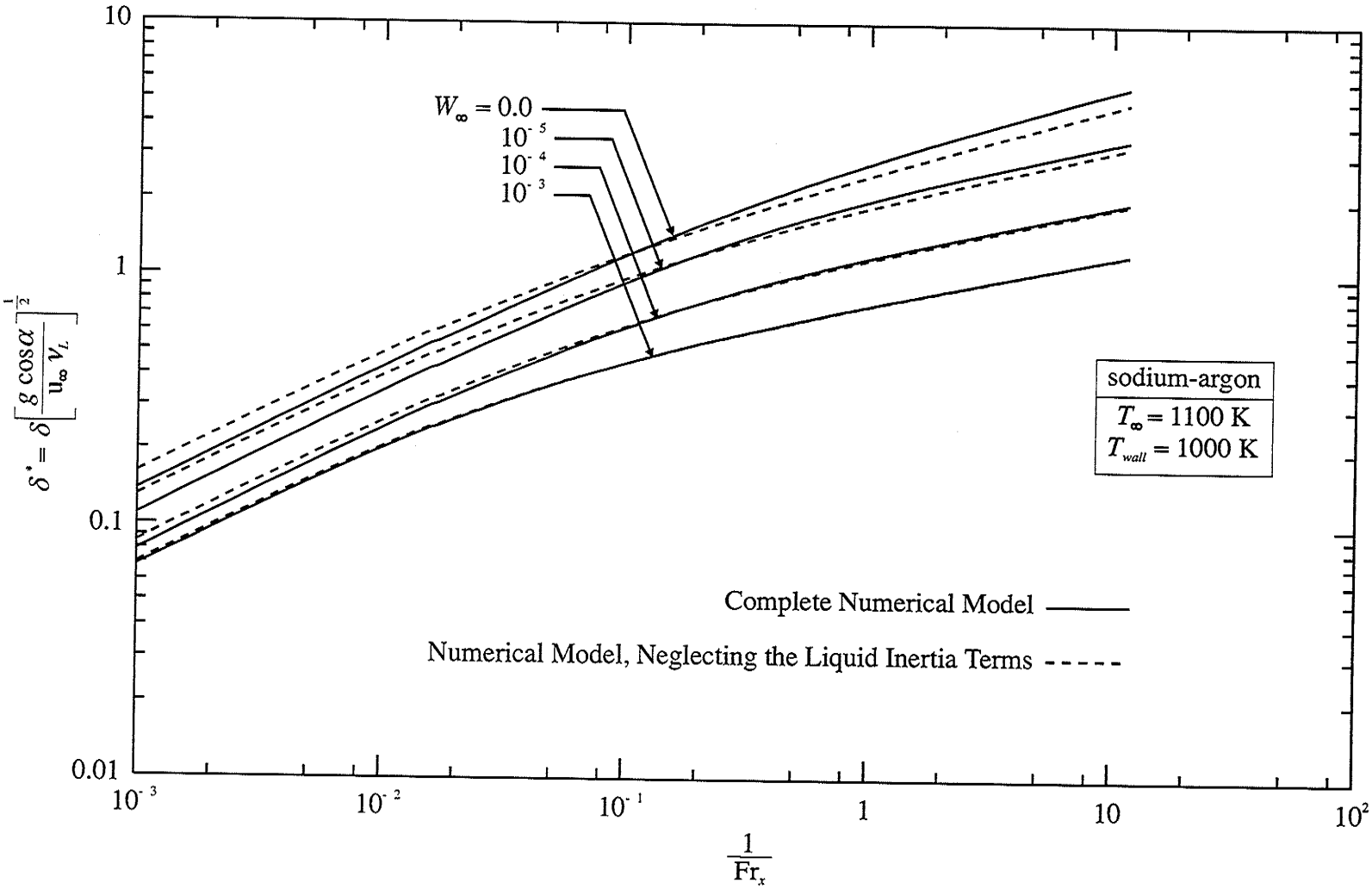

Figure 6.7: Dimensionless liquid film thickness for a sodium-argon mixture at $T_\infty = 1100$ K, and $T_{wall} = 1000$ K.

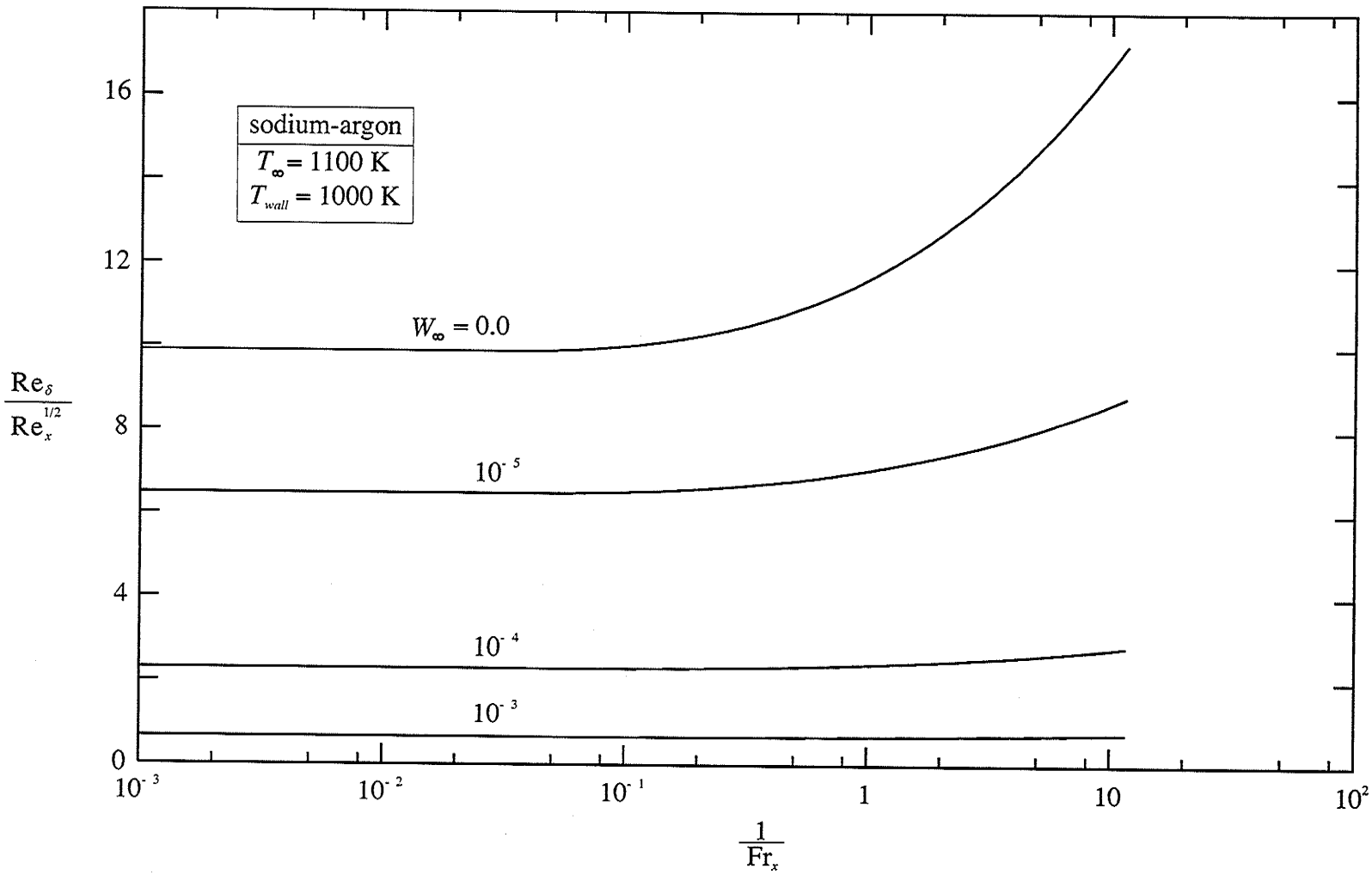

Figure 6.8: Film Reynolds number for a sodium-argon mixture at T_∞= 1100 K, and T_{wall} = 1000 K.

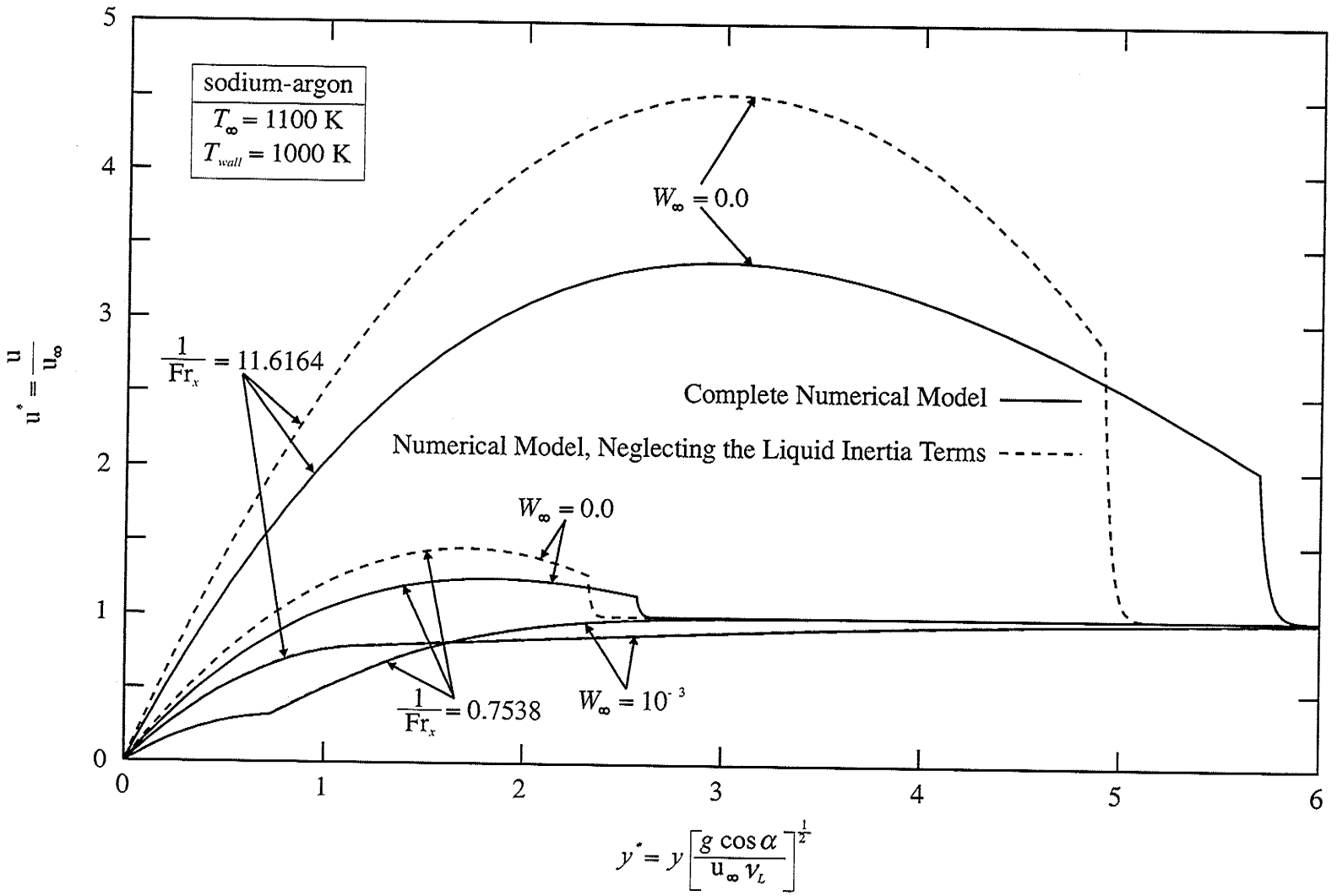

Figure 6.9: Dimensionless velocity profiles for a sodium-argon mixture at $T_\infty = 1100$ K, $T_{wall} = 1000$ K and $W_\infty = 0.0$ and 10^{-3}.

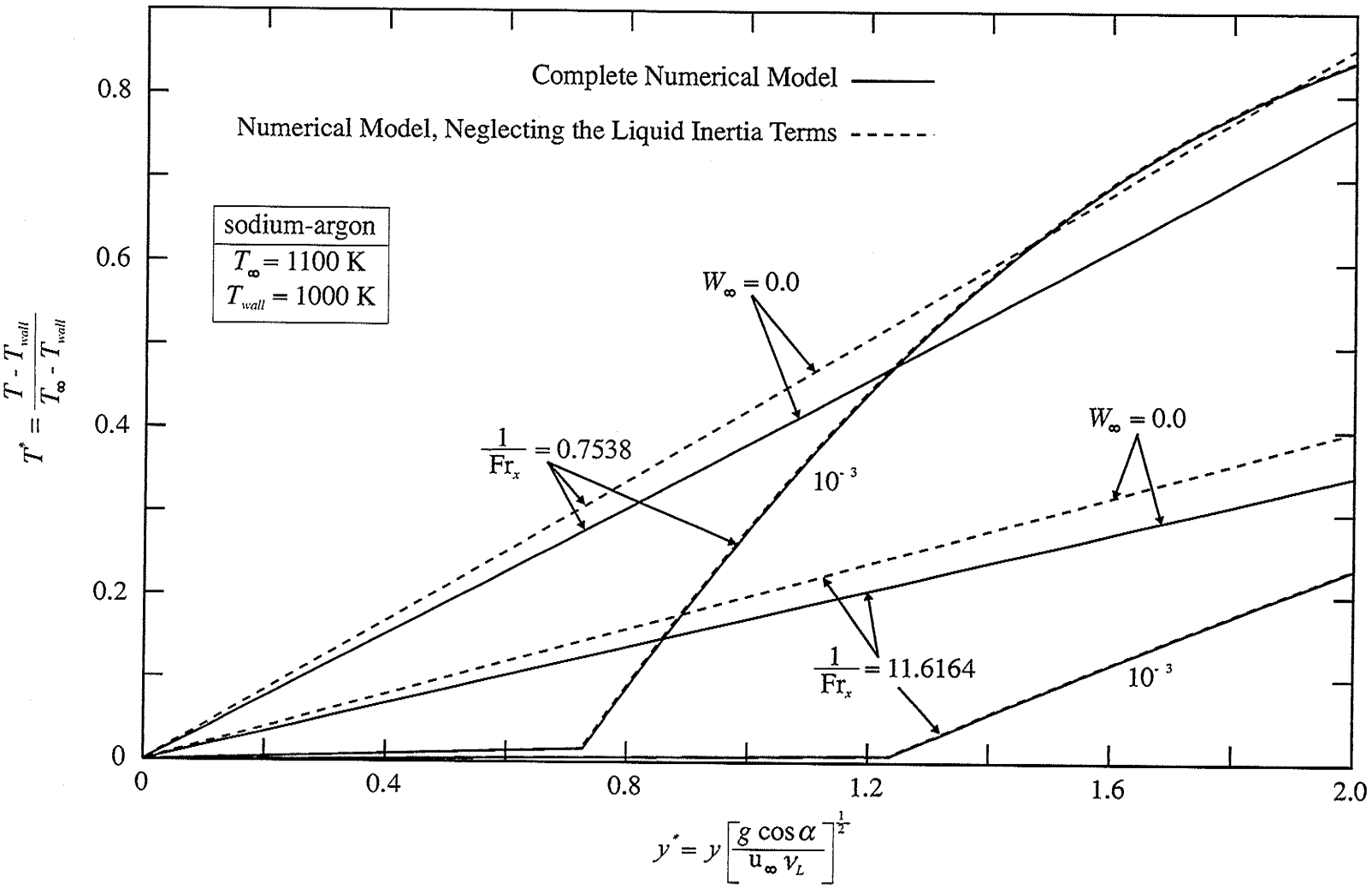

Figure 6.10: Dimensionless temperature profiles for a sodium-argon mixture at T_∞= 1100 K, T_{wall} = 1000 K and W_∞ = 0.0 and 10^{-3}.

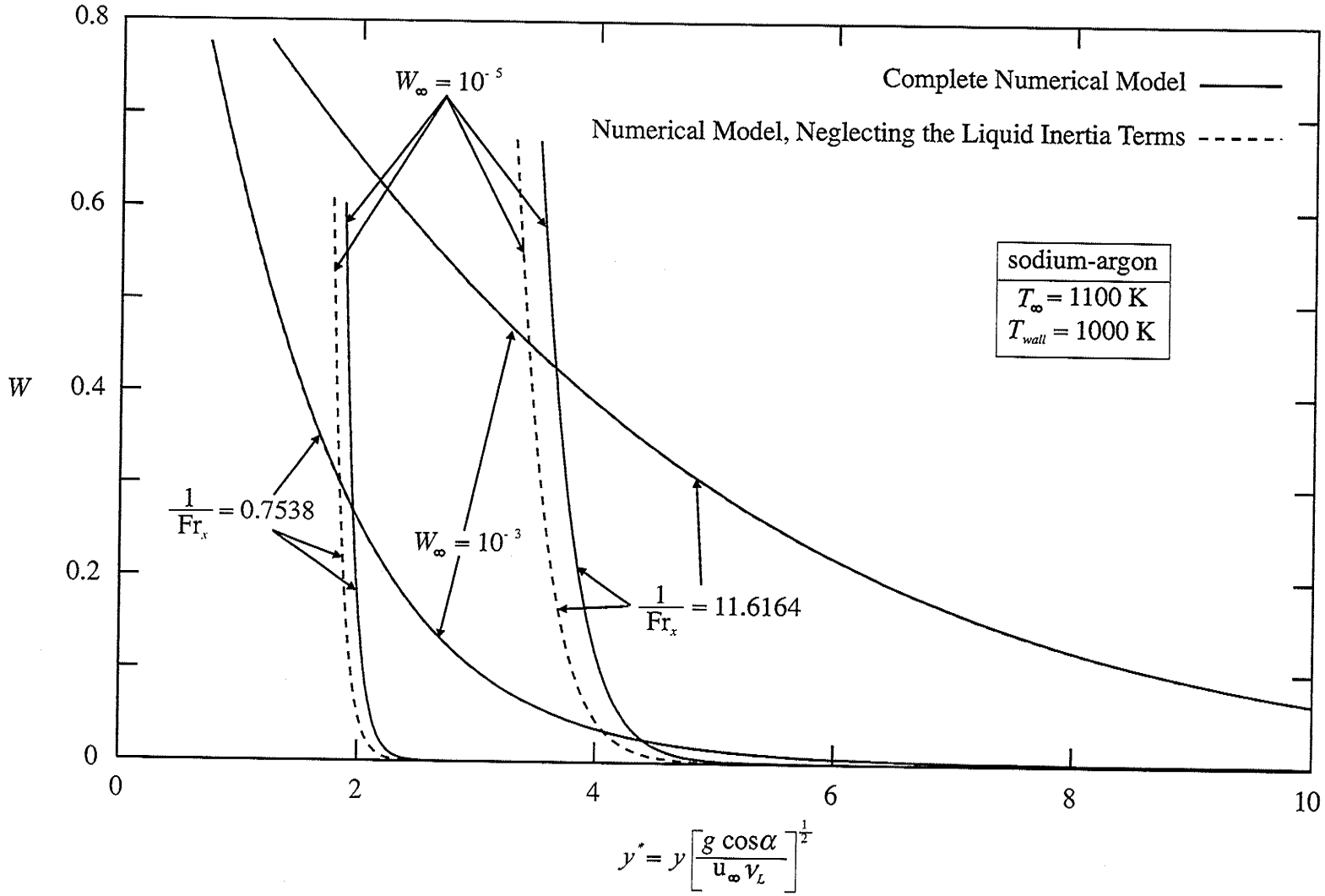

Figure 6.11: Gas mass fraction profiles for a sodium-argon mixture at $T_\infty = 1100$ K, $T_{wall} = 1000$ K and $W_\infty = 10^{-5}$ and 10^{-3}.

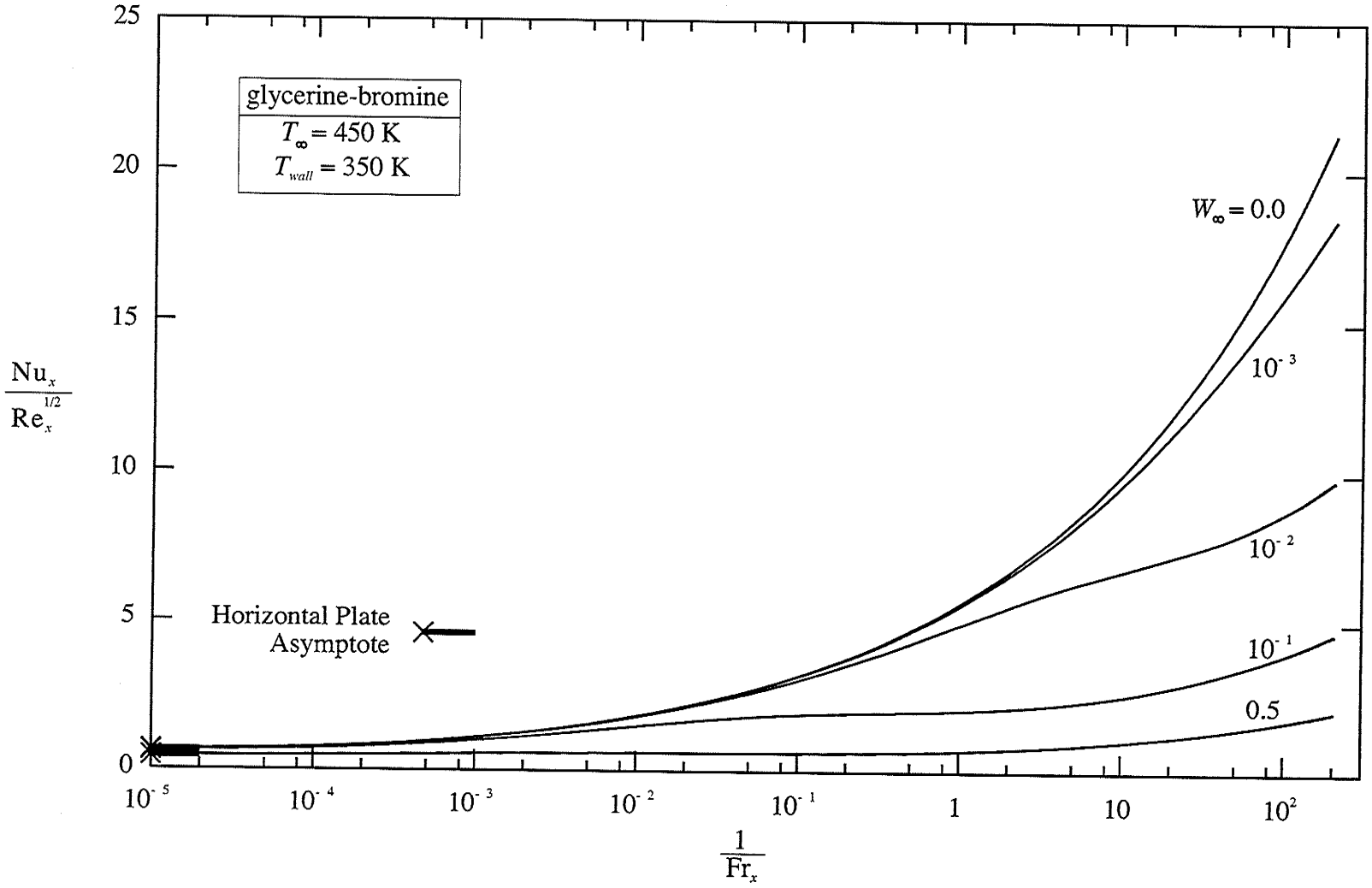

Figure 6.12: Effect of W_∞ on the heat transfer for a glycerine-bromine mixture at $T_\infty = 450$ K, and $T_{wall} = 350$ K.

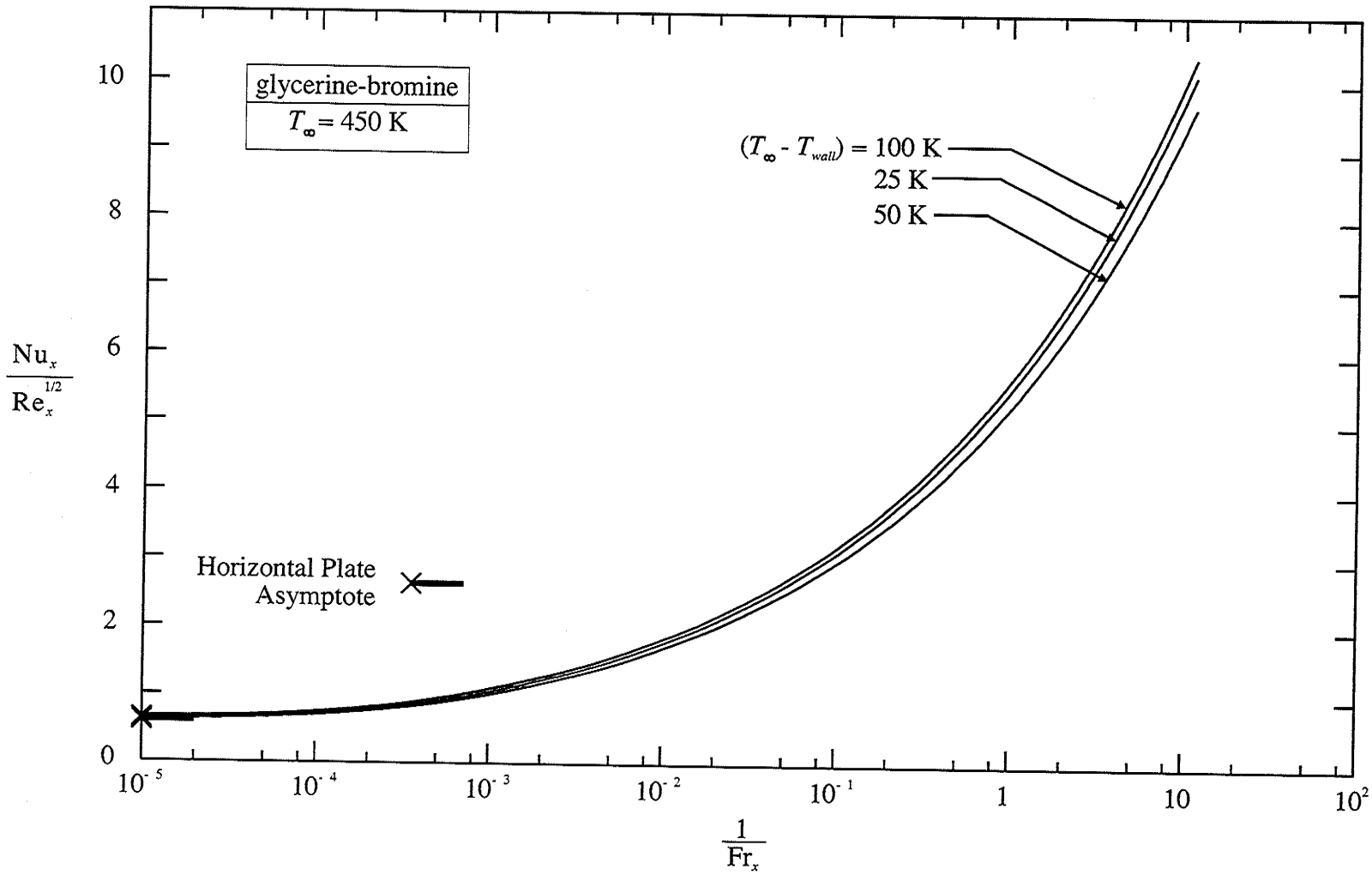

Figure 6.13: Effect of $(T_\infty - T_{wall})$ on the heat transfer for pure glycerine at T_∞ = 450 K.

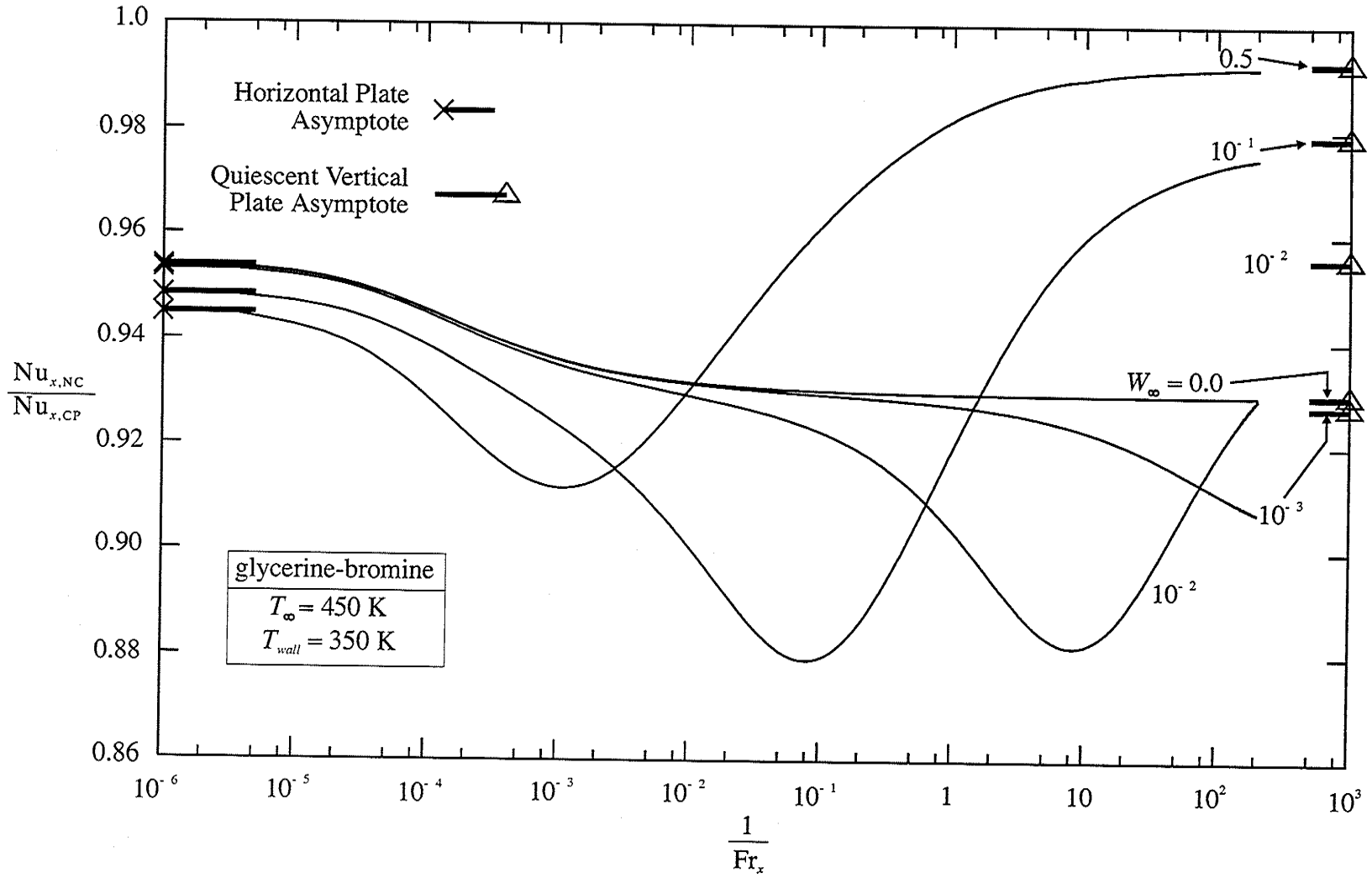

Figure 6.14: Effect of energy convection terms in the liquid energy equation for a glycerine-bromine mixture at $T_\infty = 450$ K, and $T_{wall} = 350$ K.

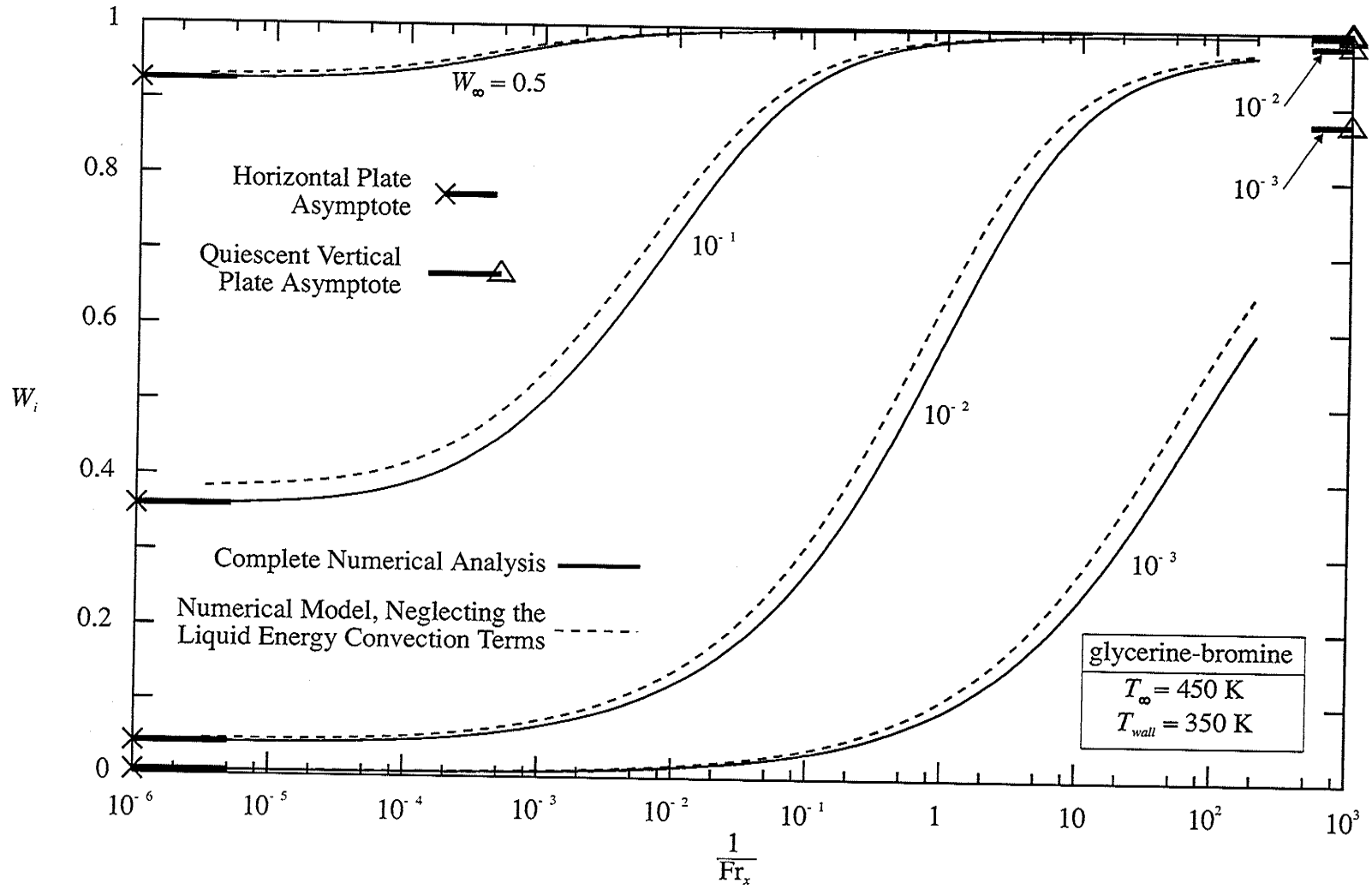

Figure 6.15: Interfacial gas concentrations for a glycerine-bromine mixture at $T_\infty = 450$ K, and $T_{wall} = 350$ K.

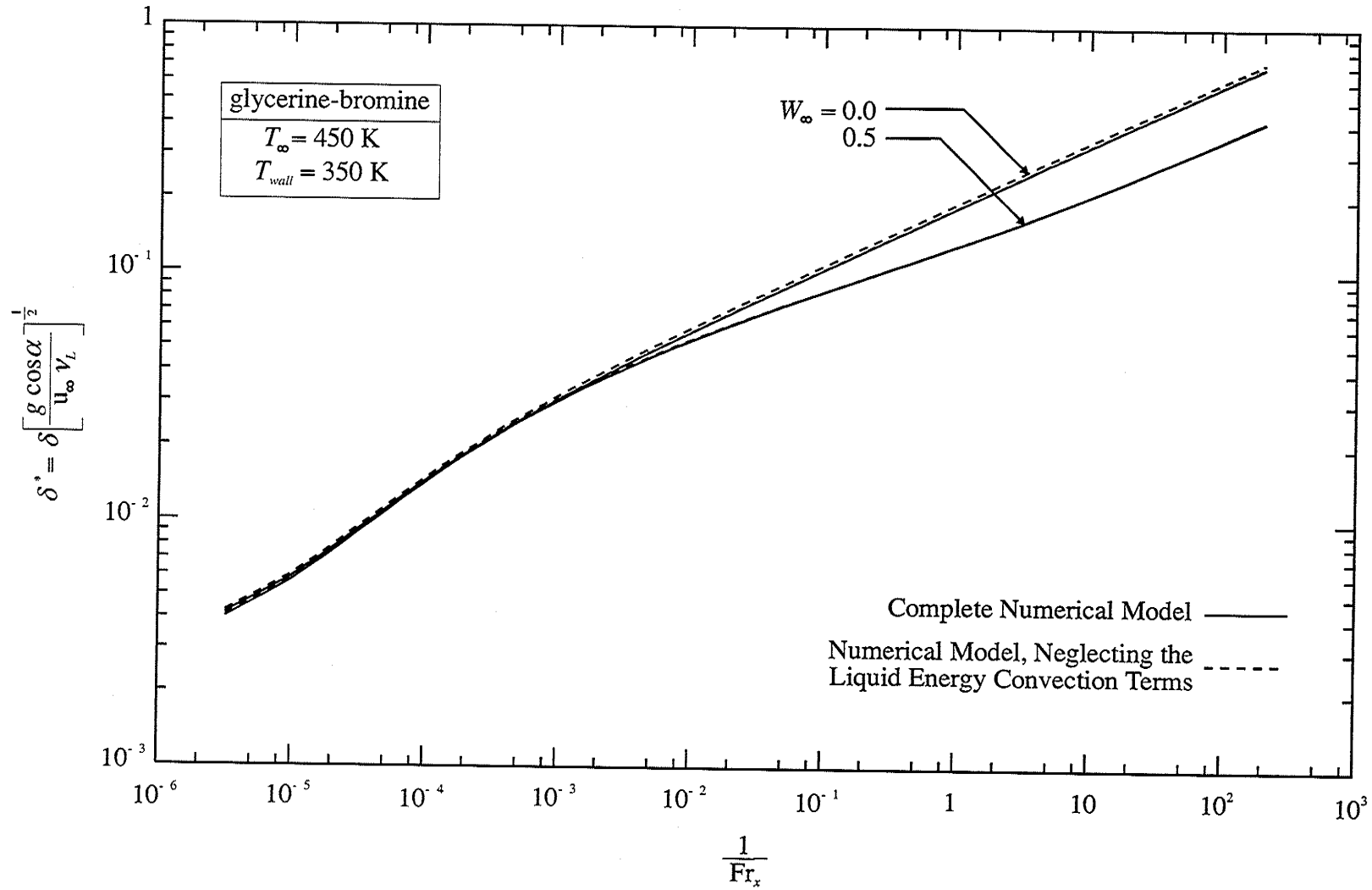

Figure 6.16: Dimensionless liquid film thickness for a glycerine-bromine mixture at T_∞ = 450 K, and T_{wall} = 350 K.

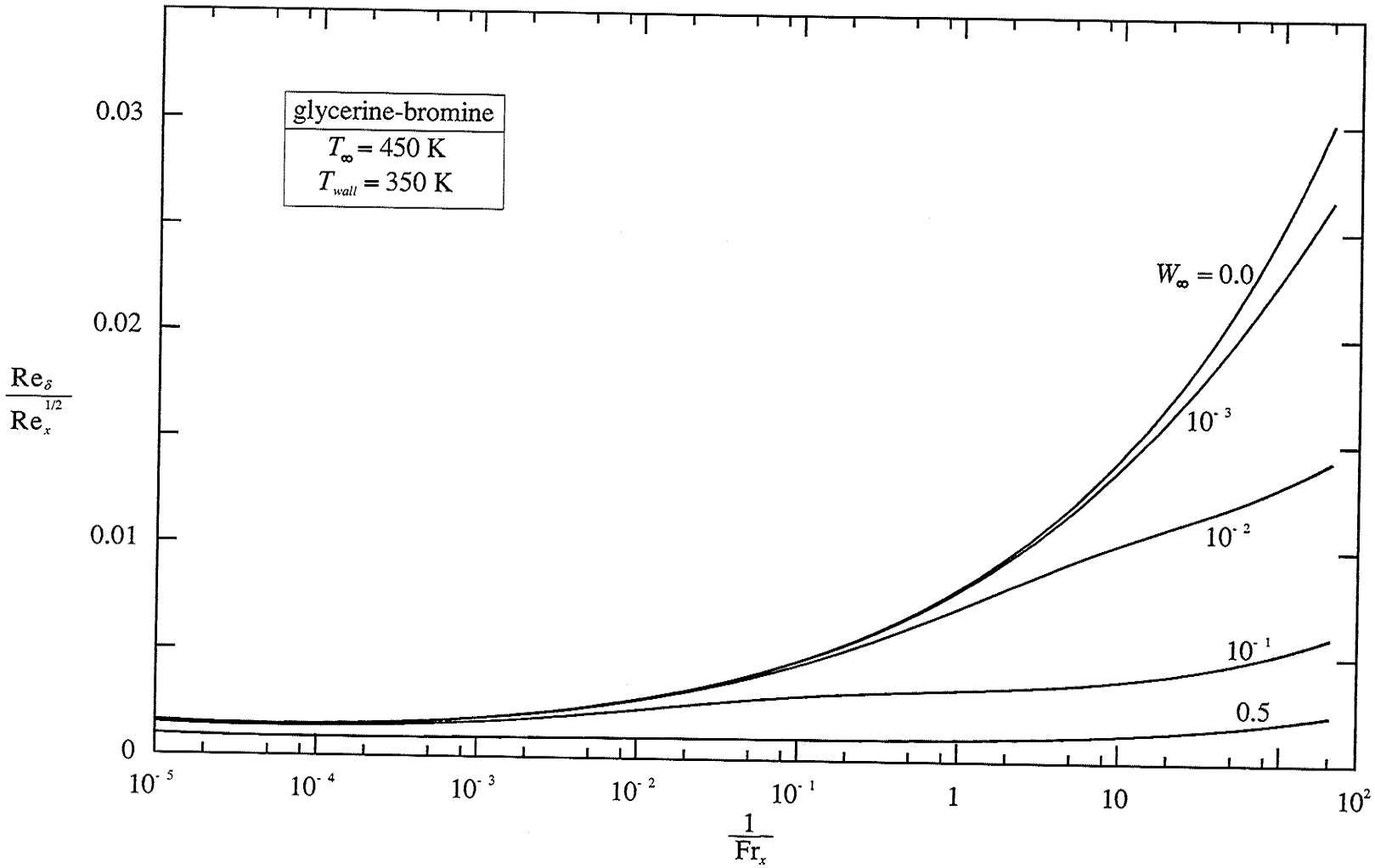

Figure 6.17: Film Reynolds number for a glycerine-bromine mixture at $T_\infty = 450$ K, and $T_{wall} = 350$ K.

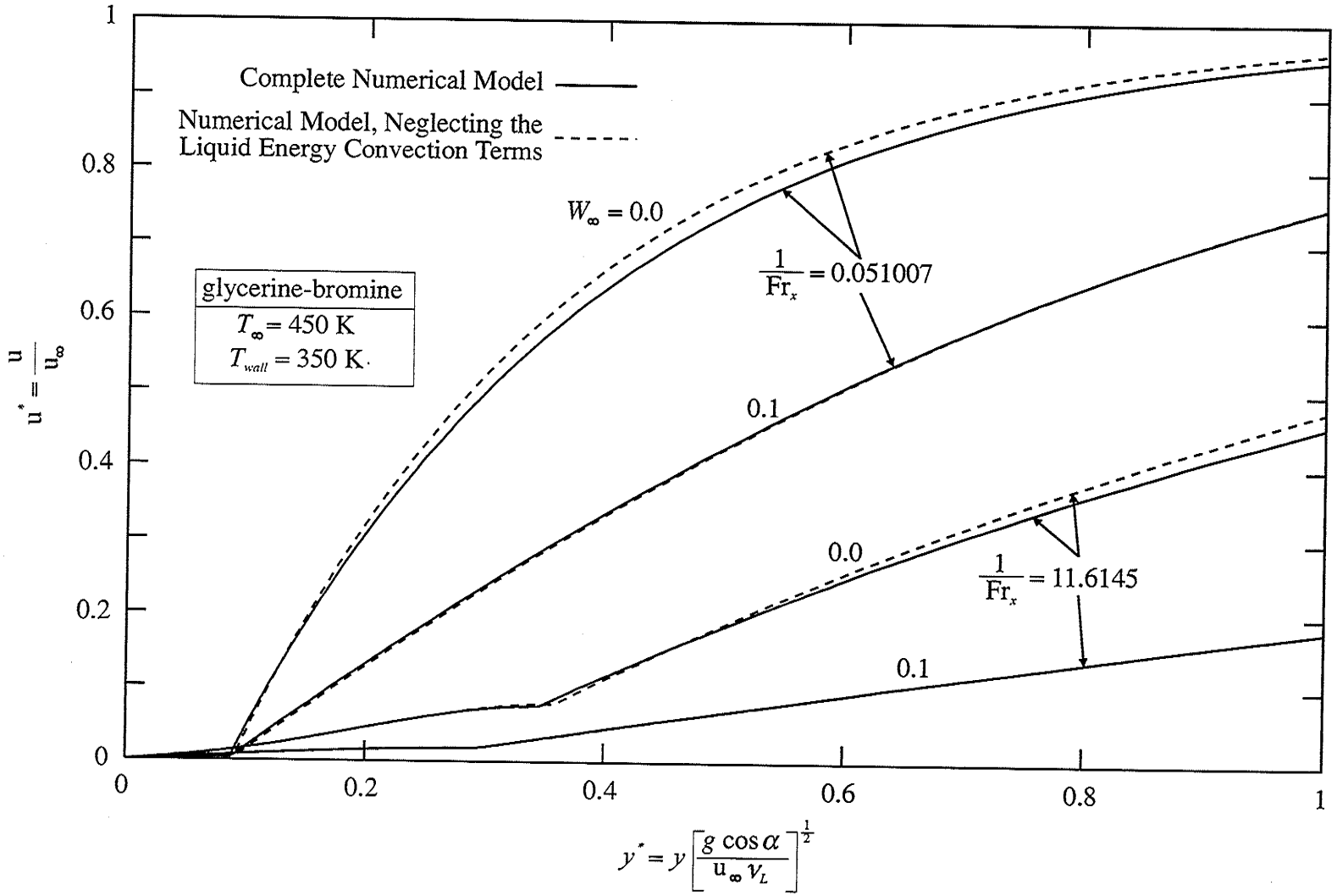

Figure 6.18: Dimensionless velocity profiles for a glycerine-bromine mixture at T_∞ = 450 K, T_{wall} = 350 K and W_∞ = 0.0 and 0.1.

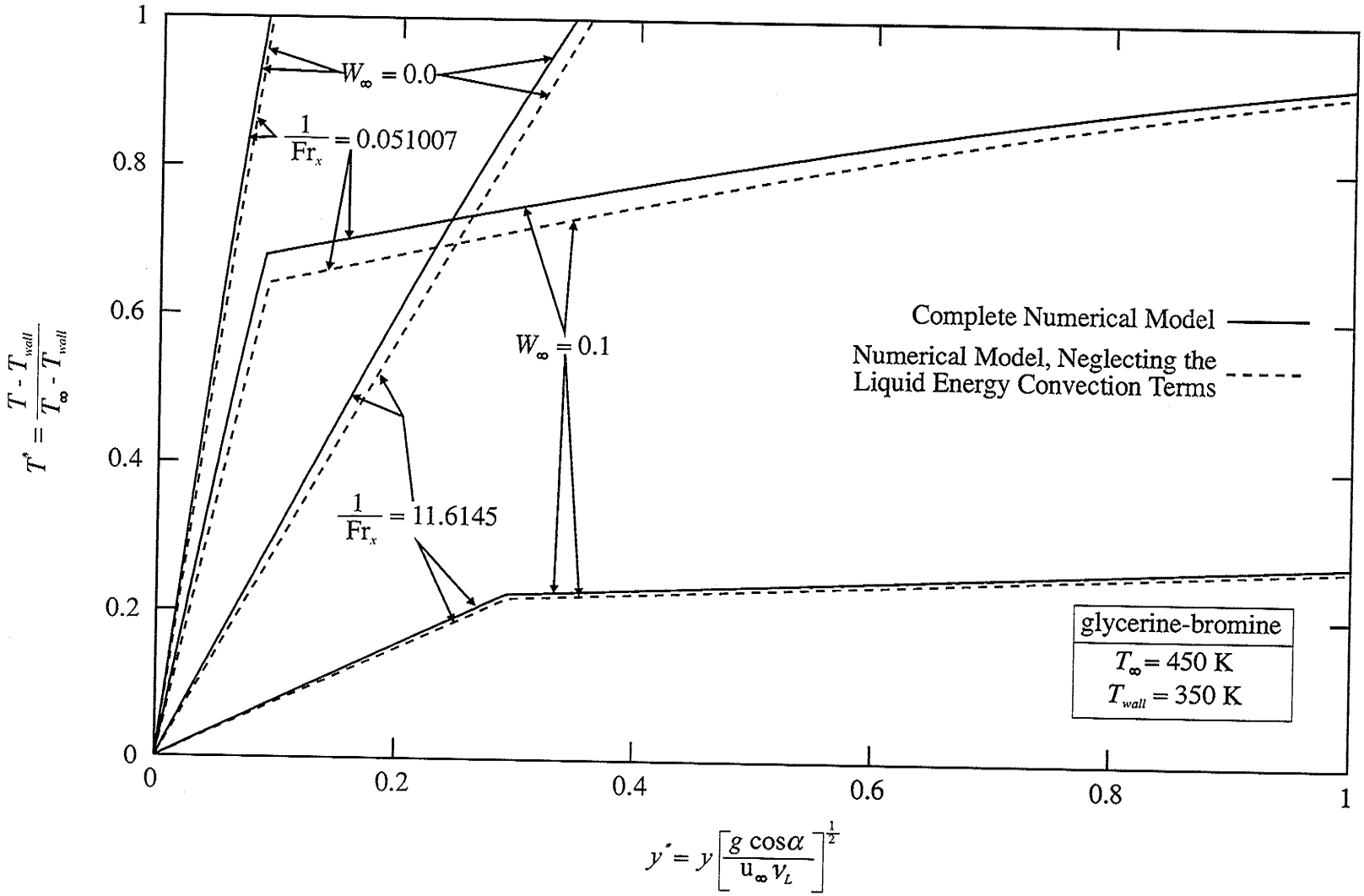

Figure 6.19: Dimensionless temperature profiles for a glycerine-bromine mixture at $T_\infty = 450$ K, $T_{wall} = 350$ K and $W_\infty = 0.0$ and 0.1.

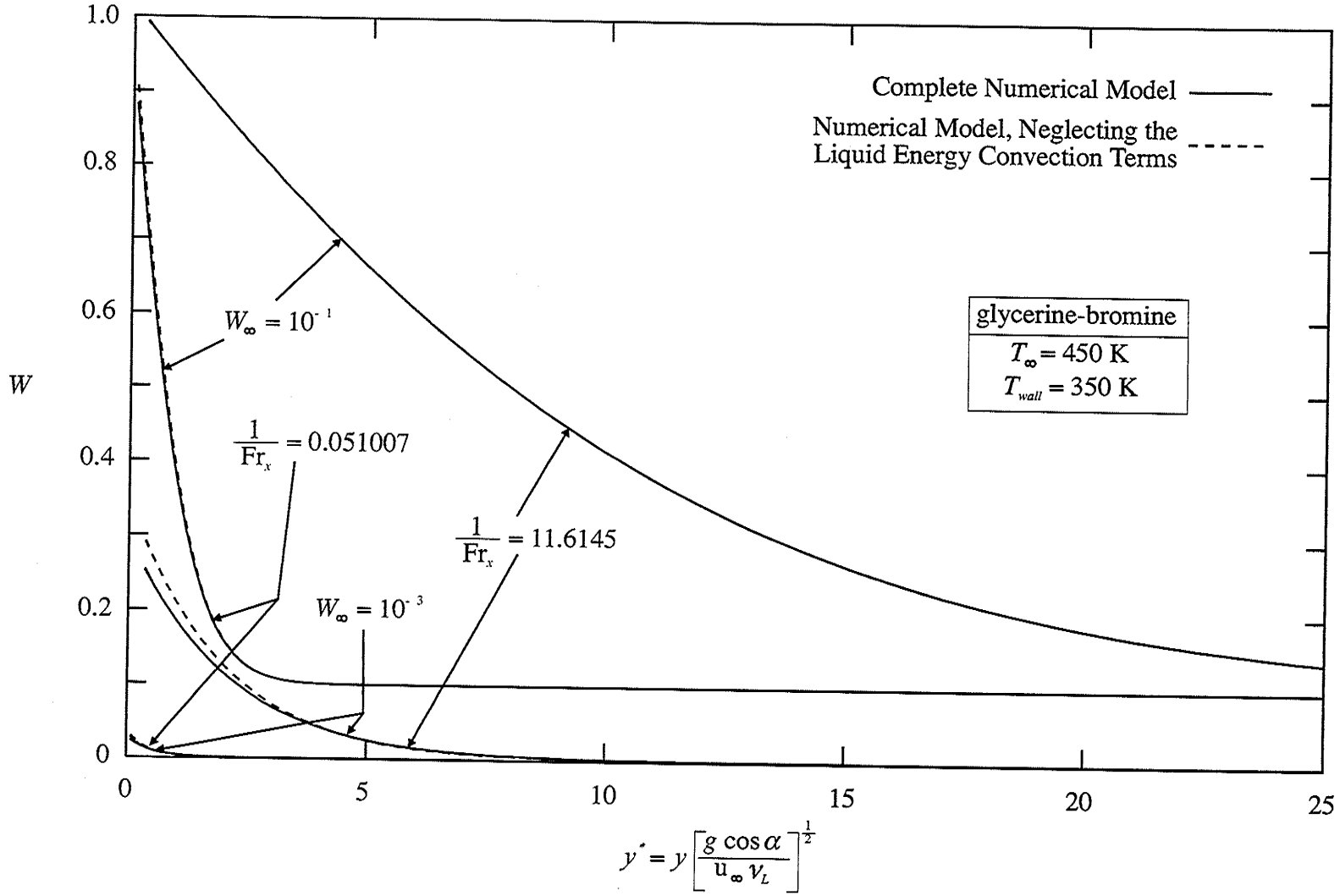

Figure 6.20: Gas mass fraction profiles for a glycerine-bromine mixture at $T_\infty = 450$ K, $T_{wall} = 350$ K and $W_\infty = 10^{-3}$ and 10^{-1}.

Chapter 7

CONCLUSIONS AND RECOMMENDATIONS

A finite control volume method is utilized for solving the complete set of two-phase boundary layer equations for laminar film condensation (natural and forced convection) in the presence of a noncondensable gas. The model accounts for the effects of inertia and buoyancy forces, as well as energy convection in the liquid and mixture layers. Therefore, there is no restriction on the applicability of the present model in terms of fluid properties (high or low Prandtl number fluids) or the type of noncondensable gas (lighter or heavier than the vapor).

Results obtained in this thesis focused on three different vapor-gas mixtures: steam-air ($Pr_L \approx 2$), sodium-argon ($Pr_L \approx 0.006$) and glycerine-bromine ($Pr_L \approx 1000$). For all three combinations, the noncondensable gas is heavier than the vapor. These results were then validated by comparison with the work by previous authors. The present results also agreed with their trends, showing that the effect of the noncondensable gas is to reduce the heat transfer, with the gas having the strongest effect on lower Pr_L fluids. Also, heat transfer is increased with higher u_∞ or ΔT.

7.1 Conclusions

Here are the conclusions of this thesis for each of the three vapor-gas mxitures regarding the effects of the inertia and energy convection terms in the governing equations:

- **Steam-Air Mixtures:**

  1. The inertia terms in the liquid momentum equation have negligible effect on the hydrodynamic and thermal characteristics of the flow.

  2. The energy convection terms in the liquid energy equation have negligible effect on the hydrodynamic and thermal characteristics of the flow.

- **Sodium-Argon Mixtures:**

  1. Due to the high thermal conductivity of liquid sodium, the energy convection terms of the liquid energy equation have negligible effect on the condensation of a sodium-argon mixture.

  2. The liquid inertia terms in the liquid momentum equation can have a strong effect on the condensation of pure sodium. This effect is diminished by the presence of argon gas in the free stream. Thus, the

inertia terms are negligible for gas concentrations higher than $W_\infty = 10^{-3}$.

3. A comparison of the heat transfer results plotted, in terms of $\mathrm{Nu}_{x,\mathrm{NI}}/\mathrm{Nu}_{x,\mathrm{CP}}$, showed that for low $1/\mathrm{Fr}_x$, the effect of neglecting the liquid inertia terms is to underpredict Nu_x. Then, as $1/\mathrm{Fr}_x$ increases, the error decreases until $\mathrm{Nu}_{x,\mathrm{NI}}/\mathrm{Nu}_{x,\mathrm{CP}}$ reaches unity. Further increases in $1/\mathrm{Fr}_x$ will then result in overpredicting Nu_x. The point at which the cross over occurs is dependent on the conditions and no conclusions about the relationship were made.

4. The error resulting from neglecting the inertia terms is greatest for $W_\infty = 0.0$ at $T_\infty = 1100$ K and $\Delta T = 100$ K, with an underprediction of Nu_x by 15 % as $1/\mathrm{Fr}_x \to 0$ and an overprediction of Nu_x by almost 18 % as $1/\mathrm{Fr}_x \to \infty$.

5. The laminar region is exceptionally short for condensation at normal gravity. Thus, the results presented for sodium-argon is more practical for micro gravity applications. The addition of a noncondensable gas will increase the length of the laminar section (distance the film grows before transition to turbulence occurs).

- **Glycerine-Bromine Mixtures:**

1. The inertia terms of the liquid momentum equation have negligible effect on the condensation of a glycerine-bromine mixture. This is due to the highly viscous nature of liquid glycerine.

2. The effect of neglecting the liquid energy convection terms is to underpredict the Nusselt number, Nu_x.

3. A comparison of the heat transfer results, plotted as $\mathrm{Nu}_{x,\mathrm{NC}}/\mathrm{Nu}_{x,\mathrm{CP}}$, showed that for $W_\infty > 0$, the greatest error occurs somewhere between the horizontal forced convection limit ($1/\mathrm{Fr}_x \to 0$) and the free convection limit ($1/\mathrm{Fr}_x \to \infty$). In addition, the maximum error could be as high as 12% even though the errors at the limits were 2% and 5%.

4. For the particular cases studied, a maximum error (12 %) occured for $W_\infty = 10^{-1}$ at $T_\infty = 450$ K and $\Delta T = 100$ K.

5. The laminar region for glycerine is exceptionally long. For example, with $W_\infty = 0.0$, $T_\infty = 450$ K and $\Delta T = 100$ K, $\mathrm{u}_\infty = 5$ m/s, $g = 9.81$ m/s^2 and $\alpha = 0$, the start of the transition occurs at $x_\delta = 11.9$ metres. The axial location at which transition occurs increases with increasing W_∞.

7.2 Recommendations

The present work can be improved or carried further through efforts to:

1. Reduce the computational time and also to reduce chances of divergence by coupling all seven boundary layer equations and the energy balance for the film thickness and solve them simultaneously.

2. Extend this work to the condensation of a vapor-gas mixture on the outside of a horizontal tube.

3. Exend work to turbulent liquid flow. This is especially important for low Pr_l fluids because of the extremely short laminar region under normal gravity.

REFERENCES

Bolz, R.E., and Tuve, G.L., 1973, *CRC Handbook of Tables for Applied Engineering Science*, Second Ed., Chemical Rubber Company, Cleveland, Ohio.

Cess, R.D., 1960, "Laminar-Film Condensation of a Flat Plate in the Absence of a Body Force", *Z. Angew. Math. Phys.*, Vol. 11, pp. 426-433.

Chen, M.M., 1961, "An Analytical Study of Laminar Film Condensation: Part 1–Flat Plates", *Journal of Heat Transfer*, Vol. 83, pp. 48-54.

Denny, V.E., and Mills, A.F., 1969, "Nonsimilar Solutions for Laminar Film Condensation on a Vertical Surface", *Int. J. Heat Mass Transfer*, Vol. 12, pp. 965-979.

Denny, V.E., Mills, A.F., and Gardiner, J.R., 1970, "Nonsimilar Solutions for Laminar Film Condensation of Liquid Metals", Paper Cs 2.1 in the Proceedings of the Fourth International Heat Transfer Conference, Paris, France.

Denny, V.E., Mills, A.F., and Jusionis, V.J., 1971, "Laminar Film Condensation From a Steam-Air Mixture Undergoing Forced Flow Down a Vertical Surface", *Journal of Heat Transfer*, Vol. 93, pp. 297-304.

Denny, V.E., and Jusionis, V.J., 1972, "Effects of Noncondensable Gas and Forced Flow on Laminar Film Condensation", *Int. J. Heat Mass Transfer*, Vol. 15, pp. 315-326.

Fujii, T., Shinzato, K., and Lee, J.B., 1992, "Free-Convection Condensation of an Air-Steam Mixture on a Vertical Surface - Comparison Between Theory and Experimental", *3rd UK National Conference Incorporating 1st European Conference on Thermal Sciences*, Vol. 1, No. 129, pp. 287-293.

Fujii, T., and Uehara, H., 1972, "Laminar Filmwise Condensation on a Vertical Surface", *Int. J. Heat Mass Transfer*, Vol. 15, pp. 217-233.

Gaddis, E.S., 1979, "Solution of the Two Phase Boundary-Layer Equations for Laminar Film Condensation of Vapour Flowing Perpendicular to a Horizontal Cylinder", *Int. J. Heat Mass Transfer*, Vol. 22, pp. 371-382.

Gallant, R.W., 1968, *Physical Properties of Hydrocarbons*, Gulf Publishing Co., Houston, Texas.

Hijikata, K., and Mori, Y., 1973, "Forced Convective Heat Transfer of a Gas With Condensing Vapour Around a Flat Plate", *Heat Transfer–Jap. Res.*, Vol. 2, pp. 81-101.

Incropera, F.P., and DeWitt, D.P., 1985, *Fundamentals of Heat and Mass Transfer*, 2nd ed., pp. 767-775, John Wiley & Sons, New York.

Irvine, T.F. Jr., and Liley, P.E., 1984, *Steam and Gas Tables with Computer Equations*, Academic Press, London.

Hultgren, R., Desai, P.D., Hawkins, D.T., Gleiser, M., Kelley, K.H., and Wagman, D.D., 1973, *Selected Values of the Thermodynamic Properties of the Elements*, American Society for Metals, Metals Park, Ohio.

Jacobs, H.R., 1966, "An Integral Treatment of Combined Body Force and Forced Convection in Laminar Film Condensation", *Int. J. Heat Mass Transfer*, Vol. 9, pp. 637-648.

Koh, J.C.Y., 1962, "Film Condensation in a Forced-Convection Boundary-Layer Flow", *Int. J. Heat Mass Transfer*, Vol. 5, pp. 941-954.

Koh, J.C.Y., Sparrow, E.M., and Hartnett, J.P., 1961, "The Two Phase Boundary Layer in Laminar Film Condensation", *Int. J. Heat Mass Transfer*, Vol. 2, pp. 69-82.

Legay-Desequelles, F., and Prunet-Foch, B., 1985, "Dynamic Behaviour of a Boundary Layer with Condensation Along a Flat Plate: Comparison with Suction", *Int. J. Heat Mass Transfer*, Vol. 28, pp. 2363-2370.

Legay-Desequelles, F., and Prunet-Foch, B., 1986, "Heat and Mass Transfer with Condensation in Laminar and Turbulent Boundary Layers Along a Flat Plate", *Int. J. Heat Mass Transfer*, Vol. 29, pp. 95-105.

Mason, E.A. and Monchik, L., 1963, *Survey of the Equation of State and Transport Properties of Moist Gases*, International Symposium on Humidity and Moisture, National Bureau of Standards, Washington, D.C..

Mills, A.F., 1965, *The Condensation of Steam at Low Pressures*, Technical Report on NSF GP-2520. Series No. 6, Issue No. 39. Space Sciences Laboratory, University of California, Berkeley.

Minkowycz, W.J., and Sparrow, E.M., 1966, "Condensation Heat Transfer in the Presence of Noncondensables, Interfacial Resistance, Superheating, Variable Properties, and Diffusion", *Int. J. Heat Mass Transfer*, Vol. 9, pp. 1125-1144.

Minkowycz, W.J., and Sparrow, E.M., 1969, "The Effect of Superheating on Condensation Heat Transfer in a Forced Convection Boundary Layer Flow", *Int. J. Heat Mass Transfer*, Vol. 12, pp. 147-154.

Nabavian, K., 1962, *Condensation Coefficient of Water*, Ph.D. Thesis, University of California, Berkeley.

Nusselt, W., 1916, "Die Oberflächenkondensation des Wasserdampfes", *Zeitschr. Ver Deutsch. Ing.*, Vol. 60, pp. 541-546 and pp. 569-575.

Patankar, S.V., 1980, *Numerical Heat Transfer and Fluid Flow*, Hemisphere Publishing Corporation, New York.

Patankar, S.V., and Spalding, D.B., 1967, "A Finite Difference Procedure for Solving the Equations of the Two-Dimensional Boundary Layer", *Int. J. Heat Mass Transfer*, Vol. 10, pp. 1389-1411.

Paul, B., 1962, "Compilation of Evaporation Coefficients", *American Rocket Society Journal*, Vol. 32, pp. 1321-1328.

Poots, G., and Miles, R.G., 1967, "Effects of Variable Physical Properties on Laminar Film Condensation of Saturated Steam on a Vertical Flat Plate", *Int. J. Heat Mass Transfer*, Vol. 10, pp. 1677-1692.

Reid, R.C., Prausnitz, J.M., and Sherwood, T.K., 1977, *The Properties of Gases and Liquids*, Third Ed., McGraw-Hill, New York.

Rohsenow, W.M., 1956, "Heat Transfer and Temperature Distribution in Laminar-Film Condensation", *Transactions of the ASME*, Vol. 78, pp. 1645-1648.

Rohsenow, W.M., Hartnett, J.P., and Ganic, E.N., 1985, *Handbook of Heat Transfer Fundamentals*, Second Ed., McGraw- Hill, New York.

Rohsenow, W.M., Webber, J.H., and Ling, A.T., 1956, "Effect of Vapor Velocity on Laminar and Turbulent-Film Condensation", *Transactions of the ASME*, Vol. 78, pp. 1637-1643.

Rose, J.W., 1969, "Condensation of a Vapour in the Presence of a Non-condensing Gas", *Int. J. Heat Mass Transfer*, Vol. 12, pp. 233-237.

Rose, J.W., 1980, "Approximate Equations for Forced-Convection Condensation in the Presence of a Non-condensing Gas on a Flat Plate and Horizontal Tube", *Int. J. Heat Mass Transfer*, Vol. 23, pp. 539-546.

Rose, J.W., 1988, "Fundamentals of Condensation Heat Transfer: Laminar Film Condensation", *JSME International Journal*, series II, Vol. 31, No. 3, pp.357-375.

Rose, J.W., 1989, "A New Interpolation Formula for Forced-Convection Condensation on a Horizontal Surface", *Journal of Heat Transfer*, Vol. 111, pp. 818-819.

Shekriladze, I.G., and Gomelauri, V.I., 1966, "Theoretical Study of Laminar Film Condensation of Flowing Vapour", *Int. J. Heat Mass Transfer*, Vol. 9, pp. 581-591.

Smith, B.D., and Srivastava, R., 1986, *Thermodynamic Data for Pure Compounds*, Elsevier, New York.

Sparrow, E.M., and Eckert, E.R.G., 1961, "Effects of Superheated Vapor and Noncondensable Gases on Laminar Film Condensation", *A.I.Ch.E. Journal*, Vol. 7, No. 3, pp. 473-477.

Sparrow, E.M., and Gregg, J.L., 1959, "A Boundary-Layer Treatment of Laminar-Film Condensation", *Journal of Heat Transfer*, Vol. 81, pp. 13-18.

Sparrow, E.M., and Lin, S.H., 1964, "Condensation Heat Transfer in the Presence of a Noncondensable Gas", *Journal of Heat Transfer*, Vol. 86, pp. 430-436.

Sparrow, E.M., Minkowycz, W.J., and Saddy, M., 1967, "Forced Convection Condensation in the Presence of Noncondensables and Interfacial Resistance", *Int. J. Heat Mass Transfer*, Vol. 10, pp. 1829-1845.

Touloukian, Y.S., Liley, P.E., and Saxena, S.C., 1970, *Thermophysical Properties of Matter*, Vols. 3, 6, and 11, IFI/Plenum, New York.

Turner, R.H., Mills, A.F., and Denny, V.E., 1973, "The Effect of Noncondensable Gas on Laminar Film Condensation of Liquid Metals", *Journal of Heat Transfer*, Vol. 95, pp. 6-11.

APPENDIX A

Transport and Thermal Properties

A.1 Introduction

This appendix contains the details of how the properties are calculated for steam, air, sodium, argon, glycerine and bromine. The final section gives details of how the separate vapor and gas properties are used to evaluate the mixture properties Equations used in the evaluation of the pressure is common to all three vapor-gas combinations are defined in this section along with the universal gas constant.

Universal gas constant: $\overline{R} = 8.3144$ kJ/kmol·K

Free Stream Pressure:

P_∞ must be calculated from the given T_∞ and W_∞. This is done by assuming that, at the free stream, the vapor exists at its saturation state. Thus the saturation temperature of the vapor is the same as the mixture temperature. The partial pressure of the vapor can then be evaluated at T_∞ and P_∞ can then be calculated from:

$$P_\infty = P_v\left[\frac{\tilde{M}_g + W_\infty\left(\tilde{M}_v - \tilde{M}_g\right)}{\tilde{M}_g - W_\infty \tilde{M}_g}\right] \tag{A.1}$$

Partial Pressure of the Gas and Vapor:

The partial pressure of the noncondensable gas, P_g, is given by:

$$P_g = P_\infty\left[\frac{W \tilde{M}_v}{\tilde{M}_g + W\left(\tilde{M}_v - \tilde{M}_g\right)}\right] \tag{A.2}$$

and the partial pressure of the vapor, P_v, is given by:

$$P_v = P_\infty - P_g \tag{A.3}$$

A.2 Water Properties

Saturation Temperature and Pressure of Steam:

Source: page 21 of Irvine and Liley (1984)

$$T_{sat} = A + \frac{B}{\ln(P_{sat}) + C} \tag{A.4}$$

where ln represents natural logarithm and the constants, A, B and C are given for two saturation pressure or temperature ranges:

$0.611 \text{ kPa} \le P_{sat} < 12.33\text{x}10^3 \text{ kPa}$	$12.33\text{x}10^3 \text{ kPa} \le P_{sat} \le 22.10\text{x}10^3 \text{ kPa}$
$273.16 \text{ K} \le T_{sat} < 600.0 \text{ K}$	$600.0 \text{ K} \le T_{sat} \le 647.3 \text{ K}$
$A = 0.426776\text{x}10^2$	$A = -0.387592\text{x}10^3$
$B = -0.389270\text{x}10^4$	$B = -0.125875\text{x}10^5$
$C = -0.948654\text{x}10^1$	$C = -0.152578\text{x}10^2$

Latent Heat of Vaporization:

Source: page 23 of Irvine and Liley (1984)

Temperature Range: $273.16 \text{ K} \le T_i \le 647.3 \text{ K}$

$$h_{fg} = 2.5009\text{x}10^3 \left[A + B t_c^{1/3} + C t_c^{5/6} + D t_c^{7/8} + \sum_{N=1}^{5} E(N) t_c^{N} \right] \tag{A.5}$$

where: $t_c = \frac{647.3 - T_i}{647.3}$

A = 0.0

B = 7.79221E-01

C = 4.62668

D = -1.07931

E(1) = -3.87446

E(2) = 2.94553

E(3) = -8.06395

E(4) = 1.15633E+01

E(5) = -6.02884

A.2.1 Water (Liquid) Properties

Water Density:

Assume that the liquid density of the steam is equal to the saturated liquid density.

Source: page 22 of Irvine and Liley (1984)

Temperature Range: $273.16\ \text{K} \leq T_L \leq 647.3\ \text{K}$

$$\rho_L = \frac{1}{3.155\text{x}10^{-3}\left[A + Bt_c^{\frac{1}{3}} + Ct_c^{\frac{5}{6}} + Dt_c^{\frac{7}{8}} + \sum_{N=1}^{5} E(N)t_c^{N}\right]} \qquad \text{(A.6)}$$

where: $t_c = \frac{647.3 - T_L}{647.3}$

A = 1.0

B = -1.9153882

C = 1.2015186E+01

D = -7.8464025

E(1) = -3.888614

E(2) = 2.0582238

E(3) = -2.0829991

E(4) = 8.2180004E-01

E(5) = 4.7549742E-01

Water Viscosity, Thermal Conductivity and Specific Heat:

Assume that μ_L, k_L and C_{P_L} is at the saturation values. A linear interpolation was used to evaluate the properties at the desired T_L from the table given below.

Source: page 774 of Incropera and DeWitt (1985)

example of linear interpolation: evaluate μ_L at $T_L = 283.0$ K

From Table A.1, select two tabulated viscosity values from the table, one at a higher temperature and the other at a lower temperature like so,

$\mu_{L1} = 1422.0 \times 10^{-6}$ N/m·s at $T_{L_1} = 280.0$

and

$\mu_{L2} = 1225.0 \times 10^{-6}$ N/m·s at $T_{L_2} = 285.0$

then,

$$\mu_L = \frac{\mu_{L_2} - \mu_{L_1}}{T_{L_2} - T_{L_1}} T_L + \mu_{L_1} - \frac{\mu_{L_2} - \mu_{L_1}}{T_{L_2} - T_{L_1}} T_{L_1}$$

$$\mu_L = 1303.8 \times 10^{-6} \text{ N/m·s}$$

Table A.1: Liquid steam properties.

T_L (K)	μ_L (N/m·s x10^6)	k_L (W/m·K x10^3)	C_{P_L} (kJ/kg·K)
273.15	1750.0	569.0	4.217
275.0	1652.0	574.0	4.211
280.0	1422.0	582.0	4.198
285.0	1225.0	590.0	4.189
290.0	1080.0	598.0	4.184
295.0	959.0	606.0	4.181
300.0	855.0	613.0	4.179
305.0	769.0	620.0	4.178
310.0	695.0	628.0	4.178
315.0	631.0	634.0	4.179
320.0	577.0	640.0	4.180
325.0	528.0	645.0	4.182
330.0	489.0	650.0	4.184
335.0	453.0	656.0	4.186
340.0	420.0	660.0	4.188
345.0	389.0	668.0	4.191
350.0	365.0	668.0	4.195
355.0	343.0	671.0	4.199
360.0	324.0	674.0	4.203
365.0	306.0	677.0	4.209
370.0	289.0	679.0	4.214
373.15	279.0	680.0	4.217
375.0	274.0	681.0	4.220
380.0	260.0	683.0	4.226
385.0	248.0	685.0	4.232
390.0	237.0	686.0	4.239
400.0	217.0	688.0	4.256
410.0	200.0	688.0	4.278

Table A.1: Liquid steam properties.

T_L (K)	μ_L (N/m·s x10^6)	k_L (W/m·K x10^3)	C_{P_L} (kJ/kg·K)
420.0	185.0	688.0	4.302
430.0	173.0	685.0	4.331
440.0	162.0	682.0	4.36
450.0	152.0	678.0	4.40
460.0	143.0	673.0	4.44
470.0	136.0	667.0	4.48
480.0	129.0	660.0	4.53
490.0	124.0	651.0	4.59
500.0	118.0	642.0	4.66
510.0	113.0	631.0	4.74
520.0	108.0	621.0	4.84
530.0	104.0	608.0	4.95
540.0	101.0	594.0	5.08
550.0	97.0	580.0	5.24
560.0	94.0	563.0	5.43
570.0	91.0	548.0	5.68
580.0	88.0	528.0	6.00
590.0	84.0	513.0	6.41
600.0	81.0	497.0	7.00
610.0	77.0	467.0	7.85
620.0	72.0	444.0	9.35
625.0	70.0	430.0	10.60
630.0	67.0	412.0	12.60
635.0	64.0	392.0	16.40
640.0	59.0	367.0	26.0
645.0	54.0	331.0	90.0
647.3	45.0	238.0	1.0e+10

A.2.2 Water Vapor (Steam) Properties

Molecular weight: steam, $\tilde{M}_v = 18.015$

Steam Vapor Density:

Approximated the vapor density of steam by the ideal gas equation of state:

$$\rho_v = \frac{P_v \tilde{M}_v}{\overline{R} T} \qquad \text{(A.7)}$$

where P_v is evaluated from Equations (A.1) to (A.3).

Steam Vapor Viscosity, Thermal Conductivity and Specific Heat:

Assume that μ_v, k_v and C_{pv} is at the saturation values. A linear interpolation was used to evaluate the properties at the desired T_v from Table A.2 below. For example of linear interpolation, see the previous section on steam vapor viscosity, thermal conductivity and specific heat.

Source: page 774 of Incropera and DeWitt (1985)

Table A.2: Vapor steam properties.

T_v (K)	μ_v (N/m·s x10^6)	k_v (W/m·K x10^3)	C_{Pv} (kJ/kg·K)
273.15	8.02	18.2	1.854
275.0	8.09	18.3	1.855
280.0	8.29	18.6	1.858
285.0	8.49	18.9	1.861
290.0	8.69	19.3	1.864
295.0	8.89	19.5	1.868
300.0	9.09	19.6	1.872
305.0	9.29	20.1	1.877
310.0	9.49	20.4	1.882
315.0	9.69	20.7	1.888
320.0	9.89	21.0	1.895
325.0	10.09	21.3	1.903
330.0	10.29	21.7	1.911
335.0	10.49	22.0	1.920
340.0	10.69	22.3	1.930
345.0	10.89	22.6	1.941
350.0	11.09	23.0	1.954
355.0	11.29	23.3	1.968
360.0	11.49	23.7	1.983
365.0	11.69	24.1	1.999
370.0	11.89	24.5	2.017
373.15	12.02	24.8	2.029
375.0	12.09	24.9	2.036
380.0	12.29	25.4	2.057
385.0	12.49	25.8	2.080
390.0	12.69	26.3	2.104
400.0	13.05	27.2	2.158
410.0	13.42	28.2	2.221
420.0	13.79	29.8	2.291
430.0	14.14	30.4	2.369
440.0	14.50	31.7	2.46
450.0	14.85	33.1	2.56
460.0	15.19	34.6	2.68
470.0	15.54	36.3	2.79
480.0	15.88	38.1	2.94
490.0	16.23	40.1	3.10
500.0	16.59	42.3	3.27
510.0	16.95	44.7	3.47

Table A.2: Vapor steam properties.

T_v (K)	μ_v (N/m·s x10^6)	k_v (W/m·K x10^3)	C_{Pv} (kJ/kg·K)
520.0	17.33	47.5	3.70
530.0	17.72	50.6	3.96
540.0	18.1	54.0	4.27
550.0	18.6	58.0	4.64
560.0	19.1	63.7	5.09
570.0	19.7	76.7	5.67
580.0	20.4	76.7	6.40
590.0	21.5	84.1	7.35
600.0	22.7	92.9	8.75
610.0	24.1	103.0	11.1
620.0	25.9	114.0	15.4
625.0	27.0	121.0	18.3
630.0	28.0	130.0	22.1
635.0	30.0	141.0	27.6
640.0	32.0	155.0	42.0
645.0	37.0	178.0	1.0e+10
647.3	45.0	238.0	1.0e+10

A.3 Air (Gas) Properties

Molecular weight: air, $\tilde{M}_g = 28.97$

Air Density:

Approximated the air density by the ideal gas equation of state.

$$\rho_g = \frac{P_g \tilde{M}_g}{\bar{R} T} \qquad \text{(A.8)}$$

where P_g is evaluated from Equations (A.1) and (A.2)

Air Viscosity:

Source: page 113 of Irvine and Liley (1984)

Temperature Range: $250\ K \leq T < 600\ K$

$$\mu_g = 1.0\text{x}10^{-6} \sum_{N=1}^{5} B(N) T^{N-1} \qquad (A.9)$$

where: b(1) = -9.8601e-01

b(2) = 9.080125e-02

b(3) = -1.17635575e-04

b(4) = 1.2349703e-07

b(5) = -5.7971299e-11

Note: The equation given on page 113 of Irvine and Liley (1984) does not give the μ_g in $N{\cdot}s/m^2$, instead, the value has been multiplied by $1.0\text{x}10^6$. This can be verified by comparing the value for μ_g obtained from equation on page 113 of Irvine and Liley to the tabulated data found on page 115 of Irvine and Liley.

Air Thermal Conductivity:

Source: page 114 of Irvine and Liley (1984)

Temperature Range: $250\ K \leq T \leq 1050\ K$

$$k_g = \sum_{N=1}^{6} C(N) T^{N-1} \qquad (A.10)$$

where: c(1) = -2.276501e-03

c(2) = 1.2598485e-04

c(3) = -1.4815235e-07

c(4) = 1.73550646e-10

c(5) = -1.066657e-13

c(6) = 2.47663035e-17

Air Specific Heat:

Source: page 97 of Irvine and Liley (1984)

Temperature Range: 250 K ≤ T ≤ 2000 K

$$C_{P_g} = 1.0\text{x}10^3 \sum_{N=1}^{5} \text{A(N)}\, T^{\text{N-1}} \qquad \text{(A.11)}$$

where: A(1) = 0.103409e+01

A(2) = -0.2848870e-03

A(3) = 0.7816818e-06

A(4) = -0.4970786e-9

A(5) = 0.1077024e-12

A.4 Sodium Properties

Saturation Temperature of Sodium:

Source: Table 32 on page 3-49 of Rohsenow *et al.* (1985)

The tabulated data is given in Table A.3 and three data points (shown in a bold font in the table) were used to obtain the following polynomial function fit:

$$T_{sat} = \frac{1}{\sum_{N=1}^{3} A(N)\left[\frac{\mathrm{Log}_{10}(P_{sat})}{1000}\right]^{N-1}} \qquad (A.12)$$

where: A(1) = 1.240664916666178E-03

A(2) = -1.852089809350434E-01

A(3) = -8.653480488567620E-01

Table A.3: Saturated temperature and pressure of sodium.

P_{sat} (kPa) tabulated	T_{sat} (K) tabulated	T_{sat} (K) calculated	% error of calculated T_{sat}
2.63100000E-08	3.80000000E+02	3.85384908E+02	1.41708095E+00
1.38500000E-07	4.00000000E+02	4.04821539E+02	1.20538477E+00
4.59400000E-06	4.50000000E+02	4.53593031E+02	7.98451310E-01
7.52300000E-05	5.00000000E+02	5.02593428E+02	5.18685601E-01
7.37700000E-04	5.50000000E+02	5.51793400E+02	3.26072687E-01
4.92600000E-03	6.00000000E+02	6.01168169E+02	1.94694768E-01
2.44500000E-02	6.50000000E+02	6.50650989E+02	1.00152078E-01
9.64900000E-02	7.00000000E+02	7.00350980E+02	5.01400588E-02
8.16000000E-01	7.50000000E+02	7.95536123E+02	6.07148313E+00
8.90400000E-01	**8.00000000E+02**	8.00000000E+02	3.94706490E-10
2.21700000E+00	8.50000000E+02	8.49962460E+02	-4.41649165E-03
4.98000000E+00	**9.00000000E+02**	9.00000001E+02	9.59687062E-08
1.02500000E+01	9.50000000E+02	9.50041342E+02	4.35182722E-03
1.96300000E+01	1.00000000E+03	1.00024215E+03	2.42145996E-02
6.00200000E+01	1.10000000E+03	1.10062823E+03	5.71118817E-02
1.50370000E+02	**1.20000000E+03**	1.20000000E+03	3.37875387E-08
3.24540000E+02	1.30000000E+03	1.29853570E+03	-1.12638554E-01
6.25380000E+02	1.40000000E+03	1.39659288E+03	-2.43365841E-01
1.10140000E+03	1.50000000E+03	1.49418330E+03	-3.87780264E-01
1.80200000E+03	1.60000000E+03	1.59109685E+03	-5.56446938E-01

Saturation Pressure of Sodium

Source: Table 32 on page 3-49 of Rohsenow *et al.* (1985)

The Newton-Raphson root search for P_{sat} requires an initial guess. This initial value, $P_{sat,guess}$, can be obtained from a polynomial function fit to all 19 data points from Table A.3:

$$P_{sat,guess} = 10^{a} \tag{A.13}$$

where: $$a = 1000 \sum_{N=1}^{19} A(N) \left(\frac{1}{T_{sat}} \right)^{N-1}$$

A(1) = 1.239454894732565E+01

A(2) = -1.598682876121705E+05

A(3) = 9.480391081632472E+08

A(4) = -3.424513464709380E+12

A(5) = 8.414236137751989E+15

A(6) = -1.485712528585111E+19

A(7) = 1.937860893550345E+22

A(8) = -1.882374805391690E+25

A(9) = 1.342829952640452E+28

A(10) = -6.633583186318712E+30

A(11) = 1.781945908436261E+33

A(12) = 2.611096134026306E+35

A(13) = -5.448172497285625E+38

A(14) = 3.006525270708681E+41

A(15) = -1.013567822244568E+44

A(16) = 2.281506512743549E+46

A(17) = -3.374631890934458E+48

A(18) = 2.989457336607413E+50

A(19) = -1.208117407392358E+52

The equation for T_{sat} as a function of P_{sat} is really a polynomial expression in terms of:

$$y = \left[\frac{1}{T_{sat}}\right] \text{ and } x = \left[\frac{\text{Log}_{10}(P_{sat})}{1000}\right],$$

$$y = a_1x + a_2x^2 + a_3x^3 \tag{A.14}$$

Given a value of T_{sat}, and we want to find P_{sat} (y is known, x is required), a function $f(x)$ is defined as:

$$f(x) = 0 = a_1x + a_2x^2 + a_3x^3 - y \tag{A.15}$$

The derivative of this function f with respect to x is:

$$f'(x) = a_1 + 2a_2x + 3a_3x^2 \tag{A.16}$$

A new value of x can then be calculated by:

$$x_{new} = x_{old} - \frac{f(x_{old})}{f'(x_{old})} \tag{A.17}$$

Starting with an initial guess as x_{old}, x_{new} is calculated, replace x_{old} with x_{new} and recalculate. Keep iterating untill the percent difference between x_{new} and x_{old} is less than $10^{-7}\%$. P_{sat} can then be obtained when x has been calculated to the desired

accuracy. Table A.4 shows the accuracy of this method because given a value for the saturated pressure, $P_{sat,1}$, the corresponding saturation temperature, T_{sat}, can be calculated. Then for T_{sat}, the Newton-Raphson root search will produce $P_{sat,2}$ which is essentially identical to $P_{sat,1}$.

Table A.4: Accuracy of Newton-Raphson root search for the saturation pressure of sodium.

$P_{sat,1}$ (kPa) starting value	T_{sat} (K) calculated with $P_{sat,1}$	$P_{sat,2}$ (kPa) calculated with T_{sat}
0.81234567890000	795.30789494101	0.81234567890000
1.1234567890000	812.15028112206	1.1234567890000
2.1234567890000	847.45692236383	2.1234567890000
3.1234567890000	870.44151764413	3.1234567890000
4.1234567890000	887.79560111635	4.1234567890000
10.1234567890000	949.13185465375	10.1234567890000
100.123456789000	1153.8224568611	100.123456789000
140.123456789000	1191.7179432855	140.123456789000

Latent Heat of Vaporization of Sodium:

Source: Table 32 on page 3-49 of Rohsenow *et al.* (1985)

The tabulated data is given in Table A.5 and seven data points (shown in a bold font in the table) were used to obtain the following polynomial function fit:

$$h_{fg} = 3.0\text{x}10^3 \sum_{N=1}^{7} A(N) T_i^{N-1} \qquad \text{(A.18)}$$

where: A(1) = 1.685133041746523E+03

A(2) = -1.269746171635577E+00

A(3) = 3.880618917880488E-03

A(4) = -6.572769601481255E-06

A(5) = 5.559618599617473E-09

A(6) = -2.322335999352337E-12

A(7) = 3.804812132246850E-16

Table A.5: Sodium latent heat of vaporization.

T_i (K) tabulated	h_{fg} (J/kg) tabulated	h_{fg} (J/kg) calculated	% error of calculated h_{fg}
3.80000000E+02	**4.50300000E+06**	4.50300000E+06	0.00000000E+00
4.00000000E+02	4.49300000E+06	4.49274094E+06	-5.76594539E-03
4.50000000E+02	4.46700000E+06	4.46674162E+06	-5.78430435E-03
5.00000000E+02	**4.43900000E+06**	4.43900000E+06	0.00000000E+00
5.50000000E+02	4.40900000E+06	4.40852280E+06	-1.08234132E-02
6.00000000E+02	4.37500000E+06	4.37485011E+06	-3.42605939E-03
6.50000000E+02	4.33800000E+06	4.33792902E+06	-1.63616741E-03
7.00000000E+02	**4.29800000E+06**	4.29800000E+06	4.33374860E-14
7.50000000E+02	4.25600000E+06	4.25549614E+06	-1.18387551E-02
8.00000000E+02	4.21200000E+06	4.21095528E+06	-2.48033320E-02
8.50000000E+02	4.16600000E+06	4.16494492E+06	-2.53259183E-02
9.00000000E+02	**4.11800000E+06**	4.11800000E+06	-4.52317909E-14
9.50000000E+02	4.07000000E+06	4.07057352E+06	1.40913727E-02
1.00000000E+03	**4.02300000E+06**	4.02300000E+06	4.62999043E-14
1.10000000E+03	3.92600000E+06	3.92802817E+06	5.16600083E-02
1.20000000E+03	3.83200000E+06	3.83281151E+06	2.11770945E-02
1.30000000E+03	**3.73500000E+06**	3.73500000E+06	-1.24675043E-14
1.40000000E+03	3.63300000E+06	3.63125740E+06	-4.79658571E-02
1.50000000E+03	3.52200000E+06	3.51917379E+06	-8.02445150E-02
1.60000000E+03	**3.40000000E+06**	3.40000000E+06	1.36959202E-13

A.4.1 Liquid Sodium Properties

Liquid Sodium Density:

Source: Table 5-34 on page 533 of Bolz and Tuve (1973)

The tabulated data is given in Table A.6 and four data points (shown in a bold font in the table) were used to obtain the following polynomial function fit:

$$\rho_L = \sum_{N=1}^{4} A(N) T_L^{N-1} \qquad (A.19)$$

where: A(1) = 1.011468326351929E+03

A(2) = -2.232792937678628E-01

A(3) = -1.511268255051431E-05

A(4) = -4.552689292179106E-10

Table A.6: Liquid sodium density.

T_L (K) tabulated	ρ_L (kg/m^3) tabulated	ρ_L (kg/m^3) calculated	% error of calculated ρ_L
3.66483300E+02	**9.27588000E+02**	9.27588000E+02	0.00000000E+00
4.77594400E+02	9.03528000E+02	9.01334641E+02	-2.42754904E-01
5.88705600E+02	**8.74692000E+02**	8.74692000E+02	0.00000000E+00
6.99816700E+02	8.49060000E+02	8.47656376E+02	-1.65314999E-01
8.10927800E+02	**8.20224000E+02**	8.20224000E+02	0.00000000E+00
9.22038900E+02	7.86582000E+02	7.92391124E+02	7.38527392E-01
1.03315000E+03	**7.64154000E+02**	7.64154000E+02	-1.48774773E-14

Liquid Sodium Viscosity:

Source: Table 5-34 on page 533 of Bolz and Tuve (1973)

The tabulated data is given in Table A.7 and all the data points were used to obtain the following polynomial function fit:

$$\mu_L = \sum_{N=1}^{10} A(N) T_L^{N-1} \qquad \text{(A.20)}$$

where: A(1) = 3.975718390107967E-01

A(2) = -4.910165819614793E-03

A(3) = 2.637551794991279E-05

A(4) = -8.079137160810898E-08

A(5) = 1.556389002843107E-10

A(6) = -1.957881246565389E-13

A(7) = 1.610499770854559E-16

A(8) = -8.364513144006752E-20

A(9) = 2.492289317896899E-23

A(10) = -3.249889547977568E-27

Table A.7: Liquid sodium viscosity.

T_L (K) tabulated	μ_L (N·s/m^2) tabulated	μ_L (N·s/m^2) calculated	% error of calculated μ_L
3.66483300E+02	7.12425000E-04	7.12425000E-04	-2.71497586E-11
4.77594400E+02	4.52235000E-04	4.52235000E-04	-2.43279303E-10
5.88705600E+02	3.29161000E-04	3.29161000E-04	-1.54055978E-09
6.99816700E+02	2.51930000E-04	2.51930000E-04	8.63837102E-10
8.10927800E+02	2.31280000E-04	2.31280000E-04	-5.51875219E-10
9.22038900E+02	1.96175000E-04	1.96175000E-04	3.46271818E-09
1.03315000E+03	1.71395000E-04	1.71395000E-04	2.31681754E-08
1.15000000E+03	1.45335110E-04		
1.17500000E+03	1.39759610E-04		
1.20000000E+03	1.34184109E-04		

Note: The last three data points were obtained by a linear extrapolation of two data points at T_L = 9.22038900E+02 K and T_L = 1.03315000E+03 K

Liquid Sodium Thermal Conductivity:

Source: Table 5-34 on page 533 of Bolz and Tuve (1973)

The tabulated data is given in Table A.8 and all the data points were used to obtain the following polynomial function fit:

$$k_L = \sum_{N=1}^{8} A(N) T_L^{N-1} \qquad \text{(A.21)}$$

where: A(1) = 1.024599115464461E+03

A(2) = -9.562595884971515E+00

A(3) = 4.040434802187922E-02

A(4) = -9.168424360561372E-05

A(5) = 1.204701441764185E-07

A(6) = -9.200634050775044E-11

A(7) = 3.796224470956367E-14

A(8) = -6.550354751627853E-18

Table A.8: Liquid sodium thermal conductivity.

T_L (K) tabulated	k_L (W/m·K) tabulated	k_L (W/m·K) calculated	% error of calculated k_L
3.66483300E+02	8.49430000E+01	8.49430000E+01	3.34597429E-13
4.77594400E+02	8.07910000E+01	8.07910000E+01	6.33227426E-13
5.88705600E+02	7.57740000E+01	7.57740000E+01	-1.61286656E-12
6.99816700E+02	6.93730000E+01	6.93730000E+01	7.59982572E-12
8.10927800E+02	6.43560000E+01	6.43560000E+01	1.48388563E-11
9.22038900E+02	6.05500000E+01	6.05500000E+01	4.01095800E-11
1.03315000E+03	5.65710000E+01	5.65710000E+01	7.38037000E-11
1.20000000E+03	5.05959341E+01		

Note: The last data points was obtained by a linear extrapolation of two data points at T_L = 9.22038900E+02 K and T_L = 1.03315000E+03 K

Liquid Sodium Specific Heat:

Source: Table on page 331 of Hultgren *et al.* (1973)

The tabulated data is given in Table A.9 and all the data points were used to obtain the following polynomial function fit:

$$C_{P_L} = \sum_{N=1}^{11} A(N) T_L^{N-1} \qquad (A.22)$$

where: A(1) = 3.358544943001141E+05

A(2) = -4.509830247988411E+03

A(3) = 2.688320266274026E+01

A(4) = -9.333074952894620E-02

A(5) = 2.090798737248267E-04

A(6) = -3.159957632594026E-07

A(7) = 3.265149237993157E-10

A(8) = -2.279100314599376E-13

A(9) = 1.029127453476702E-16

A(10) = -2.716345589650161E-20

A(11) = 3.184489760703564E-24

Table A.9: Liquid sodium specific heat.

T_L (K) tabulated	C_{P_L} (J/kg·K) tabulated	C_{P_L} (J/kg·K) calculated	% error of calculated C_{P_L}
4.00000000E+02	1.37041297E+03	1.37041297E+03	2.84214404E-11
5.00000000E+02	1.32855440E+03	1.32855440E+03	7.12984528E-11
6.00000000E+02	1.29579553E+03	1.29579553E+03	2.40920770E-11
7.00000000E+02	1.27395628E+03	1.27395628E+03	-1.46334438E-10
8.00000000E+02	1.25939678E+03	1.25939678E+03	1.41970796E-09
9.00000000E+02	1.25393696E+03	1.25393696E+03	1.04611655E-09
1.00000000E+03	1.25939678E+03	1.25939678E+03	-1.51055656E-09
1.10000000E+03	1.27213634E+03	1.27213634E+03	2.02905682E-09
1.15620000E+03	1.28487590E+03	1.28487590E+03	-1.85859213E-09
1.20000000E+03	1.29579553E+03	1.29579553E+03	7.67263341E-09
1.30000000E+03	1.35767340E+03	1.35767340E+03	1.47976321E-08

A.4.2 Sodium Vapor Properties

Molecular weight: steam, $\tilde{M}_v = 22.9898$

Sodium Vapor Density:

Approximated the vapor density of steam by the ideal gas equation of state.

$$\rho_v = \frac{P_v \tilde{M}_v}{\bar{R} T} \qquad \text{(A.23)}$$

where P_v is evaluated from Equations (A.1) to (A.3)

Sodium Vapor Viscosity and Thermal Conductivity:

Source: Reid *et al.* (1977)

Viscosity: Equation (9-3.9) of Reid *et al.*

$$\mu_v = 26.69 \frac{\sqrt{\tilde{M}_v T}}{\sigma^2 \Omega} 1.0\text{x}10^{-7} \qquad \text{(A.24)}$$

Thermal Conductivity: Equation (10-2.2) of Reid *et al.*

$$k_v = \frac{1.989\text{x}10^{-4} \left(\frac{T}{\tilde{M}_v} \right)^{1/2}}{\sigma^2 \Omega} 418.4 \qquad \text{(A.25)}$$

where: k_b = boltzman's constant = $1.3805\text{x}10^{-16}$ ergs/K

ω = accentric factor, from equation (2-3.3) of Reid *et al.*

$$= \frac{3}{7} \frac{T_b/T_c}{1 - T_b/T_c} \text{Log}_{10}(P_c) - 1$$

ε = potential energy, from equation (2-7.3) of Reid *et al.*

$= k_b T_c (0.7915 + 0.1693\omega)$, ergs

σ = potential length constant, from equation (2-7.2) of Reid *et al.*

$= (2.3551 - 0.087\omega)\left(\frac{T_c}{P_c}\right)^{1/3}$, Å

P_c = critical pressure = 365.1604 atm
T_c = critical temperature = 2500.0 K
T_b = normal boiling temperature = 1155.0 K

} Source: Table 10 of Rohsenow *et al.* (1985)

Ω = collision integral, from equation (9-4.3) of Reid *et al.*

$$= \left(\frac{A}{T'^{B}}\right) + \frac{C}{\exp(DT')} + \frac{E}{\exp(FT')}$$

$$T' = \frac{k_b T}{\varepsilon}$$

A = 1.16145

B = 0.14874

C = 0.52457

D = 0.77320

E = 2.16178

F = 2.43787

Sodium Vapor Specific Heat:

Source: Table on page 331 of Hultgren *et al.* (1973)

The specific heat of sodium vapor is constant over the range of $300 \leq T \leq 1700$ K.

C_{Pv} = 905.114268 J/kg·K (A.26)

A.5 Argon Gas Properties

Molecular weight: argon, $\tilde{M}_g = 39.948$

Argon Density:

Approximated the vapor density of argon by the ideal gas equation of state.

$$\rho_g = \frac{P_g \tilde{M}_g}{\bar{R} T} \qquad \text{(A.27)}$$

where P_g is evaluated from Equations (A.1) and (A.2)

Argon Viscosity and Thermal Conductivity:

Source: Reid *et al.* (1977)

Viscosity: Equation (9-3.9) of Reid *et al.*

$$\mu_g = 26.69 \frac{\sqrt{\tilde{M}_g T}}{\sigma^2 \Omega} 1.0\text{x}10^{-7} \qquad \text{(A.28)}$$

Thermal Conductivity: Equation (10-2.2) of Reid *et al.*

$$k_g = \frac{1.989\text{x}10^{-4}\left(\frac{T}{\tilde{M}_g}\right)^{1/2}}{\sigma^2 \Omega} 418.4 \qquad \text{(A.29)}$$

where: k_b = boltzman's constant = $1.3805\text{x}10^{-16}$ ergs/K

ω = accentric factor, from equation (2-3.3) of Reid *et al.*

$$= \frac{3}{7}\frac{T_b/T_c}{1 - T_b/T_c} \text{Log}_{10}(P_c) - 1$$

ε = potential energy, from equation (2-7.3) of Reid *et al.*

$= k_b T_c (0.7915 + 0.1693\omega)$, ergs

σ = potential length constant, from equation (2-7.2) of Reid *et al.*

$= (2.3551 - 0.087\omega)\left(\frac{T_c}{P_c}\right)^{1/3}$, Å

P_c = critical pressure = 49.346 atm
T_c = critical temperature = 151.0 K
T_b = normal boiling temperature = 87.2 K

} Source: Table 10 of Rohsenow *et al.* (1985)

Ω = collision integral, from equation (9-4.3) of Reid *et al.*

$$= \left(\frac{A}{T'^{B}}\right) + \frac{C}{\exp(DT')} + \frac{E}{\exp(FT')}$$

$$T' = \frac{k_b T}{\varepsilon}$$

A = 1.16145

B = 0.14874

C = 0.52457

D = 0.77320

E = 2.16178

F = 2.43787

Argon Specific Heat:

Source: Table AVII.2 on page 118 of Irvine and Liley (1984)

The specific heat of argon is constant over the range of $200 \le T \le 1600$ K.

$$C_{Pg} = 520.8870534 \text{ J/kg·K} \qquad \text{(A.30)}$$

A.6 Glycerine Properties

Saturation Temperature of Glycerine:

Source: Table on page 297 of Smith and Srivastava (1986)

Some of the tabulated data is given in Table A.10 and three data points (shown in a bold font in table) were used to obtain the following polynomial function fit:

$$T_{sat} = 10^{a} \tag{A.31}$$

where: $$a = \left[\sum_{N=1}^{3} A(N) \left[\mathrm{Log}_{10}(P_{sat}) \right]^{N-1} \right]$$

A(1) = 2.641156035945220E+00

A(2) = 4.642589471283395E-02

A(3) = 2.293023884903247E-03

Table A.10: Saturation temperature and pressure of glycerine.

P_{sat} (kPa) tabulated	T_{sat} (K) tabulated	T_{sat} (K) calculated	% error of calculated T_{sat}
4.04000000E-05	**3.03000000E+02**	3.03000000E+02	-3.75204085E-14
1.01300000E-03	3.34000000E+02	3.33195315E+02	-2.40923504E-01
8.62600000E-03	**3.59000000E+02**	3.59000000E+02	1.58338214E-13
9.57200000E-01	4.33000000E+02	4.36792222E+02	8.75801878E-01
3.16900000E+01	**5.20000000E+02**	5.20000000E+02	6.55885602E-14

Saturation Pressure of Glycerine:

Source: Table on page 297 of Smith and Srivastava (1986)

The Newton-Raphson root search for P_{sat} requires an initial guess. This initial value, $P_{sat,guess}$ can be obtained from a polynomial function fit to three data points shown in bold text in Table A.11:

$$P_{sat,guess} = 10^{a} \tag{A.32}$$

where: $$a = \left[\sum_{N=1}^{3} A(N) \left[\mathrm{Log}_{10}(T_{sat}) \right]^{N-1} \right]$$

A(1) = -3.388954032804762E+02

A(2) = 2.350010713865879E+02

A(3) = -4.037962956705267E+01

The equation T_{sat} as a function of P_{sat} is really a polynomial expression in terms of $y = \mathrm{Log}_{10}(T_{sat})$ and $x = \mathrm{Log}_{10}(P_{sat})$,

$$y = a_1 x + a_2 x^2 + a_3 x^3 \tag{A.33}$$

Given a value of T_s, and we want to find P_s (y is known, x is required), a function $f(x)$ is defined as:

$$f(x) = 0 = a_1 x + a_2 x^2 + a_3 x^3 - y \tag{A.34}$$

The derivative of this function f with respect to x is:

$$f'(x) = a_1 + 2a_2 x + 3a_3 x^2 \tag{A.35}$$

A new value of x can then be calculated by:

$$x_{new} = x_{old} - \frac{f(x_{old})}{f'(x_{old})} \tag{A.36}$$

Starting with an initial guess as x_{old}, x_{new} is calculated, replace x_{old} with x_{new} and recalculate. Keep iterating untill the percent difference between x_{new} and x_{old} is less than $10^{-7}\%$. P_{sat} can then be obtained when x has been calculated to the desired accuracy. Table A.11 shows the accuracy of this method because given a value for the saturated pressure, $P_{sat,1}$, the corresponding saturation temperature, T_{sat}, can be calculated. Then for T_{sat}, the Newton-Raphson root search will produce $P_{sat,2}$ which is essentially identical to $P_{sat,1}$.

Table A.11: Accuracy of Newton-Raphson root search for the saturation pressure of glycerine.

$P_{sat,1}$ (kPa) starting value	T_{sat} (K) calculated with $P_{sat,1}$	$P_{sat,2}$ (kPa) calculated with T_{sat}	% error of $P_{sat,2}$
9.370E-06	2.92206582E+02	9.370E-06	7.95505863E-13
3.305E-02	3.77951011E+02	3.305E-02	-1.25970842E-12
3.143E+00	4.62181839E+02	3.143E+00	-1.89334884E-12

Latent Heat of Vaporization of Glycerine:

Source: Graph on page 128 of Gallant (1968)

A polynomial function was fitted to data points read off the graph for a temperature range of $330 \leq T_i \leq 500$ K:

$$h_{fg} = \sum_{N=1}^{9} A(N) T_i^{N-1} \qquad (A.37)$$

where: A(1) = -5.810894555687108E+08

A(2) = 1.001196016043278E+07

A(3) = -7.471516784621120E+04

A(4) = 3.161775088262917E+02

A(5) = -8.303921138847964E-01

A(6) = 1.386824715066246E-03

A(7) = -1.439113569425394E-06

A(8) = 8.487920085844089E-10

A(9) = -2.179359930628292E-13

A.6.1 Liquid Glycerine Properties

Liquid Glycerine Density:

Source: Graph on page 131 of Gallant (1968)

A polynomial function was fitted to data points read off the graph for a temperature range of $275 \leq T_L \leq 580$ K:

$$\rho_L = \sum_{N=1}^{3} A(N) T_L^{N-1} \qquad (A.38)$$

where: A(1) = 1.409866697761959E+03

A(2) = -3.622528402899021E-01

A(3) = -4.649950125339035E-04

Liquid Glycerine Viscosity:

Source: Graphs on pages 132 and 134 of Gallant (1968)

A polynomial function was fitted to data points read off the graph for a temperature range of $350 \leq T_L \leq 450$ K:

$$\mu_L = \sum_{N=1}^{10} A(N) T_L^{N-1} \qquad \text{(A.39)}$$

where: A(1) = -6.957169365731268E+05

A(2) = 1.589091193872878E+04

A(3) = -1.610197061889472E+02

A(4) = 9.500214155495478E-01

A(5) = -3.596820637773954E-03

A(6) = 9.062278194615016E-06

A(7) = -1.519484353266230E-08

A(8) = 1.634960898168976E-11

A(9) = -1.024422133977335E-14

A(10) = 2.847850144465320E-18

Liquid Glycerine Thermal Conductivity:

Source: Graphs on page 138 of Gallant (1968)

A polynomial function was fitted to data points read off the graph for a temperature range of $290 \leq T_L \leq 480$ K:

$$k_L = \sum_{N=1}^{3} A(N) T_L^{N-1} \qquad (A.40)$$

where: A(1) = 2.414345354596216E-02

A(2) = 8.425167491085949E-06

A(3) = 1.510687869353571E-08

Liquid Glycerine Specific Heat:

Source: Graphs on page 130 of Gallant (1968)

A polynomial function was fitted to data points read off the graph for a temperature range of $290 \leq T_L \leq 473$ K:

$$C_{P_L} = \sum_{N=1}^{5} A(N) T_L^{N-1} \qquad (A.41)$$

where: A(1) = -1.807730903928356E+04

A(2) = 2.010518236927689E+02

A(3) = -7.396441193821263E-01

A(4) = 1.226531151819975E-03

A(5) = -7.583886819026206E-07

A.6.2 Glycerine Vapor Properties

Molecular weight: glycerine, $\tilde{M}_v = 92.095$

Glycerine Vapor Density:

Approximated the vapor density of steam by the ideal gas equation of state.

$$\rho_v = \frac{P_v \tilde{M}_v}{\overline{R} T} \tag{A.42}$$

where P_v is evaluated from (A.1) to (A.3)

Glycerine Vapor Viscosity:

Source: Graphs on page 132 of Gallant (1968)

A polynomial function was fitted to data points read off the graph for a temperature range of $270 \le T \le 770$ K:

$$\mu_v = 1.0 \times 10^{-4} \sum_{N=1}^{3} A(N) T^{N-1} \tag{A.43}$$

where: A(1) = 2.738639920749575E-03

A(2) = 2.379199522295590E-04

A(3) = 5.187274325086972E-09

Glycerine Vapor Thermal Conductivity:

Source: Graphs on page 136 of Gallant (1968)

A polynomial function was fitted to data points read off the graph for a temperature range of $323 \le T \le 750$ K:

$$k_v = \sum_{N=1}^{6} A(N) T^{N-1} \tag{A.44}$$

where: A(1) = 1.182122606510318E-01

A(2) = -1.223059600744010E-03

A(3) = 5.162974967214564E-06

A(4) = -1.029589882569102E-08

A(5) = 1.020841500354680E-11

A(6) = -3.973121834282032E-15

Glycerine Vapor Specific Heat:

Source: Graphs on page 128 of Gallant (1968)

A polynomial function was fitted to data points read off the graph for a temperature range of $270 \leq T \leq 773$ K:

$$C_{P_v} = \sum_{N=1}^{6} A(N) T^{N-1} \qquad \text{(A.45)}$$

where: A(1) = 1.502927809943238E+03

A(2) = -4.066408070553585E+00

A(3) = 2.590494599585174E-02

A(4) = -4.956541257228084E-05

A(5) = 4.424333480192872E-08

A(6) = -1.572853351236986E-11

A.7 Bromine Gas Properties

Molecular weight: bromine, $\tilde{M}_g = 159.808$

Bromine Density:

Approximated the vapor density of bromine by the ideal gas equation of state.

$$\rho_g = \frac{P_g \tilde{M}_g}{\overline{R} T} \tag{A.46}$$

where P_g is evaluated from (A.1) and (A.2)

Bromine Viscosity:

Source: Touloukian *et al.* (1970)

A polynomial function was fitted to data points for a temperature range of $280 \leq T \leq 800$ K:

$$\mu_g = \sum_{N=1}^{3} A(N) T^{N-1} \tag{A.47}$$

where: A(1) = 2.318181818181828E-06

A(2) = 4.174242424242419E-08

A(3) = 7.575757575757632E-12

Bromine Thermal Conductivity:

Source: Touloukian *et al.* (1970)

A polynomial function was fitted to data points given for saturated bromine vapor for a temperature range of $300 \leq T \leq 500$ K:

$$k_g = \sum_{N=1}^{4} A(N) T^{N-1} \qquad \text{(A.48)}$$

where: A(1) = -1.142773279352228E-01

A(2) = 1.114839502602661E-03

A(3) = -2.746168305378834E-06

A(4) = 2.740023134759979E-09

Bromine Specific Heat:

Source: Touloukian *et al.* (1970)

Touloukian *et al.* suggested the following polynomial function for a temperature range of $200 \leq T \leq 590$ K:

$$C_{P_g} = 4.184 \times 10^3 \sum_{N=1}^{4} A(N) T^{N-1} \qquad \text{(A.49)}$$

where: A(1) = 4.184200000000000E-02

A(2) = 7.345570000000000E-05

A(3) = -1.381880000000000E-07

A(4) = 9.044155560000001E-11

A.8 Mixture Property Evaluation

Diffusion Coefficient for a Steam-Air Mixture

Source: Equation 11-4.1 on page 554 of Reid *et al.* (1977)

$$D = 10^{-4}\left\{\frac{10^{-3}\,T^{1.75}\left[\frac{\tilde{M}_g+\tilde{M}_v}{\tilde{M}_g\,\tilde{M}_v}\right]^{0.5}}{\frac{P_\infty}{101.33}\left[\gamma_g^{1/3}+\gamma_v^{1/3}\right]^2}\right\} \qquad \text{(A.50)}$$

where: $\gamma_g = 20.1$, $\gamma_v = 12.7$ } Table 11-1 on page 554 of Reid *et al.* (1977)

Diffusion Coefficient for Sodium-Argon mixture and Glycerine-Bromine Mixture:

Source: Equation (11-3.2) from Reid *et al.* 1977)

$$D = 1.858\text{x}10^{-3}\,T^{3/2}\frac{\left[\frac{\tilde{M}_v+\tilde{M}_g}{\tilde{M}_v\,\tilde{M}_g}\right]^{1/2}}{\frac{P_\infty}{101.325}\sigma_{vg}^{\,2}\,\Omega}\,1.0\text{x}10^{-4} \qquad \text{(A.51)}$$

where: $\sigma_{vg} = \frac{\sigma_v+\sigma_g}{2}$, from equation (11-3.5) of Reid *et al.*

σ_v, σ_g = potential length constant, from equation (2-7.2) of Reid *et al.*

$$= (2.3551 - 0.087\omega)\left(\frac{T_c}{P_c}\right)^{1/3},\ \text{Å}$$

ω = accentric factor, from equation (2-3.3) of Reid *et al.*

$$= \frac{3}{7}\frac{T_b/T_c}{1-T_b/T_c}\text{Log}_{10}(P_c) - 1$$

$\varepsilon_{vg} = (\varepsilon_v\,\varepsilon_g)^{1/2}$, from equation (11-3.4) of Reid *et al.*

$\varepsilon_v, \varepsilon_g$ = potential energy, from equation (2-7.3) of Reid *et al.*

$$= k_b\,T_c\,(0.7915 + 0.1693\omega),\ \text{ergs}$$

k_b = boltzman's constant = $1.3805\text{x}10^{-16}$ ergs/K

Ω = collision integral, from equation (11-3.6) of Reid *et al.*

$$= \left(\frac{A}{T'^{B}}\right) + \frac{C}{\exp(DT')} + \frac{E}{\exp(FT')} \frac{G}{\exp(HT')}$$

$$T' = \frac{k_b T}{\varepsilon}$$

A = 1.06036

B = 0.15610

C = 0.19300

D = 0.47635

E = 1.03587

F = 1.52996

G = 1.76474

H = 3.89411

$$P_c = \begin{cases} 365.1604 \text{ atm}, & \text{sodium} \\ 49.346 \text{ atm}, & \text{argon} \\ 66.0 \text{ atm}, & \text{glycerine} \\ 102.0 \text{ atm}, & \text{bromine} \end{cases}$$

$$T_c = \begin{cases} 2500.0 \text{ K}, & \text{sodium} \\ 151.0 \text{ K}, & \text{argon} \\ 726.0 \text{ K}, & \text{glycerine} \\ 584.0 \text{ K}, & \text{bromine} \end{cases}$$

$$T_b = \begin{cases} 1155.0 \text{ K}, & \text{sodium} \\ 87.2 \text{ K}, & \text{argon} \\ 563.0 \text{ K}, & \text{glycerine} \\ 331.9 \text{ K}, & \text{bromine} \end{cases}$$

Mixture Density:

$$\rho = \rho_v + \rho_g \qquad \text{(A.52)}$$

- Mixture Viscosity:

  Source: Equation 9-5.4 on page 411 of Reid *et al.* (1977)

$$\mu = \frac{\gamma_g \mu_g}{\gamma_g + \gamma_v \varphi_{gv}} + \frac{\gamma_v \mu_v}{\gamma_v + \gamma_g \varphi_{vg}} \qquad \text{(A.53)}$$

where: $\gamma_g = \frac{P_g}{P_\infty}$

$$\gamma_v = \frac{P_v}{P_\infty}$$

$$\varphi_{gv} = \frac{\left[1 + \left(\frac{\mu_g}{\mu_v}\right)^{1/2} \left(\frac{\tilde{M}_v}{\tilde{M}_g}\right)^{1/4}\right]^2}{\left[8\left(1 + \frac{\tilde{M}_g}{\tilde{M}_v}\right)\right]^{1/2}}$$

$$\varphi_{vg} = \varphi_{gv}\left[\frac{\mu_v \tilde{M}_g}{\mu_g \tilde{M}_v}\right]$$

Mixture Thermal Conductivity:

Source: Equation 10-6.1 on page 508 of Reid *et al.* (1977)

$$k = \frac{\gamma_g k_g}{\gamma_g + \gamma_v \varphi_{gv}} + \frac{\gamma_v k_v}{\gamma_v + \gamma_g \varphi_{vg}} \qquad \text{(A.54)}$$

where: $\gamma_g = \frac{P_g}{P_\infty}$

$$\gamma_v = \frac{P_v}{P_\infty}$$

$$\varphi_{gv} = \frac{\left[1+\left(\frac{\mu_g \tilde{M}_v}{\mu_v \tilde{M}_g}\right)^{1/2}\left(\frac{\tilde{M}_g}{\tilde{M}_v}\right)^{1/4}\right]^2}{\left[8\left(1+\frac{\tilde{M}_g}{\tilde{M}_v}\right)\right]^{1/2}}$$

$$\varphi_{vg} = \frac{\left[1+\left(\frac{\mu_v \tilde{M}_g}{\mu_g \tilde{M}_v}\right)^{1/2}\left(\frac{\tilde{M}_v}{\tilde{M}_g}\right)^{1/4}\right]^2}{\left[8\left(1+\frac{\tilde{M}_v}{\tilde{M}_g}\right)\right]^{1/2}}$$

Mixture Specific Heat:

$$C_p = W C_{P_g} + (1-W) C_{Pv} \qquad \text{(A.55)}$$

APPENDIX B

Discretization of Boundary Layer

Equations and Boundary Conditions

This appendix gives detailed information on the discretization of the boundary layer equations and their boundary conditions. It also contains the details of the interpolation equations used to evaluate the value of ϕ and $\frac{\partial \phi}{\partial \eta}$ at the control volume faces. The boundary layer equations are as follows:

- **Liquid Continuity Equation**

$$\frac{\partial}{\partial \chi}(\delta \rho_L u_L) - \frac{d\delta}{d\chi}\frac{\partial}{\partial \eta}(\eta \rho_L u_L) + \frac{\partial}{\partial \eta}(\rho_L v_L) = 0 \qquad \text{(B.1)}$$

- Liquid Momentum Equation

$$\frac{\partial}{\partial \chi}(\delta \rho_L u_L u_L) - \frac{d\delta}{d\chi}\frac{\partial}{\partial \eta}(\eta \rho_L u_L u_L) + \frac{\partial}{\partial \eta}(\rho_L v_L u_L) = \frac{\partial}{\partial \eta}\left(\frac{\mu_L}{\delta}\frac{\partial u_L}{\partial \eta}\right) + \delta g (\rho_L - \rho_\infty)\cos\alpha \qquad \text{(B.2)}$$

- Liquid Energy Equation

$$\frac{\partial}{\partial \chi}(\delta \rho_L c_{P_L} u_L T_L) - \frac{d\delta}{d\chi}\frac{\partial}{\partial \eta}(\eta \rho_L c_{P_L} u_L T_L) + \frac{\partial}{\partial \eta}(\rho_L c_{P_L} v_L T_L) = \frac{\partial}{\partial \eta}\left(\frac{k_L}{\delta}\frac{\partial T_L}{\partial \eta}\right) \qquad \text{(B.3)}$$

- Mixture Continuity Equation

$$\frac{\partial}{\partial \chi}(\delta \rho u) - \frac{d\delta}{d\chi}\frac{\partial}{\partial \eta}(\eta \rho u) + \frac{\partial}{\partial \eta}(\rho v) = 0 \qquad \text{(B.4)}$$

- Mixture Momentum Equation

$$\frac{\partial}{\partial \chi}(\delta \rho u u) - \frac{d\delta}{d\chi}\frac{\partial}{\partial \eta}(\eta \rho u u) + \frac{\partial}{\partial \eta}(\rho v u) = \frac{\partial}{\partial \eta}\left(\frac{\mu}{\delta}\frac{\partial u}{\partial \eta}\right) + \delta g (\rho - \rho_\infty)\cos\alpha \qquad \text{(B.5)}$$

- Mixture Energy Equation

$$\frac{\partial}{\partial \chi}(\delta \rho c_P u T) - \frac{d\delta}{d\chi}\frac{\partial}{\partial \eta}(\eta \rho c_P u T) + \frac{\partial}{\partial \eta}(\rho c_P v T) = \frac{\partial}{\partial \eta}\left(\frac{k}{\delta}\frac{\partial T}{\partial \eta}\right) + \frac{\partial}{\partial \eta}\left(\frac{\rho D\left(c_{P_g} - c_{P_v}\right)}{\delta} T \frac{\partial W}{\partial \eta}\right) \quad \text{(B.6)}$$

- Mixture Mass Diffusion Equation

$$\frac{\partial}{\partial \chi}(\delta \rho u W) - \frac{d\delta}{d\chi}\frac{\partial}{\partial \eta}(\eta \rho u W) + \frac{\partial}{\partial \eta}(\rho v W) = \frac{\partial}{\partial \eta}\left(\frac{\rho D}{\delta}\frac{\partial W}{\partial \eta}\right) \quad \text{(B.7)}$$

The boundary conditions are:

- At the plate surface $(\eta = 0)$:

$$u_L = 0 \quad \text{(B.8)}$$

$$v_L = 0 \quad \text{(B.9)}$$

$$T_L = T_{wall} \quad \text{(B.10)}$$

- At the free stream $(\eta \rightarrow \infty)$:

$$u = u_\infty \quad \text{(B.11)}$$

$$T = T_\infty \quad \text{(B.12)}$$

$$W = W_\infty \quad \text{(B.13)}$$

- At the liquid-mixture interface $(\eta = 1)$:

$$u_L = u \quad \text{(B.14)}$$

$$\mu_L \frac{\partial u_L}{\partial \eta} = \mu \frac{\partial u}{\partial \eta} \tag{B.15}$$

$$T_L = T = T_i \tag{B.16}$$

$$T_i = T_{v,sat,i}\left(W_i, W_\infty, T_\infty, \tilde{M}_v, \tilde{M}_g\right) \tag{B.17}$$

$$\dot{m}'' = \rho_L u_L \frac{d\delta}{d\chi} - \rho_L v_L = \rho u \frac{d\delta}{d\chi} - \rho v \tag{B.18}$$

$$\dot{m}'' W + \frac{\rho D}{\delta} \frac{\partial W}{\partial \eta} = 0 \tag{B.19}$$

The transformed form of the energy balance used to evaluate δ is:

$$\frac{k_L}{\delta}\left(\frac{\partial T_L}{\partial \eta}\right)_{\eta=1} = \frac{k}{\delta}\left(\frac{\partial T}{\partial \eta}\right)_{\eta=1} + h_{fg} \frac{d}{d\chi} \int_0^1 \rho_L u_L \delta \, d\eta \tag{B.20}$$

B.1 Staggered Grid Spacing

The following alogrithim was used to calculate the grid boundaries to obtain a staggered grid spacing. The grid spacing is staggered such that the nodes are more closely packed near the start and the spacing increases further down the axis. The variable "factor" defines how tightly packed the nodes are near the start and the rate of expansion. Values for "factor" varies between 1.0 (uniform grid spacing) and infinity, but generally it doesn't need to exceed 50,000. The following example shows how the alogrithim is used to calculate the staggered grid along the *x* axis.

Using the following nomenclature:

$factor$ = expansion variable
m = number of nodes
x_{start} = start of the x axis
x_{end} = end of the x axis
x_b = array containing the location of the grid boundaries

Now let define:

$$d\ell = \frac{\mathrm{Log}_{10}(factor + 1.0)}{m - 1} \tag{B.21}$$

The variable $\ell(i)$ is solved for $1 \leq i \leq m$ by using:

$$\left.\begin{aligned} \ell(1) &= 0.0 \\ \ell(i) &= \ell(i-1) + d\ell \end{aligned}\right\} \tag{B.22}$$

Now take the exponential of $\ell(i)$ and subtract 1.0 as given by:

$$e(i) = \exp[\ell(i)] - 1.0 \tag{B.23}$$

The grid boundaries along the x axis is then given by:

$$x_b(i) = \left[\frac{x_{end} - x_{start}}{factor}\right] e(i) + x_{start} \tag{B.24}$$

B.2 Interpolation Formulas

To discretize the continuity and general transport equations, interpolation formulas are required to determine the value of ϕ at the four faces and it's gradient $\frac{\partial \phi}{\partial \eta}$ at the north

and south faces. In keeping with the assumption of a foreward marching type solution where the downstream has no effect, the east and west faces can be estimated by using upstream grid point as follows:

$$\phi_e = \phi_P \quad \text{or} \quad \phi_e(i,j) = \phi(i,j) \tag{B.25}$$

$$\phi_w = \phi_W \quad \text{or} \quad \phi_w(i,j) = \phi(i-1,j) \tag{B.26}$$

The same upwind interpolation scheme is also used to evaluate the properties at the east and west faces. For the north and south faces, a different approach is used. An analytical equation is obtained by solving a simplified form of the general transport equation, given by Equation (B.73), between two adjacent grid points labeled (i, j) and $(i, j+1)$. This expression will then yield an approximation for ϕ and it's gradient at the north face as a function of the two grid point values $\phi(i,j)$ and $\phi(i,j+1)$. The general transport equation is simplified by neglecting the variation of ϕ in the χ direction and ignoring the source term. This gives:

$$-\frac{d\delta}{d\chi}\frac{\partial}{\partial\eta}(\xi\eta G_x\phi) + \frac{\partial}{\partial\eta}(\xi G_y\phi) = \frac{\partial}{\partial\eta}\left(\frac{\Gamma}{\delta}\xi\frac{\partial\phi}{\partial\eta}\right) \tag{B.27}$$

Subject to the boundary conditions:

$$\phi = \phi_P = \phi(i,j) \text{ at } \eta = \eta_P = \eta(i,j) \tag{B.28}$$

$$\phi = \phi_N = \phi(i,j+1) \text{ at } \eta = \eta_N = \eta(i,j+1)$$

Now neglect the variation of the properties, ηG_x and G_y across $\Delta\eta_+$ and evaluate them at the boundary between the two grid points. The equation can then be written as:

$$-\eta_n G_{x,n}\frac{d\delta}{d\chi}\frac{\partial\phi}{\partial\eta} + G_{y,n}\frac{\partial\phi}{\partial\eta} = \frac{\Gamma_n}{\delta}\frac{\partial^2\phi}{\partial\eta^2} \tag{B.29}$$

Rearrange to obtain:

$$\left(G_{y,n} - \eta_n G_{x,n} \frac{d\delta}{d\chi}\right)\frac{\partial \phi}{\partial \eta} = \frac{\Gamma_n}{\delta}\frac{\partial^2 \phi}{\partial \eta^2} \qquad \text{(B.30)}$$

Integrate across $\Delta\chi$, and evaluate $\frac{1}{\delta}$ at δ_m. This would give:

$$\left[G_{y,n}\Delta\chi - \eta_n G_{x,n}(\delta_e - \delta_w)\right]\frac{\partial \phi}{\partial \eta} = \frac{\Gamma_n}{\delta_m}\frac{\partial^2 \phi}{\partial \eta^2}\Delta\chi \qquad \text{(B.31)}$$

Recall that the mass flow across the north face is:

$$\dot{m}_n = \Delta\chi\, G_{y,n} - (\delta_e - \delta_w)\eta_n G_{x,n} \qquad \text{(B.32)}$$

Results in:

$$\frac{\dot{m}_n}{\Delta\chi}\frac{\partial \phi}{\partial \eta} = \frac{\Gamma_n}{\delta_m}\frac{\partial^2 \phi}{\partial \eta^2} \quad \text{or} \quad \frac{\partial^2 \phi}{\partial \eta^2} - \frac{\dot{m}_n \delta_m}{\Delta\chi\,\Gamma_n}\frac{\partial \phi}{\partial \eta} = 0 \qquad \text{(B.33)}$$

The general solution would be:

$$\phi = C_1 + C_2 \exp\left(\frac{\dot{m}_n \delta_m}{\Delta\chi\,\Gamma_n}\eta\right) \qquad \text{(B.34)}$$

The two coefficients are then obtained by applying the two boundary conditions. This results in an interpolation formula to determine a value for ϕ.

$$\phi = \phi_P + (\phi_N - \phi_P)\left\{\frac{\exp\left(\mathrm{Pe}_n \frac{\eta - \eta_P}{\Delta\eta_+}\right) - 1}{\exp(\mathrm{Pe}_n) - 1}\right\} \quad ,\eta_P \le \eta \le \eta_N \qquad \text{(B.35)}$$

$$\text{where} \quad \mathrm{Pe}_n = \frac{\delta_m \dot{m}_n \Delta\eta_+}{\Gamma_n \Delta\chi} \qquad \text{(B.36)}$$

This equation is then used to define the value of ϕ and it's gradient at the north and south faces. They are as follows:

$$\phi_n(i,j) = \phi(i,j) + \alpha_n(i,j)\left[\phi(i,j+1) - \phi(i,j)\right] \tag{B.37}$$

$$\left(\frac{\partial\phi(i,j)}{\partial\eta}\right)_n = \frac{\delta_m(i)\dot{m}_n(i,j)}{\Gamma_n(i,j)\Delta\chi(i)}\beta_n(i,j)\left[\phi(i,j+1) - \phi(i,j)\right] \tag{B.38}$$

$$\phi_s(i,j) = \phi(i,j-1) + \alpha_s(i,j)\left[\phi(i,j) - \phi(i,j-1)\right] \tag{B.39}$$

$$\left(\frac{\partial\phi(i,j)}{\partial\eta}\right)_s = \frac{\delta_m(i)\dot{m}_n(i,j-1)}{\Gamma_n(i,j-1)\Delta\chi(i)}\beta_s(i,j)\left[\phi(i,j) - \phi(i,j-1)\right] \tag{B.40}$$

where: $$\alpha_n(i,j) = \frac{\exp\left[\mathrm{Pe}_n(i,j)\frac{\eta_n(j) - \eta(j)}{\Delta\eta_+(j)}\right] - 1}{\exp\left[\mathrm{Pe}_n(i,j)\right] - 1} \tag{B.41}$$

$$\beta_n(i,j) = \frac{\exp\left[\mathrm{Pe}_n(i,j)\frac{\eta_n(j) - \eta(j)}{\Delta\eta_+(j)}\right]}{\exp\left[\mathrm{Pe}_n(i,j)\right] - 1} \tag{B.42}$$

$$\mathrm{Pe}_n(i,j) = \frac{\delta_m(i)\dot{m}_n(i,j)\Delta\eta_+(j)}{\Gamma_n(i,j)\Delta\chi(i)} \tag{B.43}$$

$$\alpha_s(i,j) = \frac{\exp\left[\mathrm{Pe}_s(i,j)\frac{\eta_n(j-1) - \eta(j-1)}{\Delta\eta_+(j-1)}\right] - 1}{\exp\left[\mathrm{Pe}_s(i,j)\right] - 1} \tag{B.44}$$

$$\beta_s(i,j) = \frac{\exp\left[\mathrm{Pe}_s(i,j)\frac{\eta_n(j-1) - \eta(j-1)}{\Delta\eta_+(j-1)}\right]}{\exp\left[\mathrm{Pe}_s(i,j)\right] - 1} \tag{B.45}$$

$$\mathrm{Pe}_s(i,j) = \frac{\delta_m(i)\dot{m}_n(i,j-1)\Delta\eta_+(j-1)}{\Gamma_n(i,j-1)\Delta\chi(i)} \tag{B.46}$$

Interpolation formulas are also required to evaluate the properties at the faces of the control volume. An upwind scheme was used to evaluate the properties at the east and west faces. Interpolation formulas by Patankar (1980) were used to evaluate the properties at the north and south faces. Using the current nomenclature, Patankar's formula for a general property, Γ, at the north face is:

$$\Gamma_n(j) = \frac{\Gamma(j)\Gamma(j+1)}{[1+f(j)]\Gamma(j+1) + f(j)\Gamma(j)} \tag{B.47}$$

where: $$f(j) = \frac{\eta(j+1) - \eta_b(j)}{\eta(j+1) - \eta(j)} \tag{B.48}$$

B.3 Continuity Equations

The two continuity equations, for the liquid and mixture, are the same. Thus only the discretization of the mixture continuity will be given in detail. The final results will be written for both the liquid and mixture. The mixture continuity equation is:

$$\frac{\partial}{\partial\chi}(\delta\rho u) - \frac{d\delta}{d\chi}\frac{\partial}{\partial\eta}(\eta\rho u) + \frac{\partial}{\partial\eta}(\rho v) = 0 \tag{B.49}$$

Using these definations for mass fluxes in the *x-y* plane:

$$G_x = \rho u \qquad G_y = \rho v \tag{B.50}$$

Equation (B.49) can be re-written as:

$$\frac{\partial}{\partial\chi}(\delta G_x) - \frac{d\delta}{d\chi}\frac{\partial}{\partial\eta}(\eta G_x) + \frac{\partial}{\partial\eta}(G_y) = 0 \tag{B.51}$$

This equation is then integrated over a control volume $\Delta\chi$ and $\Delta\eta$ as shown in Figure 4.3.

$$\int_w^e \int_s^n \frac{\partial}{\partial \chi}(\delta G_x)\, d\eta\, d\chi \;-\; \int_w^e \int_s^n \frac{d\delta}{d\chi}\,\frac{\partial}{\partial \eta}(\eta G_x)\, d\eta\, d\chi + \int_w^e \int_s^n \frac{\partial}{\partial \eta}(G_y)\, d\eta\, d\chi \;=\; 0 \tag{B.52}$$

For simplicity, the three terms are integrated separately. The first term represented by:

$$\mathrm{I} \;=\; \int_w^e \int_s^n \frac{\partial}{\partial \chi}(\delta G_x)\, d\eta\, d\chi \tag{B.53}$$

Assuming that δ and G_x are indepent of η will result in:

$$\mathrm{I} \;=\; \Delta\eta \int_w^e \frac{\partial}{\partial \chi}(\delta G_x)\, d\chi \;=\; \Delta\eta\left(\delta_e G_{x,e} - \delta_w G_{x,w}\right) \tag{B.54}$$

The second term is:

$$\mathrm{II} \;=\; \int_w^e \int_s^n \frac{d\delta}{d\chi}\,\frac{\partial}{\partial \eta}(\eta G_x)\, d\eta\, d\chi \tag{B.55}$$

Integrate w.r.t. η first:

$$\mathrm{II} \;=\; \int_w^e \frac{d\delta}{d\chi}\left[\eta_n G_{x,n} - \eta_s G_{x,s}\right] d\chi \tag{B.56}$$

Now, assume that G_{xn} and G_{xs} are independant of χ and integrate to give:

$$\text{II} = \left[\eta_n G_{x,n} - \eta_s G_{x,s}\right] \int_w^e \frac{d\delta}{d\chi} d\chi = \left[\eta_n G_{x,n} - \eta_s G_{x,s}\right]\left[\delta_e - \delta_w\right] \quad \text{(B.57)}$$

The third term is given by:

$$\text{III} = \int_w^e \int_s^n \frac{\partial}{\partial \eta}\left(G_y\right) d\eta \, d\chi \quad \text{(B.58)}$$

Assume that G_y is independant of χ and integrate to obtain:

$$\text{III} = \int_w^e \left[G_{y,n} - G_{y,s}\right] d\chi = \Delta\chi \left[G_{y,n} - G_{y,s}\right] \quad \text{(B.59)}$$

The discretized form of Equation (B.52) is then given by combining the three parts.

$$\begin{aligned} \Delta\eta\left(\delta_e G_{x,e} - \delta_w G_{x,w}\right) - \left[\eta_n G_{x,n} - \eta_s G_{x,s}\right]\left[\delta_e - \delta_w\right] \\ + \Delta\chi\left[G_{y,n} - G_{y,s}\right] = 0 \end{aligned} \quad \text{(B.60)}$$

Equation (B.60) contains mass fluxes which are directed in *x-y* coordinate system, and the cross-sectional areas are given in the χ-η coordinate plane. Figure B.1 shows the relationship between the two coordinate systems by showing a control volume in *x-y* coordinate system along with the cross sectional areas. Now define the mass flows across each of the four faces in Figure B.1:

$$\begin{aligned} \dot{m}_e &= \text{mass flow across east face, out of the control volume} \\ &= \Delta\eta\,\delta_e G_{x,e} \end{aligned} \quad \text{(B.61)}$$

$$\begin{aligned} \dot{m}_w &= \text{mass flow across west face, into the control volume} \\ &= \Delta\eta\,\delta_w G_{x,w} \end{aligned} \quad \text{(B.62)}$$

$$\dot{m}_n = \text{mass flow across north face, out of the control volume} = \Delta\chi\, G_{y,n} - (\delta_e - \delta_w)\eta_n\, G_{x,n} \quad \text{(B.63)}$$

$$\dot{m}_s = \text{mass flow across south face, into the control volume} = \Delta\chi\, G_{y,s} - (\delta_e - \delta_w)\eta_s\, G_{x,s} \quad \text{(B.64)}$$

and the discretized continuity equation for (i,j) can be rewritten as:

$$\dot{m}_w(i,j) - \dot{m}_e(i,j) + \dot{m}_s(i,j) - \dot{m}_n(i,j) = 0 \quad \text{(B.65)}$$

The upwind scheme is then used to evaluate the mass flows at the east and west faces from the known u-velocity profile:

$$\begin{aligned} \dot{m}_e(i,j) &= \rho_L(i,j)\mathrm{u}_L(i,j)\Delta\eta_L(j)\delta(i) \\ \dot{m}_w(i,j) &= \dot{m}_e(i-1,j) \end{aligned} \quad \text{(B.66)}$$

B.3.1 Liquid Continuity Equation

For $j_L = 1$, application of the boundary condition at the wall, $\mathrm{v}_L = 0$ gives:

$$\dot{m}_s(i,1) = 0 \quad \text{(B.67)}$$

and with $\dot{m}_{L,w}(i,1) = \dot{m}_{L,e}(i,1) = 0$, because $\Delta\eta_L(1) = 0.0$, the discretized continuity equation for $(i,1)$ is:

$$\dot{m}_{L,n}(i,1) = \dot{m}_{L,w}(i,1) - \dot{m}_{L,e}(i,1) = 0.0 \quad \text{(B.68)}$$

For $2 \le j_L \le n\text{-}1$, the discretized continuity equation is:

$$\dot{m}_{L,n}(i,j_L) = \dot{m}_{L,w}(i,j_L) - \dot{m}_{L,e}(i,j_L) + \dot{m}_{L,s}(i,j_L) \quad \text{(B.69)}$$

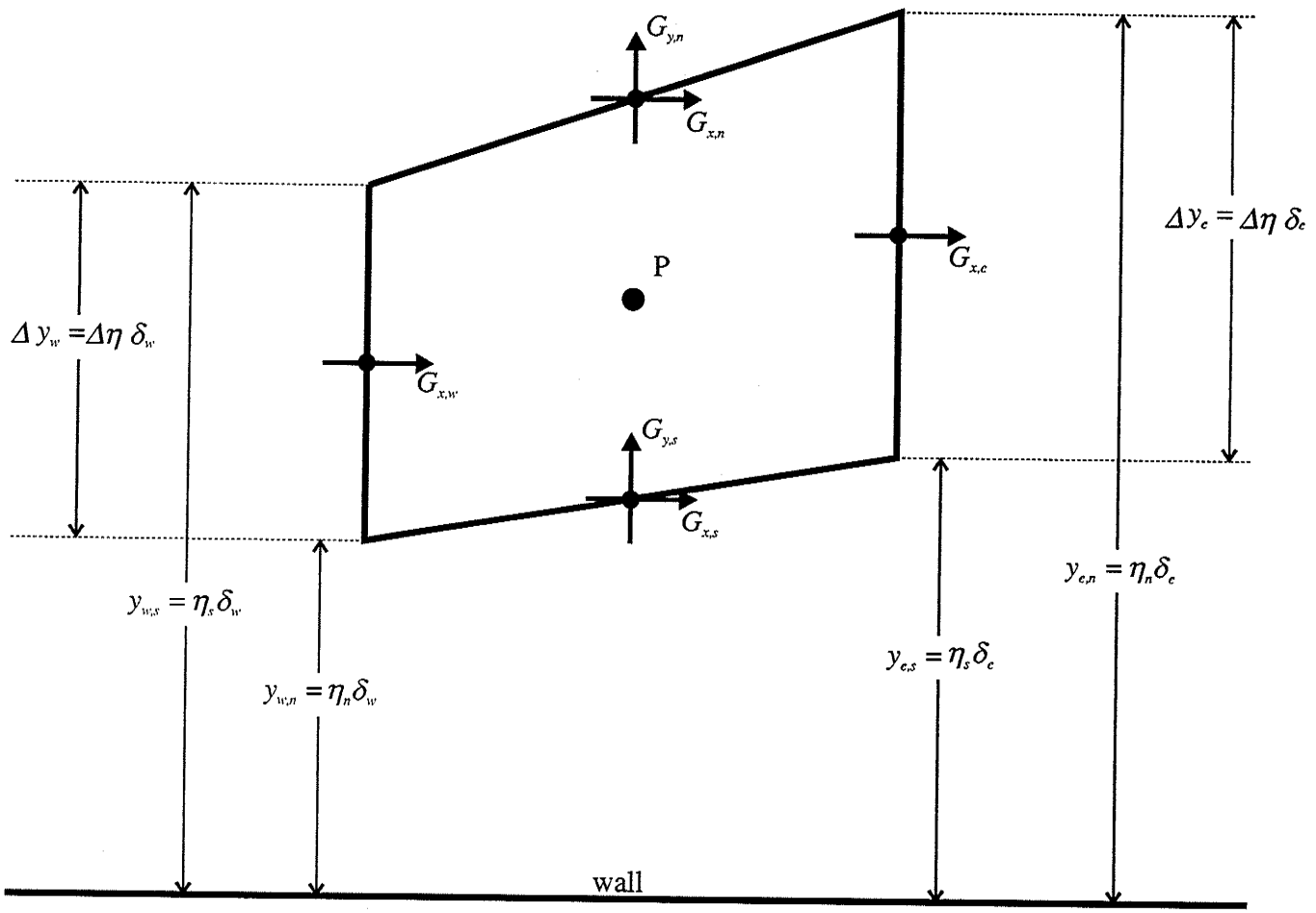

Figure B.1: Mass fluxes across a control volume.

B.3.2 Mixture Continuity Equation

For j = 1, application of the boundary condition, given by Equation (B.18), at the interface:

$$\dot{m}'' = \rho_L u_L \frac{d\delta}{d\chi} - \rho_L v_L = \rho u \frac{d\delta}{d\chi} - \rho v \tag{B.70}$$

with a zero thickness control volume ($\Delta\eta = 0$) show that:

$$\dot{m}_n(i, j=1) = \dot{m}_{L,n}(i, j_L = n-1) \tag{B.71}$$

For $2 \le j \le nv\text{-}1$, the discretized continuity equation is:

$$\dot{m}_n(i,j) = \dot{m}_w(i,j) - \dot{m}_e(i,j) + \dot{m}_s(i,j) \tag{B.72}$$

B.4 General Transport Equation

The five equations for the liquid momentum, liquid energy, mixture momentum, mixture energy and mixture diffusion all have a similiar form. Thus they can be re-written in a general form:

$$\frac{\partial}{\partial\chi}(\xi\delta G_x\phi) - \frac{d\delta}{d\chi}\frac{\partial}{\partial\eta}(\xi\eta G_x\phi) + \frac{\partial}{\partial\eta}(\xi G_y\phi) = \frac{\partial}{\partial\eta}\left(\frac{\Gamma}{\delta}\xi\frac{\partial\phi}{\partial\eta}\right) + S \tag{B.73}$$

with G_x and G_y as defined by Equation (B.50) and the general variables, ϕ, ξ, Γ, and S as defined in Table B.1

Table B.1: Definition of general variables in the general transport equation.

Equation	ϕ	ξ	Γ	S
Liquid Momentum	u_L	1	μ_L	$\delta\, g\, (\rho_L - \rho_\infty)\cos\alpha$
Liquid Energy	T_L	c_{P_L}	k_L / c_{P_L}	0
Mixture Momentum	u	1	μ	$\delta\, g\, (\rho - \rho_\infty)\cos\alpha$
Mixture Energy	T	c_P	k / c_P	$\frac{\partial}{\partial\eta}\left(\frac{\rho D\left(c_{P_s} - c_{P_v}\right)}{\delta} T \frac{\partial W}{\partial\eta}\right)$
Mixture Diffusion	W	1	ρD	0

B.4.1 Discretization of the General Transport Equation

Equation (B.73) is discretized over a control volume $\Delta\chi$ and $\Delta\eta$ as shown in Figure 4.3.

$$\int_s^n \int_w^e \frac{\partial}{\partial\chi}(\xi\delta\, G_x\phi)\, d\chi\, d\eta \;-\; \int_s^n \int_w^e \frac{d\delta}{d\chi}\frac{\partial}{\partial\eta}(\xi\eta\, G_x\phi)\, d\chi\, d\eta$$

$$+ \int_s^n \int_w^e \frac{\partial}{\partial\eta}(\xi\, G_y\phi)\, d\chi\, d\eta \;=\; \int_s^n \int_w^e \frac{\partial}{\partial\eta}\left(\frac{\Gamma}{\delta}\xi\frac{\partial\phi}{\partial\eta}\right) d\chi\, d\eta \qquad \text{(B.74)}$$

$$+ \int_s^n \int_w^e S\, d\chi\, d\eta$$

The first term on the right hand side of Equation (B.74) is integrated as follows:

$$I = \int_s^n \int_w^e \frac{\partial}{\partial \chi}(\xi \delta G_x \phi)\, d\chi\, d\eta \tag{B.75}$$

Integrate with respect to χ to obtain:

$$I = \int_s^n \left[\xi_e \delta_e G_{x,e} \phi_e - \xi_w \delta_w G_{x,w} \phi_w\right] d\eta \tag{B.76}$$

Neglecting the variance in the η direction to give:

$$I = \Delta\eta \left[\xi_e \delta_e G_{x,e} \phi_e - \xi_w \delta_w G_{x,w} \phi_w\right] \tag{B.77}$$

The second term of Equation (B.74) is:

$$II = \int_s^n \int_w^e \frac{d\delta}{d\chi} \frac{\partial}{\partial \eta}(\xi \eta G_x \phi) d\chi\, d\eta \tag{B.78}$$

Assume that $\frac{\partial}{\partial \eta}(\xi \eta G_x \phi)$ doesn't vary with χ.

$$II = \int_s^n (\delta_e - \delta_w) \frac{\partial}{\partial \eta}(\xi \eta G_x \phi) d\eta \tag{B.79}$$

$$II = (\delta_e - \delta_w)\left[\xi_n \eta_n G_{x,n} \phi_n - \xi_s \eta_s G_{x,s} \phi_s\right] \tag{B.80}$$

The third term of Equation (B.74) is:

$$III = \int_s^n \int_w^e \frac{\partial}{\partial \eta}(\xi G_y \phi) d\chi\, d\eta \tag{B.81}$$

Neglect variance with respect to χ,

$$\text{III} = \int_s^n \Delta\chi \frac{\partial}{\partial\eta}\left(\xi G_y \phi\right) d\eta \tag{B.82}$$

$$\text{III} = \Delta\chi \left[\xi_n G_{y,n} \phi_n - \xi_s G_{y,s} \phi_s\right] \tag{B.83}$$

The fourth term of Equation (B.74) is:

$$\text{IV} = \int_s^n \int_w^e \frac{\partial}{\partial\eta}\left(\frac{\Gamma}{\delta}\xi \frac{\partial\phi}{\partial\eta}\right) d\chi\, d\eta \tag{B.84}$$

Neglect the variance of Γ, ξ and $\frac{\partial\phi}{\partial\eta}$ with respect to χ. Assume a piecewise linear profile for δ between the east and west faces and replace δ with the mean value, δ_m:

$$\text{IV} = \frac{\Delta\chi}{\delta_m} \int_s^n \frac{\partial}{\partial\eta}\left(\Gamma \xi \frac{\partial\phi}{\partial\eta}\right) d\eta \tag{B.85}$$

$$\text{IV} = \frac{\Delta\chi}{\delta_m}\left[\Gamma_n \xi_n \left(\frac{\partial\phi}{\partial\eta}\right)_n - \Gamma_s \xi_s \left(\frac{\partial\phi}{\partial\eta}\right)_s\right] \tag{B.86}$$

The integration of the source term will be shown in the appropriate section later in this appendix. Each of the discretized terms are then recombined to form the discretized general transport equation:

$$\begin{aligned}
&\Delta\eta\left[\xi_e \delta_e G_{x,e} \phi_e \;-\; \xi_w \delta_w G_{x,w} \phi_w\right] \\
&\quad - \;(\delta_e - \delta_w)\left[\xi_n \eta_n G_{x,n} \phi_n - \xi_s \eta_s G_{x,s} \phi_s\right] \\
&\quad + \;\Delta\chi\left[\xi_n G_{y,n} \phi_n - \xi_s G_{y,s} \phi_s\right] \\
&\quad = \;\frac{\Delta\chi}{\delta_m}\left[\Gamma_n \xi_n \left(\frac{\partial\phi}{\partial\eta}\right)_n - \Gamma_s \xi_s \left(\frac{\partial\phi}{\partial\eta}\right)_s\right] \;+\; \int_s^n \int_w^e S \, d\chi \, d\eta
\end{aligned} \tag{B.87}$$

Rearange to form:

$$\begin{aligned}
&\left(\Delta\eta \delta_e G_{x,e}\right)\xi_e \phi_e \;-\; \left(\Delta\eta \delta_w G_{x,w}\right)\xi_w \phi_w \\
&\quad + \;\left[\Delta\chi G_{y,n} - (\delta_e - \delta_w)\eta_n G_{x,n}\right]\xi_n \phi_n \\
&\quad - \;\left[\Delta\chi G_{y,s} - (\delta_e - \delta_w)\eta_s G_{x,s}\right]\xi_s \phi_s \\
&\quad = \;\frac{\Delta\chi \Gamma_n \xi_n}{\delta_m}\left(\frac{\partial\phi}{\partial\eta}\right)_n \;-\; \frac{\Delta\chi \Gamma_s \xi_s}{\delta_m}\left(\frac{\partial\phi}{\partial\eta}\right)_s \;+\; \int_s^n \int_w^e S \, d\chi \, d\eta
\end{aligned} \tag{B.88}$$

Apply the definations for mass flows across the east, west, nort and south faces as given by Equations (B.61) to (B.64):

$$\begin{aligned}
&\dot{m}_e \xi_e \phi_e \;-\; \dot{m}_w \xi_w \phi_w \;+\; \dot{m}_n \xi_n \phi_n \;-\; \dot{m}_s \xi_s \phi_s \\
&\quad = \;\frac{\Delta\chi \Gamma_n \xi_n}{\delta_m}\left(\frac{\partial\phi}{\partial\eta}\right)_n \;-\; \frac{\Delta\chi \Gamma_s \xi_s}{\delta_m}\left(\frac{\partial\phi}{\partial\eta}\right)_s \;+\; \int_s^n \int_w^e S \, d\chi \, d\eta
\end{aligned} \tag{B.89}$$

Use the interpolation formulas, given by Equations (B.37) to (B.40) to evaluate ϕ and $\frac{\partial\phi}{\partial\eta}$ at the four faces of the control volume to obtain an equation in terms ϕ_P, ϕ_N, ϕ_S, and ϕ_W:

$$\dot{m}_e \xi_e \phi_P - \dot{m}_w \xi_w \phi_W + \dot{m}_n \xi_n \left[\phi_P + \alpha_n (\phi_N - \phi_P)\right] - \dot{m}_s \xi_s \left[\phi_S + \alpha_s (\phi_P - \phi_S)\right] \quad \text{(B.90)}$$

$$= \xi_n \dot{m}_n \beta_n (\phi_N - \phi_P) - \xi_s \dot{m}_s \beta_s (\phi_P - \phi_S) + \int_s^n \int_w^e S \, d\chi \, d\eta$$

Add $\dot{m}_s \xi_s \phi_P - \dot{m}_s \xi_s \phi_P$ to the left hand side of Equation (B.90):

$$\dot{m}_e \xi_e \phi_P - \dot{m}_w \xi_w \phi_W + \dot{m}_n \xi_n \phi_P + \dot{m}_n \xi_n \alpha_n (\phi_N - \phi_P) - \dot{m}_s \xi_s \phi_S + \dot{m}_s \xi_s \phi_P - \dot{m}_s \xi_s \phi_P - \dot{m}_s \xi_s \alpha_s (\phi_P - \phi_S) \quad \text{(B.91)}$$

$$= \xi_n \dot{m}_n \beta_n (\phi_N - \phi_P) - \xi_s \dot{m}_s \beta_s (\phi_P - \phi_S) + \int_s^n \int_w^e S \, d\chi \, d\eta$$

Rearrange to obtain:

$$\phi_P \left[\dot{m}_e \xi_e + \dot{m}_n \xi_n - \dot{m}_s \xi_s + \dot{m}_n \xi_n (\beta_n - \alpha_n) + \dot{m}_s \xi_s (1 - \alpha_s + \beta_s)\right] = \dot{m}_w \xi_w \phi_W + \phi_N \left[\dot{m}_n \xi_n (\beta_n - \alpha_n)\right] + \phi_S \left[\dot{m}_s \xi_s (1 - \alpha_s + \beta_s)\right] \quad \text{(B.92)}$$

$$+ \int_s^n \int_w^e S \, d\chi \, d\eta$$

This has the form of:

$$a_P \phi_P = a_N \phi_N + a_S \phi_S + b_P \quad \text{(B.93)}$$

where: $$a_N = \dot{m}_n \xi_n (\beta_n - \alpha_n) \quad \text{(B.94)}$$

$$a_S = \dot{m}_s \xi_s (1 - \alpha_s + \beta_s) \quad \text{(B.95)}$$

$$b_P = \dot{m}_w \xi_w \phi_W + \int_s^n \int_w^e S \, d\chi \, d\eta \quad \text{(B.96)}$$

$$a_P = \dot{m}_e \xi_e + \dot{m}_n \xi_n - \dot{m}_s \xi_s + a_N + a_S \tag{B.97}$$

From the defination of the interpolation formulas:

$$(\beta_n - \alpha_n) = \frac{\exp\left(Pe_n \frac{\eta_n - \eta}{\Delta\eta_+}\right)}{\exp(Pe_n) - 1} - \frac{\exp\left(Pe_n \frac{\eta_n - \eta}{\Delta\eta_+}\right) - 1}{\exp(Pe_n) - 1} \tag{B.98}$$

$$(\beta_n - \alpha_n) = \frac{1}{\exp(Pe_n) - 1} \tag{B.99}$$

$$\begin{aligned}(1 - \alpha_s + \beta_s) = 1 &- \frac{\exp\left(Pe_s \frac{\eta_s - \eta_S}{\Delta\eta_-}\right) - 1}{\exp(Pe_s) - 1} \\ &+ \frac{\exp\left(Pe_s \frac{\eta_s - \eta_S}{\Delta\eta_-}\right)}{\exp(Pe_s) - 1}\end{aligned} \tag{B.100}$$

$$(1 - \alpha_s + \beta_s) = \frac{\exp(Pe_s)}{\exp(Pe_s) - 1} \tag{B.101}$$

Applying Equations (B.99) and (B.101) to Equations (B.93) through to (B.97) will result in:

$$a_P \phi_P = a_N \phi_N + a_S \phi_S + b_P \tag{B.102}$$

where: $$a_N = \dot{m}_n \xi_n \left[\frac{1}{\exp(Pe_n) - 1}\right] \tag{B.103}$$

$$a_S = \dot{m}_s \xi_s \left[\frac{\exp(Pe_s)}{\exp(Pe_s) - 1}\right] \tag{B.104}$$

$$b_P = \dot{m}_w \xi_w \phi_W + \int_s^n \int_w^e S \, d\chi \, d\eta \tag{B.105}$$

$$a_P = \dot{m}_e \xi_e + \dot{m}_n \xi_n - \dot{m}_s \xi_s + a_N + a_S \tag{B.106}$$

For the equations where $\xi = 1$, there is one more simplification, since the continuity equation states that:

$$\dot{m}_w = \dot{m}_e + \dot{m}_n - \dot{m}_s \tag{B.107}$$

The a_P cofficient can be simplified to:

$$a_P = \dot{m}_w + a_N + a_S \tag{B.108}$$

Rewriting Equations (B.102) to (B.106) in terms of the (i, j) indice:

$$a_P(i,j)\phi(i,j) = a_N(i,j)\phi(i,j+1) + a_S(i,j)\phi(i,j-1) + b_P(i,j) \tag{B.109}$$

where: $$a_N(i,j) = \dot{m}_n(i,j)\xi_n(i,j)\left[\frac{1}{\exp(Pe_n)-1}\right] \tag{B.110}$$

$$Pe_n = \frac{\dot{m}_n(i,j)\delta_m(i)\Delta\eta_+(j)}{\Gamma_n(i,j)\Delta\chi(i)} \tag{B.111}$$

$$a_S(i,j) = \dot{m}_n(i,j-1)\xi_n(i,j-1)\left[\frac{\exp(Pe_s)}{\exp(Pe_s)-1}\right] \tag{B.112}$$

$$Pe_s = \frac{\dot{m}_n(i,j-1)\delta_m(i)\Delta\eta_+(j-1)}{\Gamma_n(i,j-1)\Delta\chi(i)} \tag{B.113}$$

$$b_P(i,j) = \dot{m}_w(i,j)\xi_w(i,j)\phi(i-1,j) + \int_s^n \int_w^e S\, d\chi\, d\eta \tag{B.114}$$

$$\begin{aligned} a_P(i,j) = {} & \dot{m}_e(i,j)\xi_e(i,j) + \dot{m}_n(i,j)\xi_n(i,j) \\ & - \dot{m}_n(i,j-1)\xi_n(i,j-1) + a_N(i,j) + a_S(i,j) \end{aligned} \tag{B.115}$$

The discretized form for each of the five transport equations is obtained by using Equations (B.109) to (B.115) and applying the appropriate boundary conditions and source term.

B.4.2 Momentum Equations

B.4.2.1 Source Term for the Momentum Equations

The source term for the two momentum equations is the bouyancy term and they are the same except for the property. The discretization of the source term for the mixture momentum equation is as follows:

$$\int_s^n \int_w^e S\, d\chi\, d\eta = \int_s^n \int_w^e \delta\, g(\rho - \rho_\infty)\cos\theta\, d\chi\, d\eta \qquad \text{(B.116)}$$

Neglect the variation of ρ within the control volume:

$$\int_s^n \int_w^e S\, d\chi\, d\eta = \int_s^n g(\rho - \rho_\infty)\cos\theta \left[\int_w^e \delta\, d\chi\right] d\eta \qquad \text{(B.117)}$$

Assume a stepwise linear profile for δ between the ease and west faces and the integral:

$$\int_w^e \delta\, d\chi = \frac{\delta_e + \delta_w}{2}\Delta\chi = \delta_m \Delta\chi \qquad \text{(B.118)}$$

Thus the source term is discretized as:

$$\int_{s}^{n}\int_{w}^{e} S\,d\chi\,d\eta \;=\; g(\rho-\rho_{\infty})\cos\theta\,\delta_{m}\,\Delta\chi\,\Delta\eta \qquad \text{(B.119)}$$

Rewrite for (i,j) indice for mixture momentum equation:

$$\int_{s}^{n}\int_{w}^{e} S\,d\chi\,d\eta \;=\; g\left[\rho(i,j)-\rho(i,nv)\right]\cos\theta\,\delta_{m}(i)\Delta\chi(i)\Delta\eta(j) \qquad \text{(B.120)}$$

Likewise for the liquid momentum equation at the (i, j_L):

$$\int_{s}^{n}\int_{w}^{e} S\,d\chi\,d\eta \;=\; g\left[\rho_{L}(i,j_{L})-\rho(i,nv)\right]\cos\theta\,\delta_{m}(i)\Delta\chi(i)\Delta\eta(j_{L}) \qquad \text{(B.121)}$$

B.4.2.2 Discretized Form of the Momentum Equation

The general transport equation has already been discretized and is given by Equations (B.109) to (B.115) and the discretization for the source term is given by either Equations (B.120) or (B.121). The use of the upwind scheme shows shows that the solution only depends on the upstream solution field and is independant of what is happening downstream. The entire solution field can then be obtain by marching along the plate and obtaining the solution field for the column at each $\chi(i)$. Thus at each χ station, there will a set of equations obtained by using Equations (B.109) to (B.115) for each j control

volume. A Tri-Diagonal Matrix Solver is then used to solve the set of equations. From Equation (B.109), the general form of the equation is:

$$a_P(i,j)\phi(i,j) = a_N(i,j)\phi(i,j+1) + a_S(i,j)\phi(i,j-1) + b_P(i,j) \qquad \text{(B.122)}$$

The following sections describe how the coefficients are obtained for each of the transport equations and how the boundary conditions are applied.

B.4.2.2.1 At the Wall $(\eta = 0)$, $j_L = 1$

The boundary condition is:

$$u_L = 0 \qquad \text{(B.123)}$$

This gives:

$$u_L(i,1) = 0.0 \qquad \text{(B.124)}$$

The coefficients for Equation (B.122) at $(i, j_L = 1)$ are:

$$\left.\begin{aligned} a_P(i, j_L = 1) &= 1.0 \\ a_S(i, j_L = 1) &= 0.0 \\ a_N(i, j_L = 1) &= 0.0 \\ b_P(i, j_L = 1) &= 0.0 \end{aligned}\right\} \qquad \text{(B.125)}$$

B.4.2.2.2 Within the Liquid, at $j_L = 2$

For the control volume at (i, j_L=2), use a linear slope for $\left(\frac{\partial u_L}{\partial \eta}\right)_s$ and with $u_{L,s} = u_{L,S}$, the coefficients of Equation (B.122) become:

$$a_N(i, j_L) = \dot{m}_{L,n}(i, j_L)\left[\frac{1}{\exp(Pe_{L,n}) - 1}\right] \tag{B.126}$$

$$Pe_{L,n} = \frac{\dot{m}_{L,n}(i, j_L)\delta_m(i)\Delta\eta_{L,+}(j_L)}{\mu_{L,n}(i, j_L)\Delta\chi(i)} \tag{B.127}$$

$$a_S(i, j_L) = \frac{\mu_{L,n}(i, j_L - 1)\Delta\chi(i)}{\delta_m(i)\Delta\eta_{L,+}(j_L - 1)} + \dot{m}_{L,s}(i, j_L) \tag{B.128}$$

$$\begin{aligned} b_P(i, j_L) = {} & \dot{m}_{L,w}(i, j_L)u_L(i-1, j_L) \\ & + g\left[\rho_L(i, j_L) - \rho(i, nv)\right]\cos\theta\,\delta_m(i)\Delta\chi(i)\Delta\eta_L(j_L) \end{aligned} \tag{B.129}$$

$$a_P(i, j_L) = \dot{m}_{L,w}(i, j_L) + a_N(i, j_L) + a_S(i, j_L) \tag{B.130}$$

B.4.2.2.3 Within the Liquid, $3 \le j_L \le n$-2

The coefficients of Equation (B.122) for the liquid momentum equation, within the liquid layer, are:

$$a_N(i, j_L) = \dot{m}_{L,n}(i, j_L)\left[\frac{1}{\exp(Pe_{L,n}) - 1}\right] \tag{B.131}$$

$$Pe_{L,n} = \frac{\dot{m}_{L,n}(i, j_L)\delta_m(i)\Delta\eta_{L,+}(j_L)}{\mu_{L,n}(i, j_L)\Delta\chi(i)} \tag{B.132}$$

$$a_S(i, j_L) = \dot{m}_{L,n}(i, j_L - 1)\left[\frac{\exp(Pe_{L,s})}{\exp(Pe_{L,s}) - 1}\right] \tag{B.133}$$

$$Pe_{L,s} = \frac{\dot{m}_{L,n}(i, j_L - 1)\delta_m(i)\Delta\eta_{L,+}(j_L - 1)}{\mu_{L,n}(i, j_L - 1)\Delta\chi(i)} \tag{B.134}$$

$$\begin{aligned} b_P(i, j_L) = {} & \dot{m}_{L,w}(i, j_L)\mathrm{u}_L(i-1, j_L) \\ & + g\left[\rho_L(i, j_L) - \rho(i, nv)\right]\cos\theta\,\delta_m(i)\Delta\chi(i)\Delta\eta_L(j_L) \end{aligned} \tag{B.135}$$

$$a_P(i, j_L) = \dot{m}_{L,w}(i, j_L) + a_N(i, j_L) + a_S(i, j_L) \tag{B.136}$$

B.4.2.2.4 Within the Liquid, at $j_L = n$-1

For the control volume at (i, j_L=n-1), use a linear slope for $\left(\frac{\partial \mathrm{u}_L}{\partial \eta}\right)_n$ and with $\mathrm{u}_{L,n} = \mathrm{u}_{L,N}$, the coefficients of Equation (B.122) become:

$$a_N(i, j_L) = \frac{\mu_{L,n}(i, j_L)\Delta\chi(i)}{\delta_m(i)\Delta\eta_{L,+}(j_L)} - \dot{m}_{L,n}(i, j_L) \tag{B.137}$$

$$a_S(i, j_L) = \dot{m}_{L,n}(i, j_L - 1)\left[\frac{\exp(Pe_{L,s})}{\exp(Pe_{L,s}) - 1}\right] \tag{B.138}$$

$$Pe_{L,s} = \frac{\dot{m}_{L,n}(i, j_L - 1)\delta_m(i)\Delta\eta_{L,+}(j_L - 1)}{\mu_{L,n}(i, j_L - 1)\Delta\chi(i)} \tag{B.139}$$

$$\begin{aligned} b_P(i, j_L) = {} & \dot{m}_{L,w}(i, j_L)\mathrm{u}_L(i-1, j_L) \\ & + g\left[\rho_L(i, j_L) - \rho(i, nv)\right]\cos\theta\,\delta_m(i)\Delta\chi(i)\Delta\eta_L(j_L) \end{aligned} \tag{B.140}$$

$$a_P(i, j_L) = \dot{m}_{L,w}(i, j_L) + a_N(i, j_L) + a_S(i, j_L) \tag{B.141}$$

B.4.2.2.5 Liquid-Mixture Interface, $j_L = n$ and $j = 1$

Both the liquid and the mixture share the same control volume located at the interface. It has a finite width, $\Delta\chi$, but a zero thickness, $\Delta\eta = 0$. Also, the following two boundary conditions must be satisified at the interface:

$$u_L = u \tag{B.142}$$

$$\frac{\mu_L}{\delta}\frac{\partial u_L}{\partial \eta} = \frac{\mu}{\delta}\frac{\partial u}{\partial \eta} \tag{B.143}$$

Using a linear approximation for the gradient for u and u_L at the interface, Equation (B.143) can be discretized as:

$$\frac{\mu_{L,n}(i,n-1)}{\delta_m}\left[\frac{u_L(i,n)-u_L(i,n-1)}{\Delta\eta_{L,+}(n-1)}\right] = \frac{\mu_n(i,1)}{\delta_m}\left[\frac{u(i,2)-u(i,1)}{\Delta\eta_+(1)}\right] \tag{B.144}$$

From Equation (B.142), $u_L(i,n) = u(i,1)$ and applying this condition to Equation (B.144) results in,

$$\frac{\mu_{L,n}(i,n-1)}{\delta_m}\left[\frac{u_L(i,n)-u_L(i,n-1)}{\Delta\eta_{L,+}(n-1)}\right] = \frac{\mu_n(i,1)}{\delta_m}\left[\frac{u(i,2)-u_L(i,n)}{\Delta\eta_+(1)}\right] \tag{B.145}$$

with the following coefficient for Equation (B.122):

$$a_S(i,n) = \frac{\mu_{L,n}(i,n-1)\Delta\chi(i)}{\Delta\eta_{L,+}(n-1)\delta_m(i)} \tag{B.146}$$

$$a_N(i,n) = \frac{\mu_n(i,1)\Delta\chi(i)}{\Delta\eta_+(1)\delta_m(i)} \tag{B.147}$$

$$a_P(i,n) = a_S(i,n) + a_N(i,n) \tag{B.148}$$

$$b_P(i,n) = 0 \tag{B.149}$$

The use of Equations (B.146) to (B.149) as the coefficients of Equation (B.122) will couple the liquid and mixture momentum equations. Thus both equations must be solved simultaneously. This is done by using a general variable ϕ to represent both the u_L and u velocities. The relationship between ϕ and the two velocities are given by:

$$\left.\begin{array}{lcll} u_L(i, j_L) & = & \phi(i, j_L) & \text{for } 1 \le j_L \le n \\ u(i, j) & = & \phi(i, n + j - 1) & \text{for } 1 \le j \le nv \end{array}\right\} \tag{B.150}$$

B.4.2.2.6 Within the Mixture, at $j = 2$

For the control volume at (i, j=2), use a linear slope for $\left(\frac{\partial u}{\partial \eta}\right)_s$ and with $u_s = u_S$, the coefficients of Equation (B.122) become:

$$a_N(i,j) = \dot{m}_n(i,j)\left[\frac{1}{\exp(\mathrm{Pe}_n) - 1}\right] \tag{B.151}$$

$$\mathrm{Pe}_n = \frac{\dot{m}_n(i,j)\delta_m(i)\Delta\eta_+(j)}{\mu_n(i,j)\Delta\chi(i)} \tag{B.152}$$

$$a_S(i,j) = \frac{\mu_n(i,j-1)\Delta\chi(i)}{\delta_m(i)\Delta\eta_+(j-1)} + \dot{m}_s(i,j) \tag{B.153}$$

$$\begin{aligned} b_P(i,j) = {} & \dot{m}_w(i,j)u(i-1,j) \\ & + g\left[\rho(i,j) - \rho(i,nv)\right]\cos\theta\,\delta_m(i)\Delta\chi(i)\Delta\eta(j) \end{aligned} \tag{B.154}$$

$$a_P(i,j) = \dot{m}_w(i,j) + a_N(i,j) + a_S(i,j) \tag{B.155}$$

B.4.2.2.7 Within the Mixture, $3 \leq j \leq nv\text{-}2$

The coefficients of Equation (B.122) for the mixture momentum equation, within the mixture layer, is given by:

$$a_N(i,j) = \dot{m}_n(i,j)\left[\frac{1}{\exp(\mathrm{Pe}_n)-1}\right] \tag{B.156}$$

$$\mathrm{Pe}_n = \frac{\dot{m}_n(i,j)\delta_m(i)\Delta\eta_+(j)}{\mu_n(i,j)\Delta\chi(i)} \tag{B.157}$$

$$a_S(i,j) = \dot{m}_n(i,j-1)\left[\frac{\exp(\mathrm{Pe}_s)}{\exp(\mathrm{Pe}_s)-1}\right] \tag{B.158}$$

$$\mathrm{Pe}_s = \frac{\dot{m}_n(i,j-1)\delta_m(i)\Delta\eta_+(j-1)}{\mu_n(i,j-1)\Delta\chi(i)} \tag{B.159}$$

$$\begin{aligned} b_P(i,j) = {} & \dot{m}_w(i,j)\mathrm{u}(i-1,j) \\ & + g\left[\rho(i,j)-\rho(i,nv)\right]\cos\theta\,\delta_m(i)\Delta\chi(i)\Delta\eta(j) \end{aligned} \tag{B.160}$$

$$a_P(i,j) = \dot{m}_w(i,j) + a_N(i,j) + a_S(i,j) \tag{B.161}$$

B.4.2.2.8 Within the Mixture, at $j = nv\text{-}1$

For the control volume at (i, j=nv-1), use a linear slope for $\left(\frac{\partial \mathrm{u}}{\partial \eta}\right)_n$ and with $\mathrm{u}_n = \mathrm{u}_N$, the coefficients of Equation (B.122) become:

$$a_N(i,j) = \frac{\mu_n(i,j)\Delta\chi(i)}{\delta_m(i)\Delta\eta_+(j)} - \dot{m}_n(i,j) \tag{B.162}$$

$$a_S(i,j) = \dot{m}_n(i,j-1)\left[\frac{\exp(\mathrm{Pe}_s)}{\exp(\mathrm{Pe}_s)-1}\right] \tag{B.163}$$

$$\mathrm{Pe}_s = \frac{\dot{m}_n(i,j-1)\delta_m(i)\Delta\eta_+(j-1)}{\mu_n(i,j-1)\Delta\chi(i)} \tag{B.164}$$

$$\begin{aligned} b_P(i,j) = {} & \dot{m}_w(i,j)\mathrm{u}(i-1,j) \\ & + g\left[\rho(i,j)-\rho(i,nv)\right]\cos\theta\,\delta_m(i)\Delta\chi(i)\Delta\eta(j) \end{aligned} \tag{B.165}$$

$$a_P(i,j) = \dot{m}_w(i,j) + a_N(i,j) + a_S(i,j) \tag{B.166}$$

B.4.2.2.9 At the Freestream, $j = nv$

At the freestream, the boundary condition states that:

$$\mathrm{u} = \mathrm{u}_\infty \tag{B.167}$$

This results in the following coefficients for Equation (B.122):

$$\left.\begin{aligned} a_P(i,nv) &= 1.0 \\ a_N(i,nv) &= 0.0 \\ a_S(i,nv) &= 0.0 \\ b_P(i,nv) &= \mathrm{u}_\infty \end{aligned}\right\} \tag{B.168}$$

B.4.3 Liquid Energy Equation

The liquid energy equation doesn't contain a source term, and is to be solved using the existing solution fields for mass flows and the properties from the last iterated temperature

field. The next several sections shows how to obtain the coefficients of Equation (B.122) for the liquid energy equation.

B.4.3.1 At the Wall, $j_L = 1$

The boundary condition is:

$$T_L = T_{wall} \tag{B.169}$$

This results in the following coefficients for Equation (B.122)

$$\left.\begin{aligned} a_P(i,1) &= 1.0 \\ a_N(i,1) &= 0.0 \\ a_S(i,1) &= 0.0 \\ b_P(i,1) &= T_{wall} \end{aligned}\right\} \tag{B.170}$$

B.4.3.2 Within the Liquid, at $j_L = 2$

For the control volume at (i, j_L=2), use a linear slope for $\left(\frac{\partial T_L}{\partial \eta}\right)_s$ and with $T_{L,s} = T_{L,S}$, the coefficients of Equation (B.122) become:

$$a_N(i, j_L) = \dot{m}_{L,n}(i, j_L)\, c_{P_{L,n}}(i, j_L)\left[\frac{1}{\exp\left(Pe_{L,n}\right)-1}\right] \tag{B.171}$$

$$Pe_{L,n} = \frac{\dot{m}_{L,n}(i, j_L)\,\delta_m(i)\,\Delta\eta_{L,+}(j_L)\, c_{P_{L,n}}(i, j_L)}{k_{L,n}(i, j_L)\,\Delta\chi(i)} \tag{B.172}$$

$$a_S(i, j_L) = c_{P_{L,n}}(i, j_L - 1)\left[\frac{k_{L,n}(i, j_L - 1)\Delta\chi(i)}{c_{P_{L,n}}(i, j_L - 1)\delta_m(i)\Delta\eta_{L,+}(j_L - 1)} + \dot{m}_{L,s}(i, j_L)\right] \quad \text{(B.173)}$$

$$b_P(i, j_L) = \dot{m}_{L,w}(i, j_L)c_{P_{L,w}}(i, j_L)T_L(i-1, j_L) \quad \text{(B.174)}$$

$$a_P(i, j_L) = \dot{m}_{L,e}(i, j_L)c_{P_{L,e}}(i, j_L) + \dot{m}_{L,n}(i, j_L)c_{P_{L,n}}(i, j_L) - \dot{m}_{L,n}(i, j_L - 1)c_{P_{L,n}}(i, j_L - 1) + a_N(i, j_L) + a_S(i, j_L) \quad \text{(B.175)}$$

B.4.3.3 Within the Liquid, $3 \le j_L \le n$-2

The coefficients for Equation (B.122) are:

$$a_N(i, j_L) = \dot{m}_{L,n}(i, j_L)c_{P_{L,n}}(i, j_L)\left[\frac{1}{\exp(Pe_{L,n}) - 1}\right] \quad \text{(B.176)}$$

$$Pe_{L,n} = \frac{\dot{m}_{L,n}(i, j_L)\delta_m(i)\Delta\eta_{L,+}(j_L)c_{P_{L,n}}(i, j_L)}{k_{L,n}(i, j_L)\Delta\chi(i)} \quad \text{(B.177)}$$

$$a_S(i, j_L) = \dot{m}_{L,n}(i, j_L - 1)c_{P_{L,n}}(i, j_L - 1)\left[\frac{\exp(Pe_{L,s})}{\exp(Pe_{L,s}) - 1}\right] \quad \text{(B.178)}$$

$$Pe_{L,s} = \frac{\dot{m}_{L,n}(i, j_L - 1)\delta_m(i)\Delta\eta_{L,+}(j_L - 1)c_{P_{L,n}}(i, j_L - 1)}{k_{L,n}(i, j_L - 1)\Delta\chi(i)} \quad \text{(B.179)}$$

$$b_P(i, j_L) = \dot{m}_{L,w}(i, j_L)c_{P_{L,w}}(i, j_L)T_L(i-1, j_L) \quad \text{(B.180)}$$

$$a_P(i, j_L) = \dot{m}_{L,e}(i, j_L)c_{P_{L,e}}(i, j_L) + \dot{m}_{L,n}(i, j_L)c_{P_{L,n}}(i, j_L) - \dot{m}_{L,n}(i, j_L - 1)c_{P_{L,n}}(i, j_L - 1) + a_N(i, j_L) + a_S(i, j_L) \quad \text{(B.181)}$$

B.4.3.4 Within the Liquid, at $j_L = n\text{-}1$

For the control volume at (i, j_L=n-1), use a linear slope for $\left(\frac{\partial T_L}{\partial \eta}\right)_n$ and with $T_{L,n} = T_{L,N}$,

the coefficients of Equation (B.122) become:

$$a_N(i, j_L) = c_{P_{L,n}}(i, j_L)\left[\frac{k_{L,n}(i, j_L)\Delta\chi(i)}{c_{P_{L,n}}(i, j_L)\delta_m(i)\Delta\eta_{L,+}(j_L)} - \dot{m}_{L,n}(i, j_L)\right] \tag{B.182}$$

$$a_S(i, j_L) = \dot{m}_{L,n}(i, j_L - 1)c_{P_{L,n}}(i, j_L - 1)\left[\frac{\exp(Pe_{L,s})}{\exp(Pe_{L,s}) - 1}\right] \tag{B.183}$$

$$Pe_{L,s} = \frac{\dot{m}_{L,n}(i, j_L - 1)\delta_m(i)\Delta\eta_{L,+}(j_L - 1)c_{P_{L,n}}(i, j_L - 1)}{k_{L,n}(i, j_L - 1)\Delta\chi(i)} \tag{B.184}$$

$$b_P(i, j_L) = \dot{m}_{L,w}(i, j_L)c_{P_{L,w}}(i, j_L)T_L(i-1, j_L) \tag{B.185}$$

$$\begin{aligned} a_P(i, j_L) = {} & \dot{m}_{L,e}(i, j_L)c_{P_{L,e}}(i, j_L) + \dot{m}_{L,n}(i, j_L)c_{P_{L,n}}(i, j_L) \\ & - \dot{m}_{L,n}(i, j_L - 1)c_{P_{L,n}}(i, j_L - 1) + a_N(i, j_L) + a_S(i, j_L) \end{aligned} \tag{B.186}$$

B.4.3.5 At the Interface, $j_L = n$

The boundary condition is:

$$T_L = T_i \tag{B.187}$$

T_i is evaluated as the saturation temperature of the vapor at it's partial pressure at the interface. The coefficients for Equation (B.122) are:

$$\left.\begin{aligned} a_P(i,n) &= 1.0 \\ a_N(i,n) &= 0.0 \\ a_S(i,n) &= 0.0 \\ b_P(i,n) &= T_i \end{aligned}\right\} \qquad \text{(B.188)}$$

B.4.4 Mixture Energy Equation

B.4.4.1 Source Term for the Mixture Energy Equation

The source term for the mixture energy equation is given by:

$$\int_s^n \int_w^e S\, d\chi\, d\eta = \int_s^n \int_w^e \frac{\partial}{\partial \eta}\left[\frac{\rho D\left(c_{P_g} - c_{P_v}\right)}{\delta} T \frac{\partial W}{\partial \eta}\right] d\chi\, d\eta \qquad \text{(B.189)}$$

To simpify the discretization, neglect the variation of properties, T and $\frac{\partial W}{\partial \eta}$ across $\Delta\chi$.

Thus Equation (B.189) can be written as:

$$\int_s^n \int_w^e S\, d\chi\, d\eta = \int_s^n \frac{\partial}{\partial \eta}\left[\rho D\left(c_{P_g} - c_{P_v}\right) T \frac{\partial W}{\partial \eta}\right] d\eta \int_w^e \frac{1}{\delta} d\chi \qquad \text{(B.190)}$$

Further simplify by assuming a stepwise profile for δ. Also, use a simple linear approximation for the gradient of W at the north and south faces. This results in:

$$\int_s^n \int_w^e S\, d\chi\, d\eta = \frac{1}{\delta_m}\Delta\chi\left\{\rho_n D_n\left(c_{P_{g,n}} - c_{P_{v,n}}\right)T_n\left(\frac{\partial W}{\partial \eta}\right)_n - \rho_s D_s\left(c_{P_{g,s}} - c_{P_{v,s}}\right)T_s\left(\frac{\partial W}{\partial \eta}\right)_s\right\} \quad \text{(B.191)}$$

where: $T_n = T_P + \alpha_n\left(T_N - T_P\right)$ (B.192)

$T_s = T_S + \alpha_s\left(T_P - T_S\right)$ (B.193)

$\left(\frac{\partial W}{\partial \eta}\right)_n = \frac{W_N - W_P}{\Delta\eta_+}$ (B.194)

$\left(\frac{\partial W}{\partial \eta}\right)_s = \frac{W_P - W_S}{\Delta\eta_-}$ (B.195)

α_n and α_s are given by Equations (B.41) and (B.44)

B.4.4.2 Discretized Form of the Mixture Energy Equation

B.4.4.2.1 At the Liquid-Mixture Interface, $j = 1$

The boundary condition at the liquid-mixture interface is:

$$T = T_i \quad \text{(B.196)}$$

T_i is evaluated as the saturation temperature of the vapor at it's partial pressure at the interface. The coefficients for Equation (B.122) are:

$$\left.\begin{aligned} a_P(i,1) &= 1.0 \\ a_N(i,1) &= 0.0 \\ a_S(i,1) &= 0.0 \\ b_P(i,1) &= T_i \end{aligned}\right\} \qquad \text{(B.197)}$$

B.4.4.2.2 Within the Mixture, at $j = 2$

For the control volume at (i, j=2), use a linear slope for $\left(\frac{\partial T}{\partial \eta}\right)_s$ and with $T_s = T_S$, the coefficients of Equation (B.122) become:

$$a_N(i,j) = \dot{m}_n(i,j)\, c_{P_n}(i,j)\left[\frac{1}{\exp(Pe_n)-1}\right] \qquad \text{(B.198)}$$

$$Pe_n = \frac{\dot{m}_n(i,j)\delta_m(i)\Delta\eta_+(j)\, c_{P_n}(i,j)}{k_n(i,j)\Delta\chi(i)} \qquad \text{(B.199)}$$

$$a_S(i,j) = c_{P_n}(i,j-1)\left[\frac{k_n(i,j-1)\Delta\chi(i)}{c_{P_n}(i,j-1)\delta_m(i)\Delta\eta_+(j-1)} + \dot{m}_s(i,j)\right] \qquad \text{(B.200)}$$

$$\begin{aligned} b_P(i,j) = {} & \dot{m}_w(i,j)\, c_{P_w}(i,j)\, T(i-1,j) \\ & + \frac{1}{\delta_m}\Delta\chi(i)\left\{\rho_n(i,j)D_n(i,j)\left[c_{P_{g,n}}(i,j) - c_{P_{v,n}}(i,j)\right]T_n\left(\frac{\partial W}{\partial \eta}\right)_n\right. \\ & \left. - \rho_n(i,j-1)D_n(i,j-1)\left[c_{P_{g,n}}(i,j-1) - c_{P_{v,n}}(i,j-1)\right]T_s\left(\frac{\partial W}{\partial \eta}\right)_s\right\} \end{aligned} \qquad \text{(B.201)}$$

$$T_n = T(i,j) + \alpha_n\left[T(i,j+1) - T(i,j)\right] \qquad \text{(B.202)}$$

$$T_s = T(i,j-1) + \alpha_s\left[T(i,j) - T(i,j-1)\right] \qquad \text{(B.203)}$$

$$\left(\frac{\partial W}{\partial \eta}\right)_n = \frac{W(i,j+1)-W(i,j)}{\Delta\eta_+(j)} \tag{B.204}$$

$$\left(\frac{\partial W}{\partial \eta}\right)_s = \frac{W(i,j)-W(i,j-1)}{\Delta\eta_+(j-1)} \tag{B.205}$$

$$\begin{aligned} a_P(i,j) = {} & \dot{m}_e(i,j)\,c_{P_e}(i,j) + \dot{m}_n(i,j)\,c_{P_n}(i,j) \\ & - \dot{m}_n(i,j-1)\,c_{P_n}(i,j-1) + a_N(i,j) + a_S(i,j) \end{aligned} \tag{B.206}$$

B.4.4.2.3 Within the Mixture, $3 \le j \le nv\text{-}2$

The coefficients for Equation (B.122) are:

$$a_N(i,j) = \dot{m}_n(i,j)\,c_{P_n}(i,j)\left[\frac{1}{\exp(Pe_n)-1}\right] \tag{B.207}$$

$$Pe_n = \frac{\dot{m}_n(i,j)\,\delta_m(i)\,\Delta\eta_+(j)\,c_{P_n}(i,j)}{k_n(i,j)\,\Delta\chi(i)} \tag{B.208}$$

$$a_S(i,j) = \dot{m}_n(i,j-1)\,c_{P_n}(i,j-1)\left[\frac{\exp(Pe_s)}{\exp(Pe_s)-1}\right] \tag{B.209}$$

$$Pe_s = \frac{\dot{m}_n(i,j-1)\,\delta_m(i)\,\Delta\eta_+(j-1)\,c_{P_n}(i,j-1)}{k_n(i,j-1)\,\Delta\chi(i)} \tag{B.210}$$

$$\begin{aligned} b_P(i,j) = {} & \dot{m}_w(i,j)\,c_{P_w}(i,j)\,T(i-1,j) \\ & + \frac{1}{\delta_m}\Delta\chi(i)\Big\{\rho_n(i,j)\,D_n(i,j)\left[c_{P_{g,n}}(i,j) - c_{P_{v,n}}(i,j)\right]T_n\left(\frac{\partial W}{\partial \eta}\right)_n \\ & - \rho_n(i,j-1)\,D_n(i,j-1)\left[c_{P_{g,n}}(i,j-1) - c_{P_{v,n}}(i,j-1)\right]T_s\left(\frac{\partial W}{\partial \eta}\right)_s\Big\} \end{aligned} \tag{B.211}$$

$$T_n = T(i,j) + \alpha_n \left[T(i,j+1) - T(i,j)\right] \tag{B.212}$$

$$T_s = T(i,j-1) + \alpha_s \left[T(i,j) - T(i,j-1)\right] \tag{B.213}$$

$$\left(\frac{\partial W}{\partial \eta}\right)_n = \frac{W(i,j+1) - W(i,j)}{\Delta\eta_+(j)} \tag{B.214}$$

$$\left(\frac{\partial W}{\partial \eta}\right)_s = \frac{W(i,j) - W(i,j-1)}{\Delta\eta_+(j-1)} \tag{B.215}$$

$$\begin{aligned} a_P(i,j) = {} & \dot{m}_c(i,j)\, c_{P_c}(i,j) + \dot{m}_n(i,j)\, c_{P_n}(i,j) \\ & - \dot{m}_n(i,j-1)\, c_{P_n}(i,j-1) + a_N(i,j) + a_S(i,j) \end{aligned} \tag{B.216}$$

B.4.4.2.4 Within the Mixture, at j = nv-1

For the control volume at (i, j=nv-1), use a linear slope for $\left(\frac{\partial T}{\partial \eta}\right)_n$ and with $T_n = T_N$, the coefficients of Equation (B.122) become:

$$a_N(i,j) = c_{P_n}(i,j)\left[\frac{k_n(i,j)\Delta\chi(i)}{c_{P_n}(i,j)\delta_m(i)\Delta\eta_+(j)} - \dot{m}_n(i,j)\right] \tag{B.217}$$

$$a_S(i,j) = \dot{m}_n(i,j-1)\, c_{P_n}(i,j-1)\left[\frac{\exp(Pe_s)}{\exp(Pe_s)-1}\right] \tag{B.218}$$

$$Pe_s = \frac{\dot{m}_n(i,j-1)\delta_m(i)\Delta\eta_+(j-1)\, c_{P_n}(i,j-1)}{k_n(i,j-1)\Delta\chi(i)} \tag{B.219}$$

$$b_P(i,j) = \dot{m}_w(i,j)\,c_{P_w}(i,j)\,T(i-1,j) + \frac{1}{\delta_m}\Delta\chi(i)\Big\{\rho_n(i,j)D_n(i,j)\left[c_{P_{g,n}}(i,j) - c_{P_{v,n}}(i,j)\right]T_n\left(\frac{\partial W}{\partial \eta}\right)_n - \rho_n(i,j-1)D_n(i,j-1)\left[c_{P_{g,n}}(i,j-1) - c_{P_{v,n}}(i,j-1)\right]T_s\left(\frac{\partial W}{\partial \eta}\right)_s\Big\} \quad \text{(B.220)}$$

$$T_n = T(i,j) + \alpha_n\left[T(i,j+1) - T(i,j)\right] \quad \text{(B.221)}$$

$$T_s = T(i,j-1) + \alpha_s\left[T(i,j) - T(i,j-1)\right] \quad \text{(B.222)}$$

$$\left(\frac{\partial W}{\partial \eta}\right)_n = \frac{W(i,j+1) - W(i,j)}{\Delta\eta_+(j)} \quad \text{(B.223)}$$

$$\left(\frac{\partial W}{\partial \eta}\right)_s = \frac{W(i,j) - W(i,j-1)}{\Delta\eta_+(j-1)} \quad \text{(B.224)}$$

$$a_P(i,j) = \dot{m}_e(i,j)\,c_{P_e}(i,j) + \dot{m}_n(i,j)\,c_{P_n}(i,j) - \dot{m}_n(i,j-1)\,c_{P_n}(i,j-1) + a_N(i,j) + a_S(i,j) \quad \text{(B.225)}$$

B.4.4.2.5 At the Freestream, $j = nv$

The boundary condition at the freestream is known, and is:

$$T = T_\infty \quad \text{(B.226)}$$

The coefficients for Equation (B.122) are:

$$\left.\begin{aligned} a_P(i,nv) &= 1.0 \\ a_N(i,nv) &= 0.0 \\ a_S(i,nv) &= 0.0 \\ b_P(i,nv) &= T_\infty \end{aligned}\right\} \quad \text{(B.227)}$$

B.4.5 Mixture Diffusion Equation

B.4.5.1 At the Liquid-Mixture Interface, $j = 1$

The boundary condition that must be satisified at the interface is:

$$\dot{m}'' W + \frac{\rho D}{\delta} \frac{\partial W}{\partial \eta} = 0 \tag{B.228}$$

This is discretized over a control volume at the interface of finite $\Delta\chi$ but with $\Delta\eta = 0$. Thus there is no variation across $\Delta\eta(j=1)$ and the equation only needs to be integrated across $\Delta\chi$.

The integration of the first term is:

$$\int_w^e \dot{m}'' W \, d\chi = W_P \int_w^e \left(\rho u \frac{d\delta}{d\chi} - \rho v \right) d\chi = -\dot{m}_n W_P \tag{B.229}$$

The second term is approximated using a linear gradient between W_P and W_N, and the average value of δ, results in:

$$\int_w^e \frac{\rho D}{\delta} \frac{\partial W}{\partial \eta} d\chi = \frac{\rho_n D_n \Delta\chi}{\delta_m} \left(\frac{W_N - W_P}{\Delta\eta_+} \right) \tag{B.230}$$

Combine the two to give the discretized form:

$$W_P \left[\dot{m}_n + \frac{\rho_n D_n \Delta\chi}{\delta_m \Delta\eta_+} \right] = W_N \left[\frac{\rho_n D_n \Delta\chi}{\delta_m \Delta\eta_+} \right] \tag{B.231}$$

Thus the coefficients for Equation (B.122) are:

$$a_N(i,1) = \frac{\rho_n(i,1) D_n(i,1) \Delta\chi(i)}{\delta_m(i) \Delta\eta_+(1)} \tag{B.232}$$

$$a_S(i,1) = 0.0 \tag{B.233}$$

$$b_P(i,1) = 0.0 \tag{B.234}$$

$$a_P(i,1) = \dot{m}_n(i,1) + a_N(i,1) \tag{B.235}$$

B.4.5.2 Within the Mixture, $j = 2$

For the control volumes at $j = 2$, the partially discretized diffusion equation is of the form:

$$\dot{m}_e W_e - \dot{m}_w W_w + \dot{m}_n W_n - \dot{m}_s W_s = \frac{\Delta\chi \rho_n D_n}{\delta_m}\left(\frac{\partial W}{\partial \eta}\right)_n - \frac{\Delta\chi \rho_s D_s}{\delta_m}\left(\frac{\partial W}{\partial \eta}\right)_s \tag{B.236}$$

However, from the boundary condition at the interface, we have:

$$\dot{m}_s W_s = \frac{\Delta\chi \rho_s D_s}{\delta_m}\left(\frac{\partial W}{\partial \eta}\right)_s \tag{B.237}$$

Applying the boundary condition to the south face of the control volume at $j = 2$, reduces the diffusion equation to:

$$\dot{m}_e W_e - \dot{m}_w W_w + \dot{m}_n W_n = \frac{\Delta\chi \rho_n D_n}{\delta_m}\left(\frac{\partial W}{\partial \eta}\right)_n \tag{B.238}$$

Thus the coefficients for Equation (B.122) are:

$$a_N(i,2) = \dot{m}_n(i,2)\left[\frac{1}{\exp\left[\mathrm{Pe}_n(i,2)\right] - 1}\right] \tag{B.239}$$

$$\mathrm{Pe}_n(i,2)=\frac{\dot{m}_n(i,2)\delta_m(i)\Delta\eta_+(2)}{\rho_n(i,2)D_n(i,2)\Delta\chi(i)} \tag{B.240}$$

$$a_S(i,2) = 0.0 \tag{B.241}$$

$$b_P(i,2)=\dot{m}_w(i,2)W(i-1,2) \tag{B.242}$$

$$a_P(i,2)=\dot{m}_e(i,2)+\dot{m}_n(i,2)+a_N(i,2) \tag{B.243}$$

B.4.5.3 Within the Mixture, $3 \leq j \leq nv\text{-}2$

The coefficeints for Equation (B.122) is:

$$a_N(i,j)=\dot{m}_n(i,j)\left[\frac{1}{\exp(\mathrm{Pe}_n)-1}\right] \tag{B.244}$$

$$\mathrm{Pe}_n=\frac{\dot{m}_n(i,j)\delta_m(i)\Delta\eta_+(j)}{\rho_n(i,j)D_n(i,j)\Delta\chi(i)} \tag{B.245}$$

$$a_S(i,j)=\dot{m}_n(i,j-1)\left[\frac{\exp(\mathrm{Pe}_s)}{\exp(\mathrm{Pe}_s)-1}\right] \tag{B.246}$$

$$\mathrm{Pe}_s=\frac{\dot{m}_n(i,j-1)\delta_m(i)\Delta\eta_+(j-1)}{\rho_n(i,j-1)D_n(i,j-1)\Delta\chi(i)} \tag{B.247}$$

$$b_P(i,j)=\dot{m}_w(i,j)W(i-1,j) \tag{B.248}$$

$$a_P(i,j)=\dot{m}_w(i,j)+a_N(i,j)+a_S(i,j) \tag{B.249}$$

B.4.5.4 Within the Mixture, $j = nv\text{-}1$

For the control volume at (i, j=nv-1), use a linear slope for $\left(\frac{\partial W}{\partial \eta}\right)_n$ and with $W_n = W_N$, the coefficients of Equation (B.122) become:

$$a_N(i,j) = \frac{\rho_n(i,j) D_n(i,j) \Delta\chi(i)}{\delta_m(i) \Delta\eta_+(j)} - \dot{m}_n(i,j) \tag{B.250}$$

$$a_S(i,j) = \dot{m}_n(i,j-1)\left[\frac{\exp(\mathrm{Pe}_s)}{\exp(\mathrm{Pe}_s)-1}\right] \tag{B.251}$$

$$\mathrm{Pe}_s = \frac{\dot{m}_n(i,j-1)\delta_m(i)\Delta\eta_+(j-1)}{\rho_n(i,j-1) D_n(i,j-1) \Delta\chi(i)} \tag{B.252}$$

$$b_P(i,j) = \dot{m}_w(i,j) W(i-1,j) \tag{B.253}$$

$$a_P(i,j) = \dot{m}_w(i,j) + a_N(i,j) + a_S(i,j) \tag{B.254}$$

B.4.5.5 At the Freestream, $j = nv$

The boundary condition at the freestream is known, and is:

$$W = W_\infty \tag{B.255}$$

The coefficients for Equation (B.122) are:

$$\left.\begin{aligned} a_P(i,nv) &= 1.0 \\ a_N(i,nv) &= 0.0 \\ a_S(i,nv) &= 0.0 \\ b_P(i,nv) &= W_\infty \end{aligned}\right\} \tag{B.256}$$

B.5 Energy Balance at the Interface

The condensate thickness is determined from the energy balance performed at the interface, as given by:

$$\frac{k_L}{\delta}\left(\frac{\partial T_L}{\partial \eta}\right)_{\eta=1} = \frac{k}{\delta}\left(\frac{\partial T}{\partial \eta}\right)_{\eta=1} + h_{fg}\frac{d}{d\chi}\int_0^1 \rho_L u_L \delta \, d\eta_L \tag{B.257}$$

The above equation is discretized over a control volume at the interface with $\Delta\eta = 0$, thus it only needs to be integrated over $\Delta\chi$.

$$\int_w^e \frac{k_L}{\delta}\left(\frac{\partial T_L}{\partial \eta}\right)_{\eta=1} d\chi = \int_w^e \frac{k}{\delta}\left(\frac{\partial T}{\partial \eta}\right)_{\eta=1} d\chi + h_{fg}\int_w^e \left[\frac{d}{d\chi}\int_0^1 \rho_L u_L \delta \, d\eta_L\right] d\chi \tag{B.258}$$

Properties are evaluated at the interface temperature, use the mean values for δ in the two diffusion terms and also assume a linear temperature profile at the interface. This gives:

$$\Delta\chi(i)\frac{k_L(i,n)}{\delta_m(i)}\left\{\frac{T_L(i,n)-T_L(i,n-1)}{\Delta\eta_{L,+}(n-1)}\right\} = \Delta\chi(i)\frac{k(i,1)}{\delta_m(i)}\left\{\frac{T(i,2)-T(i,1)}{\Delta\eta_+(1)}\right\} + \delta(i)h_{fg}(i)\int_0^1 G_{x,e}\, d\eta_L - \delta(i-1)h_{fg}(i)\int_0^1 G_{x,w}\, d\eta_L \tag{B.259}$$

Recall that the defination of δ_m is:

$$\delta_m(i) = \frac{\delta(i)+\delta(i-1)}{2} \tag{B.260}$$

Also, let:
$$A = \Delta\chi(i)k_L(i,n)\left\{\frac{T_L(i,n)-T_L(i,n-1)}{\Delta\eta_{L,+}(n-1)}\right\} - \Delta\chi(i)k(i,1)\left\{\frac{T(i,2)-T_L(i,1)}{\Delta\eta_{+}(1)}\right\} \quad \text{(B.261)}$$

$$B = h_{fg}(i)\int_0^1 G_{x,e}\,d\eta_L = h_{fg}(i)\sum_{j_L=1}^{n}\frac{\dot{m}_{L,e}(i,j_L)}{\delta(i)} \quad \text{(B.262)}$$

$$C = h_{fg}(i)\int_0^1 G_{x,w}\,d\eta_L = h_{fg}(i)\sum_{j_L=1}^{n}\frac{\dot{m}_{L,w}(i,j_L)}{\delta(i-1)} \quad \text{(B.263)}$$

Using the above definations, Equation (B.259) is simplified to:

$$A = B\delta(i)\left(\frac{\delta(i)-\delta(i-1)}{2}\right) - C\delta(i-1)\left(\frac{\delta(i)-\delta(i-1)}{2}\right) \quad \text{(B.264)}$$

This simplifies to:

$$0 = B\delta(i)^2 + \delta(i)\delta(i-1)(B-C) - C\delta(i-1)^2 - 2A \quad \text{(B.265)}$$

Now apply the following definations:

$$a = B = h_{fg}(i)\sum_{j_L=1}^{n}\frac{\dot{m}_{L,e}(i,j_L)}{\delta(i)} \quad \text{(B.266)}$$

$$b = \delta(i-1)(B-C) = \delta(i-1)h_{fg}(i)\left\{\sum_{j_L=1}^{n}\frac{\dot{m}_{L,e}(i,j_L)}{\delta(i)} - \sum_{j_L=1}^{n}\frac{\dot{m}_{L,w}(i,j_L)}{\delta(i-1)}\right\} \quad \text{(B.267)}$$

$$
\begin{aligned}
c &= -C\delta(i-1)^2 - 2A \\
&= -\delta(i-1)^2 h_{fg}(i) \sum_{j_L=1}^{n} \frac{\dot{m}_{L,w}(i, j_L)}{\delta(i-1)} \\
&\quad - 2\Delta\chi(i) k_L(i, n-1) \left\{ \frac{T_L(i,n) - T_L(i,n-1)}{\Delta\eta_{L,+}(n-1)} \right\} \\
&\quad + 2\Delta\chi(i) k(i,1) \left\{ \frac{T(i,2) - T(i,1)}{\Delta\eta_{+}(1)} \right\}
\end{aligned}
\tag{B.268}
$$

Applying Equations (B.266) - (B.268) to Equation (B.265) yields the following quadratic equation for $\delta(i)$:

$$
0 = a\delta(i)^2 + b\delta(i) + c \tag{B.269}
$$

The solution of Equation (B.269) is given by:

$$
\delta(i) = \frac{-b \pm \sqrt{b^2 - 4ac}}{2a} \tag{B.270}
$$

The defination of a,b,c as given by Equations (B.266) - (B.268) show that:

$$
a > 0, \qquad b > 0, \qquad c < 0
$$

Thus Equation (B.270) can be rewritten as:

$$
\delta(i) = \frac{-b \pm \sqrt{b^2 + |4ac|}}{2a} \tag{B.271}
$$

and since $\delta(i) > 0$,

$$
\delta(i) = \frac{-b + \sqrt{b^2 - 4ac}}{2a} \tag{B.272}
$$

APPENDIX C

Initial Guess Solution Fields

To iteratively solve the discretized equations, as given in Appendix B, for $i = 2$, an initial guess solution field is needed. This appendix contains the details of the initial guess solution fields used for the three vapor-gas mixtures. The guess field for the liquid properties were calculated at T_{wall} and the mixture properties were evaluated at T_∞ and W_∞.

C.1 Steam-Air Mixture

$$\delta(i) = \left[\frac{4 k_L \mu_L (T_\infty - T_{wall}) \chi_b(i)}{h_{fg}\, g\, \rho_L^2}\right]^{1/4} \tag{C.1}$$

$$T_L(j_L) = (T_{sat} - T_{wall})\eta_L(j_L) + T_{wall} \tag{C.2}$$

where: T_{sat} is evaluated at W_∞ and T_∞.

$$u_L(j_L) = \delta(i)^2\left[\frac{0.5\rho_L g}{\mu_L}\right]\left[2\eta_L(j_L) - \eta_L(j_L)^2\right] \tag{C.3}$$

$$u(j) = u_\infty \tag{C.4}$$

$$T(j) = T_\infty \tag{C.5}$$

$$W(j) = W_\infty \tag{C.6}$$

The liquid and mixture continuity equations are then solved using the guessed velocity profiles given by Equations (C.3) and (C.4). The properties are then re-evaluated using the resulting solution field obtained from the above equations.

C.2 Sodium-Argon Mixture

$$\delta(i) = \delta_{guess} \tag{C.7}$$

where: δ_{guess} is given by the user

$$u_L(j_L) = \delta(i)^2\left[\frac{0.5\rho_L g}{\mu_L}\right]\left[2\eta_L(j_L) - \eta_L(j_L)^2\right] \tag{C.8}$$

$$T_L(j_L) = (T_i - T_{wall})\eta_L(j_L) + T_{wall} \tag{C.9}$$

$$T_i = T_{wall} - \frac{\dot{m}_{L,n}(n-1)h_{fg}\delta(i)}{k_L\,\Delta\chi(i)} \tag{C.10}$$

$$W_i = \frac{\frac{P_{g,i}}{P_\infty}\tilde{M}_g}{\frac{P_{g,i}}{P_\infty}\tilde{M}_g + \frac{P_{v,i}}{P_\infty}\tilde{M}_v} \tag{C.11}$$

where: $\dot{m}_{L,n}(n-1)$ was obtained by solving the liquid continuity equation.

$P_{v,i}$ is the partial pressure of the vapor at the interface.

$P_{g,i}$ is the partial pressure of the gas at the interface.

$$u(j) = u_L(n) + [u_\infty - u_L(n)]\frac{\exp\left[Pe_u\frac{\eta(j)-1}{\eta(nv)-1}\right] - 1}{\exp[Pe_u] - 1} \tag{C.12}$$

where: $$Pe_u = \frac{\dot{m}_{L,n}(n-1)\delta(i)[\eta(nv)-1]}{\mu\,\Delta\chi(i)} \tag{C.13}$$

$$T(j) = T_i + (T_\infty - T_i)\frac{\exp\left[Pe_T\frac{\eta(j)-1}{\eta(nv)-1}\right] - 1}{\exp[Pe_T] - 1} \tag{C.14}$$

where: $$Pe_T = \frac{c_P \dot{m}_{L,n}(n-1)\delta(i)[\eta(nv)-1]}{k\,\Delta\chi(i)} \quad \text{(C.15)}$$

$$W(j) = W_i + (W_\infty - W_i)\frac{\exp\left[Pe_W \frac{\eta(j)-1}{\eta(nv)-1}\right] - 1}{\exp[Pe_W] - 1} \quad \text{(C.16)}$$

where: $$Pe_W = \frac{\dot{m}_{L,n}(n-1)\delta(i)[\eta(nv)-1]}{\rho\, D\,\Delta\chi(i)} \quad \text{(C.17)}$$

The properties were then re-evaluated using the guess temperature and gas concentration fields and the liquid and mixture continuity equations used to obtain the mass flows across the north faces.

C.3 Glycerine-Bromine Mixture

$$\delta(i) = \delta_{guess} \quad \text{(C.18)}$$

where: δ_{guess} was given by the user.

$$u_L(j_L) = \delta(i)^2\left[\frac{0.5\rho_L g}{\mu_L}\right]\left[2\eta_L(j_L) - \eta_L(j_L)^2\right] \quad \text{(C.19)}$$

$$T_L(j_L) = (T_i - T_{wall})\eta_L(j_L) + T_{wall} \quad \text{(C.20)}$$

where: $$T_i = T_{wall} - \frac{\dot{m}_{L,n}(j_L = n)h_{fg}\,\delta(i)}{k_L\,\Delta\chi(i)} \quad \text{(C.21)}$$

and $\dot{m}_{L,n}(j_L = n)$ was obtained by solving the liquid continuity equation.

$$u(j) = u_\infty \quad \text{(C.22)}$$

$$T(j) = T_\infty \quad \text{(C.23)}$$

$$W(j) = W_{\infty} \tag{C.24}$$

The properties were then re-evaluated using the guess temperature and gas concentration fields and the liquid and mixture continuity equations used to obtain the mass flows across the north faces.

APPENDIX D

Dimensionless Groups

This appendix determines the dimensionless groups that are used to present the results. To obtain these dimensionless groups, the following assumptions are applied to the complete boundary layer equations and conditions.

1. Constant properties.
2. Forced-convection condensation.
3. vertical or inclined plate (excluding the horizontal).

This will result in the following set of boundary layer equations:

- Liquid continuity equation

$$\frac{\partial u_L}{\partial x} + \frac{\partial v_L}{\partial y} = 0 \qquad \text{(D.1)}$$

- Liquid momentum equation

$$u_L \frac{\partial u_L}{\partial x} + v_L \frac{\partial u_L}{\partial y} = \nu_L \frac{\partial^2 u_L}{\partial y^2} + g\left(1 - \frac{\rho_\infty}{\rho_L}\right)\cos\alpha \qquad \text{(D.2)}$$

The $\cos\alpha$ accounts for the component of gravity directed along the plate.

- Liquid energy equation

$$u_L \frac{\partial T_L}{\partial x} + v_L \frac{\partial T_L}{\partial y} = \frac{\nu_L}{Pr_L} \frac{\partial^2 T_L}{\partial y^2} \qquad \text{(D.3)}$$

- Mixture continuity equation

$$\frac{\partial u}{\partial x} + \frac{\partial v}{\partial y} = 0 \qquad \text{(D.4)}$$

- Mixture momentum equation

$$u\frac{\partial u}{\partial x} + v\frac{\partial u}{\partial y} = \nu\frac{\partial^2 u}{\partial y^2} + g\left(1 - \frac{\rho_\infty}{\rho}\right)\cos\alpha \qquad \text{(D.5)}$$

The $\cos\alpha$ accounts for the component of gravity directed along the plate.

- Mixture energy equation

$$u\frac{\partial T}{\partial x} + v\frac{\partial T}{\partial y} = \frac{\nu}{\Pr}\frac{\partial^2 T}{\partial y^2} + \frac{C_{Pg} - C_{Pv}}{C_P}\frac{\partial}{\partial y}\left(DT\frac{\partial W}{\partial y}\right) \qquad \text{(D.6)}$$

- Mixture mass diffusion equation

$$u\frac{\partial W}{\partial x} + v\frac{\partial W}{\partial y} = \frac{\partial}{\partial y}\left(D\frac{\partial W}{\partial y}\right) \qquad \text{(D.7)}$$

The twelve applicable boundary conditions are:

- At the plate surface $(y = 0)$:

$$u_L = 0 \qquad \text{(D.8)}$$

$$v_L = 0 \qquad \text{(D.9)}$$

$$T_L = T_{wall} \qquad \text{(D.10)}$$

- At the free stream $(y \to \infty)$:

$$u = u_\infty \qquad \text{(D.11)}$$

$$T = T_\infty \qquad \text{(D.12)}$$

$$W = W_\infty \qquad \text{(D.13)}$$

- At the liquid-mixture interface $(y = \delta)$:

$$u_L = u \qquad \text{(D.14)}$$

$$\mu_L \frac{\partial u_L}{\partial y} = \mu \frac{\partial u}{\partial y} \tag{D.15}$$

$$T_L = T = T_i \tag{D.16}$$

$$T_i = T_{v,sat,i}\left(W_i, W_\infty, T_\infty, \tilde{M}_v, \tilde{M}_g\right) \tag{D.17}$$

$$\dot{m}'' = \rho_L u_L \frac{d\delta}{dx} - \rho_L v_L = \rho u \frac{d\delta}{dx} - \rho v \tag{D.18}$$

$$\dot{m}'' W + \rho D \frac{\partial W}{\partial y} = 0 \tag{D.19}$$

- Plus the energy balance at the interface:

$$k_L \frac{\partial T_L}{\partial y} = k \frac{\partial T}{\partial y} + h_{fg} \dot{m}'' \tag{D.20}$$

Define the following dimensionless groups:

$$x^* = \frac{g x \cos\alpha}{u_\infty^2} \tag{D.21}$$

$$y^* = y\sqrt{\frac{g \cos\alpha}{u_\infty \nu_L}} \tag{D.22}$$

$$u^* = \frac{u}{u_\infty} \tag{D.23}$$

$$v^* = \frac{v}{\sqrt{g x \cos\alpha}} \tag{D.24}$$

$$T^* = \frac{T - T_{wall}}{T_\infty - T_{wall}} \tag{D.25}$$

Use the above definations to nondimensionalize Equations (D.1) to (D.20) to obtain:

- Liquid boundary layer equations

$$\frac{\partial u_L^*}{\partial x^*} + \left(\frac{u_\infty x}{\nu_L}\right)^{1/2} \frac{\partial v_L^*}{\partial y^*} = 0 \tag{D.26}$$

$$u_L^* \frac{\partial u_L^*}{\partial x^*} + \left(\frac{u_\infty x}{\nu_L}\right)^{1/2} v_L^* \frac{\partial u_L^*}{\partial y^*} = \frac{\partial^2 u_L^*}{\partial y^{*2}} + \left(1 - \frac{\rho_\infty}{\rho_L}\right) \tag{D.27}$$

$$u_L^* \frac{\partial T_L^*}{\partial x^*} + \left(\frac{u_\infty x}{\nu_L}\right)^{1/2} v_L^* \frac{\partial T_L^*}{\partial y^*} = \frac{1}{\mathrm{Pr}_L} \frac{\partial^2 T_L^*}{\partial y^{*2}} \tag{D.28}$$

- Mixture boundary layer equations

$$\frac{\partial u^*}{\partial x^*} + \left(\frac{u_\infty x}{\nu_L}\right)^{1/2} \frac{\partial v^*}{\partial y^*} = 0 \tag{D.29}$$

$$u^* \frac{\partial u^*}{\partial x^*} + \left(\frac{u_\infty x}{\nu_L}\right)^{1/2} v^* \frac{\partial u^*}{\partial y^*} = \frac{\nu}{\nu_L} \frac{\partial^2 u^*}{\partial y^{*2}} + \left(1 - \frac{\rho_\infty}{\rho}\right) \tag{D.30}$$

$$u^* \frac{\partial T^*}{\partial x^*} + \left(\frac{u_\infty x}{\nu_L}\right)^{1/2} v^* \frac{\partial T^*}{\partial y^*} = \frac{\nu}{\nu_L \mathrm{Pr}} \frac{\partial^2 T^*}{\partial y^{*2}} + \frac{C_{Pg} - C_{Pv}}{C_P} \frac{\partial}{\partial y^*}\left(\frac{D}{\nu_L} T^* \frac{\partial W}{\partial y^*}\right) \tag{D.31}$$

$$u^* \frac{\partial W}{\partial x^*} + \left(\frac{u_\infty x}{\nu_L}\right)^{1/2} v^* \frac{\partial W}{\partial y^*} = \frac{\partial}{\partial y^*}\left(\frac{D}{\nu_L} \frac{\partial W}{\partial y^*}\right) \tag{D.32}$$

- Boundary conditions at the plate surface $\left(y^* = 0\right)$:

$$u_L^* = 0 \tag{D.33}$$

$$v_L^* = 0 \tag{D.34}$$

$$T_L^* = 0 \tag{D.35}$$

- Boundary conditions at the free stream $\left(y^* \rightarrow \infty\right)$:

$$u^* = 1 \tag{D.36}$$

$$T^* = 1 \tag{D.37}$$

$$W = W_\infty \tag{D.38}$$

- Boundary conditions at the liquid-mixture interface $\left(y^* = \delta^*\right)$:

$$u_L^* = u^* \tag{D.39}$$

$$\frac{\partial u_L^*}{\partial y^*} = \frac{\mu}{\mu_L}\frac{\partial u^*}{\partial y^*} \tag{D.40}$$

$$T_L^* = T^* = T_i^* \tag{D.41}$$

$$T_i^* = \frac{T_{v,sat,i}\left(W_i, W_\infty, T_\infty, \tilde{M}_v, \tilde{M}_g\right) - T_{wall}}{T_\infty - T_{wall}} \tag{D.42}$$

$$u_L^*\frac{d\delta^*}{dx^*} - \left(\frac{u_\infty x}{\nu_L}\right)^{1/2} v_L^* = \left(\frac{\rho}{\rho_L}\right)u^*\frac{d\delta^*}{dx^*} - \left(\frac{\rho}{\rho_L}\right)\left(\frac{u_\infty x}{\nu_L}\right)^{1/2} v^* \tag{D.43}$$

$$u_L^*\frac{d\delta^*}{dx^*} - \left(\frac{u_\infty x}{\nu_L}\right)^{1/2} v_L^* + \left(\frac{\rho}{\rho_L}\right)\left(\frac{D}{\nu_L}\right)\frac{1}{W}\frac{\partial W}{\partial y^*} = 0 \tag{D.44}$$

Plus the energy balance at the interface:

$$\frac{\partial T_L^*}{\partial y^*} = \left(\frac{k}{k_L}\right)\frac{\partial T^*}{\partial y^*} + \left[\frac{h_{fg}}{C_{P_L}\left(T_\infty - T_{wall}\right)}\right]\mathrm{Pr}_L\left[u_L^*\frac{d\delta^*}{dx^*} - \left(\frac{u_\infty x}{\nu_L}\right)^{1/2} v_L^*\right] \tag{D.45}$$

The transformed Equations (D.26) to (D.45) show that all of the properties can be defined by the following dimensionless groups:

$$\frac{\rho_\infty}{\rho_L}\ ,\ \mathrm{Pr}_L\ ,\ \frac{\nu}{\nu_L}\ ,\ \mathrm{Pr}\ ,\ \frac{C_{P_g}-C_{P_v}}{C_P}\ ,\ \frac{D}{\nu}\ ,\ \frac{\rho}{\rho_L}\ ,\ \frac{k}{k_L}\ ,\ \text{and}\ \frac{C_{P_L}\left(T_\infty - T_{wall}\right)}{h_{fg}} \qquad \text{(D.46)}$$

For a constant property problem, all of these dimensionless groups are known if the vapor-gas combination is given along with T_∞ , T_{wall} , and W_∞ .

From Equations (D.26) to (D.32) and (D.45), the eight dependent dimensionless variables are:

$$u_L^*\ ,\ v_L^*\left(\frac{u_\infty x}{\nu_L}\right)^{1/2}\ ,\ T_L^*\ ,\ u^*\ ,\ v^*\left(\frac{u_\infty x}{\nu_L}\right)^{1/2}\ ,\ T^*\ ,\ \delta^*\ ,\ \text{and}\ W \qquad \text{(D.47)}$$

Each of these eight dependent variables are a function of x^* and y^*, as well as the dimensionless groups defined in Equation (D.46).

One more dimensionless group is required to present the heat transfer results . This can be obtained by examining the heat flux to the wall (at $y = 0$). The heat flux is given by:

$$q = -k_L\left(\frac{\partial T_L}{\partial y}\right)_{y=0} \qquad \text{(D.48)}$$

Rewriting it in terms of the heat transfer coefficient, h_x and applying the dimensionless groups given by Equations (D.21) and (D.25) to give:

$$h_x\left(T_\infty - T_{wall}\right) = -k_L\frac{T_\infty - T_{wall}}{\sqrt{\frac{u_\infty \nu_L}{g\cos\alpha}}}\left(\frac{\partial T_L^*}{\partial y^*}\right)_{y^*=0} \qquad \text{(D.49)}$$

Apply the defination for the Nu_x:

$$\mathrm{Nu}_x = \frac{h_x x}{k_L} = -\sqrt{\frac{g x \cos\alpha}{\mathrm{u}_\infty^{\,2}}}\ \mathrm{Re}_x^{\,1/2} \left(\frac{\partial T_L^*}{\partial y^*}\right)_{y^*=0} \tag{D.50}$$

Which can be rewritten as:

$$\frac{\mathrm{Nu}_x}{\mathrm{Re}_x^{\,1/2}} = -\left(x^*\right)^{1/2} \left(\frac{\partial T_L^*}{\partial y^*}\right)_{y^*=0} = f\left(x^*\right) \tag{D.51}$$

Thus Equation (D.51) shows that the heat transfer results along the plate is only a function of x^*.

The advantages of presenting the results using the above dimensionless groups is that the dependent variables can be plotted independently of u_∞, g and angle of inclination. Thus, only a single plot of $\mathrm{Nu}_x\ \mathrm{Re}_x^{\,-1/2}$ *vs.* $x^* = \frac{g x \cos\alpha}{\mathrm{u}_\infty^{\,2}}$ is required to represent results for different values of u_∞, g and angle of inclination.

With variable properties, the above dimensionless analysis isn't valid. However, results generated using the numerical code with variable properties can still be presented using the above dimensionless variables and the independence from u_∞, g and angle of inclination is still valid. This is done by first obtaining the variable property solution, and then nondimensionalizing the results using properties evaluated at:

$$T_r = T_{wall} + 0.31\left(T_\infty - T_{wall}\right) \tag{D.52}$$

To validate the use of the dimensionless variables in the presentation of variable property solution, two sets of results were obtained for a glycerine-bromine mixture at $T_\infty = 450$ K, $T_{wall} = 350$ K, and $W_\infty = 0.1$. One solution set was obtained with $u_\infty = 5.0$ m/s and $g = 9.81$ m/s^2. The second set was obtained with $u_\infty = 3.535533906$ m/s and $g = 4.905$ m/s^2. These results were then nondimensionalized and plotted in Figures D.1 to D.6. Each curve in those figures, represent the solution obtained at:

$$u_\infty = 5.0 \text{ m/s and } g = 9.81 \text{ m/s}^2$$

and

$$u_\infty = 3.535533906 \text{ m/s and } g = 4.905 \text{ m/s}^2$$

This shows that the variable property results obtained from the numerical code can be presented using these dimensionless parameters to display the results independently of u_∞, g and angle of inclination (variation of α is the same as varying g).

The numerical solution is only valid for laminar flow, thus the film reynolds number must be evaluated to ensure that the flow is laminar. The film Reynolds number is defined as:

$$\text{Re}_\delta = \frac{4\Gamma}{\mu_L} \quad \text{(for laminar flow, } \text{Re}_\delta < 30\text{)} \tag{D.53}$$

Performing a non-dimensional analysis on:

$$\Gamma = \int_0^\delta \rho_L u_L \, dy \tag{D.54}$$

Applying the dimensionless groups given by Equations (D.22) and (D.23) to obtain:

$$\frac{\sqrt{\frac{g\cos\alpha}{u_\infty \nu_L}}\,\Gamma}{u_\infty \rho_L} = \int_0^\delta u_L^* \, dy^* \qquad \text{(D.55)}$$

Rearrange the left side of Equation (D.55) to get:

$$\frac{Re_\delta}{4\,Re_x}\sqrt{\frac{g\,x^2\cos\alpha}{u_\infty \nu_L}} = \int_0^\delta u_L^* \, dy^* \qquad \text{(D.56)}$$

$$\frac{Re_\delta}{4\,Re_x^{1/2}\,Fr_x^{1/2}} = \int_0^\delta u_L^* \, dy^* \qquad \text{(D.57)}$$

This gives:

$$\frac{Re_\delta}{Re_x^{1/2}} = 4\,Fr_x^{-1/2}\int_0^\delta u_L^* \, dy^* = f\left(x^*\right) \qquad \text{(D.58)}$$

Thus Equation (D.58) shows that the film reynolds number can be presented for all g, u_∞ and angle of inclination by plotting $Re_\delta\, Re_x^{-1/2}$ *vs.* Fr_x^{-1}. This is shown by the two curves for two different W_∞ at various g, u_∞ and angle of inclination in Figure D.7.

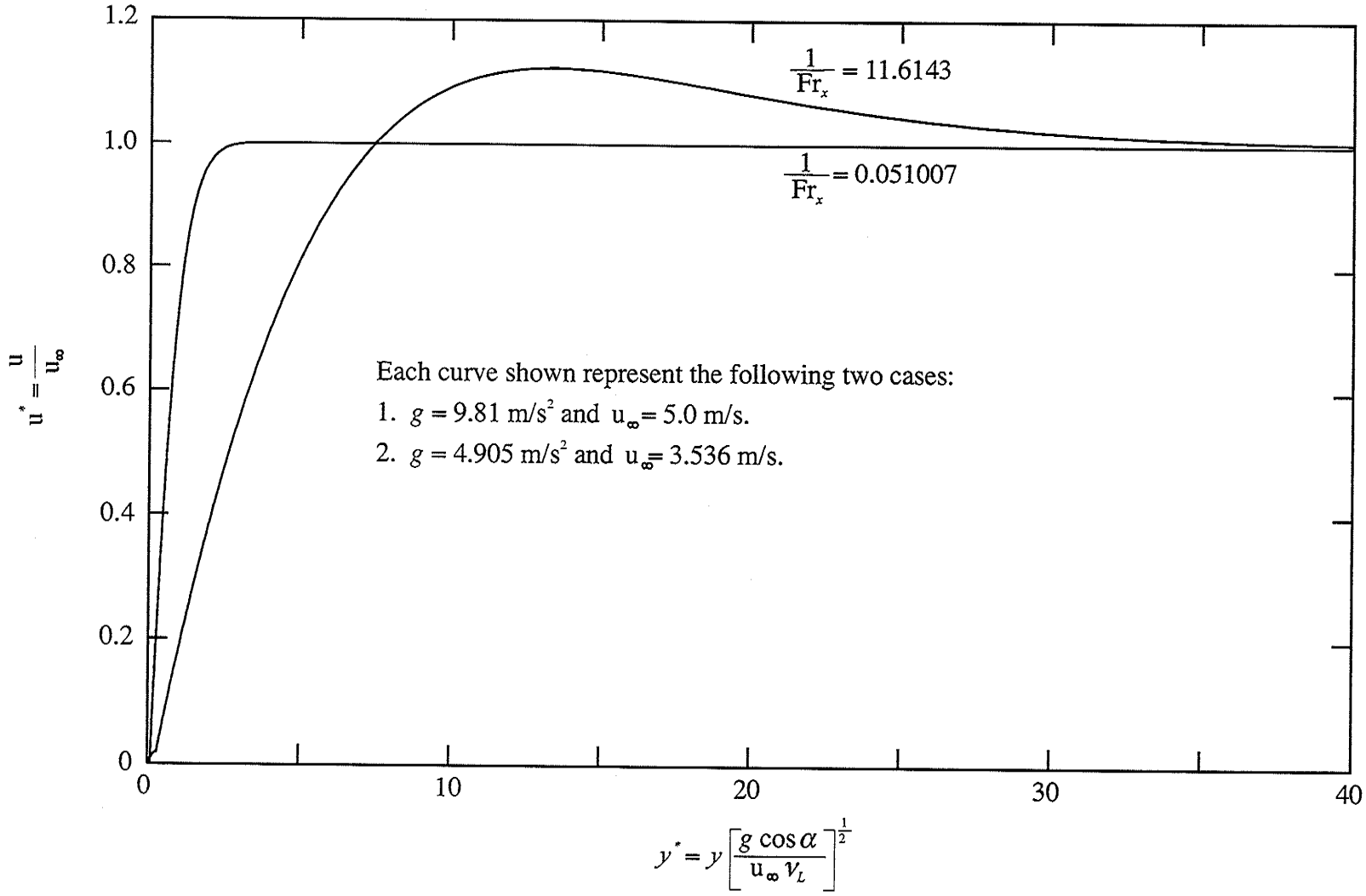

Figure D.1: Vapor velocity profiles for glycerine-bromine at $T_\infty = 450$ K, $T_{wall} = 350$ K and $W_\infty = 0.1$.

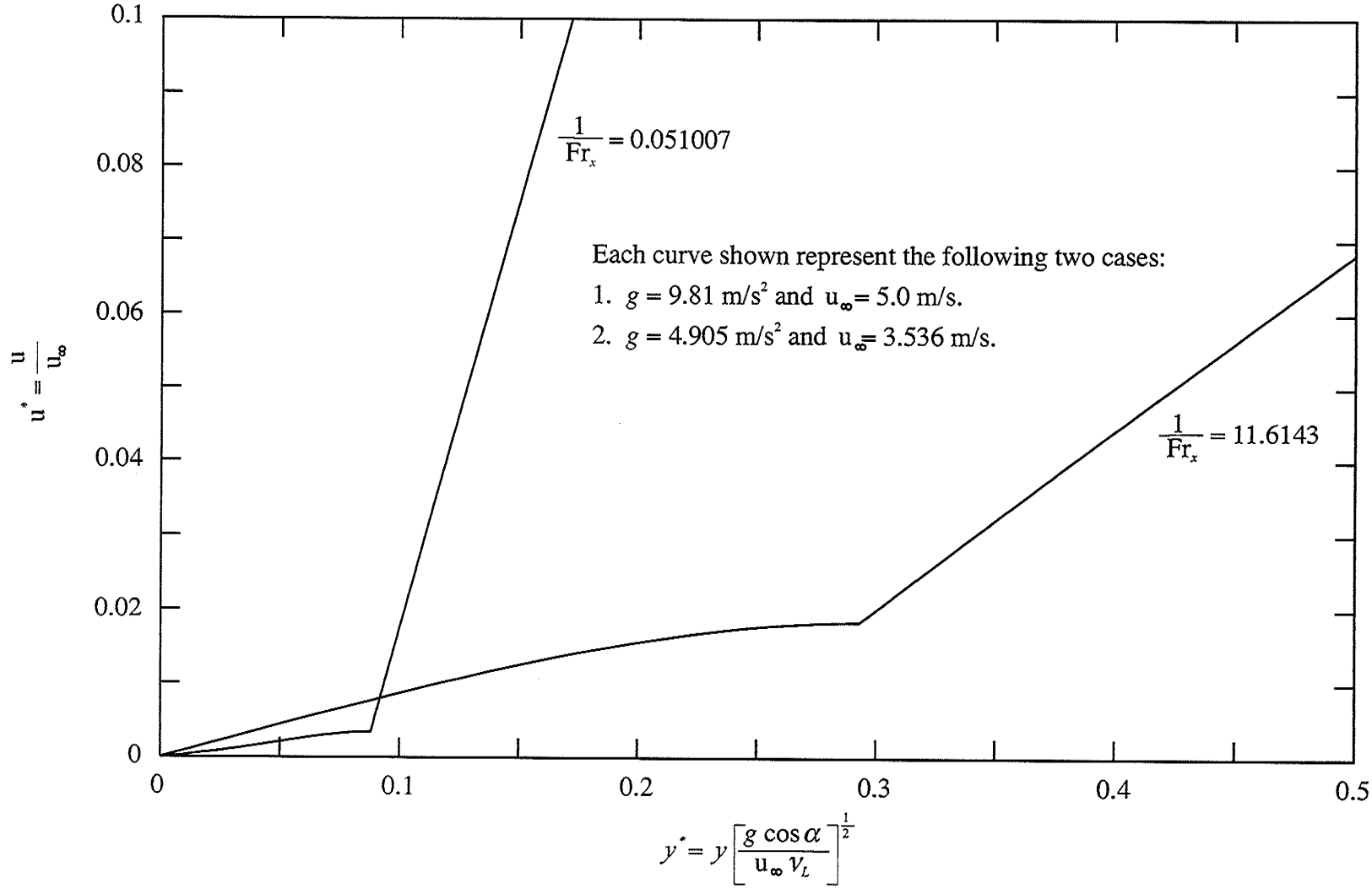

Figure D.2: Liquid velocity profiles for glycerine-bromine at $T_\infty = 450$ K, $T_{wall} = 350$ K and $W_\infty = 0.1$.

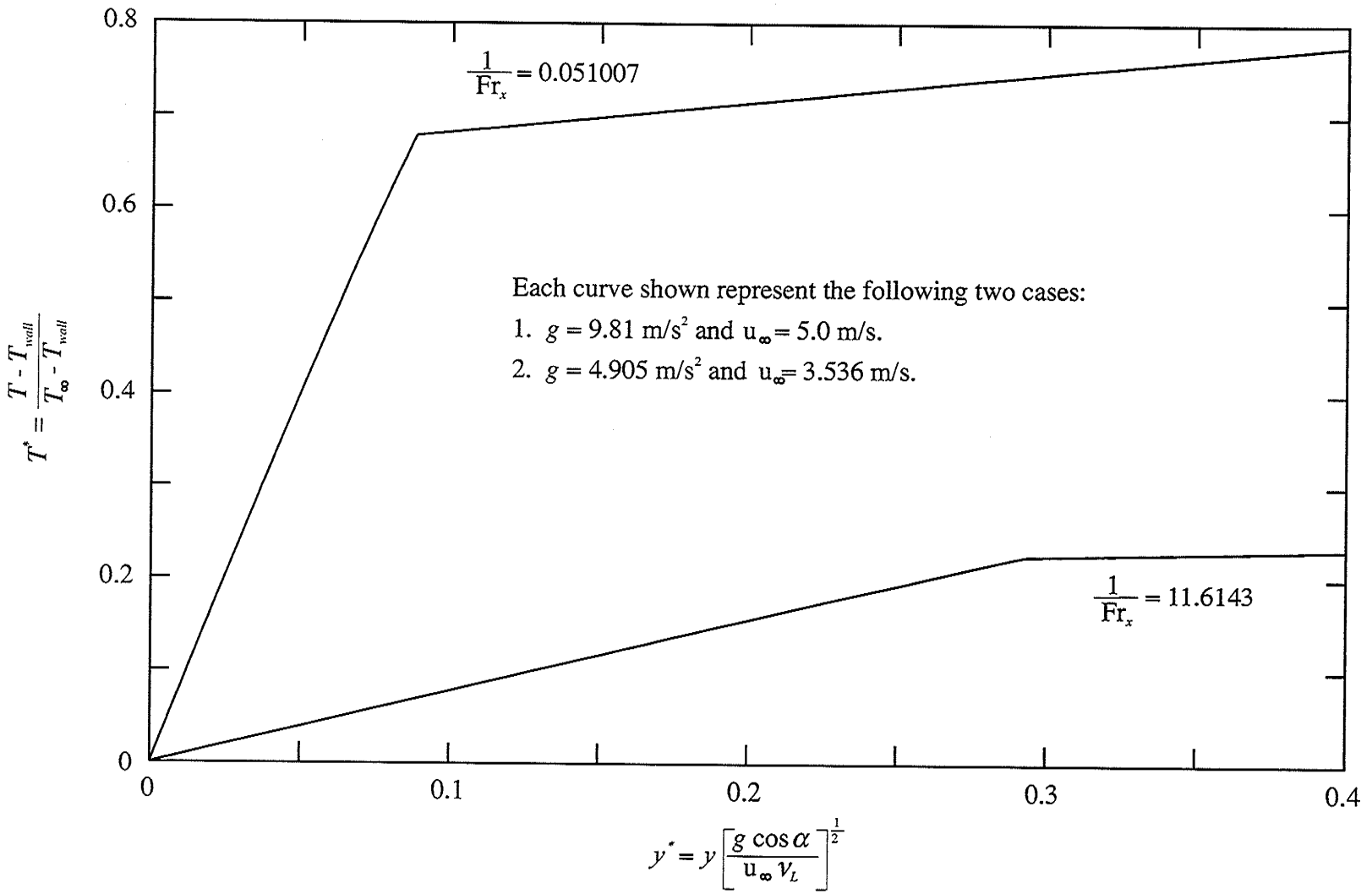

Figure D.3: Temperature profiles for glycerine-bromine at $T_\infty = 450$ K, $T_{wall} = 350$ K and $W_\infty = 0.1$.

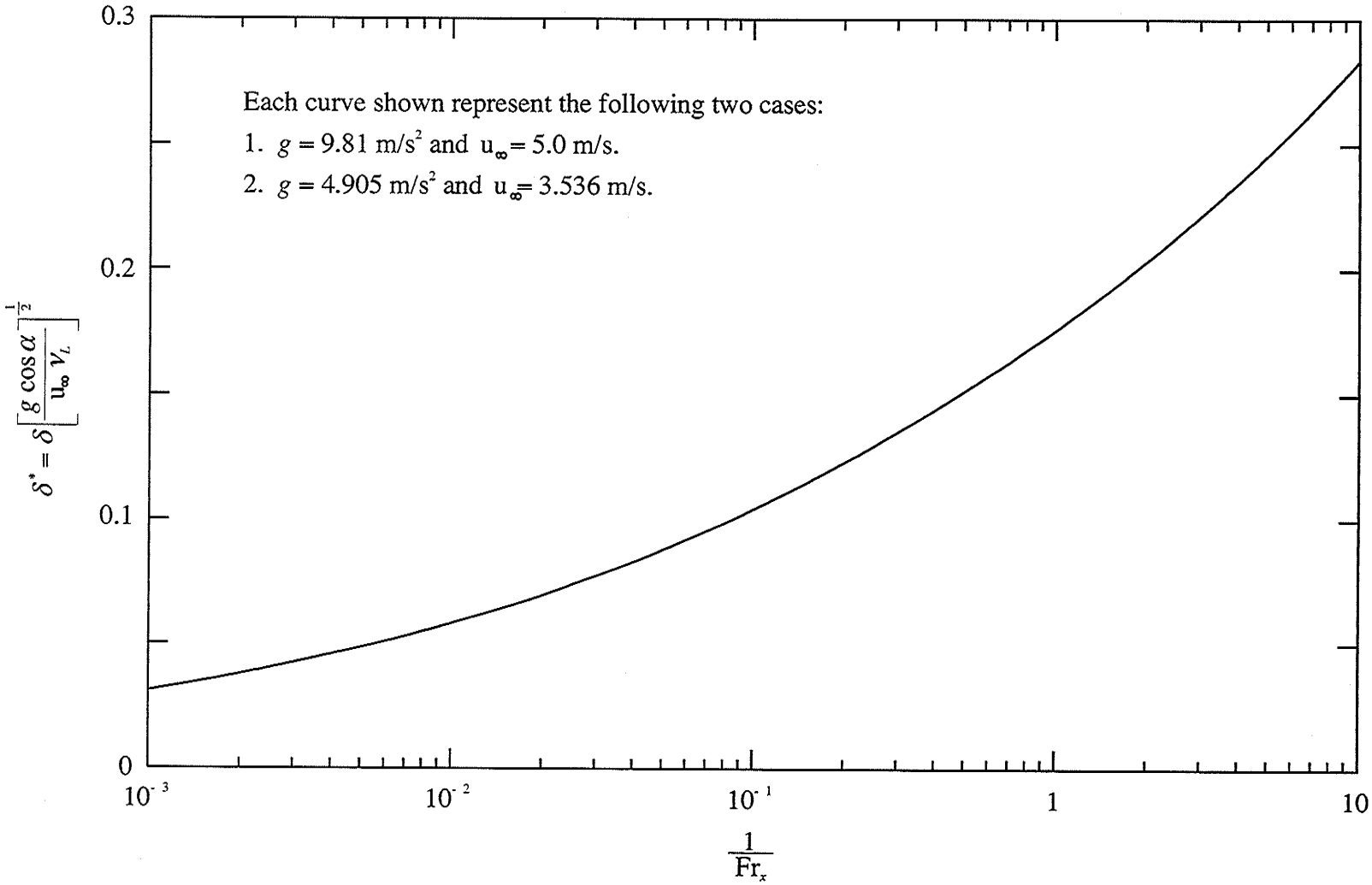

Figure D.4: Liquid film thickness for glycerine-bromine at T_∞= 450 K, T_{wall} = 350 K and W_∞ = 0.1.

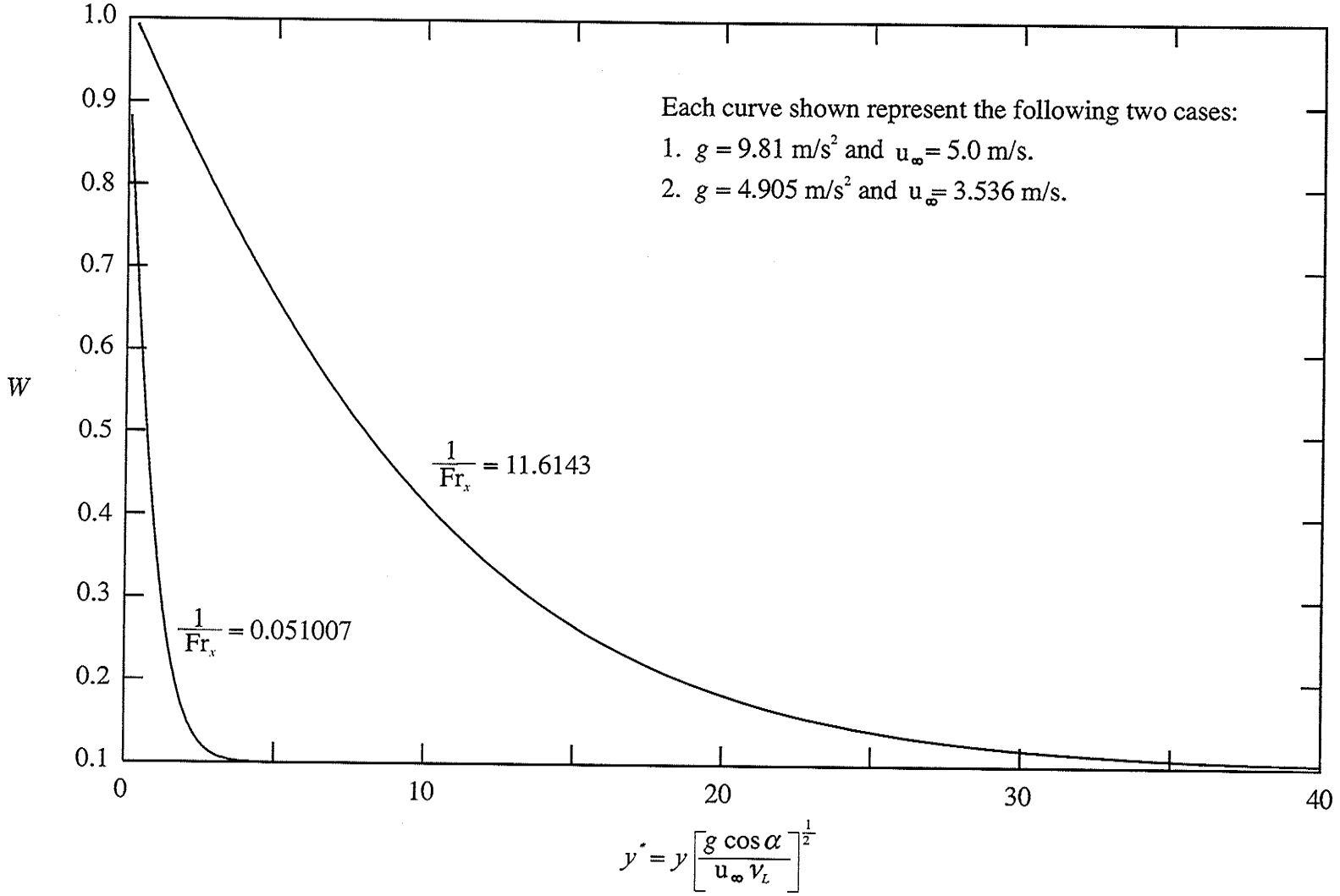

Figure D.5: Gas concentration profiles for glycerine-bromine at $T_\infty = 450$ K, $T_{wall} = 350$ K and $W_\infty = 0.1$.

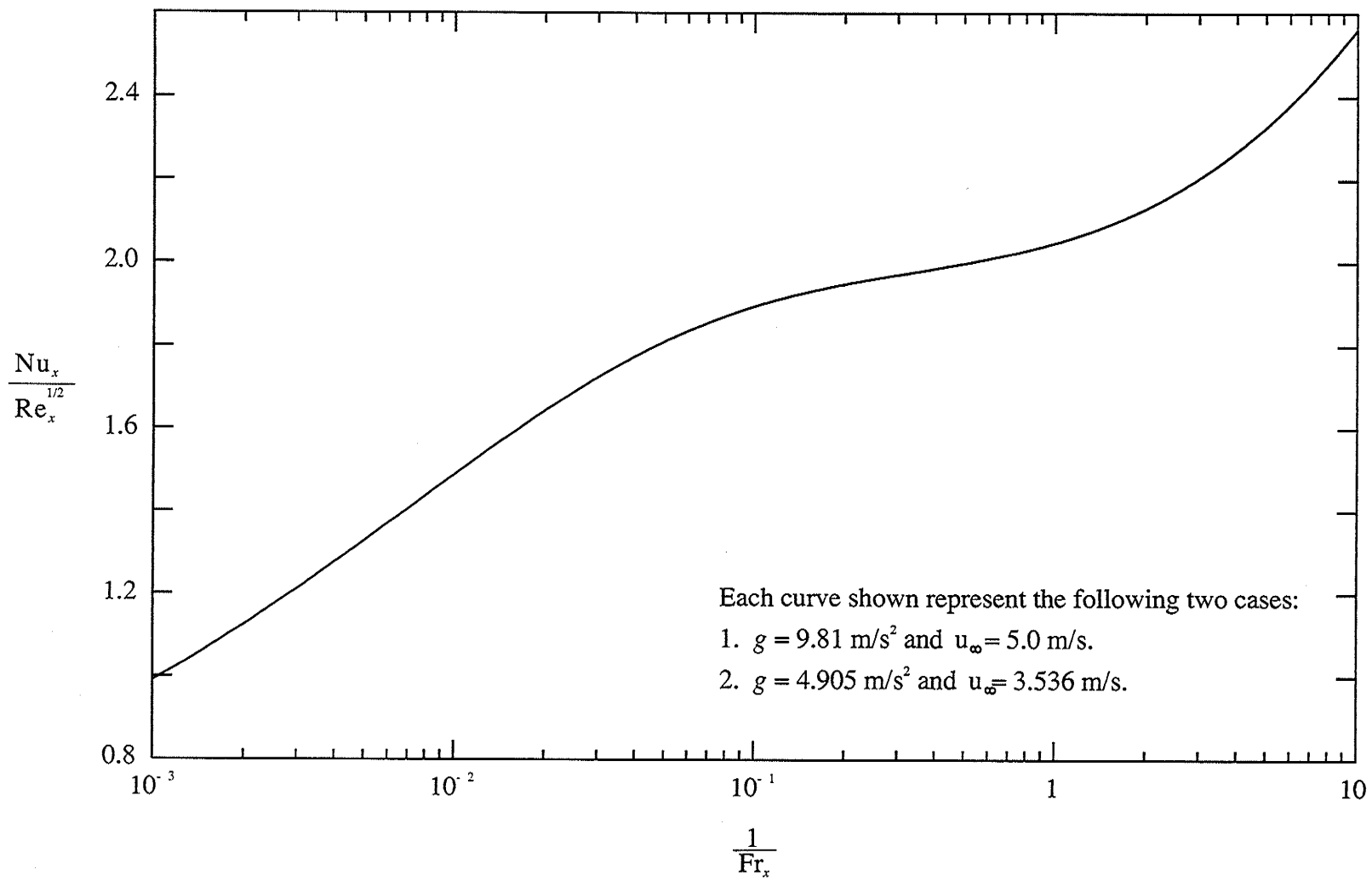

Figure D.6: Heat transfer results for glycerine-bromine at $T_\infty = 450$ K, $T_{wall} = 350$ K and $W_\infty = 0.1$.

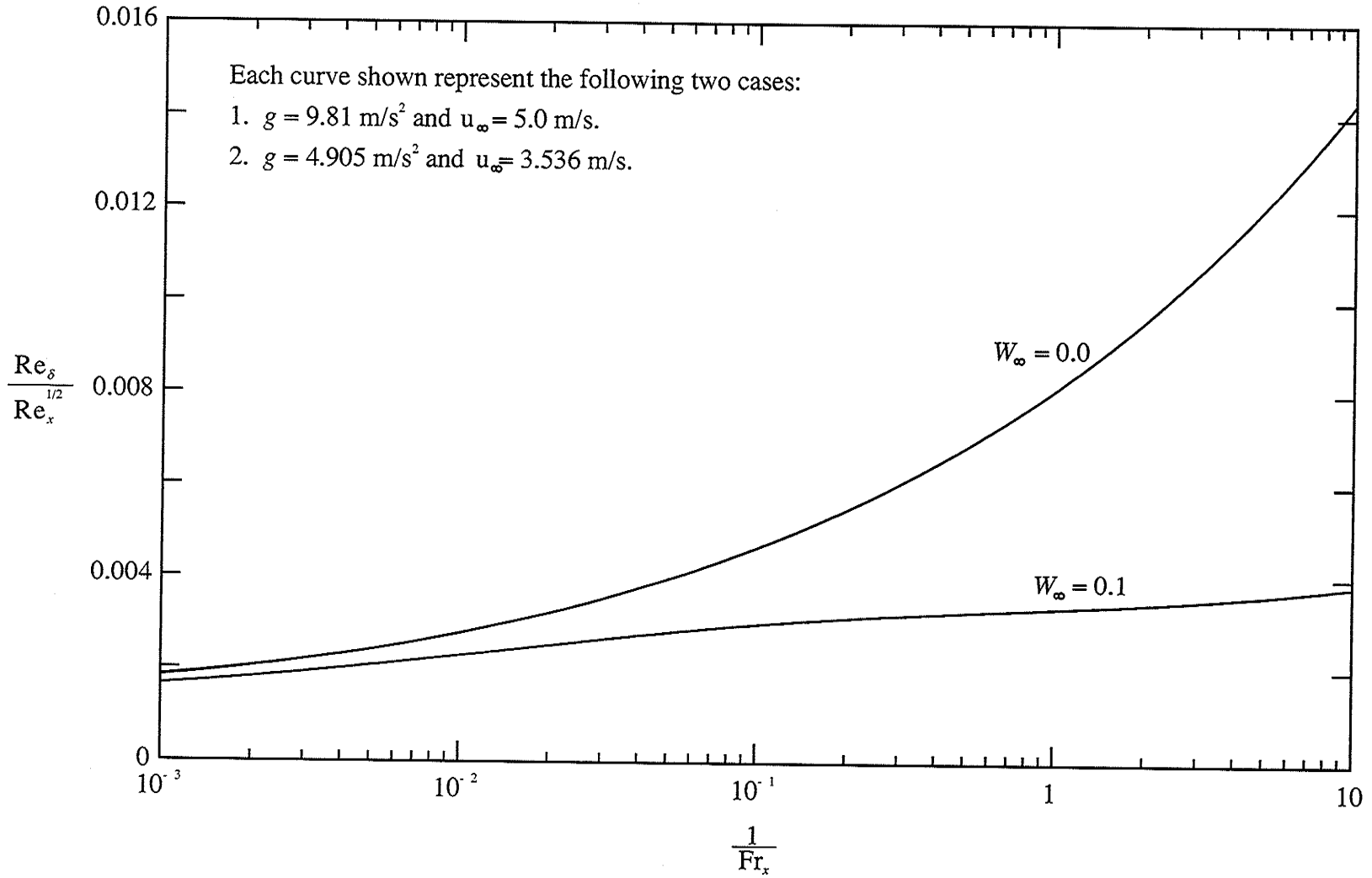

Figure D.7: Film Reynolds number for glycerine-bromine at T_∞ = 450 K, T_{wall} = 350 K and W_∞ = 0.0 and 0.1.